

Ministry of Water Resources

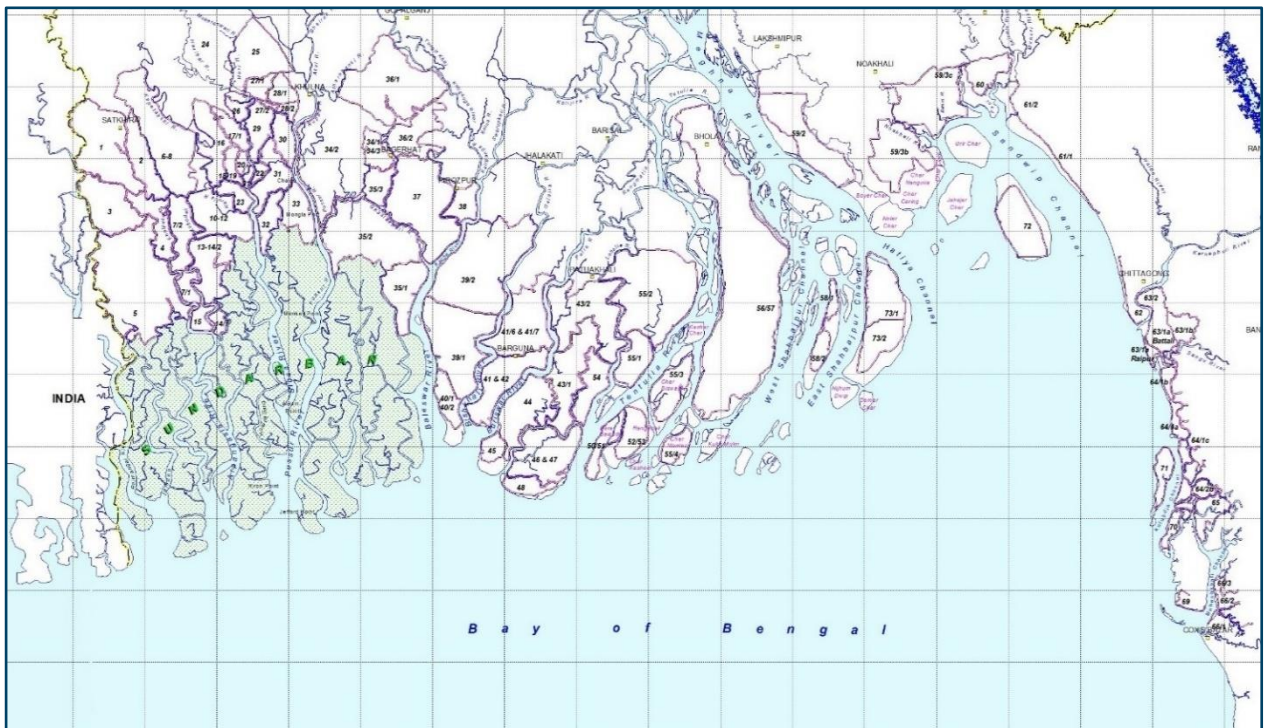


Bangladesh Water Development Board

Coastal Embankment Improvement Project, Phase-I (CEIP-I)

Long Term Monitoring, Research and Analysis of Bangladesh Coastal Zone (Sustainable Polders Adapted to Coastal Dynamics)

Macro scale morphology current situation & future projections



Joint Venture of



The expert in **WATER ENVIRONMENTS**

&



in association with



University of Colorado, Boulder, USA
Columbia University, USA

Ministry of Water Resources



Bangladesh Water Development Board

Coastal Embankment Improvement Project, Phase-I (CEIP-I)

Long Term Monitoring, Research and Analysis of Bangladesh Coastal Zone (Sustainable Polders Adapted to Coastal Dynamics)

Macro scale morphology current situation & future scenarios

May 2022

Joint Venture of



The expert in **WATER ENVIRONMENTS**

&



in association with



Water Environment & Climate

University of Colorado, Boulder, USA
Columbia University, USA

Long Term Monitoring, Research and Analysis of Bangladesh Coastal Zone (Sustainable Polders Adapted to Coastal Dynamics)

Macro scale morphology - current situation & future projections

Client	Bangladesh Water Development Board WAPDA Building
Contact	Mr. Syed Hasan Imam (BWDB project director) Swarna Kazi (World Bank)
Reference	Referenties
Keywords	Delta scale morphodynamics, climate change, sea level rise, numerical modelling, Delft3D Flexible Mesh, Hydrotrend

Document control

Version	1.0
Date	06-05-2022
Project nr.	1220745-000
Document ID	1220745-000-ZKS-0009
Pages	90
Classification	
Status	final

Main author(s)

	Reinier Schrijvershof	Deltares
	Dano Roelvink	Deltares - IHE
	Zheng Wang	Deltares
	Mick van der Wegen	Deltares - IHE
	Johan Reynolds	Deltares - IHE
	Irina Overeem	University of Colorado Boulder
	Abigail Eckland	University of Colorado Boulder

Doc. version	Author	Reviewer	Approver	Publish
1.0	Reinier Schrijvershof 	Jebbe van der Werf 	Bob Hoogendoorn 	

Summary

The main objective of the “long-term monitoring, research and analysis of the Bangladesh coastal zone” project is to create a framework for polder design to support sustainable polder management, based on understanding of the long-term and large-scale dynamics of the Ganges-Brahmaputra-Meghna (GBM) delta. Currently, there is insufficient knowledge about sediment budgets in the delta. This includes sediment input, transport and distribution in the river system and the estuaries. The knowledge on hydrodynamics and sediment dynamics, at present and in the future under climate change and human interventions is essential for the framework of polder design.

The macro-scale modelling work described in this report is the first component in a cascade of spatial and temporal scales that are studied in order to fill this knowledge gap. The purpose of this report, is to understand the large-scale annual sediment dynamics and long-term (decadal) morphodynamics of the GBM delta and predict changes in external forcing conditions (due to climate change and anthropogenic activity) and their consequences for the morphodynamics of the GBM delta.

To reach these objectives three types of models were set up and applied, each of them having a specific task in describing the governing processes. A basin scale hydrology model – HydroTrend – was developed to model water and sediment fluxes at the apex of the GBM delta. After calibration with observed discharges at the Ganges and Brahmaputra rivers, the sediment yield of the model was compared to literature for validation. The model was applied to estimate future water and sediment loads, driven by four different climate scenarios. On the scale of the delta, first a 1D river branch model was developed as a computational efficient tool. By comparison to observations and literature, the model is considered appropriate to simulate the tidal dynamics, and the distribution of discharge and suspended sediment over the main tributaries of the GBM delta. Secondly, a 2D large-scale coastal model was developed to simulate the coupled hydrodynamics, sediment transport (bed- and suspended load), and morphological change in the GBM delta. The model produces a physically reasonable bed composition, suspended sediment concentration patterns, net sedimentation areas, and agrees well to gross and net bed level changes compared to observations. Therefore, the model is considered suitable to assess future morphodynamic trends forced by climate change and anthropogenic activity.

Model simulations for the present-day situation were performed to investigate the current delta development. The results show that about 1/3th of the fluvial sediment input is exported to the deep sea, and the other 2/3th is deposited in the delta area, which agrees with literature. At a smaller scale, results show that the major part of the river discharge and fluvial sediment input is transported through the Lower Meghna, being the active delta building estuary. Here, the estuary bifurcates into multiple outlets and the 2D model results show that the most eastern outlet is increasing in importance, indicating that the eastwards building up of the delta, as reported in the geological studies, is continuing. This is supported by the 1D model results, concerning ebb and flood tidal volumes: the most eastern branch has the largest ebb and flood tidal volume whereas the west branch of the Lower Meghna has a larger net (seaward) discharge. The modelling results show that most sedimentation takes place in the mouth area of the active delta building estuary, the lower Meghna, and that the tidal channels in the Sundarbans (west of this) do not show aggradation. This result is, however, considered unrealistic and attributed to the absence of realistic mangrove vegetation effects and 3D density-driven currents (leading to landward transport) in the depth-averaged models used for the study. Including these processes, however, was not feasible considering the long-term simulations required.

The model results on future projections indicate that changes in flow discharge and sediment transport regime from the upstream rivers have more effect on the sediment dynamics in the delta than sea level rise (SLR) does. The river flow regime and the sediment transport regime are influenced by climate change (change in precipitation) and human interferences in the river

basins. The SLR and land subsidence, together the relative SLR, have a relatively minor influence on the sediment dynamics, and thus also limited influence on the sedimentation-erosion dynamics. This is best illustrated by an analysis on land loss versus land gain between present and the end of the century (2100). Relative SLR causes land loss and future accelerated SLR can turn the present net gain into net loss. According to the model results, this occurs when a value of 1.0 m for SLR is used if the upstream sediment supply remains unchanged. This effect is further aggravated when the upstream supply of water and sediment is significantly reduced, emphasizing the controlling factor of the upstream supply.

The study shows that the macro scale development of the GBM delta is dominated by sediment supply. The importance of the changes in river flow regime and sediment input from the rivers, as learned from the model results, implies that the distribution of the river discharge and sediment transport to the distributaries, like the Gorai river and Arial Khan river, will be a controlling factor for the future development of the different parts of the delta. Regulation of the distributions to these distributaries are possibly important measures for the future management of the delta.

Handtekening: 

E-mail: reinier.schrijvershof@deltares.nl

Handtekening: 

E-mail: jebbe.vanderwerf@deltares.nl

Handtekening: 

E-mail: bob.hoogendoorn@deltares.nl

Contents

1	Introduction.....	8
1.1	Background and project context	8
1.2	Objectives and approach.....	9
1.3	Outline of the report.....	10
2	Macro scale delta dynamics.....	11
2.1	Introduction	11
2.2	Sediment dynamics.....	12
2.2.1	River Sediment	12
2.2.2	Sediment transport forcing	13
2.3	Morphodynamics.....	14
2.4	Previous modelling efforts	16
2.5	Motivation for the modelling approach	16
3	Modelling approach.....	19
3.1	Model development.....	19
3.1.1	Catchment hydrology model (Hydrotrend).....	19
3.1.2	River branch model (Delft3D-FM 1D).....	20
3.1.3	Coastal model (Delft3D-FM 2D).....	21
3.2	Definition of scenario conditions	23
3.2.1	Upstream discharge	23
3.2.2	Sea level rise	26
3.2.3	Subsidence	27
3.2.4	Anthropogenic interventions	28
3.3	Scenario simulations	28
3.4	Analysis of the results	30
4	Model results on present-day situation.....	33
4.1	Hydrodynamics (1D).....	33
4.1.1	Tidal propagation	33
4.1.2	Gross and net discharge volumes	33
4.2	Sediment dynamics.....	37
4.2.1	Sediment fluxes.....	37
4.2.2	Distribution of surface sediment (2D).....	41
4.3	Morphodynamics.....	42
4.3.1	Tidal prism and cross-sectional area (1D).....	42
4.3.2	Volumetric balance (2D)	44
4.3.3	Detailed sedimentation/erosion maps (2D)	46
4.4	Integration of model results	50
5	Model results on future projections	51
5.1	Hydrodynamics (1D).....	51
5.1.1	Tidal propagation	51
5.1.2	Gross and net tidal discharge	52
5.2	Sediment dynamics.....	55
5.2.1	Sediment fluxes.....	55
5.2.2	Distribution of sediment concentrations (2D).....	60
5.3	Morphodynamics in 1D.....	62
5.3.1	Tidal prism and cross-sectional area	62
5.4	Morphodynamics in 2D.....	64

5.4.1	Bed evolution	64
5.4.2	Sedimentation/erosion patterns and differences	69
5.4.3	Volume balances and scenario effects.....	73
5.4.4	Land gain and loss	76
6	Discussion	81
6.1	Performance of the models.....	81
6.2	Lessons learned from the model results and future research	82
7	Conclusions	84
7.1	Conclusions on model development	84
7.2	Insights into the delta development and effects of climate change and human interference.....	84
8	References	86
A	Data.....	90
B	Development catchment hydrology model (HydroTrend).....	90
C	Development river network model (Delft3D-FM 1D)	90
D	Development coastal model (Delft3D-FM 2D)	90

FIGURES

Figure 1.1 Cascade of modelling scales, the macro-scale is studied in this report.....	9
Figure 2.1 Names of the major river branches in the GBM delta.	11
Figure 2.2 Sediment transport modes defined from sediment origin and transport mechanism. From Jansen et al. (1979).....	12
Figure 2.3 Development of the rivers in the Bengal delta over the past centuries (from Sarker et al., 2013).	15
Figure 2.4 Changes of the delta in the period 1985-2016 according to Aqua Monitor. Green areas: water turned into land, blue areas land turned into water.	15
Figure 2.5 The GBM delta divided into the sub-areas, from east to west: Active delta (with delta forming estuaries), Polder area, Sundarbans, and sub-aqueous delta	17
Figure 2.6 Conceptual model of sediment transport pathways in the GBM delta. Q_s is the rate of sediment delivery; S is the rate of subsidence. From Wilson and Goodbred (2015).	18
Figure 3.1 Catchments of the Brahmaputra and Ganges that are included in the Basin scale Hydrotrend model.....	20
Figure 3.2 Model domains of the 1D (in red) and 2D (in blue) Delft3D Flexible Mesh models that cover the entire Bengali part of the GBM delta.	22
Figure 3.3 Model network and bathymetry for the 2D Delft3D Flexible Mesh models that cover the entire Bengali part of the GBM delta. Darker shading reflects higher resolution, which goes from 8km near the southern boundary (not shown here) to 1km on the outer shelf, 500m on the inner shelf and Lower Meghna, 250m in the Sundarbans and locally to 100 m in Pussur-Sibsa and Baleswar-Bishkhali.	23
Figure 3.4 Calculation of a mean hydrograph (black lines) from shifted annual discharge data (gray lines), established from the observed discharge for the Ganges (a), Jamuna (b), Upper Meghna (c), and the confluence of Jamuna and Ganges into the Padma (d).	24
Figure 3.5 Cumulative distribution of the mean discharge (blue dots) and the 5 th up to and including 95 th percentiles (black circles) with 10 th percentile steps, for the Ganges (a), Jamuna (b), Upper Meghna (c), and the confluence of Jamuna and Ganges in to the Padma (d).	25
Figure 3.6 Constructed future boundary conditions for the future scenarios. Discharge in $10^3 \text{ m}^3/\text{s}$	25
Figure 3.7 Approximated sea level rise curves used as boundary conditions.	26
Figure 3.8 Spatially varying subsidence in the lower part of the GBM delta.	27
Figure 3.9 River kilometres used for the presentation of the 1D model results, see Figure 2.1 for the names of the rivers.	31
Figure 3.10 Polygons used for the presentation of the 2D model results.	32
Figure 4.1 Maps (top) and longitudinal distance plots (bottom) of the amplitude of the M_2 tidal constituent, shown for both the reference scenarios simulated with the 1D model.....	34
Figure 4.2 Distribution of the annual mean (black) and peak (blue) discharge, in $1 \cdot 10^3 \text{ m}^3/\text{s}$. Figures show the reference scenarios simulated with the 1D model. Vectors indicate the relative size of the mean annual discharge.	35
Figure 4.3 Flood (black) and ebb (blue) tidal volumes, in $1 \cdot 10^6 \text{ m}^3$. Left figure shows the south-western part of the delta and right figure the south-eastern part.	35
Figure 4.4 Flood (positive) and ebb (negative) tidal volumes (left y-axis) and net discharge (bars, right y-axis) along the length of the estuaries.....	36
Figure 4.5 Net annual suspended sediment load for cohesive (black) and non-cohesive (blue) material, in MT/yr. Positive numbers indicate a net transport in the seaward (i.e., ebb) direction, and negative numbers a net transport in the landward (i.e., flood) direction. For readability purposes, some transport vectors are not displayed.	38
Figure 4.6 Net annual total (sand and mud) suspended sediment sediment flux (bars) along the length of the estuaries, with positive (negative) numbers for the flood (ebb) direction. The fluxes for estuaries with multiple outlet systems are summed to total quantities.....	39
Figure 4.7 Yearly cumulative mud transports (left pane) and sand transports (right pane), mind the different vector scales.....	40
Figure 4.8 Yearly cumulative mud transports in gigatons with amounts per cross-section	41
Figure 4.9 Mud volume percentage in upper bed layer after 15 years. The remaining percentage consists of sand.	42

Figure 4.10 Scatterplot and linear fit of the cross-sectional area (A) versus the ebb tidal prism (P), for the estuarine systems of the Bengal delta modelled with the Delft3D-FM 1D model.....	43
Figure 4.11 Sediment volume balance over 20 years (2000-2019) computed with the 2D model (positive numbers indicate sedimentation; negative numbers erosion).	45
Figure 4.12 Cumulative sediment volume change over time for different areas over the period 2000-2019. .	46
Figure 4.13 Cumulative sediment volume change over 2000-2019 for different areas, where 'c' refers to the coastal areas and 'o' refers to the most ocean directed areas. For the exact polygon locations, see Figure 3.10.	46
Figure 4.14 Simulated sedimentation-erosion pattern, Meghna estuary, 2000-2009.	47
Figure 4.15 Observed sedimentation-erosion pattern, Meghna estuary, 2000-2009.	47
Figure 4.16 Simulated bed level changes, 2000-2019.	48
Figure 4.17 Observed land to water (blue) and water to land (green) changes, 2000-2019 (Source: Aqua Monitor).....	49
Figure 4.18 Simulated bed level changes, 2000-2019; left panel: bed level 2000; right panel: bed level 2019.....	49
Figure 5.1 Relative change in the M_2 tidal amplitude . Positive (negative) numbers indicate an increase (decrease) in the future scenarios with respect to the reference scenario.....	53
Figure 5.2 Relative change in the net tidal discharge. Positive (negative) numbers indicate an increase (decrease) in the future scenarios with respect to the reference scenario.....	54
Figure 5.3 Relative change in the total (sand and mud) suspended sediment load. Positive (negative) numbers indicate an increase (decrease) in the future scenarios with respect to the reference scenario.	56
Figure 5.4 Scenario 1.0m SLR, discharge RCP4.5 with yearly averaged sediment fluxes over the 2020-2100 period for (a) mud fraction; (b) sand fraction. Arrows indicate sediment transport direction and magnitude.	57
Figure 5.5 Scenario no SLR, discharge RCP4.5 with yearly averaged sediment fluxes over the 2020-2100 period for (a) mud fraction; (b) sand fraction. Arrows indicate sediment transport direction and magnitude.	58
Figure 5.6 Scenario 0.5m SLR, anthropic effects Q with yearly averaged sediment fluxes over the 2020-2100 period for (a) mud fraction; (b) sand fraction. Arrows indicate sediment transport direction and magnitude.	58
Figure 5.7 Scenario 1.0m SLR, discharge RCP8.5 with yearly averaged sediment fluxes over the 2020-2100 period for (a) mud fraction; (b) sand fraction. Arrows indicate sediment transport direction and magnitude.	59
Figure 5.8 Scenario 0.5m SLR, anthropic effects Q, no subsidence with yearly averaged sediment fluxes over the 2020-2100 period for (a) mud fraction; (b) sand fraction. Arrows indicate sediment transport direction and magnitude.....	59
Figure 5.9 Scenario 0.5m SLR, anthropic effects Q, 50% SSC with yearly averaged sediment fluxes over the 2020-2100 period for (a) mud fraction; (b) sand fraction. Arrows indicate sediment transport direction and magnitude.....	60
Figure 5.10 Mud sediment concentrations in g/l throughout the delta, averaged over 2040-2050 for different scenario runs.	61
Figure 5.11 Relative change in the ratio of the cross-sectional area (A) and the ebb tidal volume (P). Positive (negative) numbers indicate an increase (decrease) in the future scenarios with respect to the reference scenario.	63
Figure 5.12 Initial model bathymetry in 2020.	64
Figure 5.13 Modelled bathymetry in 2050 for runs as defined in Table 3.3.	65
Figure 5.14 Modelled bathymetry in 2100 for runs as defined in Table 3.3.	65
Figure 5.15 Area averaged bottom level change [m] between 2020 and 2050 for the different runs defined in Table 3.3. Red: deposition, blue: erosion.	66
Figure 5.16 Effect of different scenarios on average bed level change between 2020 and 2050 averaged over different subareas in the GBM delta. Subarea definitions can be found in Figure 3.10.	66
Figure 5.17 Area averaged bottom level change [m] between 2020 and 2100 for the different runs defined in Table 3.3.	67
Figure 5.18 Effect of different scenarios on average bed level change between 2020 and 2100 averaged over different subareas in the GBM delta. Subarea definitions can be found in Figure 3.10.	68

Figure 5.19 Cumulative sedimentation and erosion patterns for different scenarios (a,b) standard 1m SLR; (c,d) no sea level rise; (e,f) high end discharge, (a,c,e) after 30 years and (b,d,f) after 80 years. Mind the logarithmic colour scale.	70
Figure 5.20 Cumulative sedimentation and erosion patterns for different scenarios (a,b) 0.5m SLR and anthropic intervention; (c,d) 0.5m SLR and anthropic intervention – no subsidence; (e,f) 0.5m SLR and anthropic intervention – 50% reduction of upstream SSC, (a,c,e) after 30 years and (b,d,f) after 80 years. Mind the logarithmic colour scale.....	71
Figure 5.21 Differences in cumulative sedimentation and erosion patterns between different scenarios after 80 years (a) effect of 1m SLR; (b) effect of subsidence; (c) effect of high end discharge, (d) effect of 50% upstream SSC reduction (e) effect of anthropic intervention. Mind the logarithmic colour scale.	72
Figure 5.22 Differences in sediment volume [Gm ³] in function of time as a result of 1m SLR within different parts of the GBM delta as defined in Figure 3.10.	73
Figure 5.23 Differences in sediment volume [Gm ³] in function of time as a result of upstream reduction in discharge within different parts of the GBM delta as defined in Figure 3.10.	74
Figure 5.24 Differences in sediment volume [Gm ³] in function of time as a result of spatially varying subsidence within different parts of the GBM delta as defined in Figure 3.10.	75
Figure 5.25 Differences in sediment volume [Gm ³] in function of time as a result of a 50% reduction of suspended sediment concentration within different parts of the GBM delta as defined in Figure 3.10.....	75
Figure 5.26 Differences in sediment volume [Gm ³] in function of time as a result of using RCP8.5 instead of RCP4.5 to define upstream discharge boundaries. The different parts of the GBM delta are defined in Figure 3.10.....	76
Figure 5.27 Two estimates of land gain (green) and loss (blue) from Aqua Monitor; 1985-2016 (top) and 2000-2020 (bottom).	77
Figure 5.28 Simulated land gain due to sedimentation (green) and loss due to erosion or inundation (blue) for 2050-2060 relative to 2020-2030, for 6 different scenarios. Gray colour bar indicates bed levels.	78
Figure 5.29 Simulated land gain due to sedimentation (green) and loss due to erosion or inundation (blue) for 2090-2100 relative to 2020-2030, for 5 different scenarios.	78
Figure 5.30 Simulated total land gain (km ²) due to sedimentation (left panel), land loss due to erosion and inundation (middle panel), and net land gain (right panel), 2020-2100.....	79

ACRONYMS AND ABBREVIATIONS

BIWTA	Bangladesh Inland Water Transport Authority
BoB	Bay of Bengal
BWDB	Bangladesh Water Development Board
CEGIS	Centre for Environmental and Geographic Information Services
CEIP	Coastal Embankment Improvement Project
DEM	Digital Elevation Model
GBM	Ganges Brahmaputra Meghna
GCM	Global Climate Model
IWM	Institute of Water Modelling
MES	Meghna Estuary Study
MWL	Mean water level
RCP	Representative Concentration Pathway
SLR	Sea Level Rise
SOB	Survey of Bangladesh
SSC	Suspended Sediment Concentration
SWRM	South West Region Model
TBM	Temporary Bench Mark
TRM	Tidal River Management
ToR	Terms of Reference

1 Introduction

1.1 Background and project context

The main objective of the “long-term monitoring, research and analysis of the Bangladesh coastal zone” project is to create a framework for polder design to support sustainable polder management, based on understanding of the long-term and large-scale dynamics of the delta. The modelling work within the project is carried out to improve our understanding of the long-term and large-scale dynamics of the Ganges-Brahmaputra-Meghna (GBM) delta. There is insufficient knowledge about sediment budgets in the delta. This includes sediment input, transport and distribution in the river system and the estuaries. The knowledge on hydrodynamics and sediment dynamics, at present and in the future under climate change and human interventions is essential for the framework of polder design.

The time scales associated with the driving processes for the morphological changes range from hours (tides) to decades or even longer (climate change). Similar, the morphological responses encompass a large range of spatial scales, from thousands of kilometres (e.g. basin scale) to a few meters (e.g. internal polder drainage and siltation of peripheral rivers). Making long-term (~25-50-100y) predictions for this system is therefore particularly challenging and will be based on a cascade of process-based morphodynamic models (see Deliverable D-1; Inception report).

The cascade of models considers three different spatial and temporal scales (see Figure 1.1):

- Macro-scale (Deliverable D-4A-1, this report): annual sediment budget of the Bengal part of the GBM delta, and long-term (up to a century) morphodynamics. This scale is necessary to get a comprehensive understanding on how the system functions as a whole, and to estimate the impact of climate change and anthropogenic works.
- Meso-scale (Deliverable D-4A-2): regional river and estuary dynamics, driven by seasonal fluctuations in forcing conditions. This scale will highlight meandering and other dynamics of main estuarine branches and how they respond to major changes in tidal volumes, translating the macro scale findings into relevant impacts on local polder level.
- Micro-scale (Deliverable D-4A-3): water-logging and polder management. This scale is necessary to provide a detailed and local reference of (future) boundary conditions for dedicated polder design and management.

This report focusses on the macro-scale morphodynamic processes in the GBM delta. The report describes the development of models covering the larger domain of the GBM basin and coastal zone. The area of interest of the models is the Bengal part of the Delta. The models are first utilized to enhance our understanding of the morphodynamic processes most important for the present state of the GBM delta, and secondly the models are used to project potential future changes in the GBM delta (driven by climate change and human interventions), and to study the relevance for its macro-scale morphodynamics.

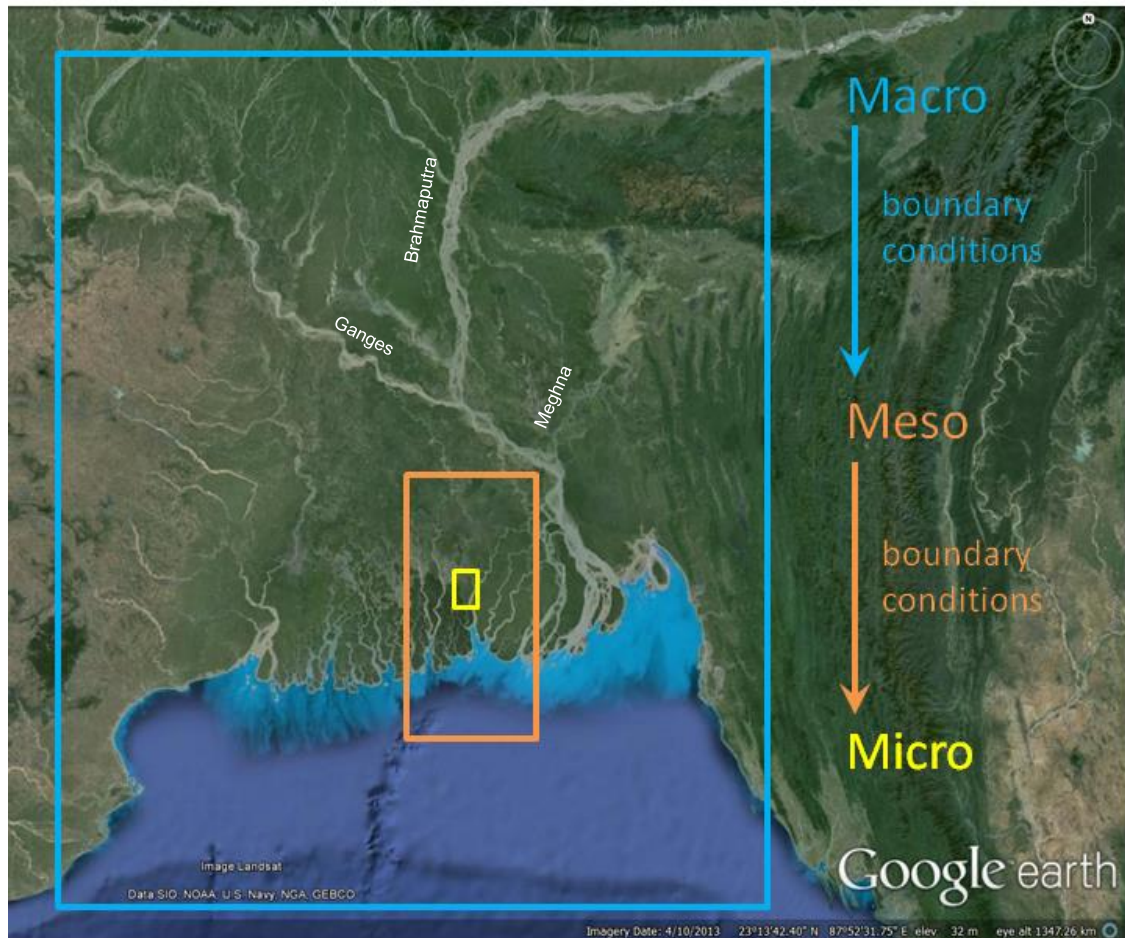


Figure 1.1 Cascade of modelling scales, the macro-scale is studied in this report.

1.2 Objectives and approach

The macro-scale morphology topic described in this report is the first component in a cascade of spatial and temporal scales that are studied. The purpose of this first part is to:

- To develop models that can simulate the morphodynamics of the GBM delta on a macro-scale;
- Improve our understanding of the macro-scale annual sediment dynamics and long-term morphodynamics of the GBM delta;
- Predict responses in the macro scale morphodynamic development of the GBM delta to climate change and anthropogenic activity.

The macro-scale morphological models are used to translate these effects to high-resolution meso-scale models (on the scale of an individual river or estuary) for their boundary conditions (separately reported in Deliverable D-4A-2). This multi-scale model approach allows for a quantitative understanding on the effect of changes in external drivers on polder sustainability and its associated design criteria.

The models are applied to establish an understanding of the long-term and large-scale sediment dynamics of the GBM delta and, based on the understanding of the current situation, identify drivers of future developments and quantify the effect of future changes in the external forcing mechanisms. To reach the objectives, three types of models are set up and applied, each of them having a specific task in describing the governing processes. These models are:

1. A catchment hydrology model (HydroTrend); the model quantifies the incoming sediment fluxes for the GBM delta, based on the catchment characteristics (i.e. drainage basin morphology and biophysical properties, and climatic conditions).
2. A river branch model (Delft3D-FM 1D); the model quantifies the distribution of incoming flow and suspended sediment fluxes over the major river branches of the GBM delta, based on the cross-sectionally averaged river bed properties (i.e. geometry, flow resistance, sediment composition).
3. A coastal model (Delft3D-FM 2D); the model quantifies the distribution of incoming flow and sediment fluxes and the morphological changes that are the result of gradients in the sediment redistribution.

1.3 Outline of the report

The report starts in the previous section with the objectives of the macro-scale morphology component and the overall methodology to reach the objectives. Chapter 2 outlines the knowledge background by providing a description on the governing hydrodynamics, sediment dynamics and historical morphological changes in the GBM delta. Previous modelling efforts done to study these delta dynamics are discussed as well, to provide a starting point of the present modelling. Chapter 3.1 gives a concise overview of the three models developed. A more detailed description of data sources, model set-up, calibration, and validation, however, is included in separate appendices (Appendices A - D). Chapter 3.2 describes the set-up of the input variables for the scenario simulations for the present-day situations and the future projections. The results of model application, addressing the objectives of the study, are subsequently presented for the present-day state of the delta in Chapter 4, and the results of the projections for future developments in the delta are described in Chapter 5. The results are integrally discussed in Chapter 6 and the report finalizes with conclusions, addressing the objectives, in Chapter 7.

2 Macro scale delta dynamics

2.1 Introduction

Setting up a numerical model requires an abundance of choices to be made such as modelling platform, spatial and temporal resolution and extent, and physical processes to be included. It is essential to have a thorough understanding of the physical system (conceptual model), model limitations, and lessons learnt from previous modelling efforts in order to make substantiated choices. This chapter gives a brief description of the system based on literature to derive a well-defined foundation for the modelling work to be executed. The chapter frequently refers to the names of the major river branches in the GBM delta. Therefore, an overview is presented in Figure 2.1.

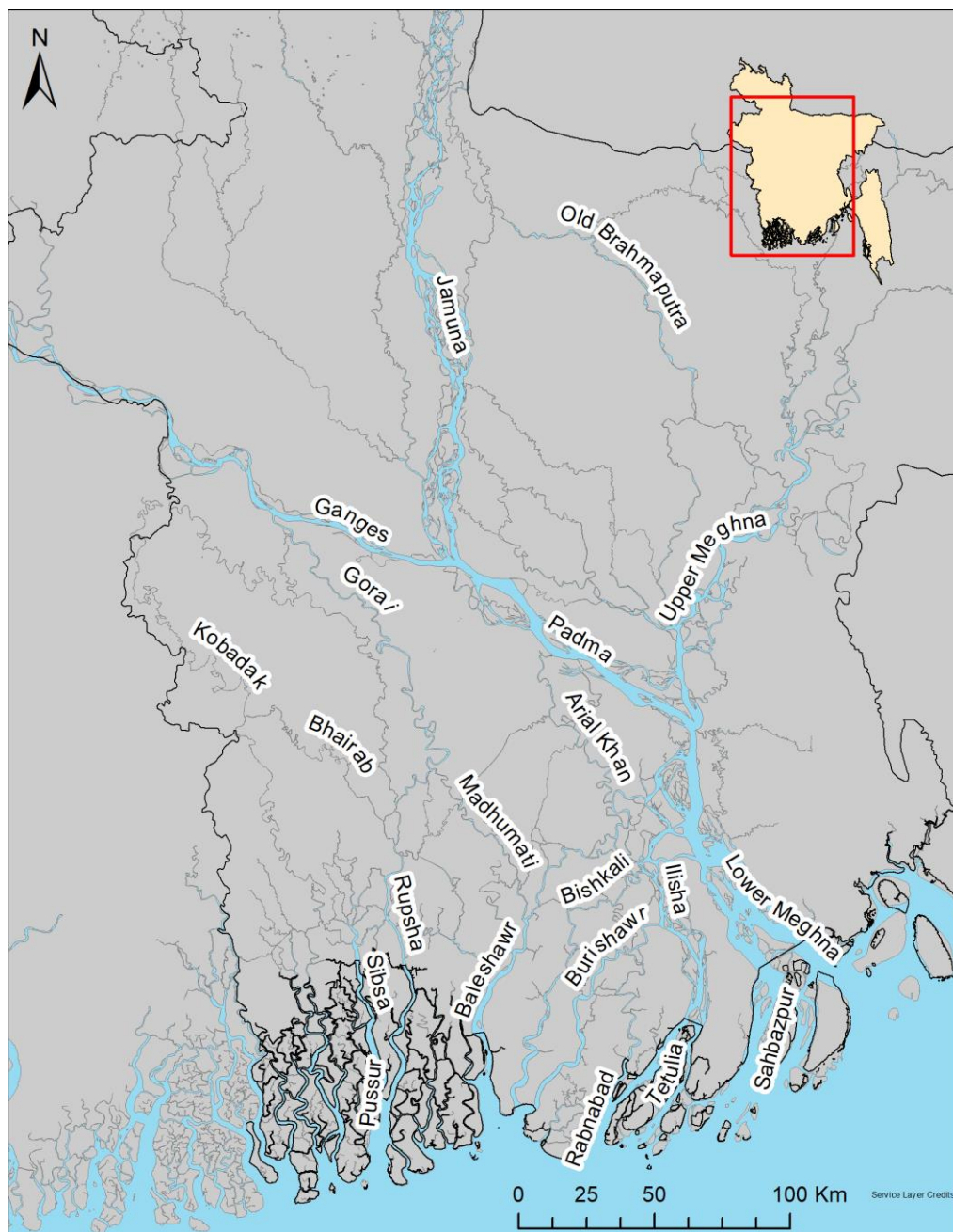


Figure 2.1 Names of the major river branches in the GBM delta.

2.2 Sediment dynamics

2.2.1 River Sediment

The concentration and distribution of sediment in the river channels are important controls on delta morphology. Understanding sediment composition and different transport mechanisms also provides insight into the reworking and accretion of material across the delta. Estimates of suspended sediment concentration (SSC) and grain size distributions have been collected across the entire GBM delta system, from the upstream portion in India, to the coastal shelf. Both in situ measurements (e.g. Kuehl et al., 1989; Barua et al., 1994; Datta and Subramanian, 1997; Singh et al., 2007) and remote sensing (Islam et al., 2001) methods have been used to make these estimates. In addition to estimates of concentration, the mineralogy of sediment samples is also recorded for the Ganga River in India (Chakrapani et al., 1995) and the Ganges, Padma, Jamuna and Meghna rivers in Bangladesh (Datta and Subramanian, 1997). Generally, the fluvial sediment input to the GBM delta is dominated by grain sizes ranging from fine sands to clays, with seasonal variability in transport due to monsoons. More detailed results from these analyses for suspended and bed load transport are summarized in the following.

Suspended Load

Like many fluvial systems, most of the sediment in the GBM delta is transported as suspended load of which a part is wash load and the remaining part belongs to bed material load (Jansen et al., 1979, see Figure 2.2). Wash load is defined as very fine sediment, which remains in near-constant suspension, even when velocities are negligible or there is slack water. This means that wash load does not participate in the exchange between water column and bed, and thus does not cause bed level change. Therefore, wash load is often ignored in morphological studies (of mostly rivers). However, for the present study it is required to consider the full suspended load including wash load because of various reasons. First, the distinction between wash load and bed material load is not everywhere the same but spatially variable. Wash load in the upstream rivers can become bed material load in the downstream estuary as the sediment settles eventually either in spatial or temporal context. This means that even the fine clay fraction of sediment does take part in the morphological changes of the GBM delta. Second, in systems with relatively high sediment concentrations like the GBM delta the influence of (total) sediment concentration on the hydrodynamics is important (Winterwerp et al., 2009, Wang et al., 2014). Considering the full suspended load without defining and excluding wash load has the consequence that more than one fractions of sediment (i.e. graded sediment) will need to be simulated in the morphodynamic models.

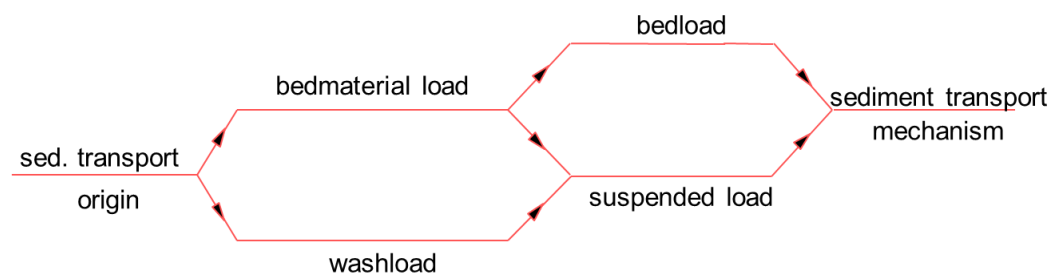


Figure 2.2 Sediment transport modes defined from sediment origin and transport mechanism. From Jansen et al. (1979).

Suspended sediment concentrations (SSC) have been assessed for several of the large rivers by measuring sediment concentrations and river discharges. Dry season estimates of SSC using Thematic Mapper (TM) and Advanced very-high-resolution radiometer (AVHRR) data resulted in average concentrations of 750 mg/L for the Brahmaputra and 500 mg/L for the Ganges River. During the monsoon season, average SSC increased to 1100 mg/L and 1250 mg/L, respectively (Islam et al., 2001). The authors argue that the increase in Ganges wet season SSC is tied to bank erosion and deposition on the floodplains during peak flooding. This increase in concentration can also be seen in sediment transport of the Padma River, where yields increase four-fold from 50 Mt/yr in the dry season

to 200 Mt/yr during the monsoon (Barua et al., 1994). Other estimates for suspended sediment load of the Brahmaputra (or Jamuna) River include 332 Mt/yr (Sarker et al., 2014), and 1060 Mt/yr for the combined system (Datta and Subramanian, 1997). Sediment moves seaward by fluvial forcing, and westward by tidal forcing (Barua et al., 1994).

In the Ganges River in India, suspended sediments range from very fine sands to medium silts (grain size 4-5.75 Φ) (Chakrapani et al., 1995; Singh et al., 2007). Suspended sediment in the main rivers of the GBM delta is finer, with predominantly fine silts and clays. Textural analysis by Datta and Subramanian (1997) showed fine silts and clays in the Ganges, Meghna, Jamuna and Padma Rivers. In their estimation, the grain size of more than 95% of the suspended material is fine silt and clays (≤ 16 microns). Median grain sizes sampled in the Meghna Estuary are similarly fine, ranging from 13.8 to 25 microns, or fine to medium silts (Kuehl et al. 1989, Barua et al., 1994).

The mineralogy of these suspended sediments has also been reported. Mineral constituents in suspended sediment samples throughout the GBM delta were predominantly quartz, followed by illite, kaolinite and feldspars (Datta and Subramanian, 1997). Trace amounts of chlorite, carbonates and montmorillonite were present at most sampling locations. Chakrapani et al. (1995) looked at the mineralogy upstream of the GBM delta system in India and noted changes in the mineral abundance moving downstream towards Bangladesh. Upstream, a high percentage of micas was noted. Towards the Bay of Bengal, smectite abundance increases, exceeding the mica abundance. In addition, samples also contain low levels of chlorites, vermis and kaolinities (Chakrapani et al., 1995).

Bed Load

Coarse sediment in fluvial systems is transported by rolling, sliding or saltating (bouncing) along the channel bed. Bed load transport is initiated when velocities near the bed are high enough to surpass a threshold for motion. In the GBM delta, bed load makes up a smaller proportion of total sediment load than suspended material.

Each of the major rivers of the GBM delta has sandy bed material (Sarker et al., 2014). Estimates for sediment transport of bed load are unknown, although some previous work supposes it may be as high as suspended transport rates (Garzanti et al., 2010) which seems very unlikely. The mineralogy of the bed load is similar to that of the suspended load. Sediments are quartz-dominated, with the presence of feldspars and clays (Datta and Subramanian, 1997).

Bed load sediments are coarser than the suspended load. Upstream of the GBM delta in India, bed load sediment is primarily fine sands (~60%) to very fine sands (~20%), with the remaining material being coarser sands, silts and clays (Singh et al., 2007). Moving into the GBM delta, bed sediment samples were 76% fine to very fine sands, with silt-sized grains making up the remaining bed layer (Datta and Subramanian, 1997). Downstream of the junction of the Ganges and Brahmaputra rivers, bed sediments are even finer. Grain sizes in that reach are very coarse silts (Singh et al., 2007). In the coastal region, samples showed the dominant size classes were also fine to very fine sands (grain size 2-4 Φ) (Stummeyer et al., 2002).

2.2.2 Sediment transport forcing

Fluvial forcing

The three main rivers of the GBM delta, the Ganges, Brahmaputra, and Meghna, deliver a total of 1 trillion (10^{12}) m³ of water and 1 billion (10^9) ton sediment per year to the Bay of Bengal through the Lower Meghna River (Akter et al., 2016). There are two other smaller branches, the Gorai River and the Arial Khan River, each delivering about 30 billion m³ of water to the bay annually (EGIS, 2001), with 30 and 25 million ton of sediment, respectively (Table 2.1).

Table 2.1 Annual discharge and sediment load of the various rivers of the GBM delta (from: Akter et al., 2016).

River	Discharge (m ³ /s)			Annual sediment load (10 ⁶ ton/yr)
	Mean	Peak	Minimum	
Jamuna	20,200	70,000	4,250	590
Ganges	11,300	52,000	600	550
Padma	32,000	95,000	4,800	1,000
Upper Meghna	-	13,700	-	-
Gorai	1,000	-	-	30
Arial Khan	1,000	-	-	25

Marine forcing

Tides along the coast of the Bengal delta (including the Indian part) are semidiurnal, with a slight diurnal inequality. The average tidal range varies from meso tidal (1.5 m) in the west to macro tidal (more than 4 m) at the NE tip of the Meghna estuary (Akter et al., 2016). The Meghna estuary, the main delta forming estuary, is a mesotidal estuary, where the tidal range varies between 2 and 4 m (MES II, 2001). The tide extends more than 100 km landwards.

2.3 Morphodynamics

The studies on the morphological development of the GBM delta on a geological time scale, carried out by Allison et al. (2003), Fergusson (1863), Goodbred & Kuehl (2000a, 2000b), Kuehl et al. (2005), Umitsu (1985, 1993), Williams (1919) and Morgan & McIntire (1959), have been summarized by Akter et al. (2016). They concluded that changes to the courses of the Ganges and Brahmaputra rivers were a consequence of the delta building process, which was itself driven by abundant sediment input from erosion of the Himalayas, conditioned by sustained sea-level rise (SLR) that began during the late Quaternary and modified internally by regional tectonics within the Bengal Basin.

On the century-scale the most important event concerns the Brahmaputra avulsion north of Madhupur Tract (where Dhaka is located): a large Pleistocene terrace from one to ten metres above the adjacent floodplains. Before the avulsion the Brahmaputra was flowing east of Madhupur Tract and after the avulsion the river now flows west of Madhupur Tract forming the present Jamuna River. Before the avulsion the two branches of Ganges had their own delta forming estuaries, separated from the one of Brahmaputra and Meghna together (Figure 2.3). The two branches Gorai and Padma were about equally important (see picture for 1776). After the avulsion the Padma River increased in importance because of the confluence of Jamuna. This has as consequence that the rivers come together with one combined delta forming estuary. After its formation the combined delta forming estuary has been shifting westwards. It is also remarked that the delta forming estuaries at present have a south-west facing orientation. This is probably due to the fact that the tidal wave in the Bengal Bay is propagating from west to east. In general, estuaries have the tendency of facing to the direction where the tidal wave comes from.

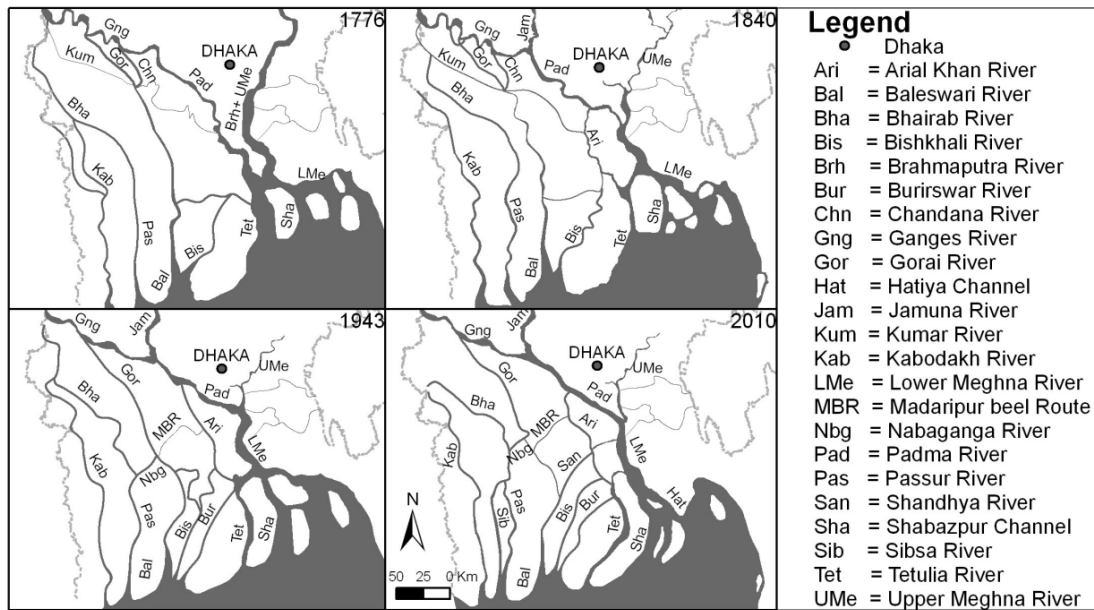


Figure 2.3 Development of the rivers in the Bengal delta over the past centuries (from Sarker et al., 2013).

On decadal timescale Akter et al. (2016) noted the changes of various bifurcations. The reported developments suggest that the western branches of bifurcations in the delta increased in dominance over eastern bifurcations. An example is that the Gorai River is now mainly discharging through the Nabaganga River instead of the Bishkhali river (see Figure 2.3).

Figure 2.4 shows the (decadal) morphological development of the delta based on satellite images between 1985 and 2016, according to Aqua Monitor developed by Deltares (Donchyts et al., 2016). The progradation of the delta at the mouth of the delta forming estuary Lower Meghna and the land formation within the estuary can be clearly observed. At the same time, the estuary is widening due to the erosion of both banks. According to Akter et al. (2016) the Shabazpur Channel is at present the main channel of the delta building estuary. However, the satellite images show that in the last years (approx. since 2009) the Hatiya Channel is increasing in importance and it seems to be the main channel in 2017 (Figure 2.4).



Figure 2.4 Changes of the delta in the period 1985-2016 according to Aqua Monitor. Green areas: water turned into land, blue areas land turned into water.

In the recent history the morphological development of the delta has also been influenced by anthropogenic activities. The building of 139 polders as part of the CEP project disconnected these former floodplains from the rivers, making sedimentation there no more possible. The subsidence in the polders increased and the tide amplified in the rivers due to loss of floodplains / tidal flats, making the local effective relative sea level rise as high as 2-3 cm/yr (Paskowski et al., 2021). The loss of floodplains / tidal flats also caused serious siltation in the river channels. The Farakka barrage on the main Ganges river, build by India in 1975, decreases the downstream river discharge by ~60% in the dry season. The decreased discharge in the Corai river has much lower sediment transport capacity, which is the reason of the increase in siltation in the river. The deltaic dynamics at present are thus a complex interplay of background natural responses to long- term change, and shorter- term responses to considerable anthropogenic activities (Paskowski et al., 2021).

2.4 Previous modelling efforts

Process-based models of the GBM delta exist, and most models are based on the MIKE¹ modelling platform. Existing 1D models like the General Model and the Super model can supply useful information for setting up the GBM 1D model to be set up in the present study. Experience and lessons learnt from the studies using these models are valuable for the set-up and application of the GBM delta models. An example is the study by Galappatti et al. (1996) who carried out a 1D morphodynamic modelling study for the main (upstream) rivers in Bangladesh. They showed that the rivers are morphologically very active. Consequently, the measured cross-sectional profiles may be less suitable for a 1D model than schematised cross-sectional profiles. Due to e.g. seasonal variation and the propagation of dunes and sand waves in the river, observed cross-sections at a certain location may fluctuate substantially depending on when the measurements are carried out. The results may vary greatly depending if the top or the trough of a sand wave is passing the measurement location at the time of observations. One important aspect, the morphodynamic development of the delta, is poorly covered by the existing models.

2.5 Motivation for the modelling approach

The GBM delta is formed by sediment from the rivers. The large scale morphodynamics of the delta are a matter of sediment supply and sediment distribution on the one hand, and relative sea-level rise on the other hand. At the macro-scale of the whole delta (Figure 1.1), fluvial input is the only sediment source. At present this sediment supply is about 1 billion ton per year (Table 2.1).

If the bulk density of sediment is 1.3 ton/m³ this sediment supply is sufficient to heighten the whole delta area of about 150,000 km² with about 5 mm/year. Considering that a large part of the delta cannot or does not need to be heightened by sedimentation, this is sufficient to compensate a quite high relative sea-level rise if the sediment can be properly distributed within the delta. However, change of the fluvial sediment supply due to climate change and human activities in the upstream river basins will directly influence the future development of the delta. Therefore, the Hydrotrend model will be set up and applied to predict the future development of the river discharge and sediment load.

At the macro-scale, the GBM delta can be divided in different areas, see Figure 2.5 where four areas are distinguished: active delta with the delta forming estuaries, polder area, Sundarbans and finally the subaqueous delta. In each of these areas the sedimentation depends on sediment supply, accommodation space and sediment transport capacity. Each of these three factors can form a limitation to the sedimentation rate:

- Sediment supply limited: Sediment source is not sufficient for fulfilling the sediment demand. As an example, if future sediment transport from the rivers to the delta will decrease or sea-level rise will accelerate, the delta as a whole will then become sediment supply limited when

¹ <https://www.mikepoweredbydhi.com/products>

the sediment transported is less than what is needed for the delta in terms of sedimentation to keep pace with sea-level rise.

- Accommodation space limited. Accommodation space depends on areas where sediment can accumulate and it increases with sea level rise (with a rate equal to the water area multiplied with sea level rise rate). In accommodation space limited areas sedimentation supply is higher than required to grow the area in line with sea level rise.
- Transport capacity limited: This is the case when there is sufficient sediment supply but accommodation space cannot be filled because the sediment transport capacity between the sediment source and the area with accommodation space is too low.

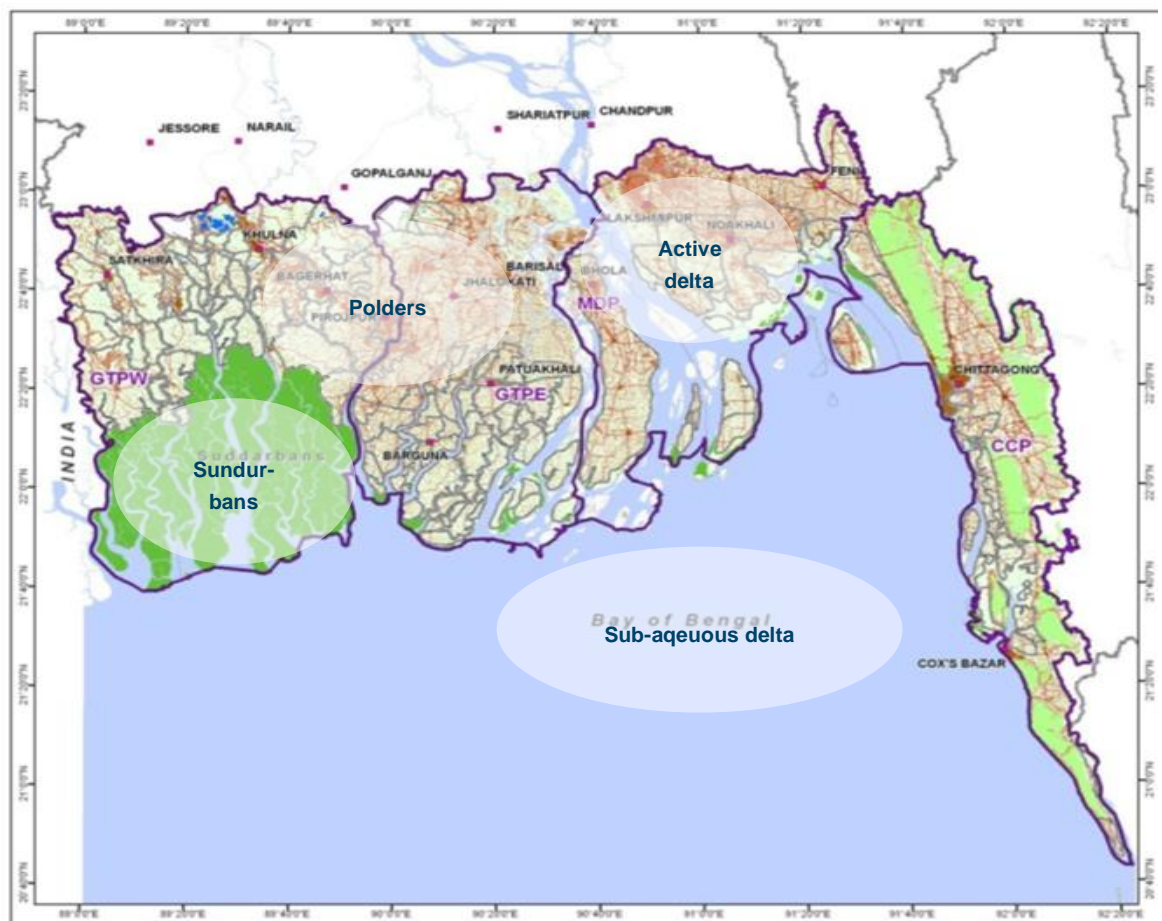


Figure 2.5 The GBM delta divided into the sub-areas, from east to west: Active delta (with delta forming estuaries), Polder area, Sundarbans, and sub-aqueous delta

Which limitation applies is important for how the area/system will respond to changing river sediment input and/or accelerating sea level rise, see Wang et al. (2018) who used this conceptual model for projecting the response of the Dutch Wadden Sea to future sea level rise scenarios.

The active delta is located in the eastern part of the overall delta, with the Lower Meghna being the main delta forming estuary. This area receives the major part of the sediment supply from the rivers. The sediment supply is thus ample, and the flow driven by river and tide provides sufficient sediment transport capacity to redistribute the sediment. The sedimentation rate here is limited by accommodation space (sediment supply is much more than needed for the area to grow with the rising sea level). As a consequence, the delta is extending seawards and a part of the sediment is transported further offshore.

The polder area is west from the active delta and east and north of the Sundarbans. Sediment supply to this area is partly via the (2nd and 3rd order) river tributaries from upstream and partly by the tidal

flow from the coastal zone. Sedimentation within the polders is transport capacity limited because sediment exchange with the river / estuary branches is practically blocked. When this blockage is removed by e.g. tidal river management (TRM) the question then arises if the sedimentation will become sediment supply limited or transport capacity limited. The river branches / channels between the polders are probably accommodation space limited at present.

For the Sundarbans the sediment supply is also partly fluvial and partly marine. At present the sedimentation seems to be accommodation space limited as the area can keep up with sea-level rise. For the future scenarios with faster sea-level rise it is the question if it will become sediment supply limited or transport capacity limited.

The marine sediment redistributed to the polder area and Sundarbans is actually sediment from the delta forming estuaries. The remaining sediment from the delta forming estuaries is contributing to the subaqueous delta further seawards where the sedimentation is per definition supply limited. This conceptual model of sediment transport pathways is summarized and visualized in Figure 2.6.

In the conceptual model for the macro-scale development of the GBM delta described above and shown in Figure 2.6 the development of the polder area and the Sundarbans depends very much on how the fluvial sediment supply is distributed via the river tributaries and how the sediment out of the delta forming estuaries is transported along the coast and landwards via the tidal estuaries. The design of sediment management measures like TRM will also rely on the understanding of this sediment distribution. Therefore, a 1D river network model and a 2D depth-averaged (2DH) model are set up for simulating the present and future macro-scale sediment distribution in and morphological development of the delta. The 1D model mainly focusses on the distribution via the river tributaries whereas the 2DH model also covers the sediment transport along the coast.

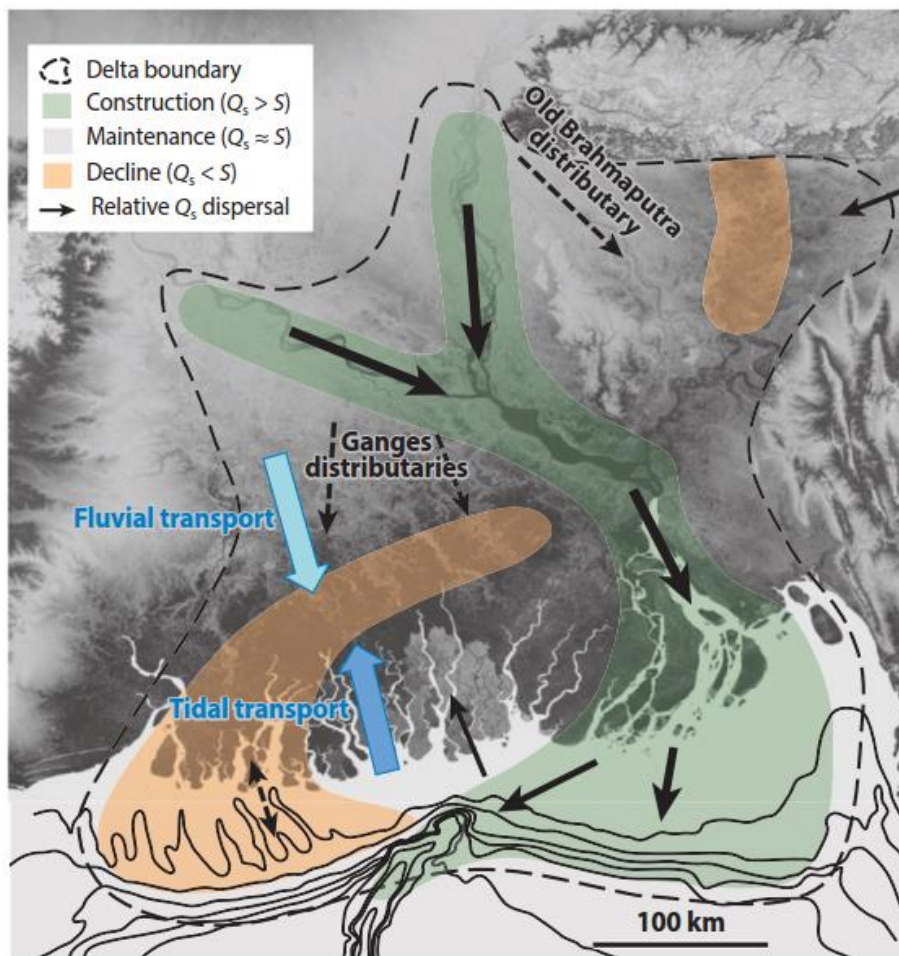


Figure 2.6 Conceptual model of sediment transport pathways in the GBM delta. Q_s is the rate of sediment delivery; S is the rate of subsidence. From Wilson and Goodbred (2015).

3 Modelling approach

3.1 Model development

Three models will be developed to study the macro scale sediment transport pathways and delta morphodynamics:

1. A catchment hydrology model (Hydrotrend)
2. A 1D river network model (Delft3D-FM 1D)
3. A 2D depth averaged coastal model (Delft3D-FM 2D)

The development of the three models is supported by numerous sources of data, which are used for analysis, model set-up, and model calibration and validation. The data include hydrographic measurements, bathymetric measurements, and oceanographic and meteorological conditions obtained from global models. The data used in the study are described in Appendix A.

3.1.1 Catchment hydrology model (Hydrotrend)

The catchment hydrology model (Hydrotrend) covers the Ganges and Brahmaputra catchments (Figure 3.1). It is a fully empirical basin-averaged model that can simulate the water and sediment fluxes towards the borders of the Bengali part of the GBM delta, as a function of basin-averaged input parameters, e.g.; precipitation and hypsometry (Kettner et al., 2008). The aim is to use the catchment hydrology model to:

- estimate incoming total annual water and sediment fluxes for each of the upstream basins of the Ganges and Brahmaputra rivers, which then can be propagated into the macro-scale morphodynamics delta models (Delft3D);
- estimate daily dynamics and analyse variability of suspended sediment fluxes for each of the Ganges and Brahmaputra rivers;
- estimate future water and sediment fluxes under projections of a changing climate and upstream dam engineering for each of the Ganges and Brahmaputra rivers.

To reach this aim, the model is calibrated against discharge measurements over a ~30 year hindcast period and observed sediment rating curves at the upstream parts of the Ganges and Jamuna river (Hardinge Bridge and Bahadurabad, respectively). Subsequently, the Hydrotrend model is used to make projections for water and sediment fluxes for the period 2006-2099. For the projections the model is forced with future conditions of precipitation and temperature in the catchment areas, obtained from four different global climate models and two emission scenarios. The analysis of the climate change conditions is described in deliverable D-4C: Meteorology. A complete description on the development of the GBM Hydrotrend model and the future climate change projections is provided in Appendix B and a submitted scientific paper on this topic (Eckland et al., submitted).

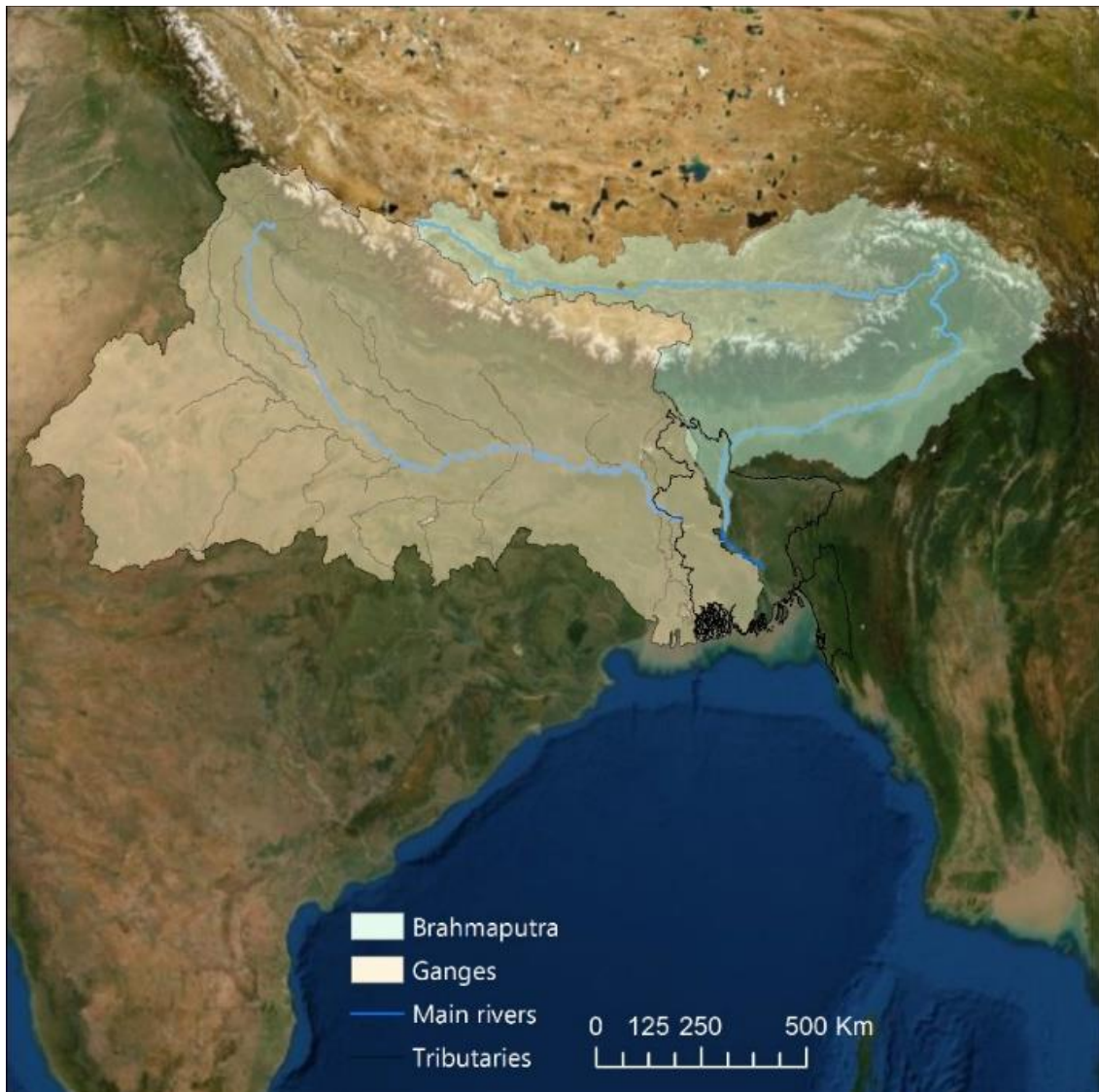


Figure 3.1 Catchments of the Brahmaputra and Ganges that are included in the Basin scale Hydrotrend model.

3.1.2 River branch model (Delft3D-FM 1D)

The river network model (Delft3D-FM 1D) covers the main branches of the Bengali part of GBM delta (Figure 3.2), from the apex up to the seaward mouth of the river estuaries. The model provides information on the distribution of flow and suspended sediment transport over the major rivers of the GBM delta. The main objectives of the model are:

- To study the large-scale tidal propagation and flow distribution, and how this is expected to change in the future;
- To derive a sediment budget for the GBM Delta, covering the largest part (major rivers) of Bangladesh;
- To apply the sediment budget model to assess the effect of scenarios of changing boundary conditions (downstream and upstream);

The model is set-up using bathymetric profile measurements and is forced with a discharge at the apex of the delta and by tidal conditions at the seaward mouths of the river estuaries, obtained from a regional model that includes the Bay of Bengal (Uddin et al., 2014). Suspended sediment concentrations are based on literature, and forced as constant values. The model is calibrated against measurements of water levels and discharge at various locations in the delta over the period 1975-

2000 and the year 2012. The model can simulate the fluvial and tidal hydrodynamics, and suspended sediment distribution over the river branches. The model is simulated in morphostatic mode; i.e. there are no bed level updates during the simulations.

The strength of the one-dimensional approach is the computationally efficient model set-up which allows for long-term calculations without the constraint of applying any input reduction scheme (schematization of boundary conditions). In this way the long-term effect of the interaction of tides and river discharge on the sediment distribution is studied using (real-time) boundary information that resembles actual conditions. The obvious weakness of a 1DH model is the assumption that the governing processes can be described by cross-sectionally averaged parameters. A full description on model development, model calibration and validation is provided in Appendix C.

3.1.3 Coastal model (Delft3D-FM 2D)

The GBM delta coastal model (Delft3D-FM 2D) covers the main branches of GBM delta and a large part of the Bay of Bengal (Figure 3.2 and Figure 3.3). The model provides information on the internal sediment distribution as a result of fluvial and tidal forcing, and information on the gross morphodynamic trends that results from gradients in the sediment transport pathways. The main objectives are:

- To study the coarse and fine sediment distribution, and how the distribution is affected by human interventions and climate change;
- To identify pathways for fine sediment;
- To study the morphology of major channels on decadal scales;
- To provide boundary conditions in terms of large-scale bed elevation change and sediment concentrations to meso-scale models.

The model is set-up using an automatic grid generation approach based on successive refinements in areas within given polygons, and the available bathymetric measurements. The model is forced by a discharge at the apex and tidal conditions derived from a global model at the seaward boundaries in the Bay of Bengal (Egbert and Erofeeva, 2002). The model is hydrodynamically calibrated against tidal conditions and discharges at various locations in the delta. The morphological model is forced by schematized boundary conditions (discharge, concentrations, wind) and calibrated against sediment concentration patterns and observed volumetric changes in the eastern part of the GBM delta and coastal zone. The coastal model proved to confidently simulate morphological developments in the delta over periods of up to decades, providing information on the redistribution of sediments and morphological adaption. A complete description on the initial development of the coastal model is provided in Appendix D.

Between the initial model setup and validation, and the application for the scenario runs over 2020-2100, several further refinements were carried out as detailed in Appendix D:

- Refinement from 500m to 250 m for large areas west of the Lower Meghna;
- Integration of the meso-scale models for Pussur-Sibsa and Baleswar-Bishkhali within the overall network;
- Inclusion of several river branches, most notably the Gorai, as curvilinear grid sections
- Adjustment of the critical bed shear stress for erosion, mainly in the Sundarbans, to account for the effect of mangroves reducing erodibility in areas above 1m above MSL.
- Adjustment of the roughness of the Gorai in order to maintain its long-term stability.
- Importantly, inclusion of large-scale bank erosion, through the 'dry cell erosion' concept, where vertical erosion due to migrating channels is converted to erosion of adjacent dry cells. This is particularly important for maintaining realistic channel and shoal geometry through very long simulations.

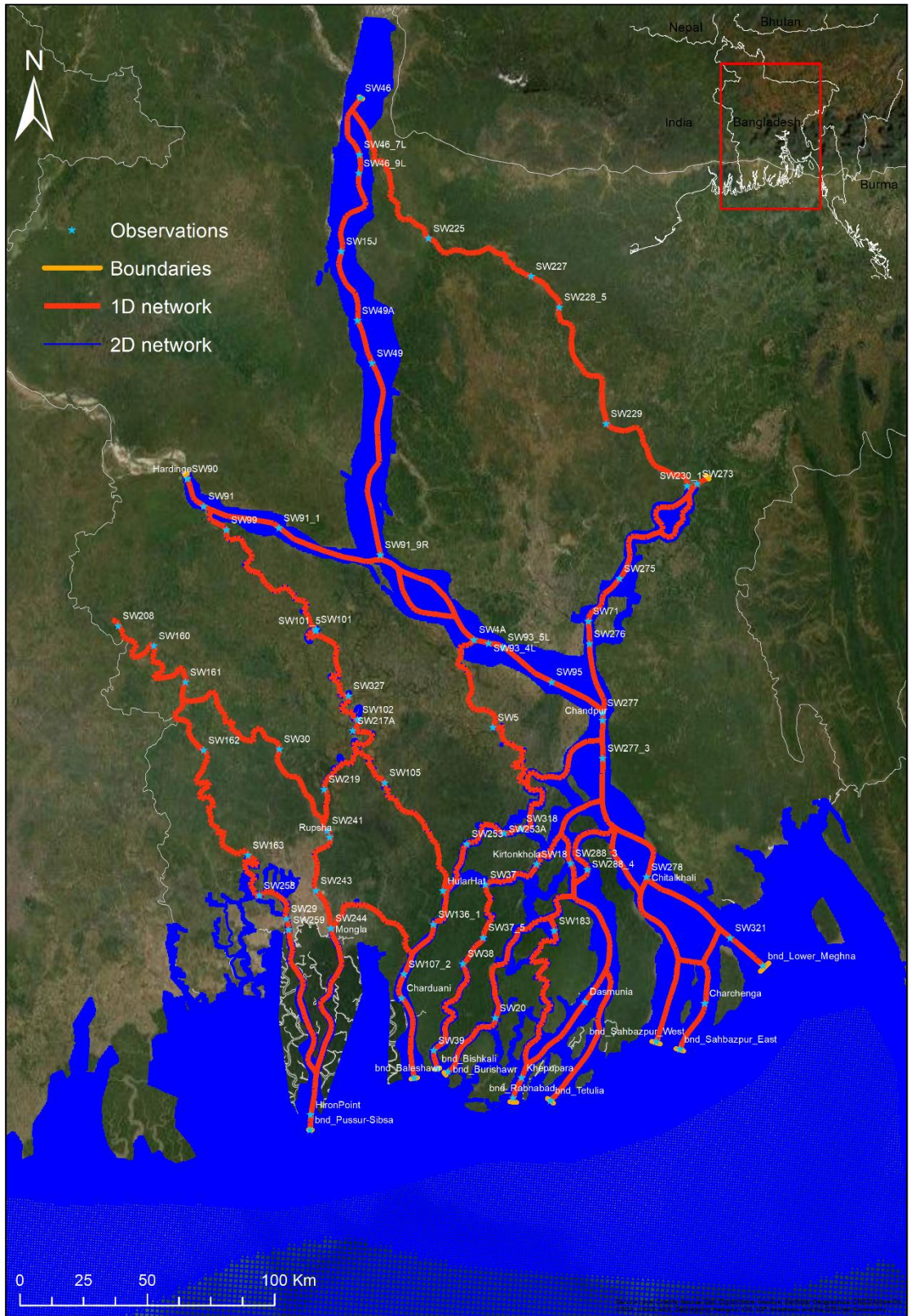


Figure 3.2 Model domains of the 1D (in red) and 2D (in blue) Delft3D Flexible Mesh models that cover the entire Bengali part of the GBM delta. delta.

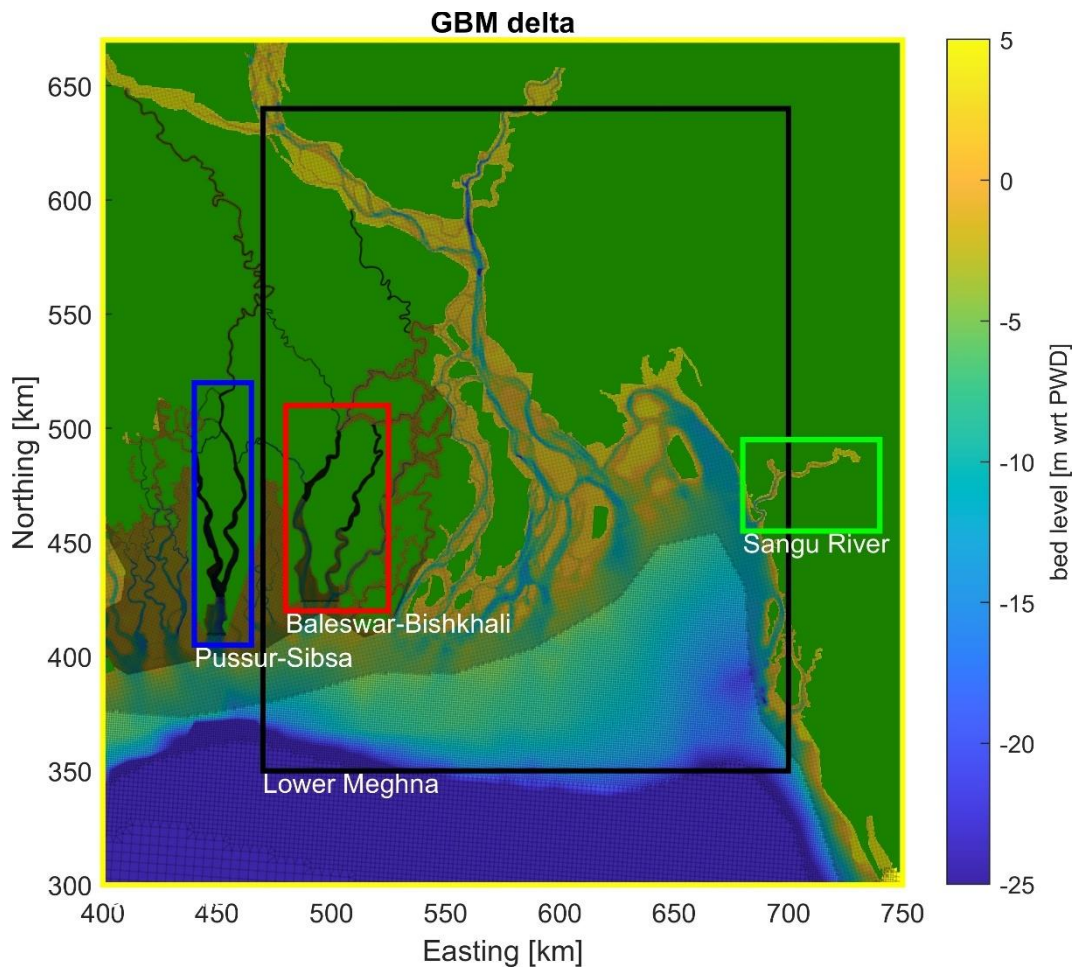


Figure 3.3 Model network and bathymetry for the 2D Delft3D Flexible Mesh models that cover the entire Bengali part of the GBM delta. Darker shading reflects higher resolution, which goes from 8km near the southern boundary (not shown here) to 1km on the outer shelf, 500m on the inner shelf and Lower Meghna, 250m in the Sundarbans and locally to 100 m in Pussur-Sibsas and Baleswar-Bishkhali.

3.2 Definition of scenario conditions

3.2.1 Upstream discharge

The historic observed discharges of the Ganges and Jamuna rivers are used in combination with the results from the Hydrotrend model to force the delta scale models at their upstream boundaries for future scenarios. The Hydrotrend results consist of timeseries for the period 2006-2095 (90 years) under two emission scenarios (RCP4.5 and RCP8.5) and four global climate models (GCM's). The large set of discharge projections needs to be schematized into reduced, but representative, boundary conditions for the models. A procedure is developed to select a series of hydrographs from the observed historic discharge data that give a proper representation of the distribution of discharge, and to increase the selected series with a factor that is determined from the Hydrotrend results. The procedure is described in the following paragraph and visualized in Figure 3.4 and Figure 3.5. The resulting timeseries that are used to force the models are shown in Figure 3.6.

The observed historical discharge data are shifted in time such that the peak day for all data coincides (see Appendix D for an explanation on the procedure). From the new dataset on annual discharge (Figure 3.4, grey lines) a representative mean hydrograph is selected (Figure 3.4, black lines). A cumulative distribution of the mean annual discharge is constructed (Figure 3.5) and the 5th – 95th percentiles (10% intervals) within this distribution are determined by linear interpolation (Figure 3.5,

black circles). A 10-year timeseries is constructed that is built up from the representative hydrograph, multiplied with the mean annual discharge values corresponding to the percentiles. The 10 hydrographs are positioned in a random order to set-up a 10-year timeseries on future discharge (the order for Ganges and Brahmaputra differs). The boundary condition time-series are constructed by concatenating the 10-year periods of randomly ordered hydrographs until 2100, while applying a multiplication factor to each hydrograph based on the increase of the mean annual discharge determined from the Hydrotrend projections (see FigureApx B.4 and FigureApx B.5 in Appendix B). The resulting timeseries (Figure 3.6) show an increase towards 2100 and a clear repetitional pattern with a period of 10 years.

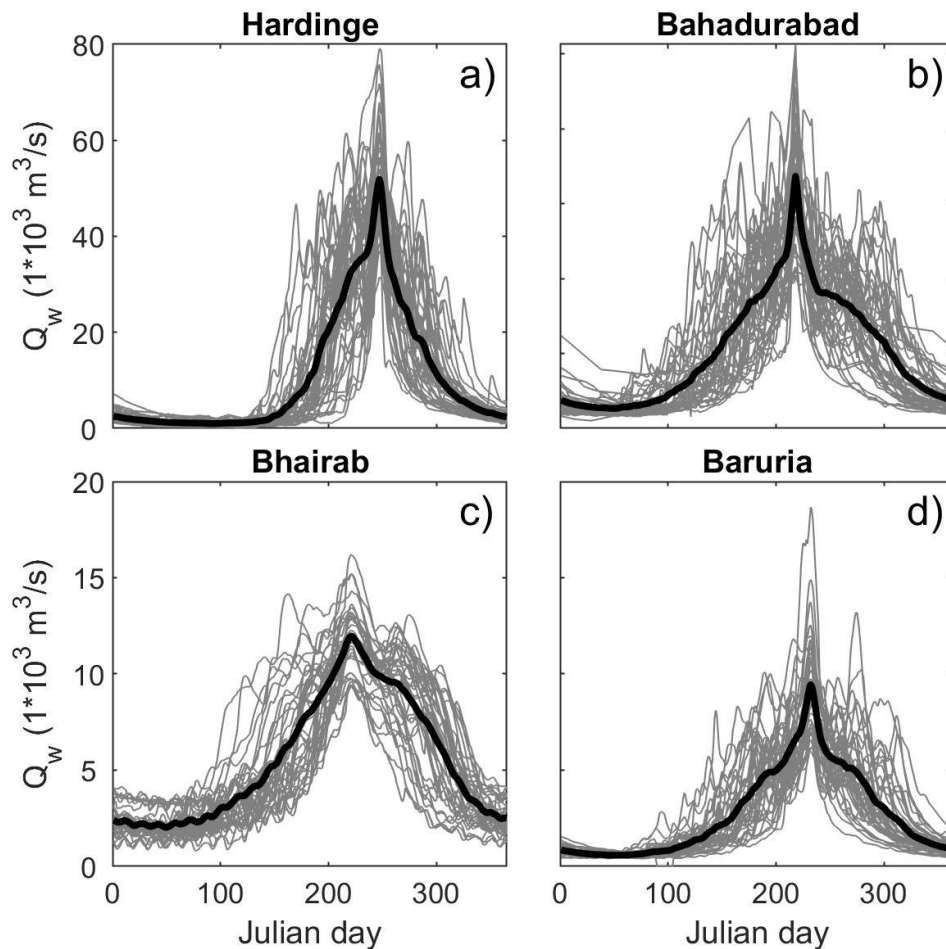


Figure 3.4 Calculation of a mean hydrograph (black lines) from shifted annual discharge data (gray lines), established from the observed discharge for the Ganges (a), Jamuna (b), Upper Meghna (c), and the confluence of Jamuna and Ganges into the Padma (d).

The boundary information (Figure 3.6) is applied directly to the 1D model and the time-series are squeezed in time to force the 2D model, that simulates the morphological change with an acceleration factor (MorFac). Suspended sediment concentrations are not derived from the Hydrotrend results but considered constant and are equal to the values used for the calibration and validation of the models (Appendix C and Appendix D).

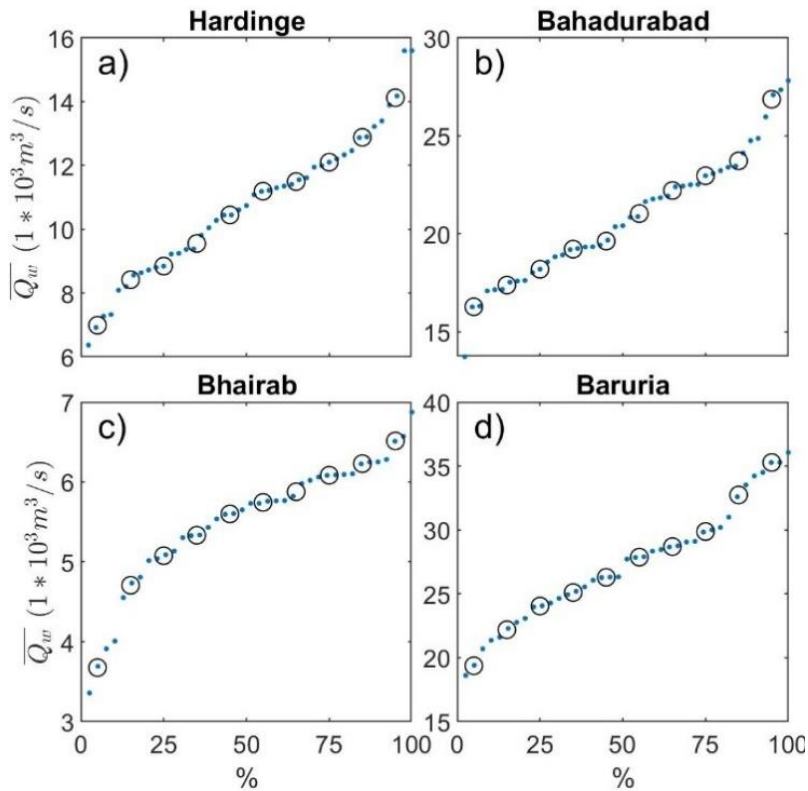


Figure 3.5 Cumulative distribution of the mean discharge (blue dots) and the 5th up to and including 95th percentiles (black circles) with 10th percentile steps, for the Ganges (a), Jamuna (b), Upper Meghna (c), and the confluence of Jamuna and Ganges in to the Padma (d).

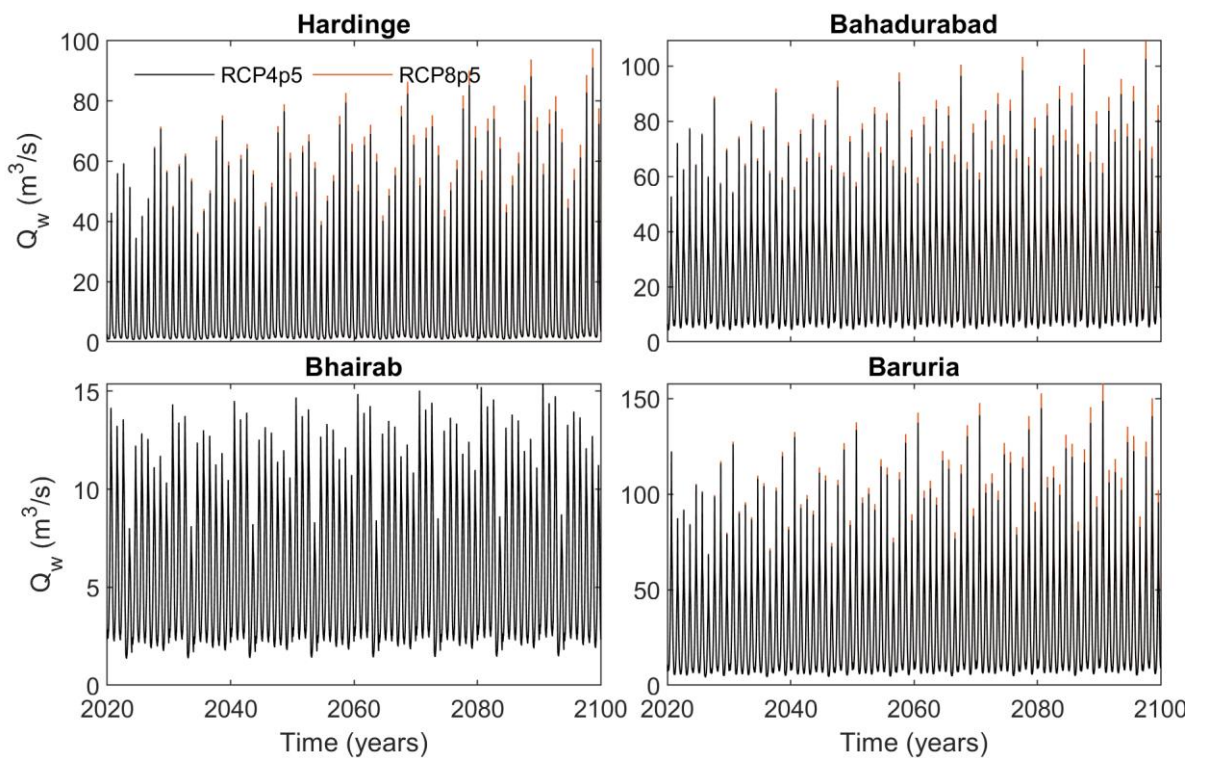


Figure 3.6 Constructed future boundary conditions for the future scenarios. Discharge in $10^3 \text{ m}^3/\text{s}$.

3.2.2 Sea level rise

Projections on absolute sea level rise values for the Bay of Bengal are derived and reported in deliverable D-4C: Meteorology. The SLR curves were extracted for five locations along the coast of Bangladesh, based on the SROCC (Special Report on the Ocean and Cryosphere in a Changing Climate) regional projections (IPCC, 2019). The analysis on SLR rates results in the conclusion that SLR can be considered spatially uniform for the Bay of Bengal. The spatially mean values for SLR up to the end of the century are shown in Figure 4.58 of the Climate Change Scenarios report (D-4C: Meteorology). The reported values include the median (50th percentile) and the associated uncertainty bands. A careful selection of the projections is made for the downstream boundary conditions for the delta scale models to ensure that the full range of projections is covered, but the number of options is limited (when combined with the upstream discharge conditions). The values of the RCP4.5 lower (5th %), RCP4.5 median (50th %), RCP8.5 median (50th %), and RCP8.5 high (95th %) projections are selected and approximated by a 2nd order polynomial (Figure 3.7).

The SLR conditions (Figure 3.7) are forced directly on the offshore boundaries of the Delft3D-FM 2D coastal model, which are located well offshore from the continental shelf. The seaward boundaries of the Delft3D-FM 1D model are, however, located at the mouths of the estuaries and SLR cannot be applied without considering the change in tidal regime. Therefore, the MIKE21 Bay of Bengal model (Uddin et al., 2014) is used to simulate the SLR projections, using the SLR values for 2100 in a one-year simulation. The output of the model is used to derive astronomical tidal constituents (amplitude and phase) and MSL for the seaward boundary conditions of the Delft3D-FM 1D model. Similar to the procedure used for model set-up of the 1D model, the tidal conditions are not derived from the 2D model to keep both delta scale models independent from each other.

To give an indication of the change in the tidal regime at the boundaries of the model, the amplitudes of the primary M₂ tidal constituent are given in Table 3.1. The table shows that the M₂ tidal amplitude increases with increasing sea level for all boundary locations, except for the Tetulia east boundary. The absolute increase differs for the boundary locations, but the trend along the coastline remains similar for all scenarios, i.e., the M₂ amplitudes generally increase from west to east but are smaller at the Tetulia and Sahbazpur estuary mouths.

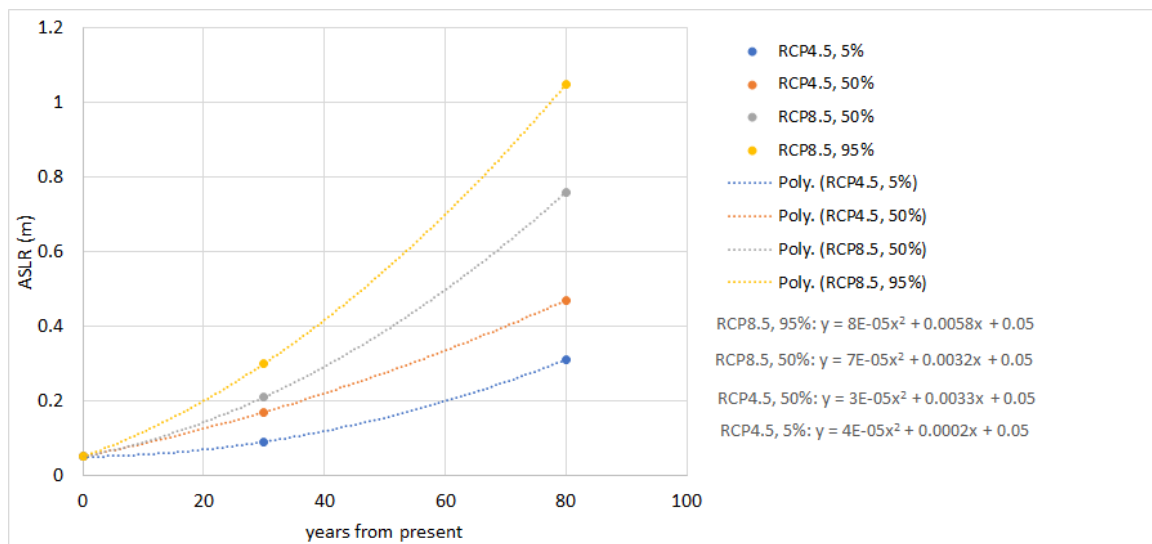


Figure 3.7 Approximated sea level rise curves used as boundary conditions.

Table 3.1 Amplitudes of the M_2 tidal constituent (in meter) for the SLR scenarios at the seaward boundaries of the Delft3D-FM model.

Boundary	SLR scenario				
	0 m	0.31 m	0.47 m	0.76 m	1.05 m
Pussur	0.84	0.86	0.87	0.89	0.90
Baleshawr	0.98	0.99	1.00	1.01	1.01
Bishkali	0.97	0.98	1.00	1.00	1.01
Burishawr	0.98	0.99	1.00	1.01	1.02
Tetulia west	0.89	0.90	0.90	0.90	0.91
Tetulia east	0.86	0.86	0.86	0.86	0.86
Sahbazpur west	0.80	0.82	0.83	0.85	0.87
Sahbazpur east	0.90	0.92	0.93	0.95	0.98
Lower Meghna	1.48	1.53	1.55	1.60	1.65

3.2.3 Subsidence

Subsidence for the GBM delta has been assessed in component D-4B: Subsidence. Based on an extensive analysis of continuous GPS measurements a contoured map of subsidence rates has been established and processed in to spatially variable subsidence rates for model input (Figure 3.7). The subsidence rates are applied as spatially variable values (but constant in time) on to the model domains, which is expressed as a lowering of the bed level height with respect to the reference level (PWD) in the model bathymetry.

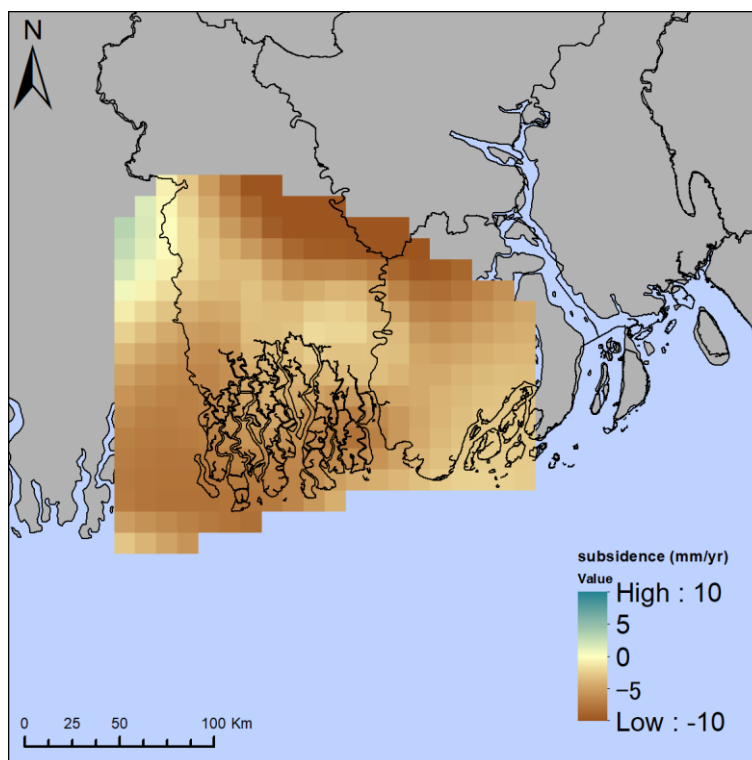


Figure 3.8 Spatially varying subsidence in the lower part of the GBM delta.

3.2.4 Anthropogenic interventions

The Indian National River Linking Project (NRLP) is a large-scale civil engineering project to connect various rivers through canals to expand agricultural production and address water scarcity (Higgins et al., 2018). Numerous dams, reservoirs, and canals are planned that will store and redistribute water to reduce temporal and spatial inconsistencies in supply. The NRLP is expected to have significant effects on the water and sediment supply to the GBM delta through three fundamental processes; (1) increases in reservoir trapping, (2) storage of high flow during the monsoon, and release during the dry season, (3) decrease of the average discharge due to increased water utilization. Higgins et al. (2018) compiled a complete database on proposed interventions within the NRLP and estimated the potential changes the interventions will have on the mean monthly water discharge and sediment load towards the GBM delta (Ganges and Brahmaputra rivers). The Brahmaputra is expected to show a relatively small decrease of 6% in the mean annual river discharge. However, as most of the NRLP interventions are planned in the Ganges basin, the mean annual discharge of this river is estimated to show a large decrease of 24%. The range in the reduction in sediment load associated to the NRLP is estimated by use of the lower and upper bounds of existing sediment rating curves and is estimated to be in the range of -9% to -25% (Brahmaputra) and -39% to -75% (Ganges).

3.3 Scenario simulations

The simulated scenarios consist of a combination of the external drivers described in the previous section (Section 3.2). The forcing conditions are combined in such a way that a full range from low impact to high impact scenarios are set-up. The simulated scenarios are slightly different for the 1D model than they are for the 2D model, because morphological change is not accounted for in the 1D model.

The scenarios for the 1D model are set-up for a current situation (T2020) and for future conditions (T2100), segregating the analysis to the first 10-year period of the simulation and to the last 10-year period of the simulation. The future scenarios are subdivided in low (S1) and high (S2) climate change impact and scenarios that include the effects of anthropogenic activity in the catchments. Furthermore, two separate scenarios are set-up that isolate the extreme of the change in upstream discharge (S4) and the extreme of sea level rise (S5). The simulations for the current situation are used as a reference scenario and the changes simulated in the future scenarios are evaluated as relative change with respect to the reference. The input for the scenarios is listed in Table 3.2.

The scenarios for the 2D coastal model are set-up for the future conditions and include the full transient variation for all forcing conditions (i.e. discharge, SLR, subsidence). The input for the scenarios is listed in Table 3.3 and Table 3.4 shows how comparison of the scenario simulations isolates the effect of the change in forcing conditions.

Table 3.2 Scenario simulations 1D river branch model.

	Scenario	RCP4.5	RCP8.5
Current (reference)	S0 _{T2020}	HYD _{RCP4.5} (2020-2030) Subsidence	
Future (projections)	S1 _{T2100} CC (low)	HYD _{RCP4.5} (2090-2100) SLR _{RCP4.5-5%} 2100 (31cm) Subsidence	HYD _{RCP8.5} (2090-2100) SLR _{RCP8.5-50%} 2100 (76cm) Subsidence
	S2 _{T2100} CC (high)	HYD _{RCP4.5} (2090-2100) SLR _{RCP4.5-50%} 2100 (47cm) Subsidence	HYD _{RCP8.5} (2090-2100) SLR _{RCP8.5-95%} 2100 (105cm) Subsidence
	S3 _{T2100} (anthro.)	HYD _{RCP4.5} (2090-2100), anthropogenic decrease SLR _{RCP4.5-5%} 2100 (31cm) Subsidence	HYD _{RCP8.5} (2090-2100), anthropogenic decrease SLR _{RCP8.5-95%} 2100 (105cm) Subsidence
Extremes isolated	S4 (HYD)	X	HYD _{RCP8.5}
	S5 (SLR)	X	HYD _{RCP8.5} SLR _{RCP8.5-95%} 2100 (105cm)

Table 3.3 Simulations 2D coastal model. Note that the runs are ordered according to variations in the forcing, rather than run number.

Run	SLR	Discharge	SSC	Subsidence	Purpose
r043	0.0	HYD _{RCP4.5}	present value	yes	no SLR
r047	0.5	HYD _{RCP4.5}	present value	yes	moderate SLR
r042	1.0	HYD _{RCP4.5}	present value	yes	high-end SLR (standard scenario)
r044	0.5	HYD _{RCP4.5} , anthro. decrease	present value	yes	decreased discharge due to damming
r045	1.0	HYD _{RCP8.5}	present value	yes	high-end CC for SLR and Q
r046	0.5	HYD _{RCP4.5} , anthro. decrease	present value	no	Influence subsidence, decreased discharge due to damming
r050	0.5	HYD _{RCP4.5} , anthro. decrease	50% present value	yes	Influence reduction sediment delivery, decreased discharge due to damming

Table 3.4 Runs used to assess process effects 2D model simulations.

Scenario	Run difference
Effect SSC reduction	r048-r044
Effect subsidence	r044-r046
Effect RCP8.5 vs RCP4.5 on Q	r045-r042
Effect damming on Q	r044-r047
Effect 1m SLR	r042-r043

3.4 Analysis of the results

The objective of this component in the project is to understand the large-scale (i.e. delta scale) annual sediment dynamics and long-term morphodynamics of the GBM delta, and to study the responses to changes in external forcing conditions driven by climate change and anthropogenic activity. To reach this objective the scenario simulations are analysed and presented for the present-day situation (Chapter 4) and for future projections (Chapter 5). The analysis is focussed on:

- Hydrodynamics
 - Tidal propagation patterns
 - The distribution of the mean annual discharge and tidal prism over the tributaries
- Sediment dynamics
 - The distribution of the mean annual sediment transport over the tributaries of the delta
 - Sediment concentration patterns
 - Bed composition patterns
- Morphodynamics
 - Tidal prism – Area relationship (qualitative)
 - Bed evolution
 - Sedimentation and erosion and differences between scenarios
 - Volumetric balances and scenario effects. From these balances the average bed level evolution is computed for each of the polygon areas defined in Figure 3.10, and these mean bed level changes are compared and their differences shown.
 - Land gain and loss. For the first time in such studies, the long-term evolution in the delta has been analysed in terms of land-to-water and water-to-land changes, their distribution and cumulative changes. The Deltares Aqua Monitor, presenting such changes based on satellite imagery, has been mimicked and overall land gain, loss and net change has been tracked through each 10-year period, from 2020 to 2100.

The scenario results simulated with the 1D model are presented as (relative) change along the longitudinal axis of the estuaries and river systems. Figure 3.9 gives an overview of the river kilometres defined along the different systems, for referencing of the longitudinal distance in the scenario plots. The origin of the river kilometres lies at the seaward boundary, except for the Upper Meghna where the origin lies as the confluences of Padma and Upper Meghna in to the Lower Meghna (see Figure 2.1 for the names of the river systems).

The scenario results simulated with the 2D model are presented as (relative change of) spatially averaged quantities within defined polygons. Figure 3.10 gives an overview of the polygons and shows the names assigned to the polygons. The names are used in the model results.

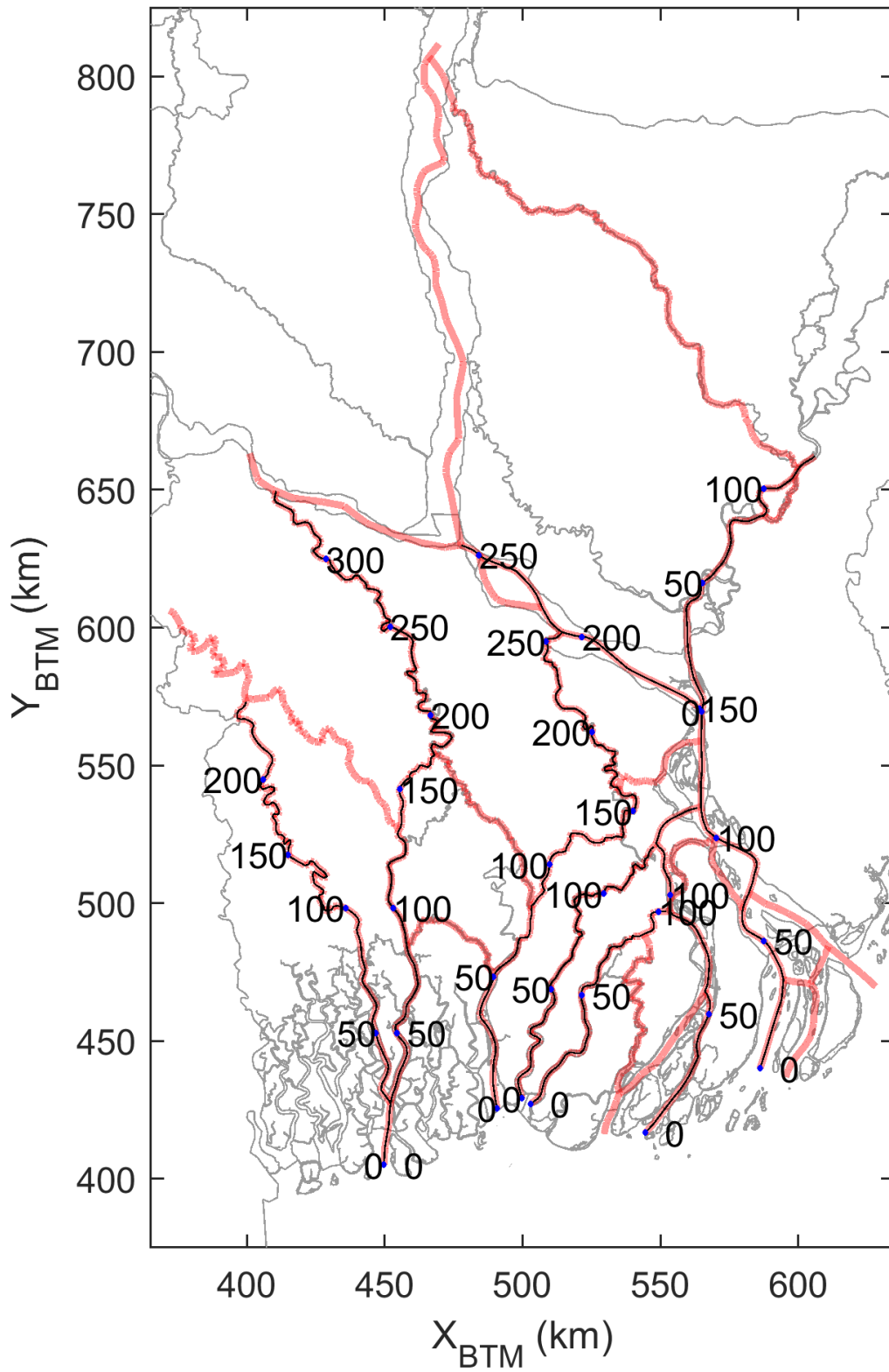
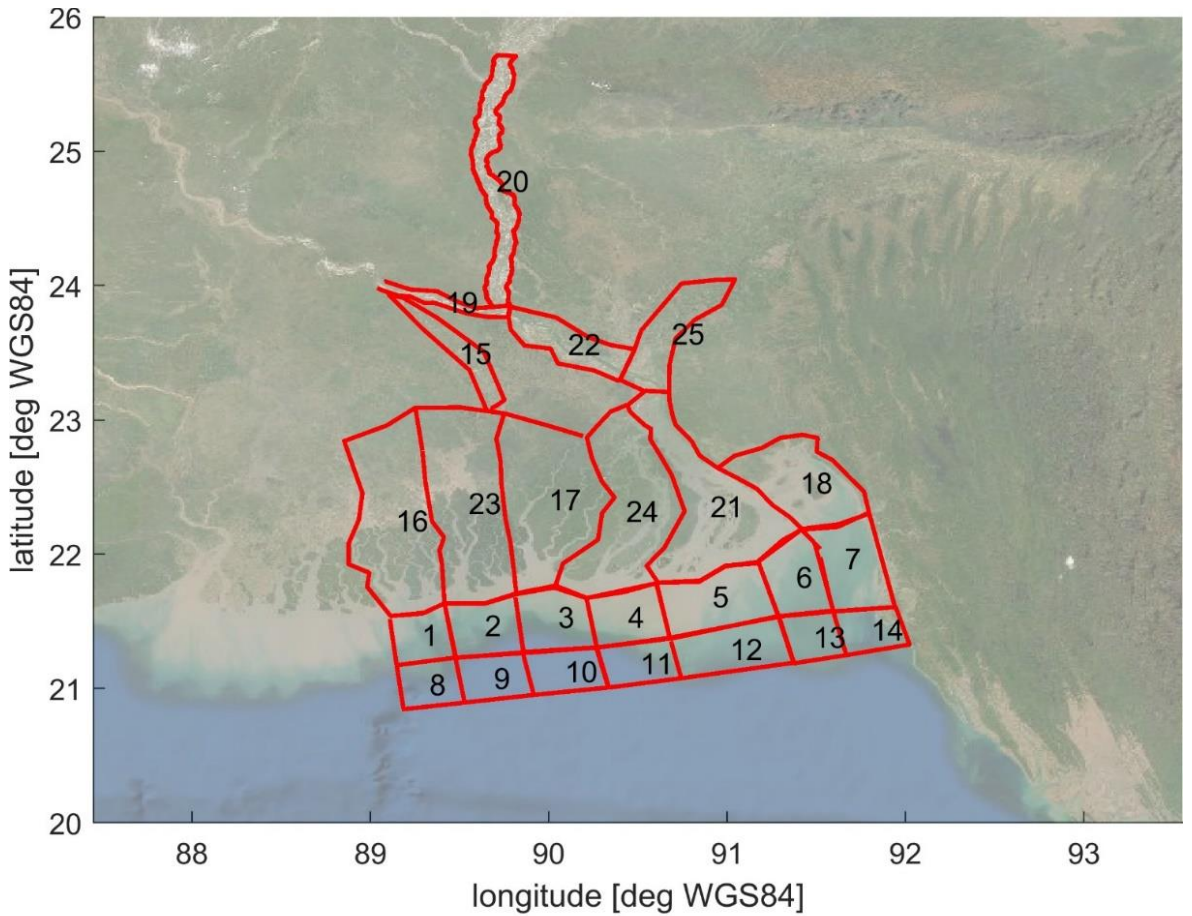


Figure 3.9 River kilometres used for the presentation of the 1D model results, see Figure 2.1 for the names of the rivers.



1. c1	10. o3	19. Ganges
2. c2	11. o4	20. Jamuna
3. c3	12. o5	21. Lower Meghna
4. c4	13. o6	22. Padma
5. c5	14. o7	23. Pussur-Sibsa
6. c6	15. Gorai	24. Tetulia
7. c7	16. Arpangasia	25. Upper Meghna
8. o1	17. Baleswar-Bishkali	
9. o2	18. Eastern Chars	

Figure 3.10 Polygons used for the presentation of the 2D model results.

4 Model results on present-day situation

4.1 Hydrodynamics (1D)

4.1.1 Tidal propagation

Figure 4.1 shows the amplitude of the M_2 tidal constituent simulated in the reference scenario with the 1D model. The figure shows that the tidal amplitude increases from west to east at the mouths of the estuaries. Along the longitudinal distance of the estuaries the tidal propagation shows a different behaviour for each system. At the Pussur system, the M_2 tidal amplitude increases – more or less – up till Mongla (~ 75 km) and subsequently it dampens out towards the point where the Pussur estuary transits into the Gorai river (~175-200 km). In the Sibsa estuary the increase is larger but there is a very abrupt transition to a decrease. The other estuaries, located eastward of the Pussur-Sibsa system, do not show this distinct increase of the M_2 tidal amplitude but show a gradual decrease along the estuary axis in the upstream direction. The M_2 tidal amplitude of the Baleshawr gradually decreases towards the Arial Khan river and dampens out at ~200 km. In the Lower Meghna, where the largest M_2 tidal amplitude is found at the mouth of the estuary, the amplitude increases slightly and subsequently decreases gradually upstream. In the Padma river the tide dampens out near the bifurcation with the Arial Khan (~200 km). In to the Upper Meghna the tide does not dampen out within the model domain but propagates up till the upstream boundary of the model.

4.1.2 Gross and net discharge volumes

Figure 4.2 shows the mean and peak annual discharges simulated with the 1D model for the present-day situation. The figures show that the mean annual discharge for all tributaries is similar to the model results used for validation of the model (Appendix C). The peak annual discharge values are, however, slightly larger than shown in Appendix C, which is to be expected as a variable (and more realistic) forcing is used for the scenario simulations. The largest part of the discharge received by the three upstream rivers (Jamuna, Ganges, Upper Meghna) is conveyed by the Padma river and subsequently the Lower Meghna. The Gorai (10% of the Ganges) and Arial Khan (5% of the Padma) rivers convey a relatively small part of the mean annual discharge, which supplies the south-western and central part of the delta.

The tidal volumes simulated with the 1D model for the tidally dominated part of the delta are shown on maps in Figure 4.3 and along the longitudinal axis of the estuaries in Figure 4.4. The figures show the mean flood and ebb volumes instead of the annual mean and peak discharges because it provides a more representative metric for the distribution of discharge in the flow-reversing (i.e., tidally dominated) branches of the delta. The difference between the ebb tidal volume and the flood tidal volume is the tidally-averaged net river discharge, which is directed seawards. The figure indicates that roughly 60% of the flood tidal prism of the shared Pussur-Sibsa system is conveyed by the Sibsa river, which shows equal flood and ebb tidal volumes as there is no river discharge feeding the Sibsa channel (the channels connecting the Pussur and Sibsa are not included in the 1D model). The flood tidal prism of the Pussur estuary decreases from $252 \cdot 10^6 \text{ m}^3$ till $66 \cdot 10^6 \text{ m}^3$ and the tidally averaged net river discharge provided by the Gorai river is approximately $40 \cdot 10^6 \text{ m}^3$ per tidal cycle. The tidally averaged net river discharge in the Baleshawr is approximately $130 \cdot 10^3 \text{ m}^3$ per tidal cycle, which is delivered by the Arial Khan that bifurcates from the Padma and connected with the Lower Meghna. The flood tidal prism conveyed by the estuaries Baleshawr, Bishkali, and Burishawr is an order of magnitude smaller than the flood tidal prism conveyed by the Pussur-Sibsa estuary. The Sahbazpur channels combined convey an approximately equal flood tidal prism as the most eastern outlet of the Lower Meghna river, and the tidally net averaged river discharge is distributed – more or less – equal as well.

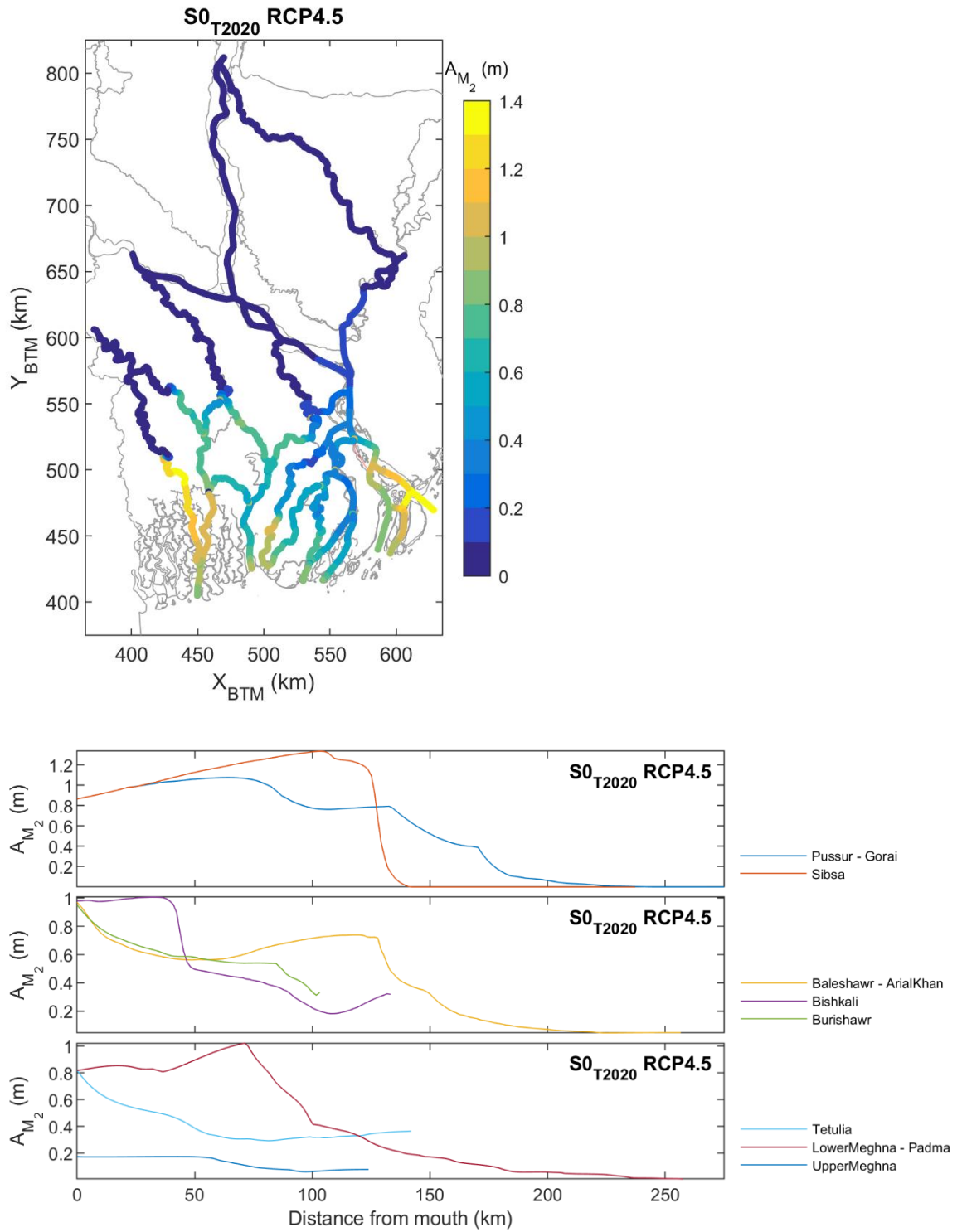


Figure 4.1 Maps (top) and longitudinal distance plots (bottom) of the amplitude of the M₂ tidal constituent, shown for both the reference scenarios simulated with the 1D model.

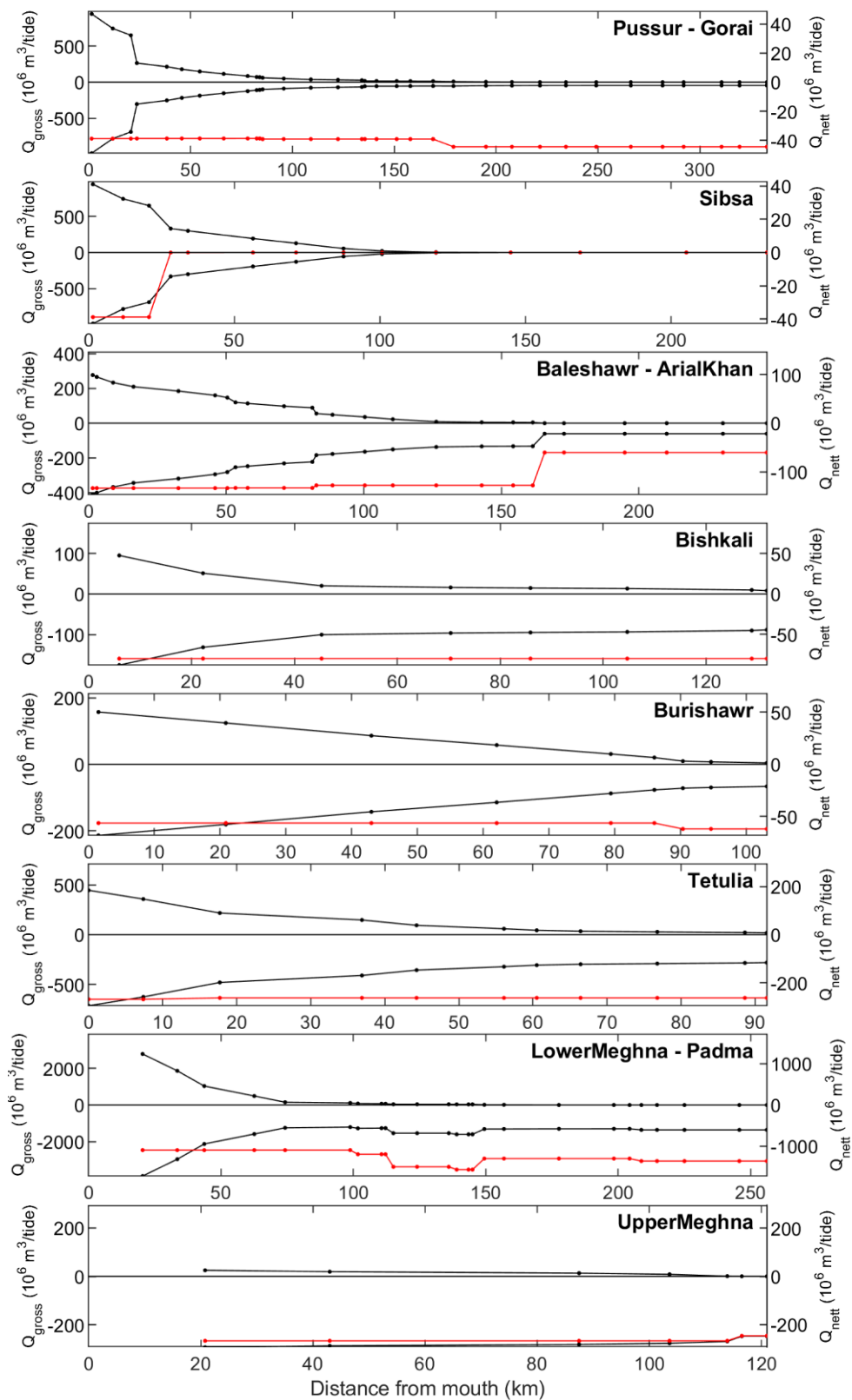


Figure 4.4 Flood (positive) and ebb (negative) tidal volumes (left y-axis) and net discharge (bars, right y-axis) along the length of the estuaries.

4.2 Sediment dynamics

4.2.1 Sediment fluxes

1D modelling results

The net (i.e. residual) suspended sediment transport fluxes simulated with the 1D model are shown as maps in Figure 4.5. Figure 4.6 shows the net transport fluxes along the length of the estuaries. In these plots the estuaries with multiple outlets (e.g., the Lower Meghna) are presented as a summed total to give an integral overview of the estuarine system as a whole.

Figure 4.5 shows that the total suspended sediment load entering the delta through the upstream boundaries of the Jamuna and Ganges is approximately 500 MT/yr for each, as expected because boundary conditions are based on these values. At the confluence of the two rivers into the Padma, however, part of the sediment load is lost and must have been deposited at the bed. Therefore, the 1D model simulates aggradation (sedimentation) for the Ganges and Jamuna rivers. The sediment load bifurcating into the Gorai river is 45 MT/yr and decreases considerably downstream. The large gradient in sediment transport means that in the simulated reference scenario sedimentation in the upstream part of the Gorai river is to be expected. The Arial Khan river receives approximately an equal amount of sediment annually as is exported towards the downstream connected Baleshawr estuary. The Arial Khan river is therefore expected to be in equilibrium.

In the tidally dominated part of the delta the net sediment flux is determined by difference between the gross sediment fluxes of import (i.e., flood directed) and export (i.e., ebb directed), and gradients in the net export give an indication for the morphological adjustment of the bed, which is not simulated with the 1D model. Figure 4.6 shows that the net sediment transport direction of the suspended sediment flux is seawards for all estuaries, except the Sibsa. The export of sediments is mainly due to the net river discharge, which explains the import at the Sibsa.

Along the length of the Pussur estuary a negative sediment transport gradient can be observed at the upstream reaches (~350 km). As described before, the results of the reference scenario indicate sedimentation in this part of the estuary. The sediment balance in the Sibsa estuary is purely determined by the tidal motion. The balance shows an import of sediment (due to tidal asymmetry), as there is no river discharge feeding the estuary from upstream. The strong gradient positive gradient at the downstream reach of the estuary indicates that erosion can be expected.

At the Baleshawr – Arial Khan a positive gradient can be found at around ~160 km, which is at the confluence where the Arial Khan and the branch connected to the Lower Meghna flow into the Baleshawr. Figure 4.5, however, shows that both these branches combined provide an approximately equal amount of sediment as is transported through the lower reaches of the Baleshawr. Therefore, the system seems to be in equilibrium in the reference scenario and no large adjustments of the morphology are expected. This is the case for the Bishkali and Upper Meghna as well.

At the upstream side of the Burishawr a negative gradient in the net sediment transport flux can be found, indicating that the upstream reaches of the estuary will show an erosive trend.

The Lower Meghna shows, interestingly, a negative and positive trend in its lower reaches between ~100 and ~150 km. The net sediment transport gradients are probably driven by the decrease of the net river discharge between at ~120 km (see Figure 4.4), which is where the Lower Meghna bifurcates into the Tetulia. Apparently, the net discharge of water bifurcates towards the Tetulia but the sediment load follows a preferable path towards the mouth of the Lower Meghna.

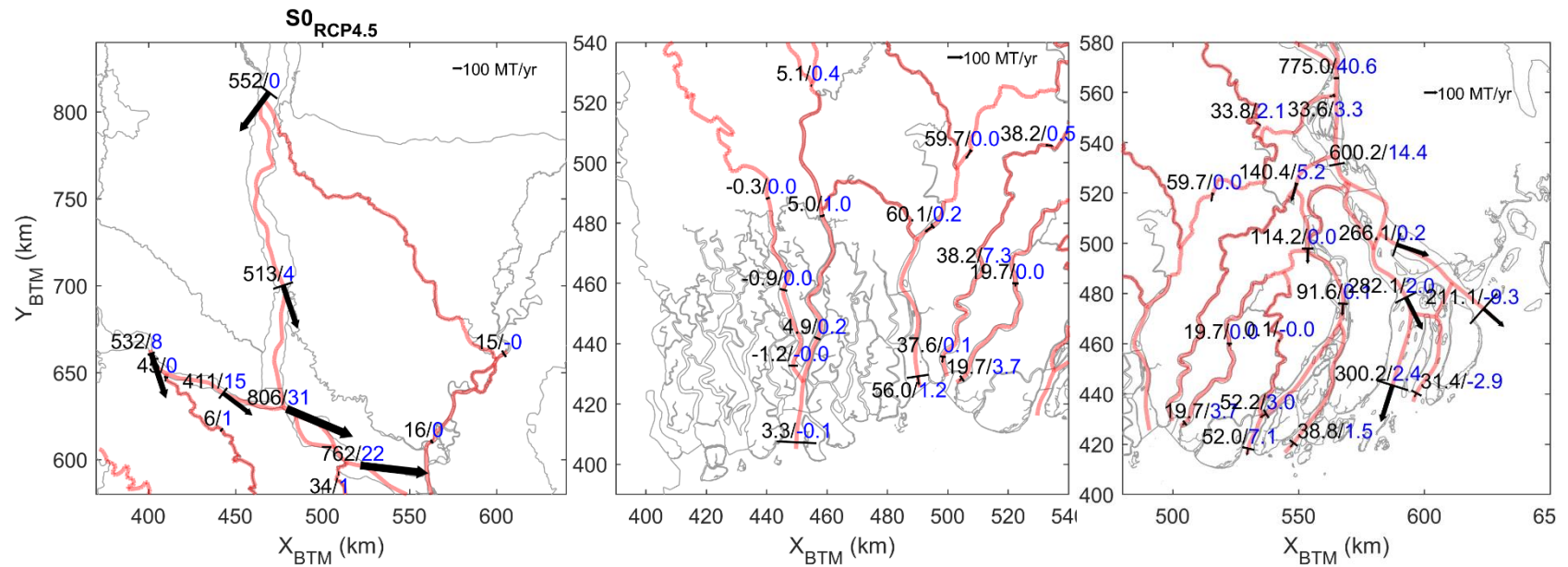


Figure 4.5 Net annual suspended sediment load for cohesive (black) and non-cohesive (blue) material, in MT/yr. Positive numbers indicate a net transport in the seaward (i.e., ebb) direction, and negative numbers a net transport in the landward (i.e., flood) direction. For readability purposes, some transport vectors are not displayed.

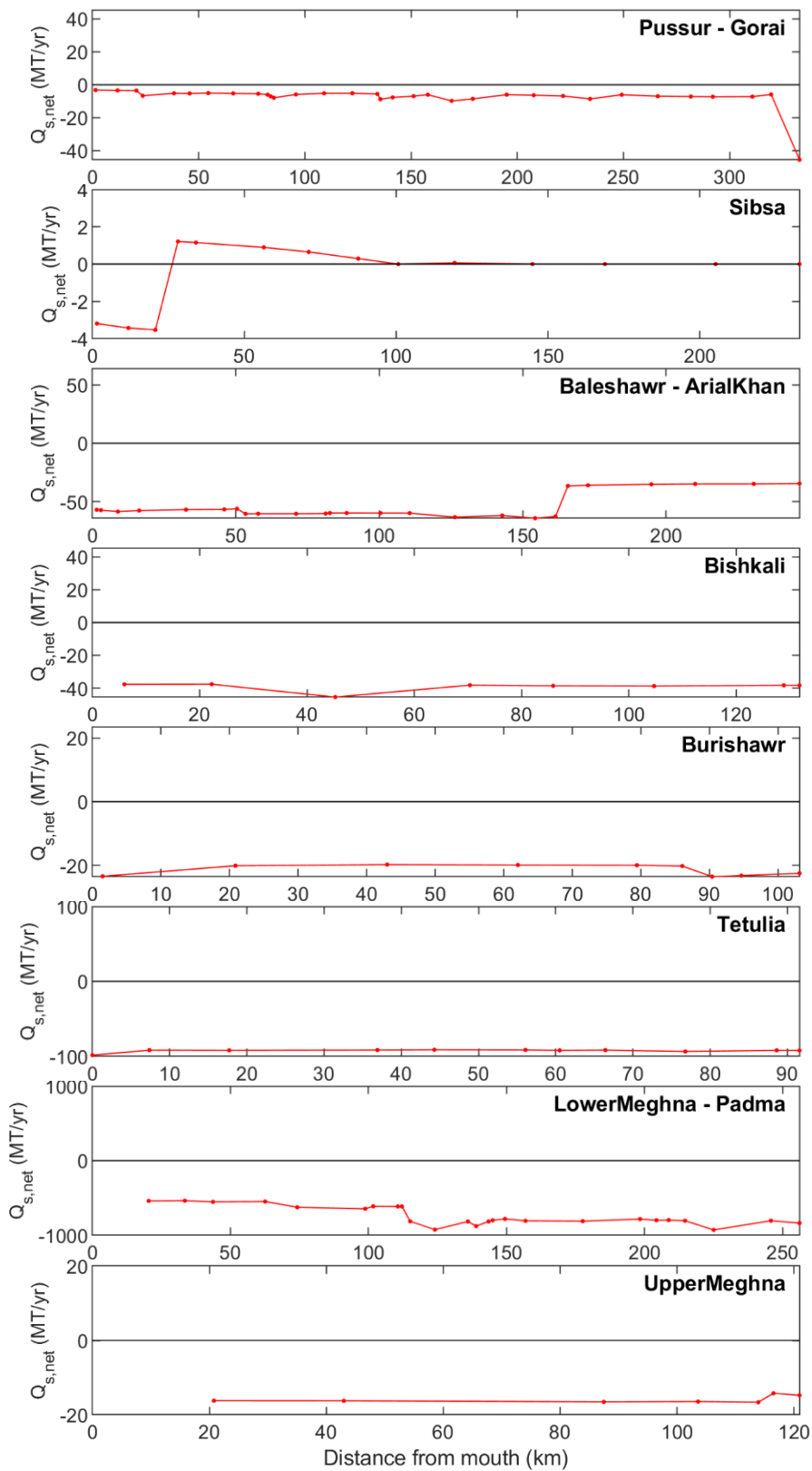


Figure 4.6 Net annual total (sand and mud) suspended sediment sediment flux (bars) along the length of the estuaries, with positive (negative) numbers for the flood (ebb) direction. The fluxes for estuaries with multiple outlet systems are summed to total quantities.

2D modelling results

The mud and sand transport under present conditions as simulated with the 2D model are shown in Figure 4.7 and Figure 4.8. The figures show significant spatial gradients in mud and sand transports. Sand transports are typically an order of magnitude smaller than mud transports. Combined sand and mud transport magnitudes amount to almost 900 Mt/year, which is similar to estimated values based on observations. The Ganges mud supply seems too low, since it should be similar to the supply by the Jamuna. This is probably due to the sediment concentration at the boundary that was set too low. Cumulative sediment transport through the Gorai is about 20 Mt/year. This is similar to estimated transports of 30 Mt/year (Table 2.1). Modelled transports through the Arial Khan are very limited compared to estimated values of 25 Mt/year. Probably the bathymetry needs improvement in this region.

Largest mud transports are found in the Padma and upper Meghna, whereas, with decreasing cumulative transports further downstream, mud deposits in the lower Meghna and on the shelf topset. Largest sand transports are found in the lower Meghna and on the eastern shelf topset, probably due to enhanced shear stresses by combined tidal action and river streamflow.

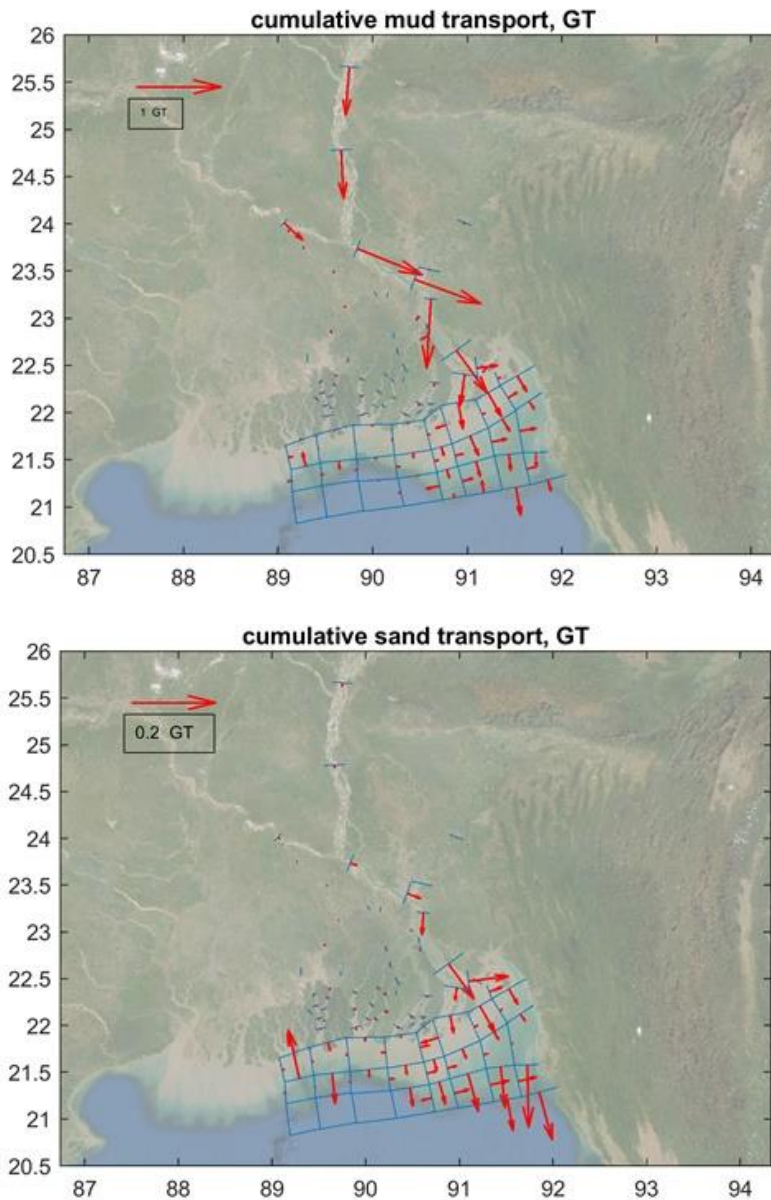


Figure 4.7 Yearly cumulative mud transports (left pane) and sand transports (right pane), mind the different vector scales

Sensitivity runs show that wave action mostly impacts the magnitude of the sand transport, which is an order of magnitude smaller than the transport of mud. Mud transport is far less affected, although transport magnitudes generally increase slightly towards the ocean due to wave action, except in the Meghna mouth, where they decrease slightly. Although most of the mud is transported towards the south, a small portion of mud transports is transported along the shore. The smaller estuaries westward of the Meghna show a yearly net export of mud towards the ocean. Given the relatively small importance of sand transport, and the extra computational effort needed to model wave fields, we do not include waves in the future scenario runs.

It is generally assumed that fine sediments discharging into the ocean from the Meghna estuary are transported alongshore in westward direction and that a large part of these fine sediments will eventually be transported landward into the Sundarbans estuaries, where they potentially play a role in the siltation of channels. However, actual alongshore transports and associated sediment transport pathways have never been measured and Figure 4.8 shows that the current model settings do not lead to significant alongshore sediment transport rates. An extended sensitivity analysis on sediment properties could reveal potential other transport directions. Additionally, 3D processes due to interaction of the freshwater plume and (saline) ocean water could impact the alongshore sediment dynamics as well.

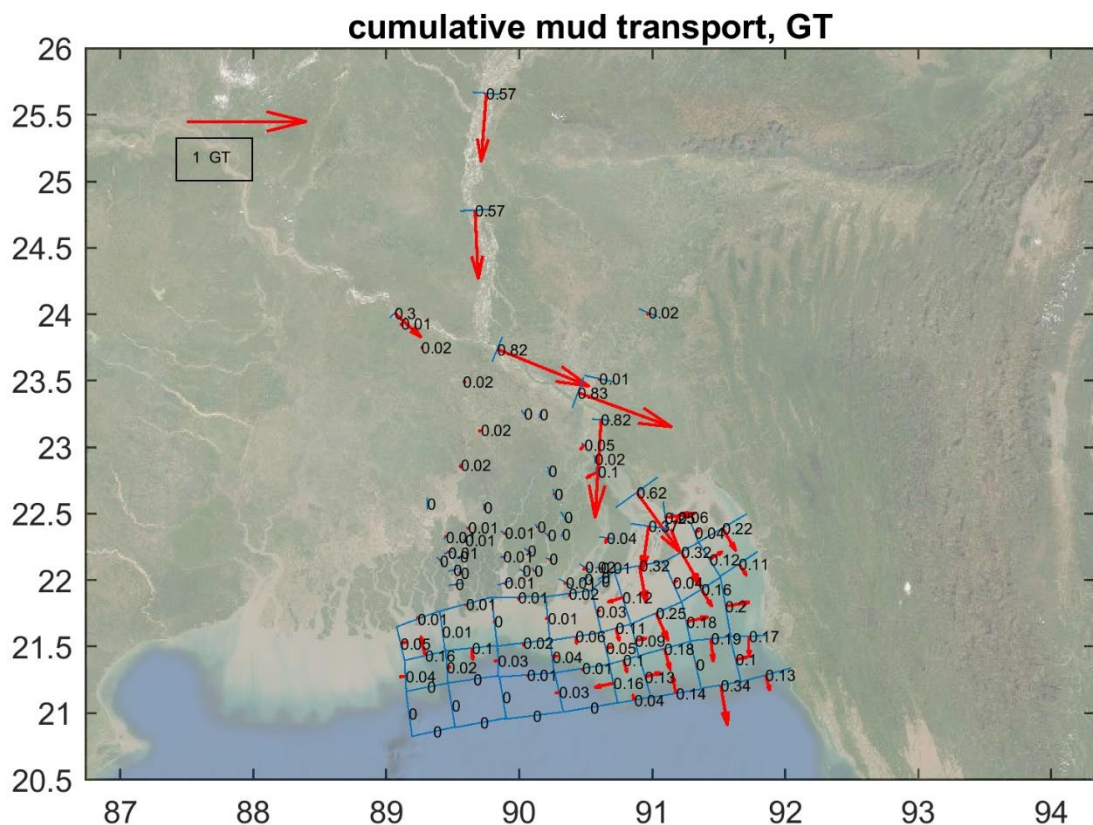


Figure 4.8 Yearly cumulative mud transports in gigatons with amounts per cross-section

4.2.2 Distribution of surface sediment (2D)

Figure 4.9 shows the presence of mud as percentage of the upper bed layer volume. In the major rivers and estuaries, the mud is distributed towards the shoals, whereas mud is washed out in the deeper channels that mainly consist of sand. Some mud deposits in the deeper coastal areas directly south of the Meghna mouth, while major mud deposition occurs in the area where the continental shelf rapidly deepens.

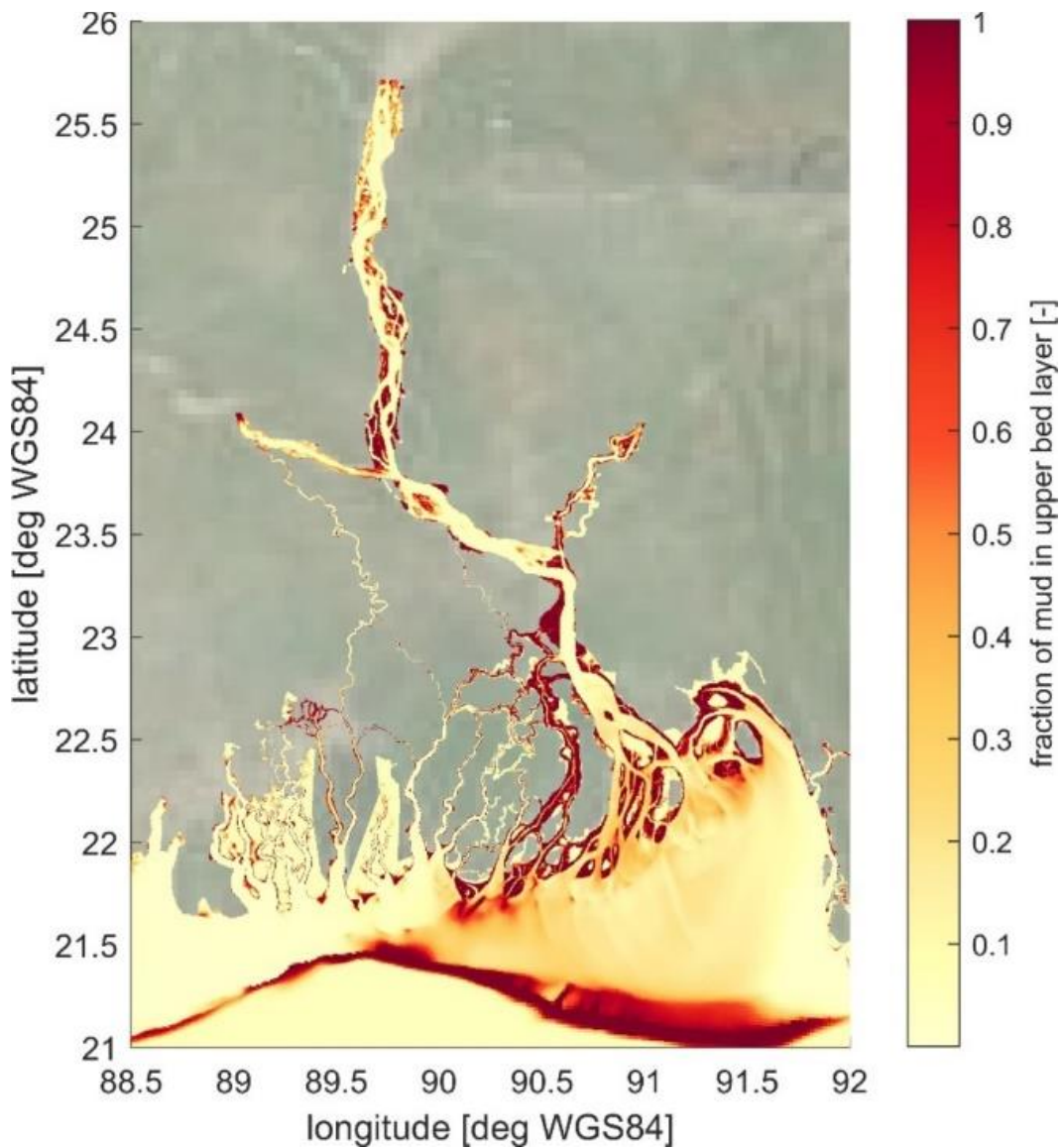


Figure 4.9 Mud volume percentage in upper bed layer after 15 years. The remaining percentage consists of sand.

4.3 Morphodynamics

4.3.1 Tidal prism and cross-sectional area (1D)

The 1D model does not calculate morphological changes that result from gradients in the simulated sediment transport. A first order assessment on the expected morphodynamic changes in the delta (besides the sediment transport balances described in the previous section), however, can be derived from the tidal prism (P) – area (A) relationship (O'Brien, 1931). The empirically derived relationship describes a dependency of the cross-sectional area to the characteristic tidal volume:

$$A = CP^n \quad (\text{Equation 1})$$

Here, A is the cross-sectional area of an inlet, P the characteristic tidal prism, and C and n are empirically determined coefficients. Although the concept of the P/A relationship was established by studying the stability of tidal inlets, the relationship is found to be valid along the length of tidal channels

(e.g., D'Alpaos et al., 2010). This suggests that the P/A relationship is valid for a range of spatial scales and a range of tidal conditions (Roelvink and Reniers, 2011). Therefore, the relationship can give a qualitative indication on the direction of morphological development (i.e., erosion or sedimentation) for the estuarine systems under the different scenarios simulated with the 1D model. Figure 4.10 shows scatter plots of the time-averaged cross-sectional area (A) versus the mean annual ebb tidal volume (P) (as representative discharge), for the estuarine systems modelled with the 1D model. The slope, intercept and the coefficient of determination (r^2) of the linear trendlines in Figure 4.10 are given in Table 4.1. The purpose of the figures and the table is not to establish equilibrium relationships in the form of Equation 1, but to show if the time-averaged mean of the cross-sectional area is correlated to the simulated ebb tidal volumes. If they are strongly correlated, the river is considered in equilibrium. The figures show that in the estuarine systems on the western part of the delta, that consist of relatively simple single channel estuaries with a small number of confluences and bifurcations, the cross-sectional area is well correlated to the tidal prism. Towards the east the delta branches increase in complexity, especially where the Lower Meghna bifurcates towards the Bishkali, Burishawr, and Tetulia (called Ilisha in Figure 2.1). The large number of confluences and bifurcations is difficult to capture well in a 1D model which is reflected by the less clear correlation in Figure 4.10. In the Upper Meghna the simulated cross-sectional area and tidal prism are, surprisingly, not correlated. This is probably because that there is still a large sediment demand in this area as the Upper Meghna historically conveyed a much larger discharge.

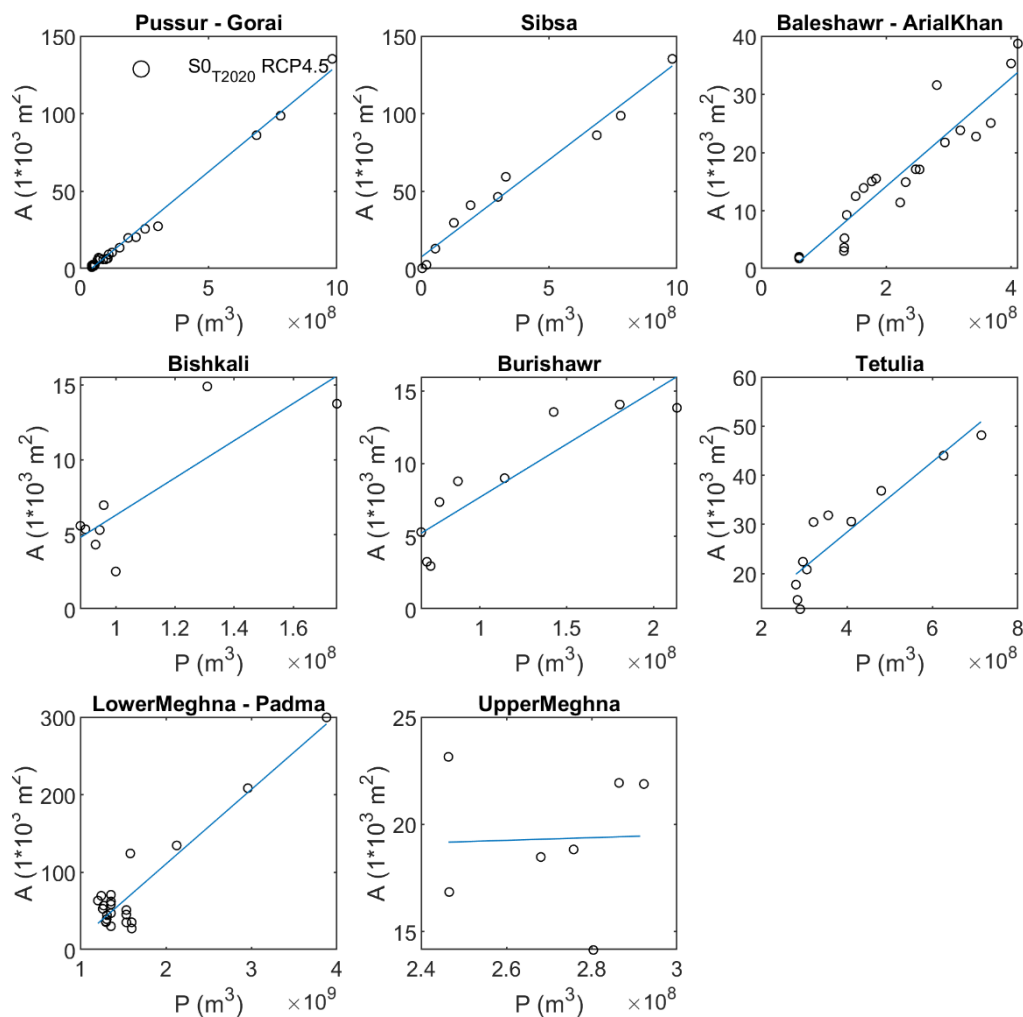


Figure 4.10 Scatterplot and linear fit of the cross-sectional area (A) versus the ebb tidal prism (P), for the estuarine systems of the Bengal delta modelled with the Delft3D-FM 1D model.

Table 4.1 Slope and intercept of the linear fit of cross-sectional area (A) versus ebb tidal volume (P)

Scenario	Slope (m ² /m ³)	Intercept (m ²)	r ²
	RCP4.5	RCP4.5	RCP4.5
Pussur - Gorai	1.50e-04	-5.74e+03	0.99
Sibsa	1.43e-04	4.50e+03	0.97
Baleshawr – Arial Khan	9.90e-05	-4.85e+03	0.89
Bishkali	3.02e-05	3.52e+03	0.68
Burishawr	7.93e-05	-3.52e+01	0.81
Tetulia west	8.26e-05	-4.29e+03	0.71
Tetulia east	5.55e-05	4.07e+03	0.49
Lower Meghna - Padma	1.20e-04	-1.15e+05	0.80
Upper Meghna	2.45e-05	1.24e+04	0.01

4.3.2 Volumetric balance (2D)

Sand and mud transport divergence will accrete and erode the bathymetry. The previous section made a sediment budget based on the cumulative transports through cross-sections in terms of sediment mass. Figure 4.11 shows the sediment budget based on the volumetric changes of predefined areas of the bathymetry. These include the different porosity values of mud and sand once deposited in the bed.

All upper reaches of the major rivers (except the Gorai River) and the area of the Tetulia and the eastern coastal area gain sediment. The Baleswar-Bishkali, the Pussur, the Sibsa and the Arpangasia areas also gain sediment volume. The western coastal area gains sediment while the eastern area loses sediment. Most of the ocean areas gain sediments.

Figure 4.12 and Figure 4.13 show that morphodynamic development is gradual with small fluctuations depending on the river flow variations, and to a much lesser extent on the varying wind and wave forcing. Many river and estuary areas (Figure 4.12) show decreasing morphodynamic activity, suggesting the development towards a (dynamic) equilibrium. This behaviour is less pronounced in coastal and ocean areas (Figure 4.13), with cumulative volume trends that are constant over time suggesting the gradual progradation of the (submerged) delta front and deposition around the eastern chars, whereas other areas with negative cumulative volumes reflect an eroding trend.

Adding the volumetric changes of Figure 4.12 leads to a net sediment deposition of about 25 Gm³ over 20 years. Considering an assumed dry bed density (averaged over sand and mud volumes) of 800 kg/m³ this corresponds to ~19 Gt over 20 years and ~0.95 Gt per year. This is similar to the ~1Gt derived in the previous section based on cross-sectional cumulative sediment transports. This implies that almost all sediments supplied towards the GBM delta deposit in the domain defined in Figure 3.10.

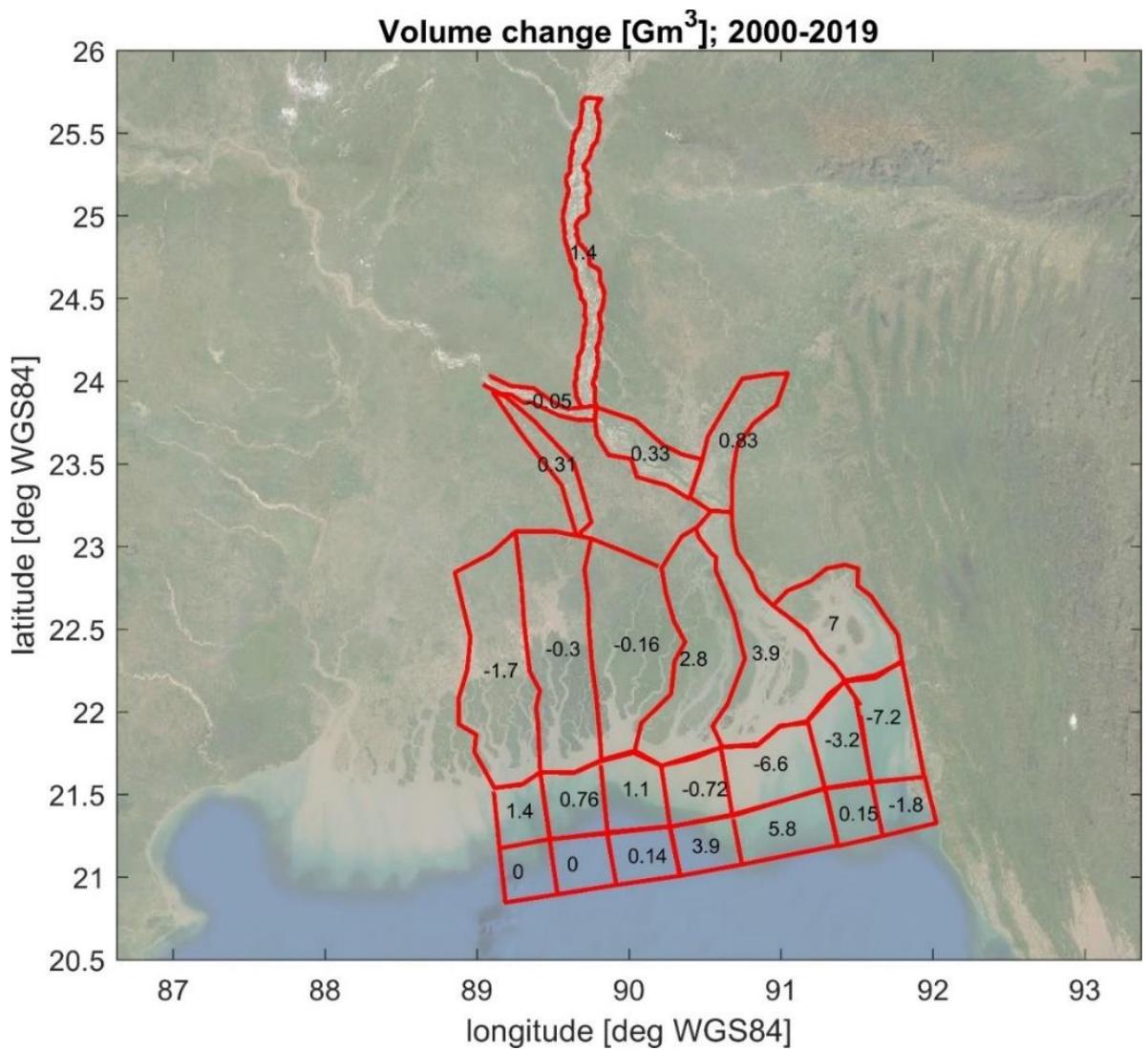


Figure 4.11 Sediment volume balance over 20 years (2000-2019) computed with the 2D model (positive numbers indicate sedimentation; negative numbers erosion).

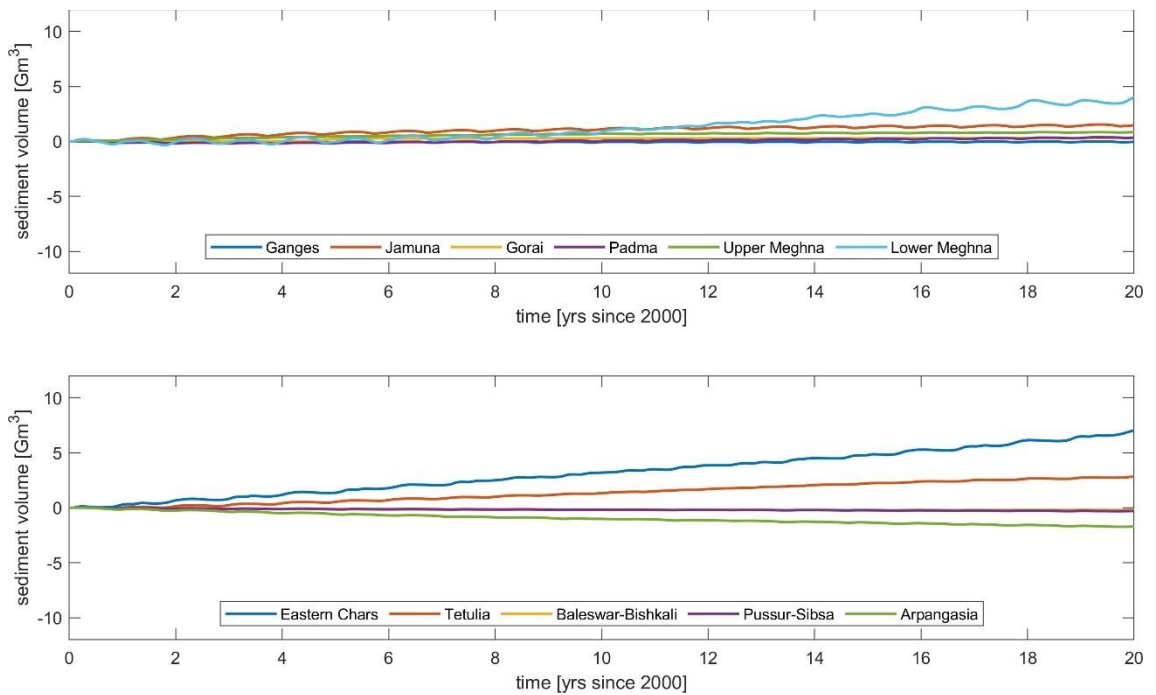


Figure 4.12 Cumulative sediment volume change over time for different areas over the period 2000-2019.

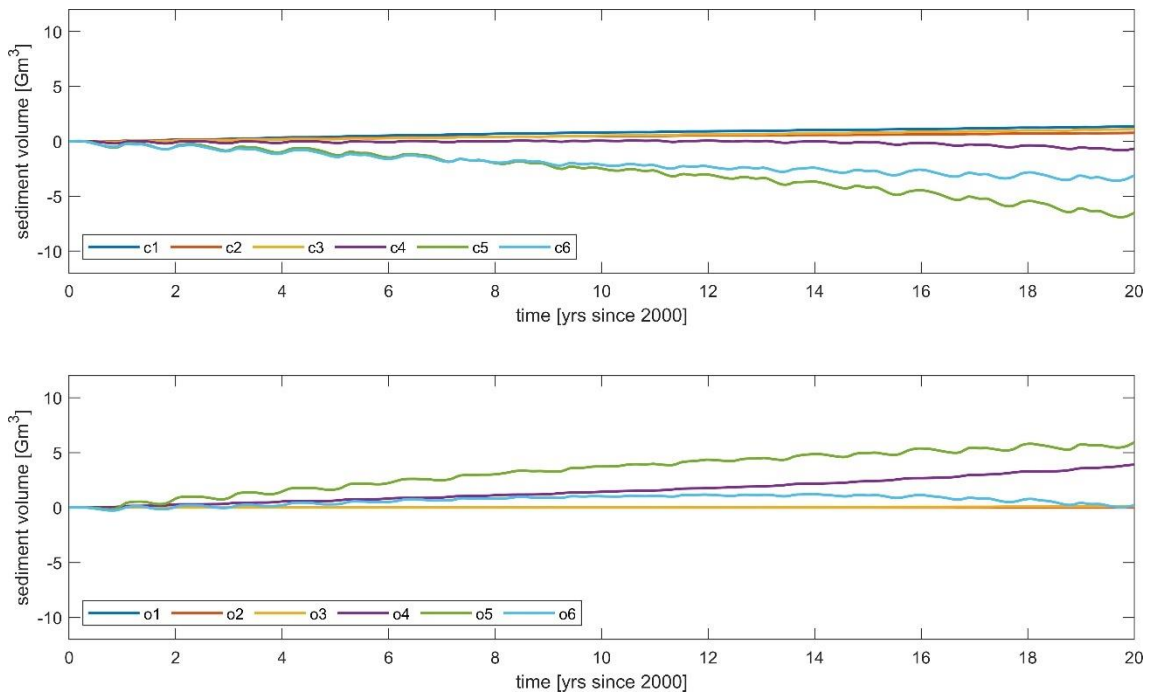


Figure 4.13 Cumulative sediment volume change over 2000-2019 for different areas, where 'c' refers to the coastal areas and 'o' refers to the most ocean directed areas. For the exact polygon locations, see Figure 3.10.

4.3.3 Detailed sedimentation/erosion maps (2D)

In this section a closer look is taken to the sedimentation-erosion patterns in the lower Meghna in comparison with the difference bathymetry maps from the EDP study (IWM, 2010), and to sedimentation/erosion patterns and bathymetry evolution in comparison with satellite-derived surface changes as provided by the Deltares Aqua Monitor.

Comparison 2000-2009 Meghna estuary

The sedimentation-erosion maps are shown in Figure 4.14 for the simulation Figure 4.15 for the observed bed level change. Clearly, there is a good qualitative agreement in the general accretion trend and details such as the encroaching channels northeast of Hatiya island and middle-east of Bhola. The channels appear to be somewhat narrower in the simulation than in the observations, but not excessively so. The mild erosion east of Sandwip island is reproduced.

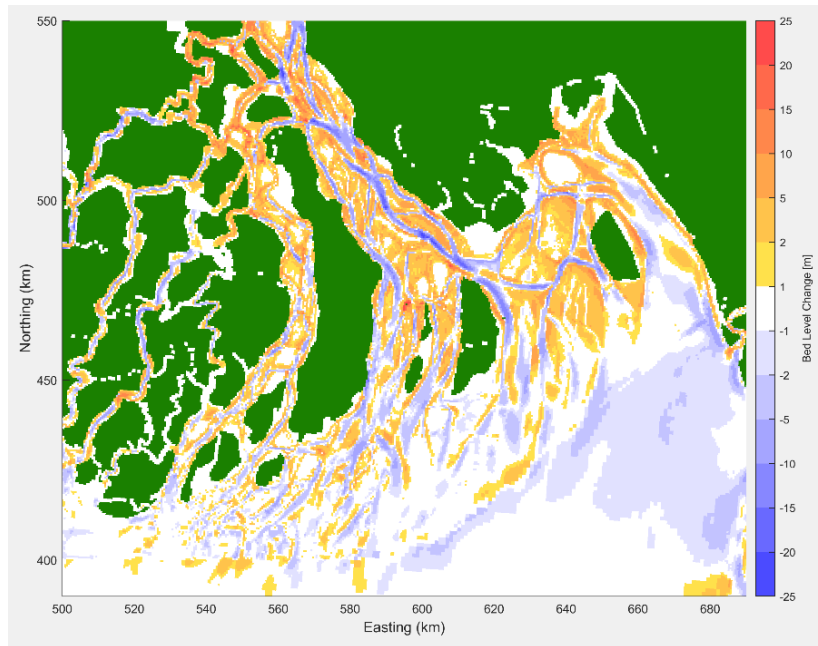


Figure 4.14 Simulated sedimentation-erosion pattern, Meghna estuary, 2000-2009.

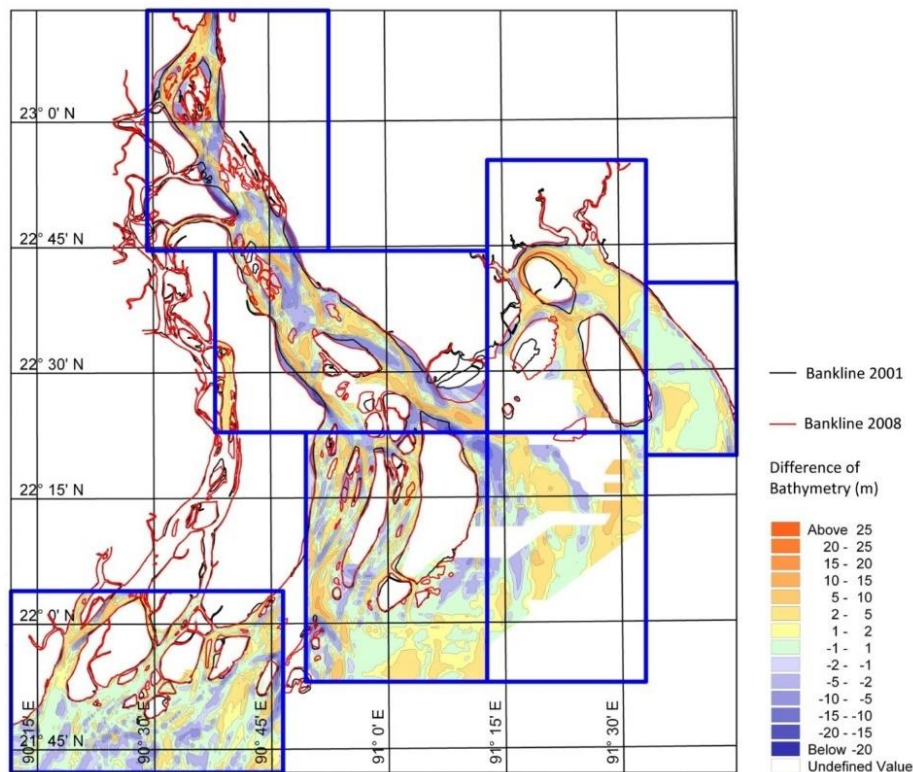


Figure 4.15 Observed sedimentation-erosion pattern, Meghna estuary, 2000-2009.

Evolution of coastal areas 2000-2019

The simulated evolution over the period 2000-2019 is visualized in the sedimentation-erosion patterns in Figure 4.16 and in the initial and final bathymetric map in Figure 4.18. For evaluating whether these simulations agree with observations of changes in land and water area can be compared to the simulated evolution with the land/water surface area changes derived from satellite imagery and presented in the Aqua Monitor of Deltares, see Figure 4.17.

While there may be important quantitative differences, a rather striking qualitative agreement in the development can be seen; this may be illustrated by describing the evolution in 6 areas denoted A through F in Figure 4.16 and Figure 4.17: In A, in the Padma, the main channel is expanding while the rest of the river bed is strongly accreting; the pattern in simulation and satellite observations is similar. Similarly, around point B in the lower Meghna, the main channel is eroded close to the bank and adjacent areas show strong accretion, which coincides with bank erosion shown in the satellite imagery. Point C is on the north side of Hatiya and shows an encroaching channel, where the imagery shows strong bank erosion. Point D, between Hatiya and Sandwip islands, is in an area of strong accretion in the model and land creation in the satellite images. Point E on the island of Bhola again shows an encroaching channel where the Aqua Monitor shows strong bank erosion. Finally, F indicates the southern tips of the Sundarbans where there is a persistent coastline retreat according to the imagery, while the simulations show a generally erosive trend in this area.

It can be concluded that the model generally reproduces the trends in the satellite imagery, though in its present form it cannot directly predict bank erosion, given the relatively coarse grid. The model does seem to be capable of accreting areas up to the high-water level, generally in areas where the satellite imagery shows water turned into land.

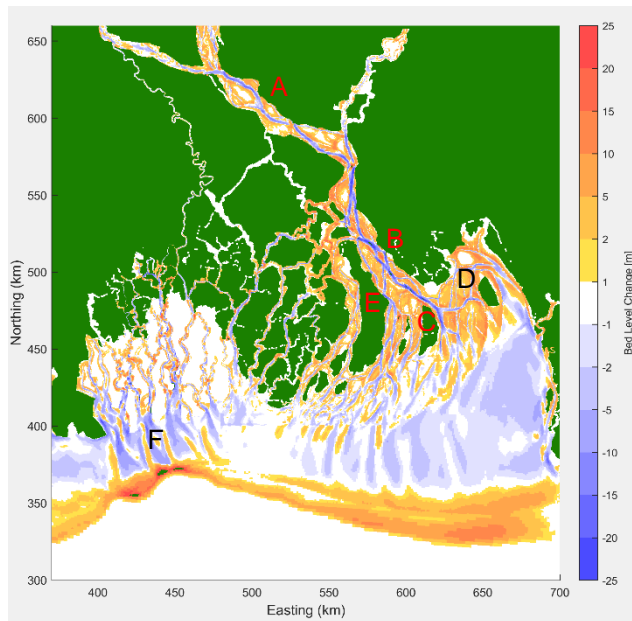


Figure 4.16 Simulated bed level changes, 2000-2019.

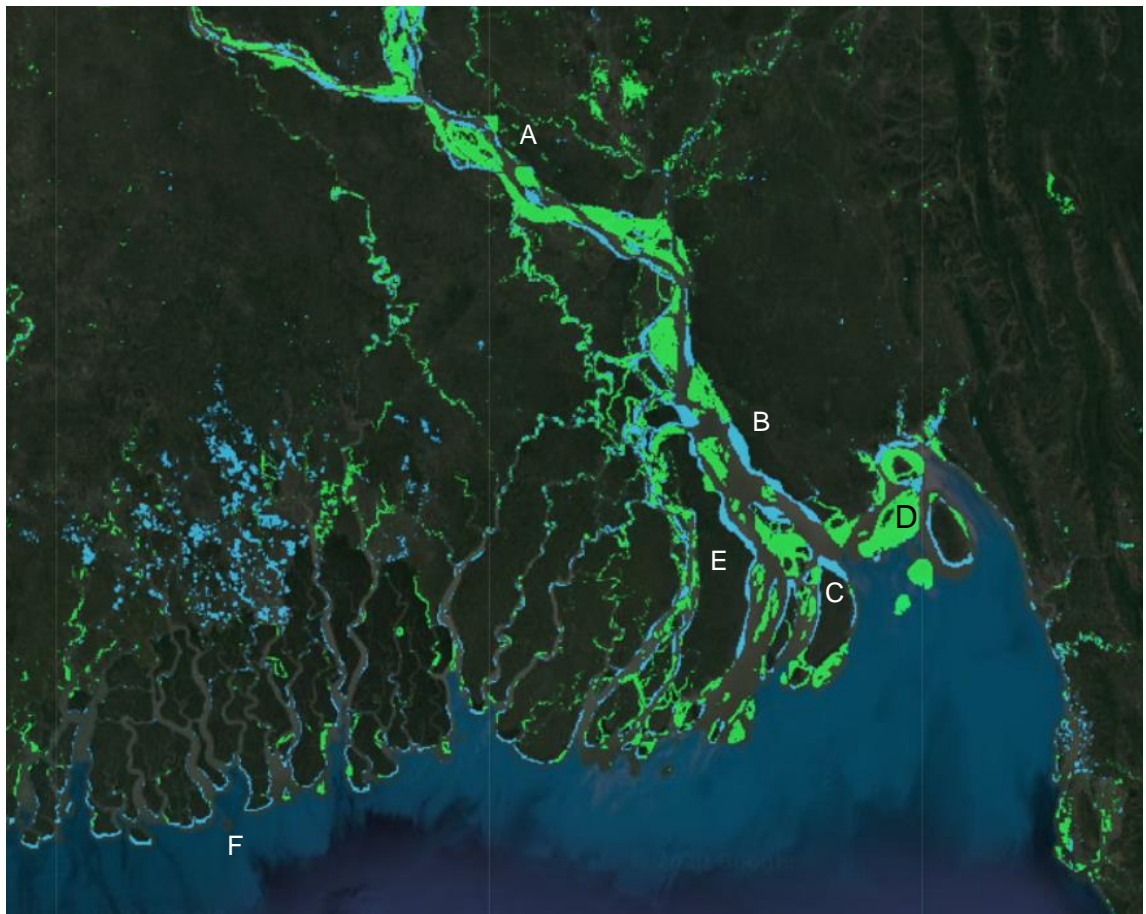


Figure 4.17 Observed land to water (blue) and water to land (green) changes, 2000-2019 (Source: Aqua Monitor).

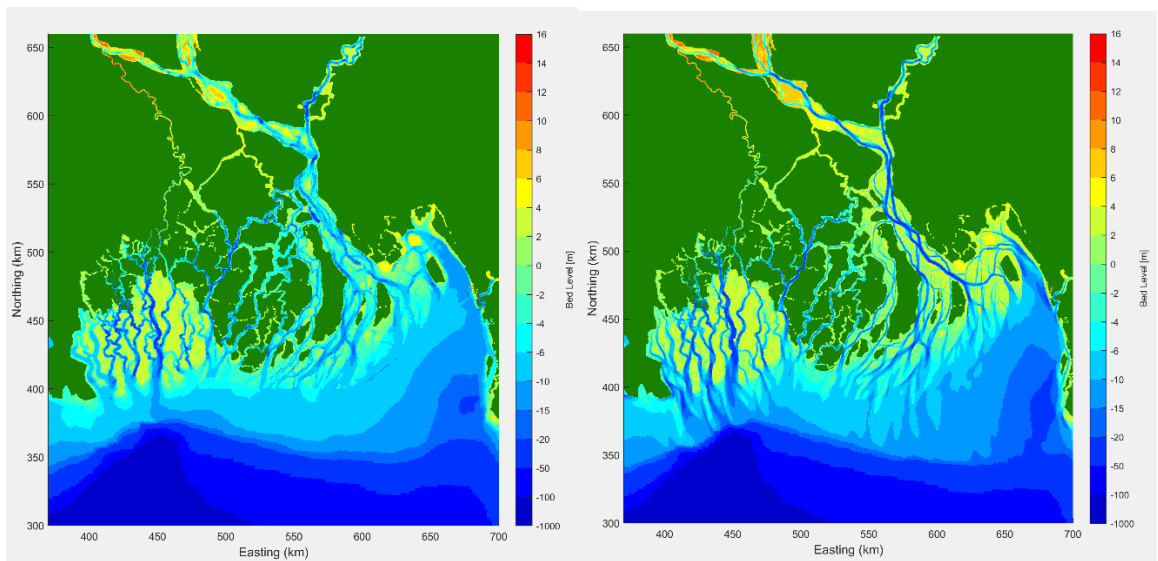


Figure 4.18 Simulated bed level changes, 2000-2019; left panel: bed level 2000; right panel: bed level 2019.

4.4 Integration of model results

The macro-scale models are set up to help understanding the large-scale annual sediment dynamics and long-term morphodynamics of the GBM delta and predicting responses in the morphodynamics of the GBM delta to changes in external forcing conditions (due to climate change and anthropogenic activity). It is important to evaluate in how far the models reproduce the reality, as this determines how the models can be used for e.g. predicting the effects of future climate change and human interference. For this purpose, the model results can be compared with the (limited) available field data, and the insights from the literature. This is done in the following for the different spatial scales.

At the mega-scale, the development of the delta as a whole is determined by the fluvial sediment input and the sediment export from the delta to the deep sea. The fluvial sediment input from the river basin is determined by the HydroTrend model and prescribed at the upstream end of the 1D and 2D Delft3D-FM models as boundary conditions. According to the 2D morphodynamic model, about 1/3 of the fluvial sediment input is exported to the deep sea (the most seaward row of cells in Fig.4.11), and the other 2/3 is deposited in the delta area. This is in agreement with literature.

At the macro-scale, the major part of the river discharge and fluvial sediment input is transported through the lower Meghna, the active delta building estuary. This is reproduced by both the 1D model and the 2D model. The discharge and sediment transport diverted by the two distributaries, the Gorai river and the Arial Khan river, are quantitatively less certain, although the order of magnitude of them simulated by the models agrees well with literature. The 1D model calculates that about 10% of the Ganges discharge is diverted to the Gorai river, and about 5% of the Padma discharge to the Arial Khan river. The sediment transport to the Gorai river is about 45 MT/yr according to the 1D model and 20 MT/yr according to the 2D model, whereas according to the literature it is about 30 MT/yr, about the same as that to the Arial Khan river. The 2D model calculates the sediment transport to the Arial Khan river as about 25 MT/yr, thus close to reported in literature. In the coastal zone, the westwards sediment transport as described in the literature is not simulated by the 2D model. It is not clear if this is a shortcoming of the model, as there the claim in the literature is not directly supported by field data. Future field measurements are required to resolve this issue and to support possible further improvement of the 2D model.

At the meso-scale, most sedimentation takes place in the mouth area of the active delta building estuary, the lower Meghna, correctly reproduced by the 2D model. The sedimentation-erosion pattern simulated by the model shows many agreements with the very limited bathymetric data, especially at a number of hotspots with relatively rapid changes. At this more detailed scale level, it is inevitable that these large-scale models also show some disagreement with observations and or reports from the literature. As an example, the results show that both the 1D and 2D models are exporting sediment in the Sundarbans area which is considered unrealistic. Causes for this are a lack of intertidal areas, mangrove vegetation effects and 3D density-driven currents leading to landward transport, which is not considered in these depth-averaged models.

In conclusion, models show satisfactory performance at the mega- and macro-scales. They can be applied for predicting the effects of future changing forcing and pressure due to climate change and/or human interference. Given shortcomings and uncertainties especially at more detailed scale levels, the models should especially be applied concerning mega- and macro-scale developments, and the model results can better be considered in relative sense by comparing the model results from different simulations, rather than use the model results in an absolute sense.

The model results of the simulations for the present-day situation already help us in understanding the current development of the delta. In the most downstream part, the active delta building estuary is bifurcated into multiple outlets. The 2D model results show that the most eastern outlet is increasing in importance, indicating that the eastwards building up of the delta, as reported in the geological studies, is continuing. This is supported by the 1D model results concerning ebb and flood tidal volumes: the most eastern branch has the largest ebb and flood tidal volume whereas the west branch has a larger net (seaward) discharge. Apparently, the tidal flow in the eastern branch is stronger due to larger tidal range, and the most fluvial sediment transport goes to the west branch causing progradation on the west side of the estuary.

5 Model results on future projections

5.1 Hydrodynamics (1D)

5.1.1 Tidal propagation

Figure 5.1 shows the change in the M_2 tidal amplitude with respect to the reference scenario. First, the results are discussed for each estuary individually to discover system-specific behaviour. Secondly, trends and main findings are discussed that are valid for all systems or for a certain scenario or process.

In the Pussur and Sibsa systems the M_2 tidal amplitude increases for all scenarios except the scenario with an increased river discharge isolated (S_{4HYD}). The largest increase is found for the RCP8.5 scenarios but the tidal limit, however, remains roughly at the same location. An increased river discharge (the effect isolated in the purple line; scenario S_{4HYD}) leads to a smaller tidal amplitude, which is due to increased friction and the mass of the increased river discharge. The high-end SLR scenario (the effect isolated in the green line; scenario S_{5SLR}) causes an increase in tidal amplitude, which is due to an increase in the mean water level. In the Sibsa estuary the effects of an increase in river discharge are limited as there is no fresh water discharge reaching the upstream reaches of this estuary. Although an increased river discharge causes a decrease of the tidal amplitude, the effect depends on the sea level rise scenario; near 80 km the tidal wave starts to amplify even further for the RCP8.5 SLR scenarios than for the RCP4.5 SLR scenarios (with lower river discharge). Apparently, SLR becomes the dominant factor controlling tidal amplification, clearly indicated by the scenario where 103 cm SLR is isolated (green line). For the Pussur system a tipping point can be identified where SLR will lead to increased tidal amplification, this point lies between 47 – 76 cm SLR.

Along the Baleshawr and Arial Khan the M_2 tidal amplitude increases for most scenarios (with respect to the reference) along the entire length of the estuary, except S_4 and the lowest climate change impact scenario $S_{1-RCP4.5}$. For all scenarios the longitudinal change shows an abrupt decrease of the tidal amplitude at approximately 130 km from the mouth. This is mainly caused by friction from the river discharge. This is clearly indicated by the tidal dampening observed for the scenario with an increased river discharge isolated (S_{4HYD} , purple line), which reaches a maximum difference here. If there is no increased river discharge at all (green line, S_5), tidal dampening is less but does not result in increased tidal amplification as observed in the Pussur estuary.

Along the Bishkali estuary the increased sea level has a more limited effect on the increase of the tidal amplitude, compared to the other estuaries. For all scenarios, even a decrease of the tidal amplitude can be observed around 90 km. This can probably be attributed to the fact that the river discharge is approximately equal to the flood tidal prism in the Bishkali (see Figure 4.3). Therefore, the effect of the increase in the mean water level (due to SLR or river discharge) is limited to the lower reaches of the estuary. Upstream of ~100 km the behaviour is different, but this is mainly controlled by the tidal propagation in the Lower Meghna estuary.

In the Burishawr estuary the increase in M_2 tidal amplitude with respect to the reference is approximately uniformly distributed up till ~85 km. Upstream of this point tidal dynamics are controlled by the river discharge and tidal propagation in the Tetulia, of which the Burishawr is a smaller bifurcating branch.

In the Tetulia estuary the scenarios show that all SLR conditions will cause the tidal amplitude to increase, up till the point where the estuary bifurcates from the Lower Meghna (~140 km), irrespective of the river discharge within these scenarios. The effect of an increased river discharge (isolated in the purple line) causes the tidal wave to dampen but the SLR conditions affect this system to a larger extent.

In the Lower Meghna the point where river discharge and an increase in mean water level compete as dominant process to affect tidal propagation is located near the mouth of the estuary (~40 km). Similar to the Pussur estuary, the tide shows increased amplification for the RCP8.5 scenarios, irrespective of the increased river discharge. The tidal limit lies at ~240 km (near the confluence of

the Ganges and Brahmaputra into the Padma) and this point of maximal tidal intrusion does not change for the simulated scenarios.

In the Upper Meghna the effect of increased river discharge is controlled by changed tidal dynamics at the confluence with the Lower Meghna, because river discharge of the Upper Meghna boundary condition is not changed in the scenario simulations. There is, however, a small extra discharge provided by the Old Brahmaputra river that confluent in to the Upper Meghna. The effects of SLR are uniformly distributed over the length of the river and show an increase of the M_2 tidal amplitude for all scenarios.

Tidal propagation – and specifically amplification and dampening of the tide – is controlled by a balance between the width convergence of the estuary and friction. Both are affected by SLR as the cross-sectional area changes with a change in the MWL. Both are affected by an increase in river discharge as well because the MWL will increase and the river discharge provides an additional source of friction. Friction caused by river discharge decreases seawards as the discharge is distributed over an increasingly larger cross-sectional area (estuaries are trumpet shaped). The scenario results show that the increase in the mean water level due to SLR allows tides to propagate more easily (less friction) into the estuaries and generally causes an increased amplification. The scenario with increased river discharge isolated clearly illustrates the frictional effect. At most systems, a point can be identified where the increased friction due to the increased river discharge dominates tidal behaviour (i.e., the tide dampens). However, for the Pussur and the Lower Meghna the results show that between 47 – 76 cm SLR a threshold is reached where the amplification of the tide is controlled less by river discharge. This can be considered as a tipping point in the response of these systems to SLR.

5.1.2 Gross and net tidal discharge

The tidal propagation patterns show that the response of the estuarine systems can be different for the simulated scenarios. Therefore, changes in the balance of net tidal volumes can be expected because the exchange in bifurcations and confluences of different river branches can function differently in the scenario simulations. These changes with respect to the reference scenario are shown in Figure 5.2. The figures show that for each system there is an increase in the tidally-averaged (net) discharge in the ebb direction (i.e., a decreasing ΔQ) for all scenarios except the S3 RCP4.5 scenario. The increase in the ebb direction is a result of the increase in discharge forced at the upstream boundaries, and the decrease in the S3 RCP4.5 scenario is a result of the decrease in the discharge. However, the scenario with sea level rise isolated ($S5_{SLR}$) shows that there can be a change in the net discharge as well because the tidal volume is distributed differently over the bifurcations and confluences of the river network.

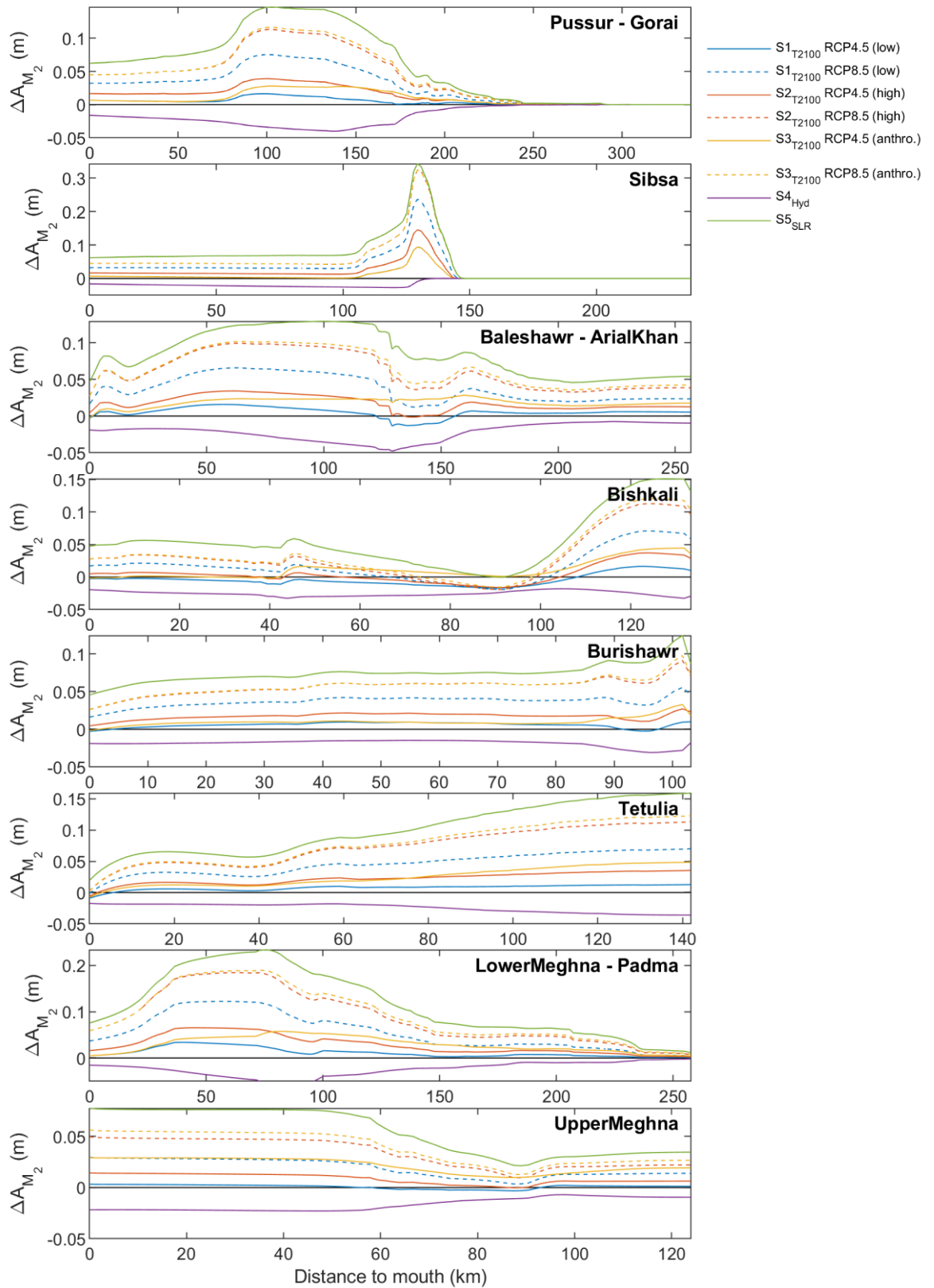


Figure 5.1 Relative change in the M_2 tidal amplitude. Positive (negative) numbers indicate an increase (decrease) in the future scenarios with respect to the reference scenario.

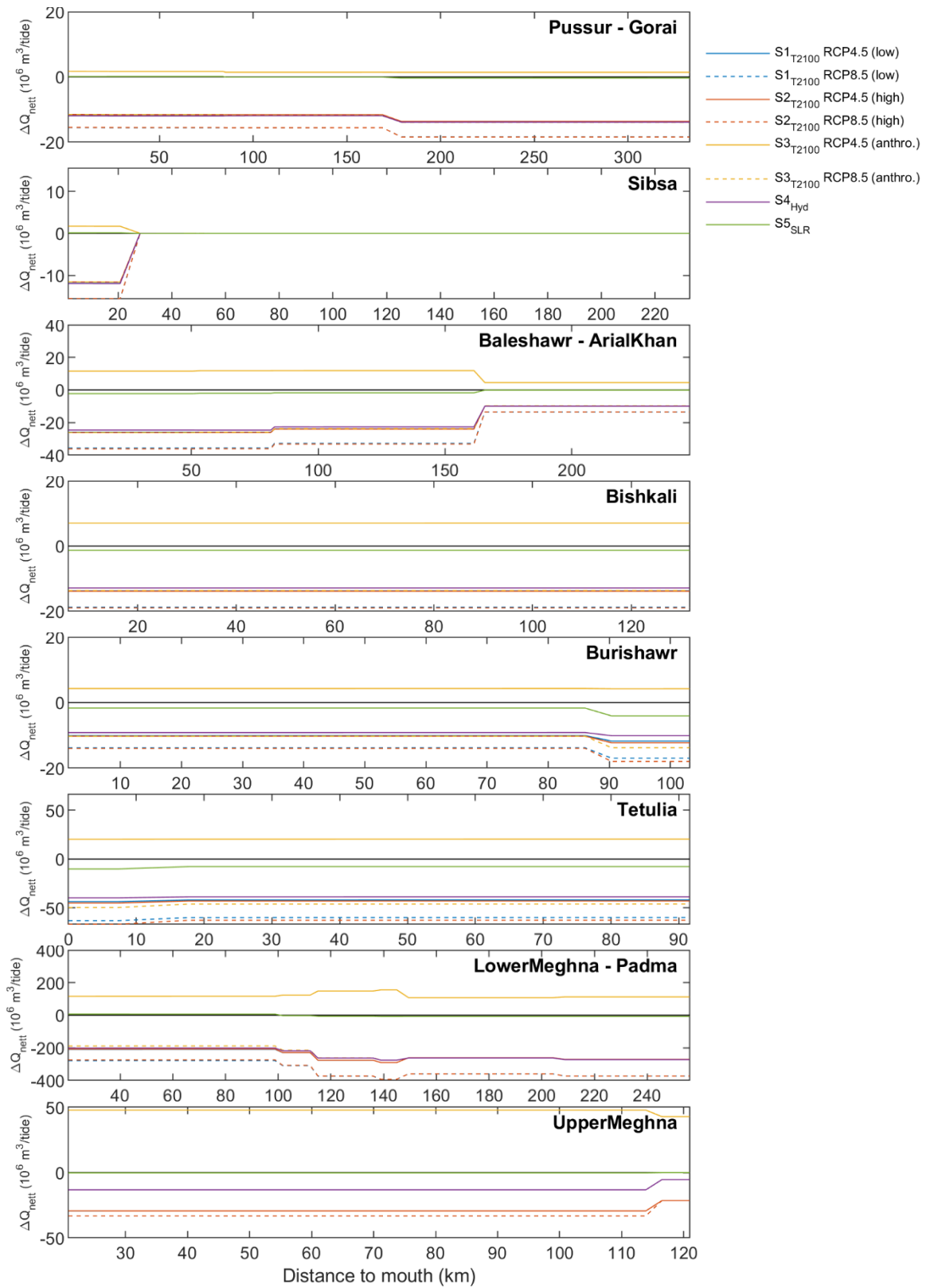


Figure 5.2 Relative change in the net tidal discharge. Positive (negative) numbers indicate an increase (decrease) in the future scenarios with respect to the reference scenario.

5.2 Sediment dynamics

5.2.1 Sediment fluxes

1D modelling results

The relative changes in the net sediment fluxes are shown in Figure 5.3. The net fluxes are basically influenced by two factors, the net tidal volume change and the change in tidal dynamics. The changes in net sediment fluxes (Figure 5.3) generally follow the same pattern as the changes in the net tidal volume. Apparently, the effect of the net tidal volume change, which is mainly the result of the change in upstream river discharge, is more important than the change in tidal dynamics. Indeed, the difference between scenario S4_{Hyd} (only upstream river discharge changed) and the reference scenario is much larger in magnitude than that between the S5_{SLR} (river discharge unchanged and only SLR) and the reference scenario. The results of the S3 RCP4.5 scenario for the Pussur-Sibsa system are an exception. The net sediment fluxes in the ebb direction in both branches increase with respect to the reference scenario although the net tidal volumes in the ebb direction show a decrease. In this case the effect of changed tidal dynamics dominates the change in net tidal volume, but mostly the changes in net tidal volume due to the changed upstream river discharges have the dominant effect on the changes in net sediment fluxes.

According to the 1D model SLR has a very limited effect on the net sediment flux in the estuaries compared to the changes of the upstream river discharges. However, it should be noted that the intertidal areas cannot be fully represented in the 1D model, especially concerning the sediment exchange with the channel. As the channel and adjacent intertidal areas at a certain location are schematized in a single cross-sectional profile, the model is not be able to model the situation of erosion in the channel and sedimentation on the intertidal shoals.

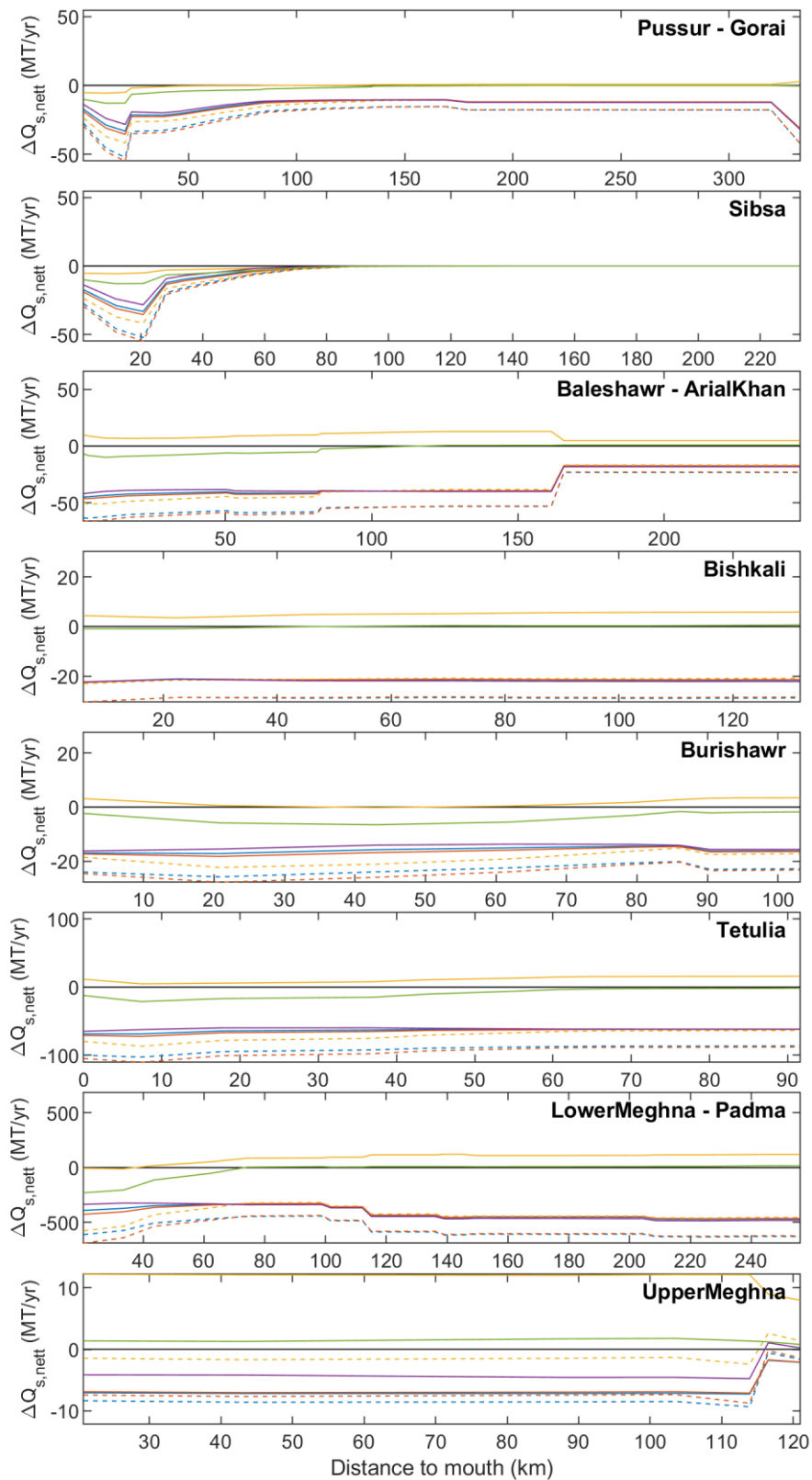


Figure 5.3 Relative change in the total (sand and mud) suspended sediment load. Positive (negative) numbers indicate an increase (decrease) in the future scenarios with respect to the reference scenario.

2D modelling results

Figure 5.4 to Figure 5.9 show the yearly-averaged sediment fluxes of mud and sand over the 2020-2100 period for all scenarios. Differences between the scenarios are typically much smaller than absolute transports with largest differences of about 50% between “Scenario 1.0m SLR” and “Scenario 0.5m SLR, anthropic effects Q, 50% SSC”. Largest mud transport take place in the major river sections. At the Meghna estuary mouth the mud disperses in all directions while a major transport occurs towards the delta front. In all scenarios some mud is transported directly westward along the coast although the alongshore transport reduces significantly at the Tetulia mouth area. Westward mud transport also occurs at a single cell at the ocean but there is no mud transported back onto the coastline.

Largest sand transports are about an order of magnitude smaller than the mud transports and mainly occur at the lower Meghna mouth and delta region. Scenario “0.5m SLR, anthropic effects Q, 50% SSC” (Figure 5.9) shows smallest averaged transports while largest transports are shown by “Scenario 1.0m SLR, discharge RCP4.5”, “Scenario no SLR, discharge RCP4.5” and “Scenario 1.0m SLR, discharge RCP8.5” (Figure 5.4, Figure 5.5, Figure 5.7, respectively).

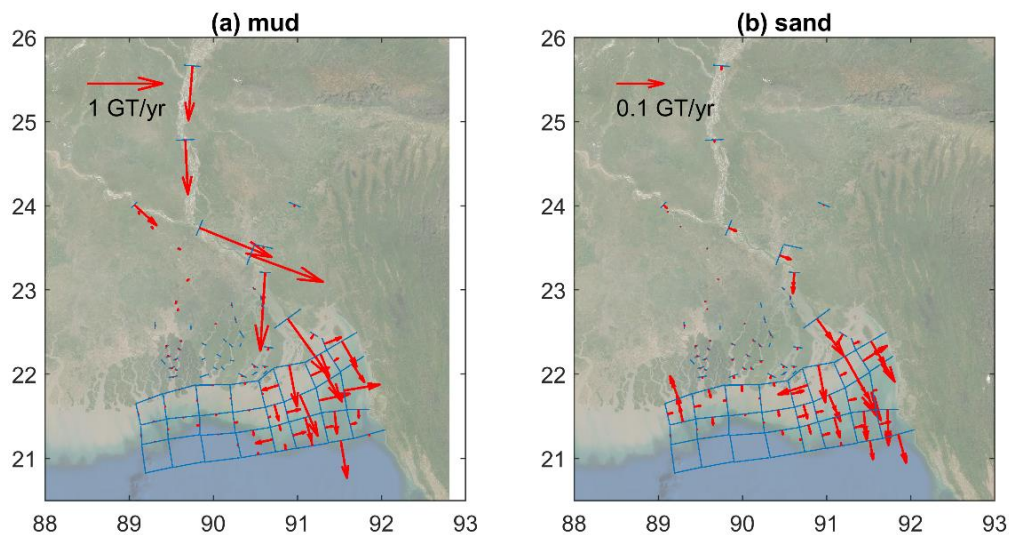


Figure 5.4 Scenario 1.0m SLR, discharge RCP4.5 with yearly averaged sediment fluxes over the 2020-2100 period for (a) mud fraction; (b) sand fraction. Arrows indicate sediment transport direction and magnitude.

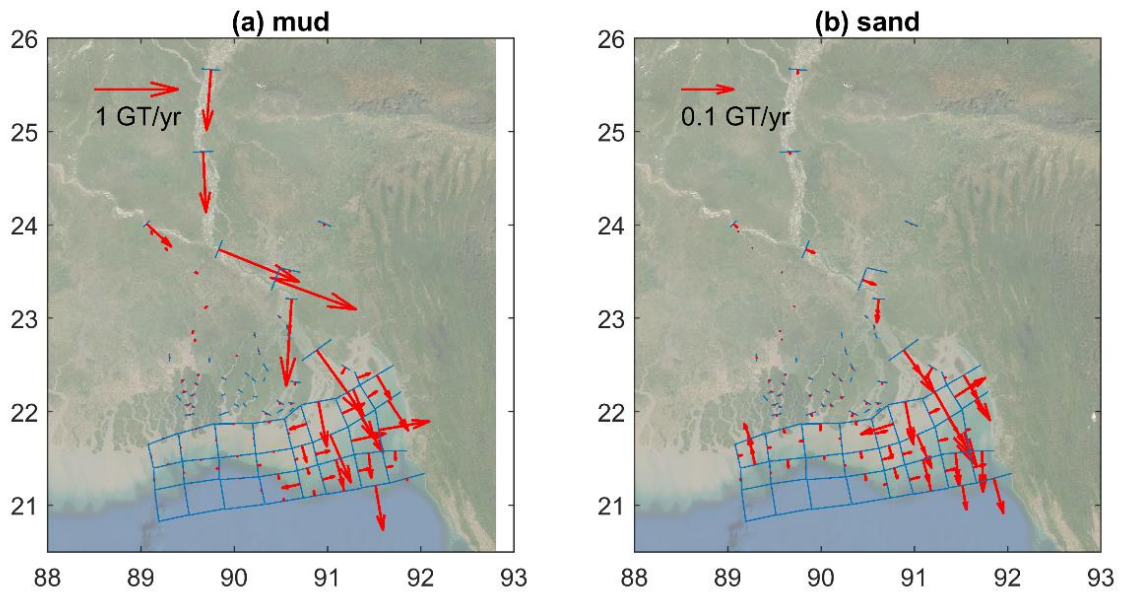


Figure 5.5 Scenario no SLR, discharge RCP4.5 with yearly averaged sediment fluxes over the 2020-2100 period for (a) mud fraction; (b) sand fraction. Arrows indicate sediment transport direction and magnitude.

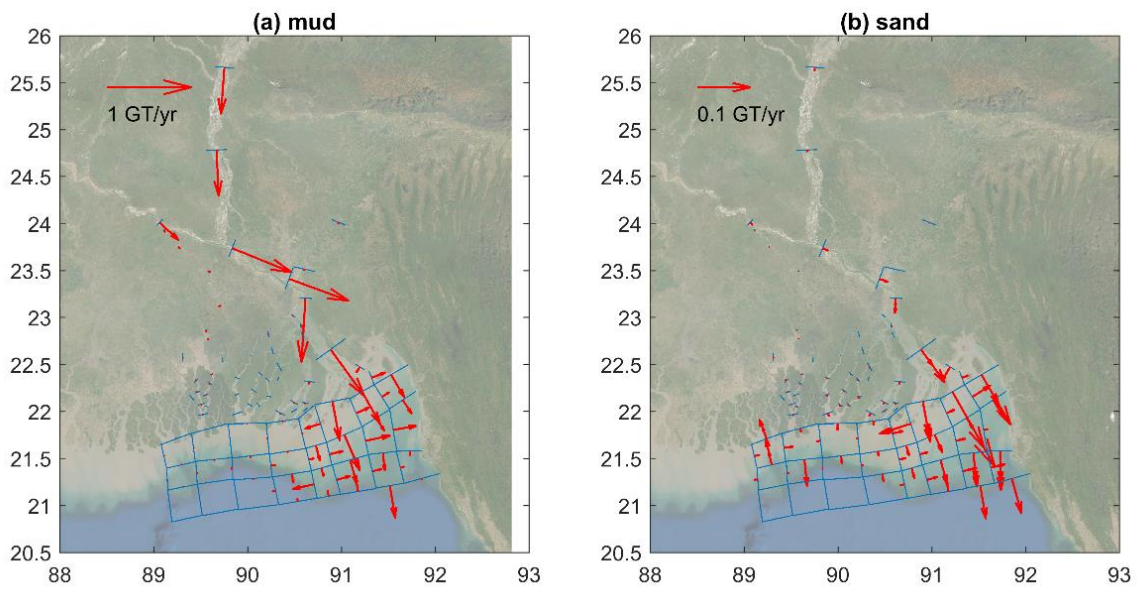


Figure 5.6 Scenario 0.5m SLR, anthropic effects Q with yearly averaged sediment fluxes over the 2020-2100 period for (a) mud fraction; (b) sand fraction. Arrows indicate sediment transport direction and magnitude.

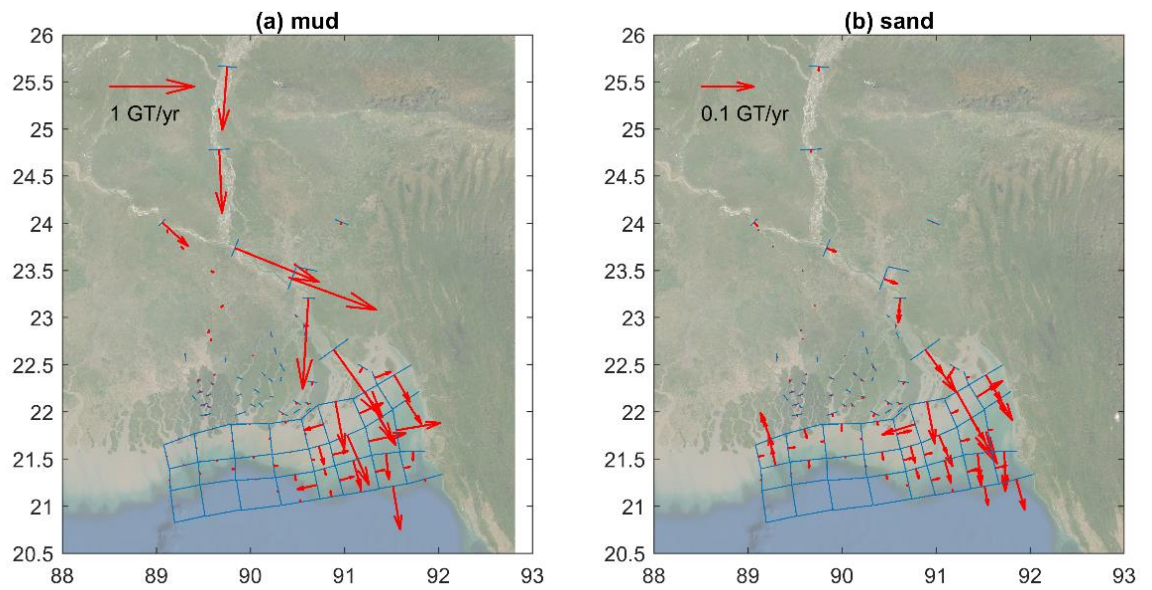


Figure 5.7 Scenario 1.0m SLR, discharge RCP8.5 with yearly averaged sediment fluxes over the 2020-2100 period for (a) mud fraction; (b) sand fraction. Arrows indicate sediment transport direction and magnitude.

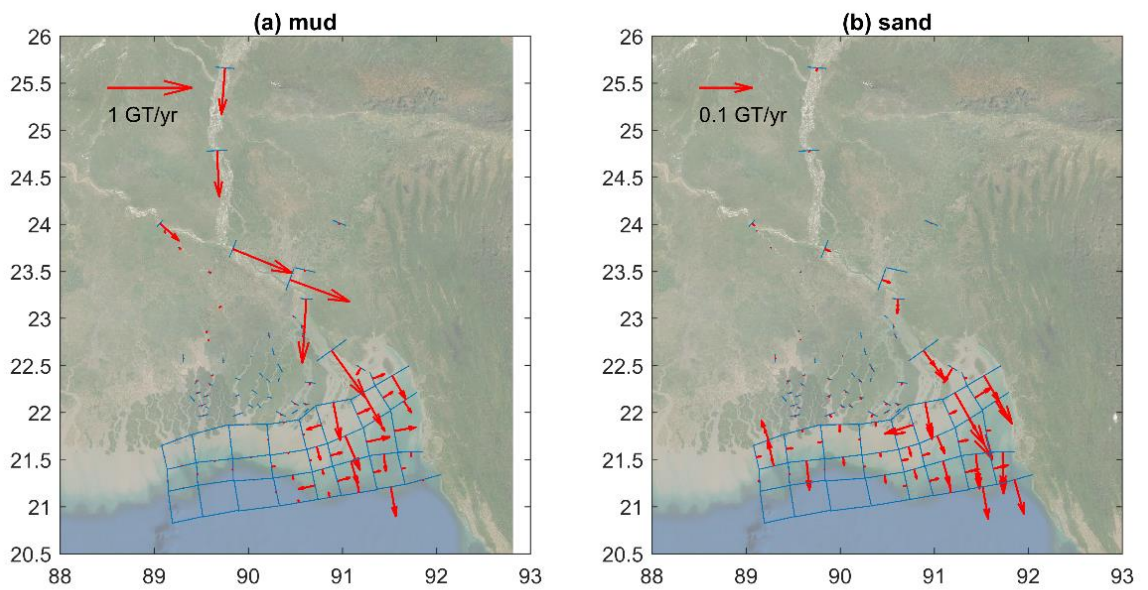


Figure 5.8 Scenario 0.5m SLR, anthropic effects Q, no subsidence with yearly averaged sediment fluxes over the 2020-2100 period for (a) mud fraction; (b) sand fraction. Arrows indicate sediment transport direction and magnitude.

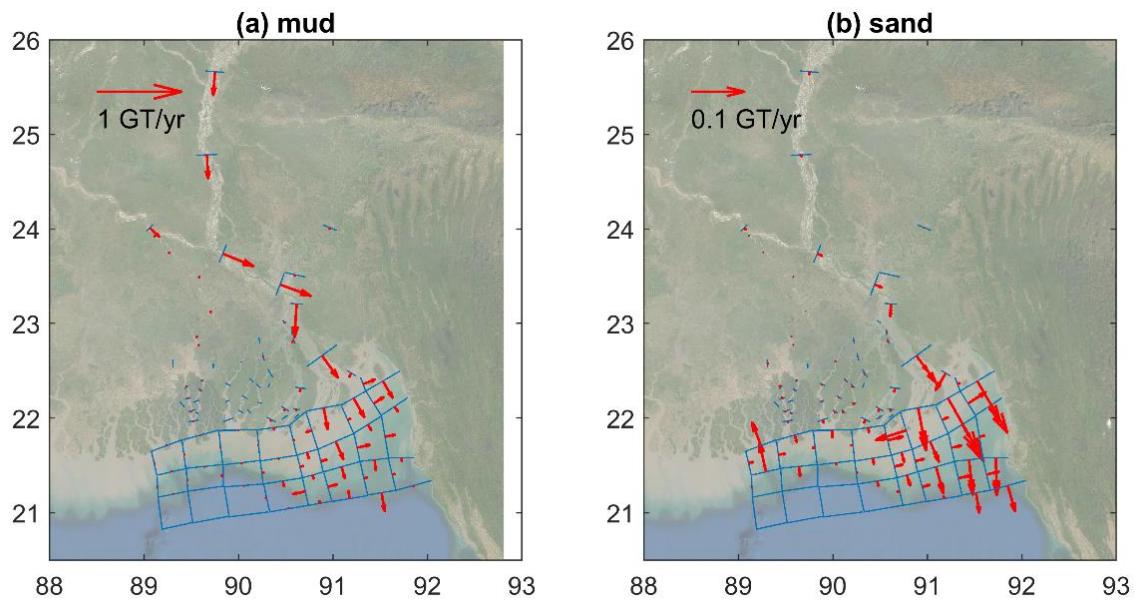


Figure 5.9 Scenario 0.5m SLR, anthropic effects Q, 50% SSC with yearly averaged sediment fluxes over the 2020-2100 period for (a) mud fraction; (b) sand fraction. Arrows indicate sediment transport direction and magnitude.

5.2.2 Distribution of sediment concentrations (2D)

The distribution of the sediment concentrations through the delta is highly variable in time and space. Apart from tidal and seasonal fluctuations it will gradually develop as the bed composition is slowly adjusting to supply from upstream and erosion and sedimentation processes. In order to give a clear comparison of the effect of the different scenarios, the mean concentration over a 10-year period is shown. We focus on the period 2040-2050, which is well after the bed composition has reached a quasi-equilibrium. The results are shown in Figure 5.10 below. We can draw the following conclusions:

- The sediment concentration is not very sensitive to the rate of sea level rise, compare (b) (no sea level rise) with (a) (1m sea level rise).
- Compared to (a,b) the effect of a lower discharge scenario (c) clearly leads to reduced sediment concentrations throughout.
- Similarly, the high-end discharge hydrograph (d) leads to slightly higher concentrations in the outflow of the Lower Meghna.
- The effect of subsidence on sediment concentration patterns is very minor (compare (c) – with subsidence with (e) – no subsidence).
- Reducing the upstream sediment concentrations in the Ganges and Brahmaputra can be seen in comparing (f) and (c) and has the largest effect on SSC

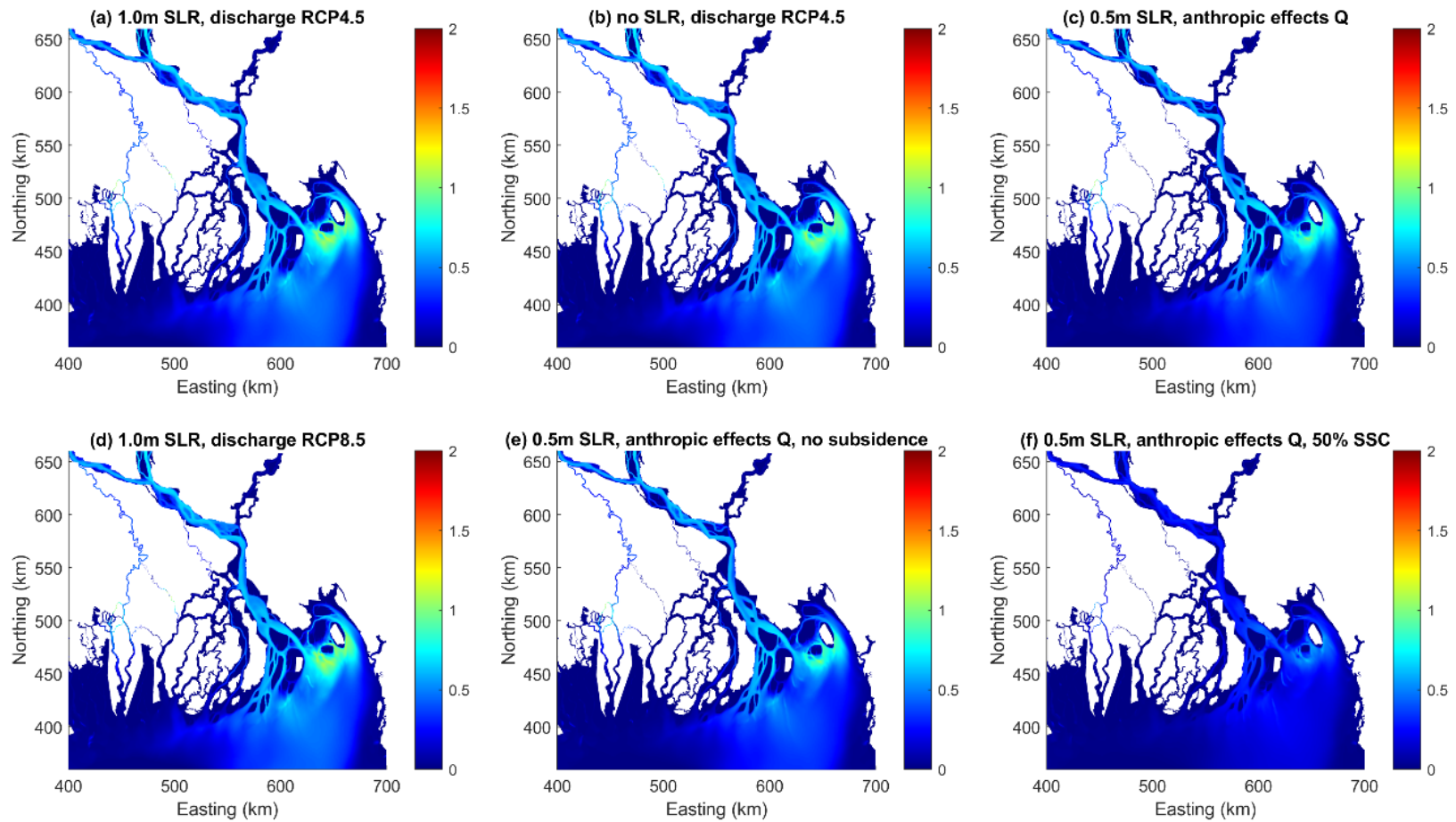


Figure 5.10 Mud sediment concentrations in g/l throughout the delta, averaged over 2040-2050 for different scenario runs.

5.3 Morphodynamics in 1D

5.3.1 Tidal prism and cross-sectional area

A change in the A/P ratio, as presented in Chapter 4.3.1 for the reference scenario, gives an indication on the future change of the morphological development. An increase of the ratio means an increase of sediment demand indicating that the morphological development tends to change in the direction of relatively more sedimentation (thus can also be less erosion), and vice versa.

Both modelled drivers, SLR and change of upstream river discharges, have influences on the A/P ratio which are not straight forward. SLR has two opposite effects on this ratio. First, the increased water level causes a direct increase of the cross-sectional area A , thus an increase of the A/P ratio. Second, SLR also causes an increase of P , the ebb volume because of the increased tidal storage volume due to increased width of the rivers/estuaries at higher water level and due to increased tidal range (increased tidal amplification because of decreased effect of friction due to larger water depth). The A/P ratio can thus increase or decrease depending on which of the two opposite effects is more dominant. The change of the ratio due to SLR can show spatial variation, even along a same river/estuary branch; decrease in relatively narrow sections and increase in relatively wide sections. Changes of upstream river discharges also influence A as well as P . An increase of the river discharge causes an increase of A because of the mean water level increase. The effect on P of an increase of the river discharge, however, is more complex. A direct increase on P follows from an increase of the ebb volume and a decrease due to damping of the tide by increased hydraulic drag/friction.

The future scenarios show a smaller A/P ratio along almost the entire length of all estuaries, indicating that, based on hydrodynamics alone, the delta will respond to the scenarios by erosion (or a reduction in sedimentation). These effects are dominated by the changes in upstream discharge; SLR has a more limited effect. Therefore, the S3 RCP4.5 (anthro) scenario, that indicates the effect of a **reduced** discharge, stands out and shows an increase of the A/P ratio. The scenario with SLR isolated ($S5_{SLR}$) shows an increase in the A/P ratio, indicating an increase in accommodation space. From the figures it can be concluded that the morphological development of the estuaries is dominated by a change in the upstream discharge, and that SLR has a subordinate effect.

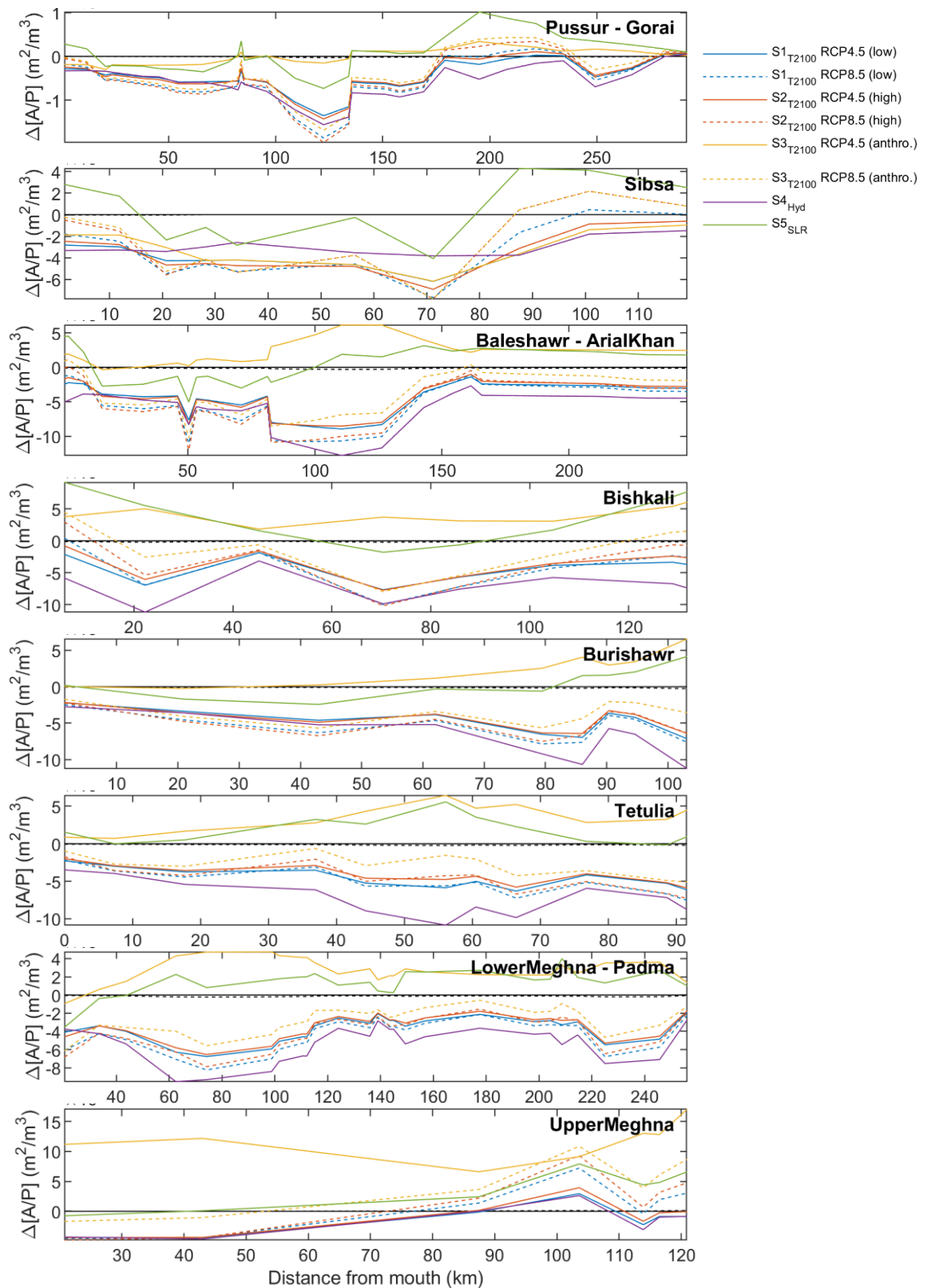


Figure 5.11 Relative change in the ratio of the cross-sectional area (A) and the ebb tidal volume (P). Positive (negative) numbers indicate an increase (decrease) in the future scenarios with respect to the reference scenario.

5.4 Morphodynamics in 2D

5.4.1 Bed evolution

The initial bathymetry in 2020 and the modelled bed levels in 2050 and 2100 are presented per run in Figure 5.12, Figure 5.13 and Figure 5.14, respectively. Averaged bottom level changes per subarea (as defined in Figure 3.10) were calculated by summing the net bed level change within a polygon over the course of the run multiplied by the cell surface area. This sum was divided by the total area of the subarea. The results are presented in Figure 5.15 and Figure 5.17.

In the first 30 years of the simulation (Figure 5.15), the differences between the separate runs are relatively limited, except for run (f) where the upstream sediment concentration value was reduced by 50% (compare Figure 5.13(f) and Figure 5.15(f)). In this last run, the relative deficit in sediment import from upstream through the Padma and the Gorai rivers results in the erosion of the Lower Meghna and the Pusur-Sibsa estuaries, whereas in all other runs these two areas are in a stable or accretionary state.

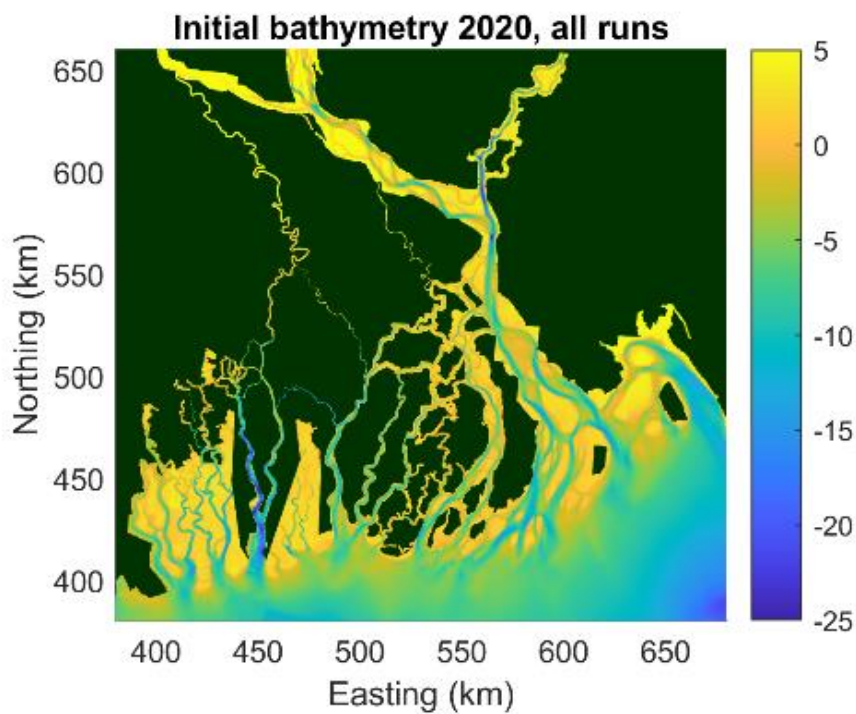


Figure 5.12 Initial model bathymetry in 2020.

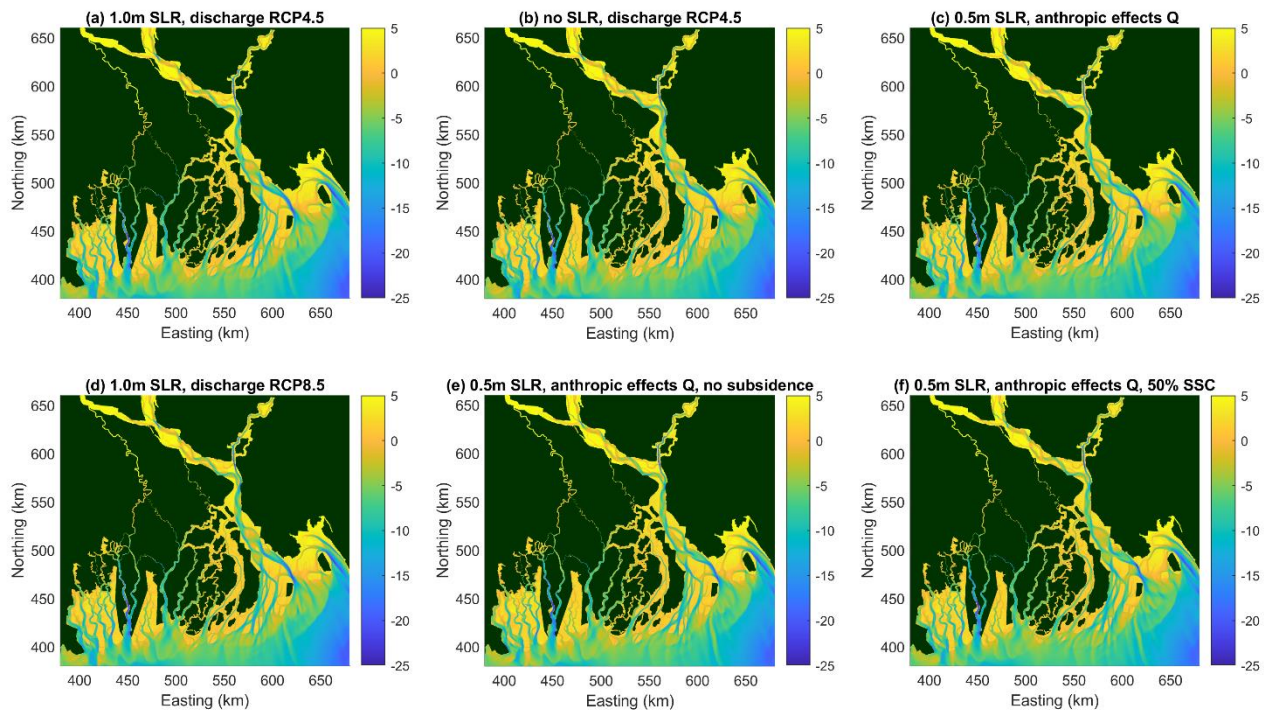


Figure 5.13 Modelled bathymetry in 2050 for runs as defined in Table 3.3.

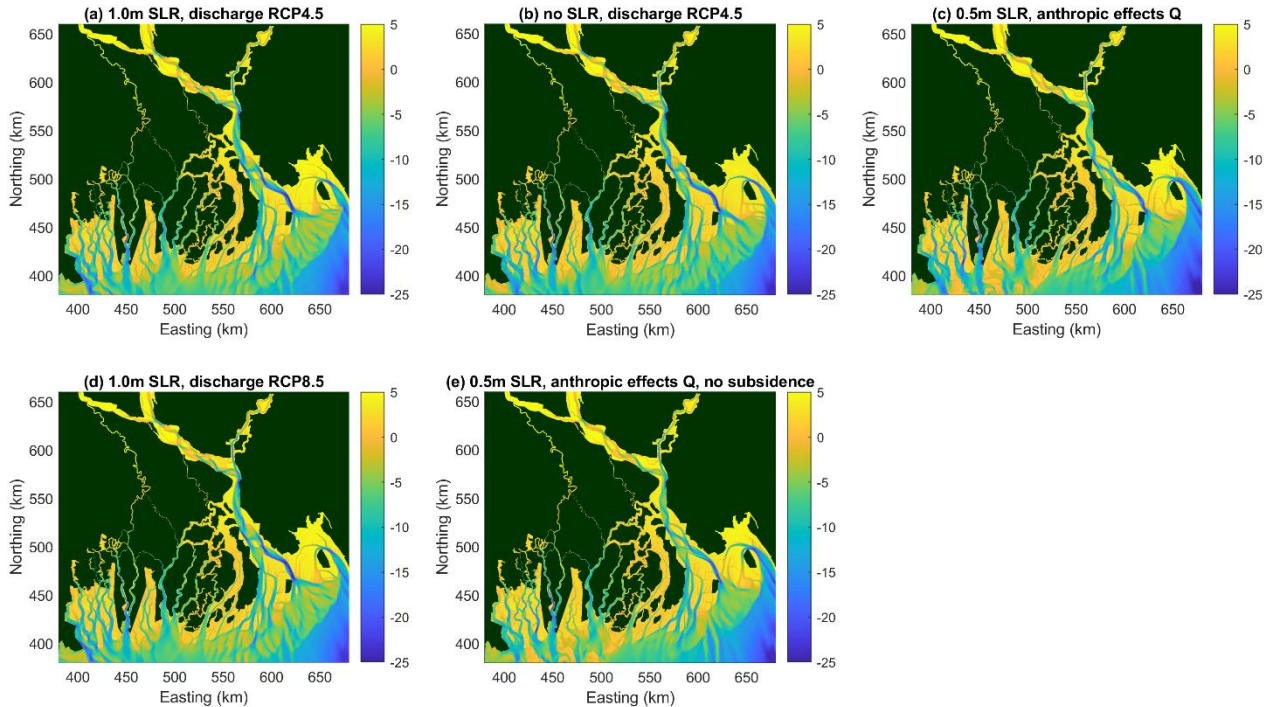


Figure 5.14 Modelled bathymetry in 2100 for runs as defined in Table 3.3.

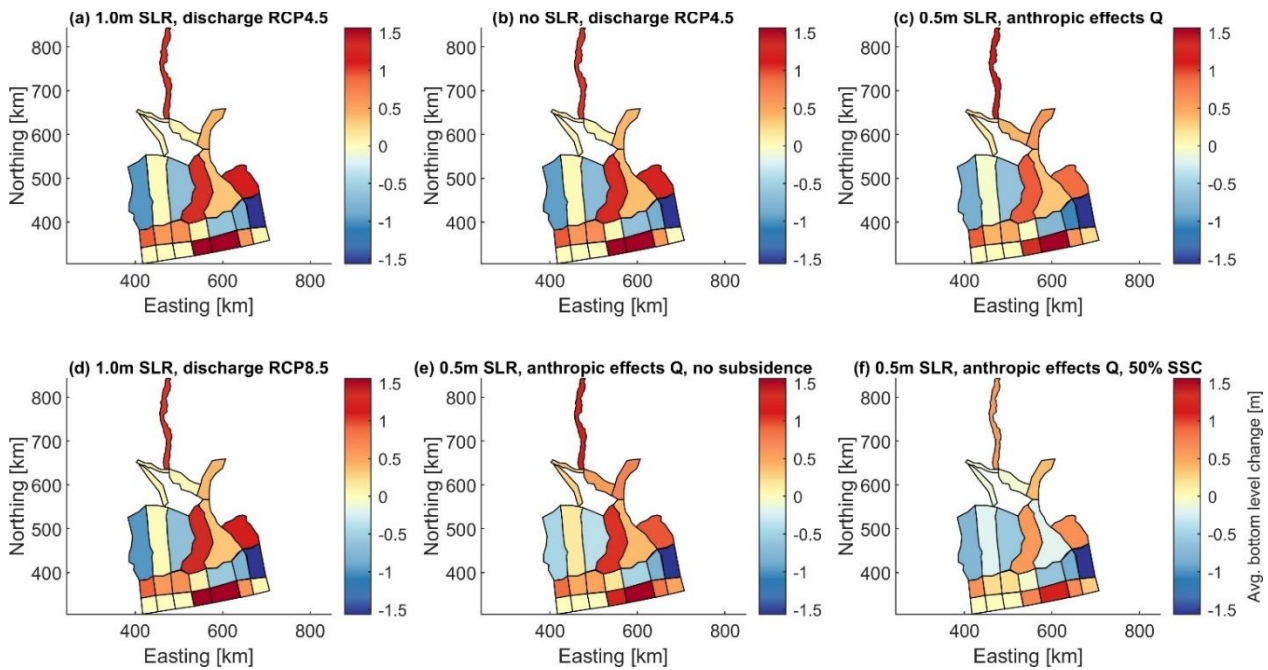


Figure 5.15 Area averaged bottom level change [m] between 2020 and 2050 for the different runs defined in Table 3.3. Red: deposition, blue: erosion.

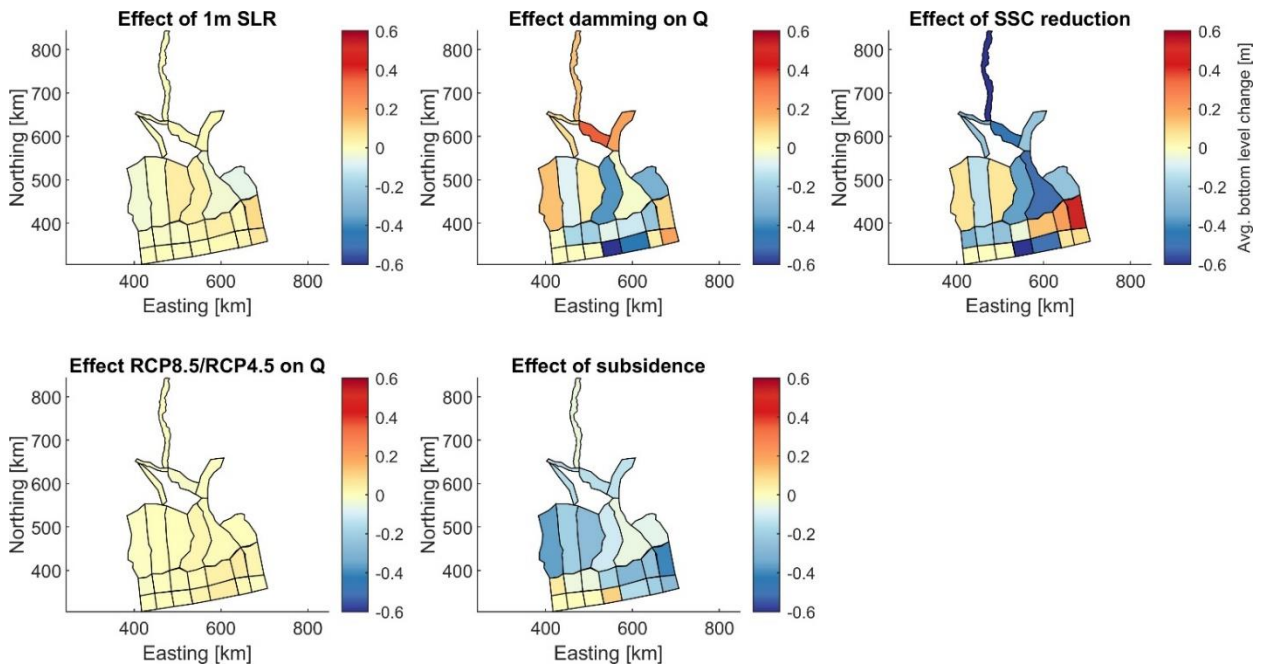


Figure 5.16 Effect of different scenarios on average bed level change between 2020 and 2050 averaged over different subareas in the GBM delta. Subarea definitions can be found in Figure 3.10.

By 2100, after 80 years of simulation, the following patterns can be observed (Figure 5.17 and Figure 5.18):

- Relative sea level rise causes erosion of the Sundarbans; this sediment is deposited on the nearby shelf (subplot (a) and subplot (b));
- A reduction of the upstream discharge by damming (anthropic effects Q) decreases the amount of sedimentation in the eastern chars, and causes a shift in deposition on the deltafront towards the west, although this is not to be interpreted as a westward transport (see section 5.4.2). The Padma shifts from a stable state to an accretionary area (subplot (c));
- An increase in upstream discharge causes more sedimentation throughout the entire domain and particularly around the Meghna mouth (subplot (d) vs subplot (a));
- Subsidence increases erosion rates and decreases accretion throughout the model area, except the southwestern parts of the delta front (subplot (e) vs subplot (c));
- The pattern of erosion and reduced accretion due to a decrease in upstream sediment concentration by 50%, noticeable after 30 years, continues until 2100. After 80 years, relatively more sediment is deposited on the delta front (subplot (e))
- Sea level rise leads to modest sedimentation overall, due to increased accommodation space (Figure 5.18a). However, for most regions the sedimentation rates are an order of magnitude smaller than the SLR itself.

Figure 5.18 clearly shows that the influence of relative sea level rise and of climate-driven changes in upstream discharges is more diffuse and gradual compared to effects related to human activities (decrease in discharge, sediment load) and subsidence.

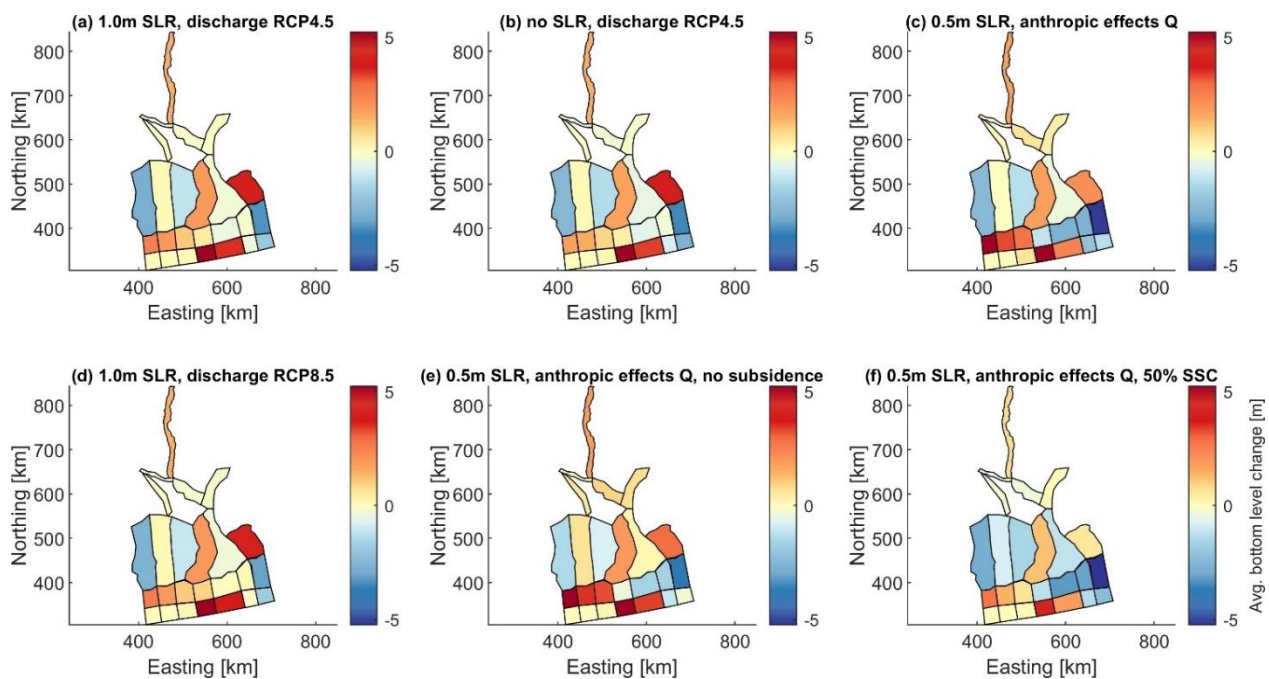


Figure 5.17 Area averaged bottom level change [m] between 2020 and 2100 for the different runs defined in Table 3.3.

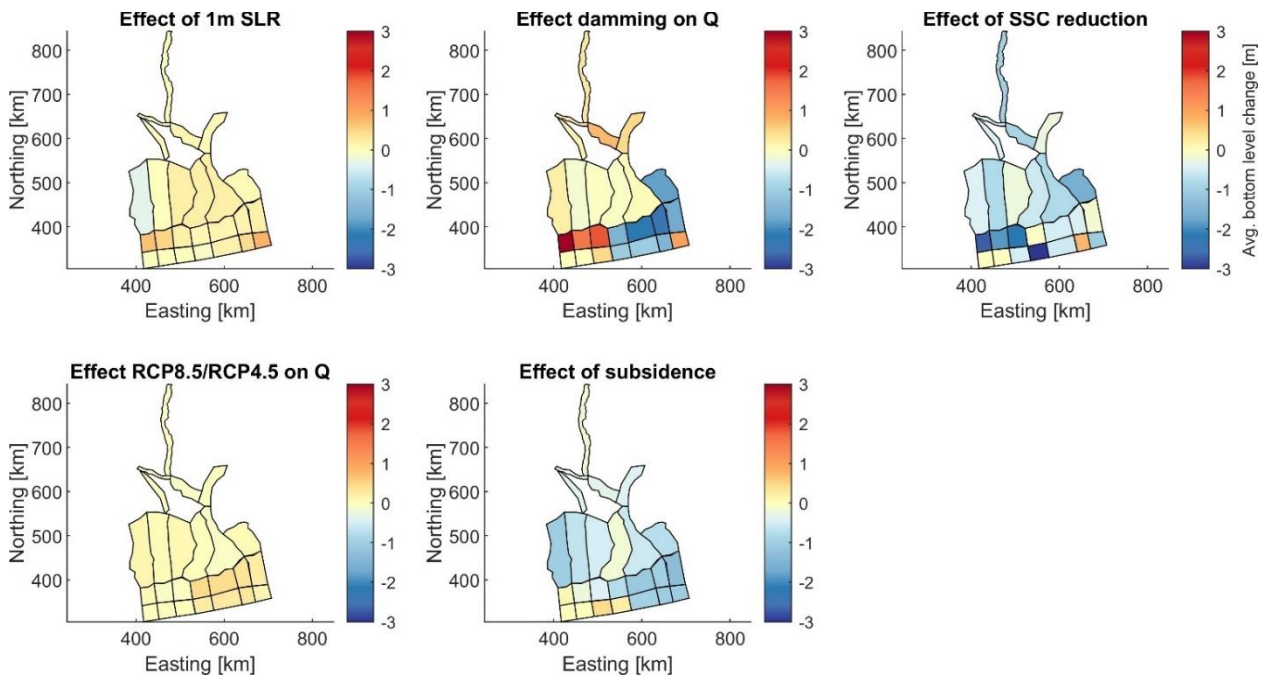


Figure 5.18 Effect of different scenarios on average bed level change between 2020 and 2100 averaged over different subareas in the GBM delta. Subarea definitions can be found in Figure 3.10.

5.4.2 Sedimentation/erosion patterns and differences

Figure 5.19 and Figure 5.20 show that there is gradual development of erosion and sedimentation patterns. That is, patterns after 80 years resemble patterns after 30 years albeit that they are more developed. All scenarios show a similar trend with patterns due to channel migration in the lower Meghna region and estuaries in the Sundarbans, accretion in the Tetulia river and the Sandwip region, deposition in ebb deltas in front of the estuaries mouths and major deposition in the form of delta expansion at the ocean. The region between estuary mouths and the delta front, the subaqueous delta, shows limited erosion.

The scenario differences plots (Figure 5.21) show that, apart from small areas at largest spatial erosion/sedimentation gradients, the differences between scenarios generally remain small compared to absolute values in Figure 5.19 and Figure 5.20.

- There is a clear signal by 1 m SLR, where, as expected, the upper parts of the Ganges and Jamuna rivers are not affected but more deposition occurs at the estuary mouths near the ocean and subaqueous Delta. The deposited sediment left the plotted domain or deposited in amounts <0.5m in case of the 0 SLR scenario.
- Subsidence leads to more erosion (or rather: bed lowering) in the Sundarban estuaries and at the subaqueous Delta. More upstream parts are less affected since subsidence rates are much lower.
- The high-end discharge enforces some additional channel dynamics in the lower Meghna and more deposition at the estuary mouths and at the ocean Delta front.
- The 50% upstream SSC reduction leads to some erosion of the upstream rivers (mainly the Jamuna), channel shifting in the lower Meghna, erosion at the Sundarban estuary mouths and the delta front and some limited deposition at the subaqueous delta due to small amounts of local sediment re-allocation.
- Anthropogenic interventions lead to deposition in the river sections, more erosion at the lower Meghna mouth and at the delta front and more deposition in the Sundarbans region. This may be interpreted as a sediment transport from the subaqueous delta towards the Sundarbans, but closer analysis of cross-sectional sediment transport volumes perpendicular to the coast shows that that is not the case. The patterns thus should be interpreted as caused by a local sediment redistribution by changes in tidal dynamics due to changes (anthropogenic lower) in river flow.

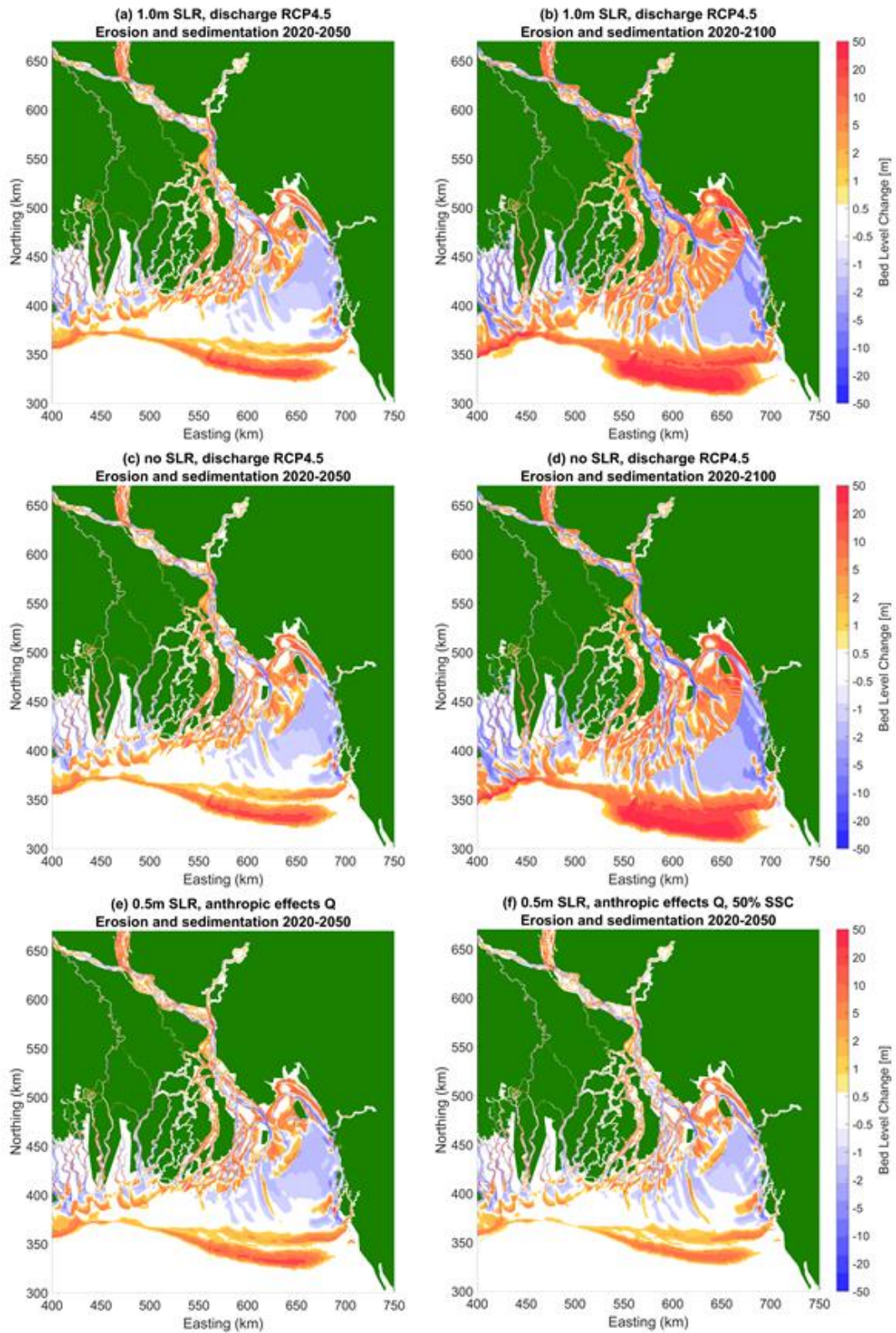


Figure 5.19 Cumulative sedimentation and erosion patterns for different scenarios (a,b) standard 1m SLR; (c,d) no sea level rise; (e,f) high end discharge, (a,c,e) after 30 years and (b,d,f) after 80 years. Mind the logarithmic colour scale.

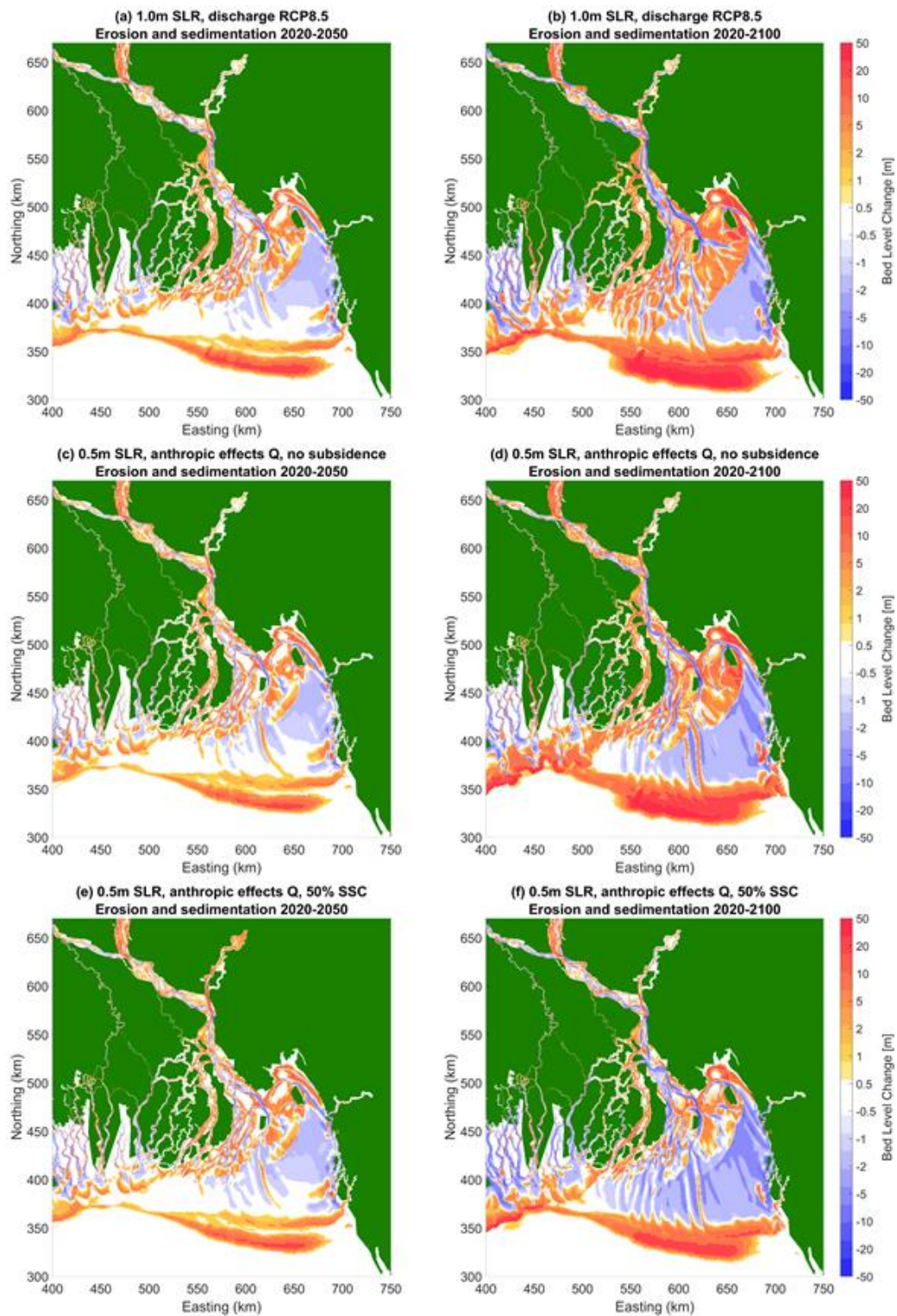


Figure 5.20 Cumulative sedimentation and erosion patterns for different scenarios (a,b) 0.5m SLR and anthropic intervention; (c,d) 0.5m SLR and anthropic intervention – no subsidence; (e,f) 0.5m SLR and anthropic intervention – 50% reduction of upstream SSC, (a,c,e) after 30 years and (b,d,f) after 80 years. Mind the logarithmic colour scale.

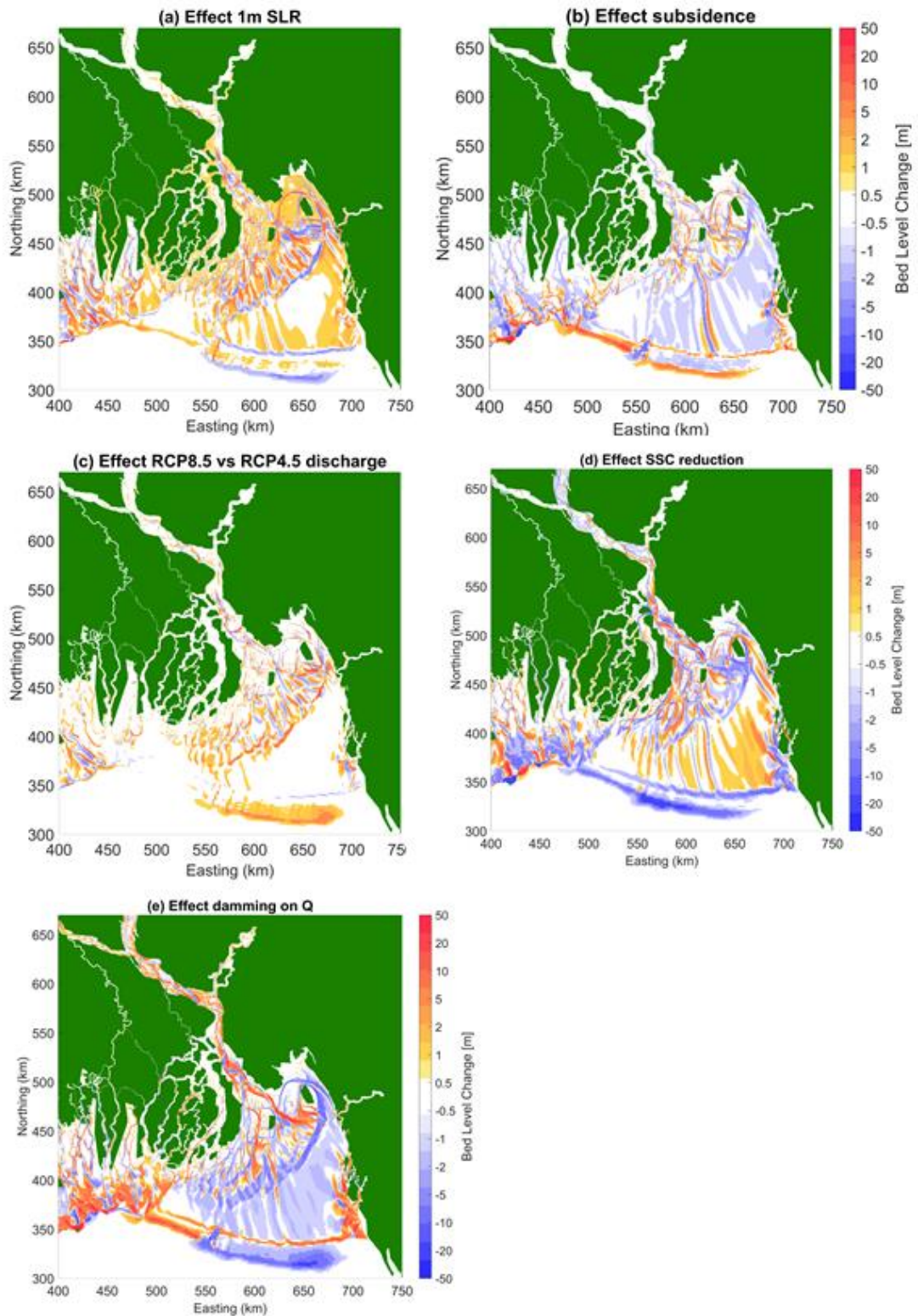


Figure 5.21 Differences in cumulative sedimentation and erosion patterns between different scenarios after 80 years (a) effect of 1m SLR; (b) effect of subsidence; (c) effect of high end discharge, (d) effect of 50% upstream SSC reduction (e) effect of anthropic intervention. Mind the logarithmic colour scale.

5.4.3 Volume balances and scenario effects

Volume time series per subarea of the model domain were constructed for every run in Table 3.3 for the period 2020-2100, by summing the product of the bed level change and the cell surface area over each polygon. To investigate the effect of the scenarios defined in Table 3.4, the relevant time series were subtracted and plotted. The results are presented in Figure 5.22 to Figure 5.26.

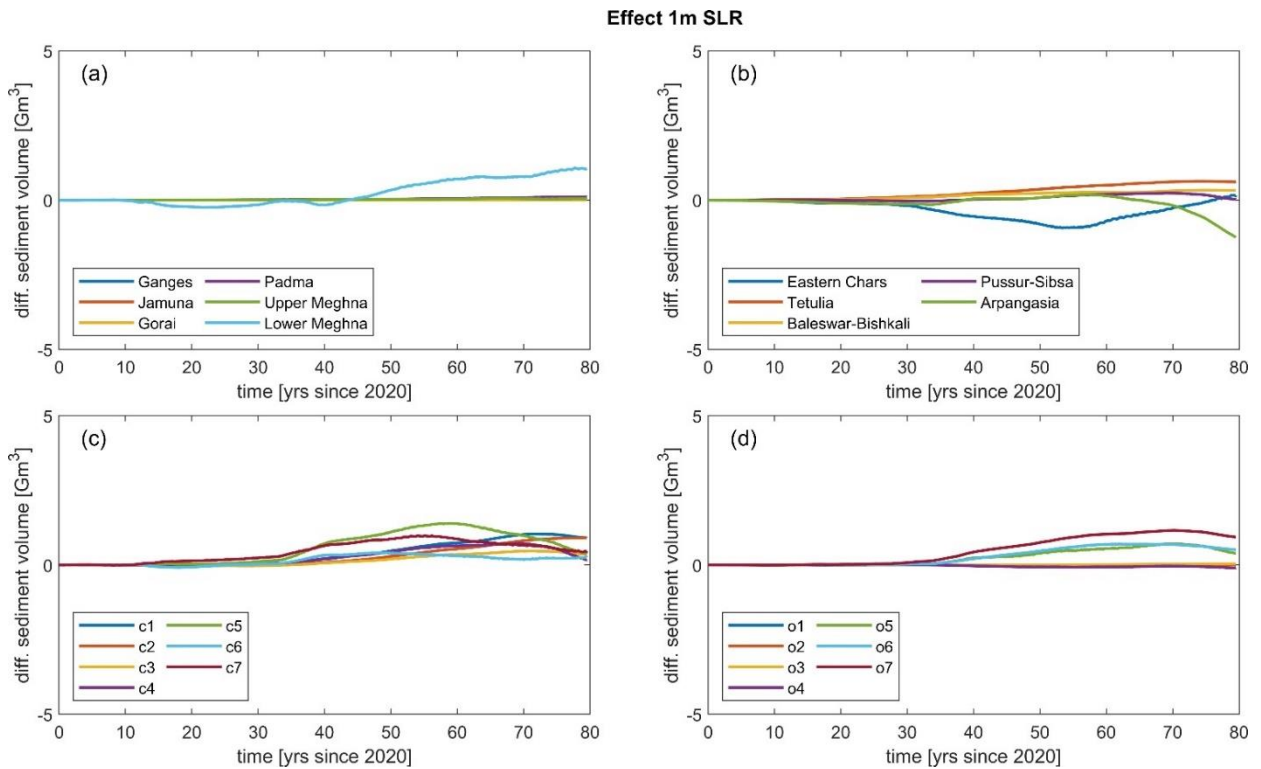


Figure 5.22 Differences in sediment volume [Gm³] in function of time as a result of 1m SLR within different parts of the GBM delta as defined in Figure 3.10.

From these plots, we observe that:

- The system is less sensitive to sea level rise and climate change driven changes in upstream discharges (compare Figure 5.22 (a)) than to human influence (damming, reduction in sediment input to the system) and subsidence (Figure 5.23 (a) and Figure 5.25 (a), see also Section 5.4.1);
- Sea level rise has almost no effect in the areas upstream of the Lower Meghna, and in the Baleswar-Bishkali, and Pussur-Sibsa estuaries (Figure 5.22a and b)). Sea level rise limits the accretion potential of the Eastern Chars (Figure 5.22(b)), and keeps relatively more sediment on the inner shelf (Figure 5.22(c,d));
- Changes in the upstream discharge because of human interventions, and the associated reduction in total yearly sediment load cause a limited enhancement of sediment retention in the upstream part of the GBM delta (Figure 5.23(a)). However, this reduction in streamflow and sediment supply has major effects in the tidal part of the system. The Eastern Chars accrete significantly less than under natural conditions, and the Sundarbans erode less (Figure 5.23(b)). The eastern part of the inner shelf erodes more in this scenario, while the western part accretes more than under natural streamflow conditions (Figure 5.23(c,d))
- Subsidence leads to decreased accretion and more erosion in the tidal parts of the delta, and on the eastern part of the inner shelf. The Sundarbans (Arpangalia and Pussur-Sibsa) are particularly sensitive to subsidence, as is the Lower Meghna. The western part of the shelf is more or less stable under subsidence conditions (Figure 5.24(a-d));

- Retaining the streamflow, but reducing the sediment load by 50% causes less accretion in the Jamuna, and turn stable bed conditions to slight erosion in the Ganges and the Padma. The Lower Meghna and the Pussur-Sibsa estuaries become erosive. The Eastern Chars and the Tetulia channel have less accretion potential. The inner shelf becomes less erosive in the east, and less accretive in the west (Figure 5.25 (a-d));
- An increase in streamflow, and in total yearly sediment load, resulting from climate change has little effect on the system as compared to the other scenarios. On the inner shelf, erosion is reduced, and accretion is enhanced due to the availability of extra sediment (Figure 5.26(a-d))

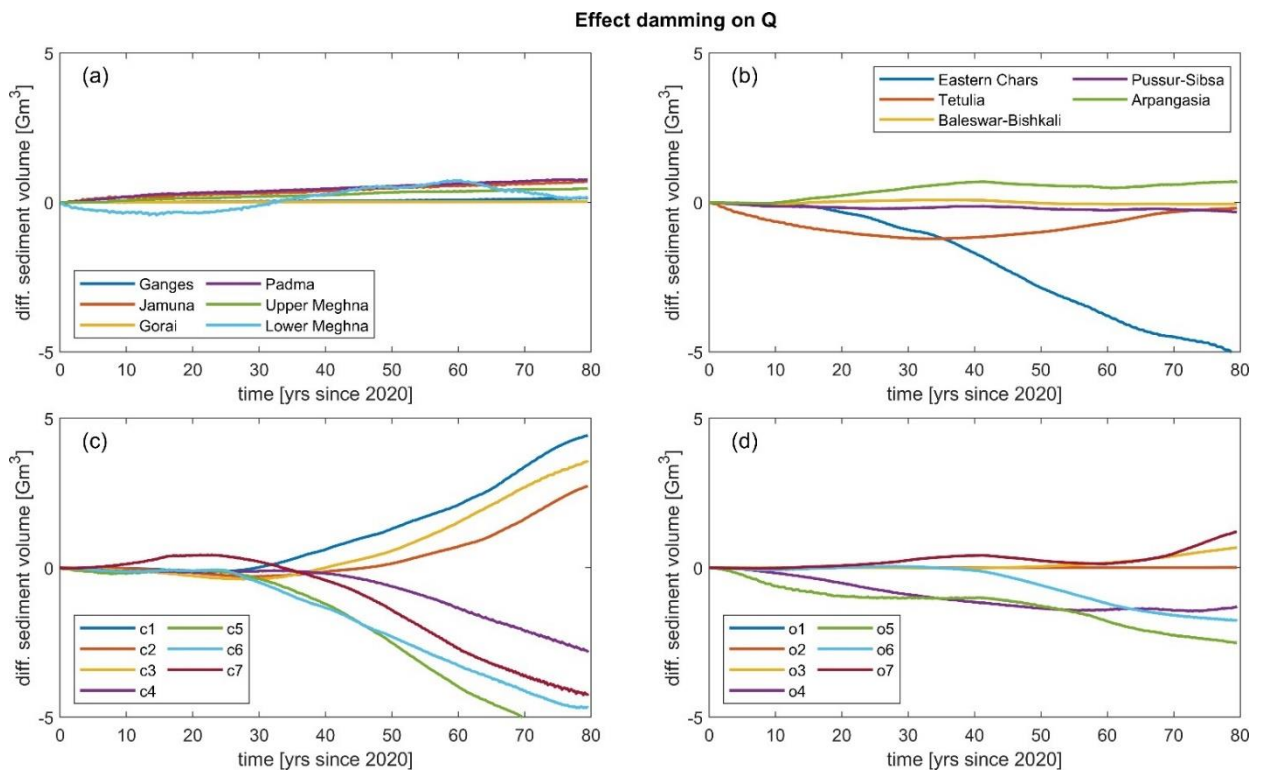


Figure 5.23 Differences in sediment volume [Gm³] in function of time as a result of upstream reduction in discharge within different parts of the GBM delta as defined in Figure 3.10.

Effect subsidence

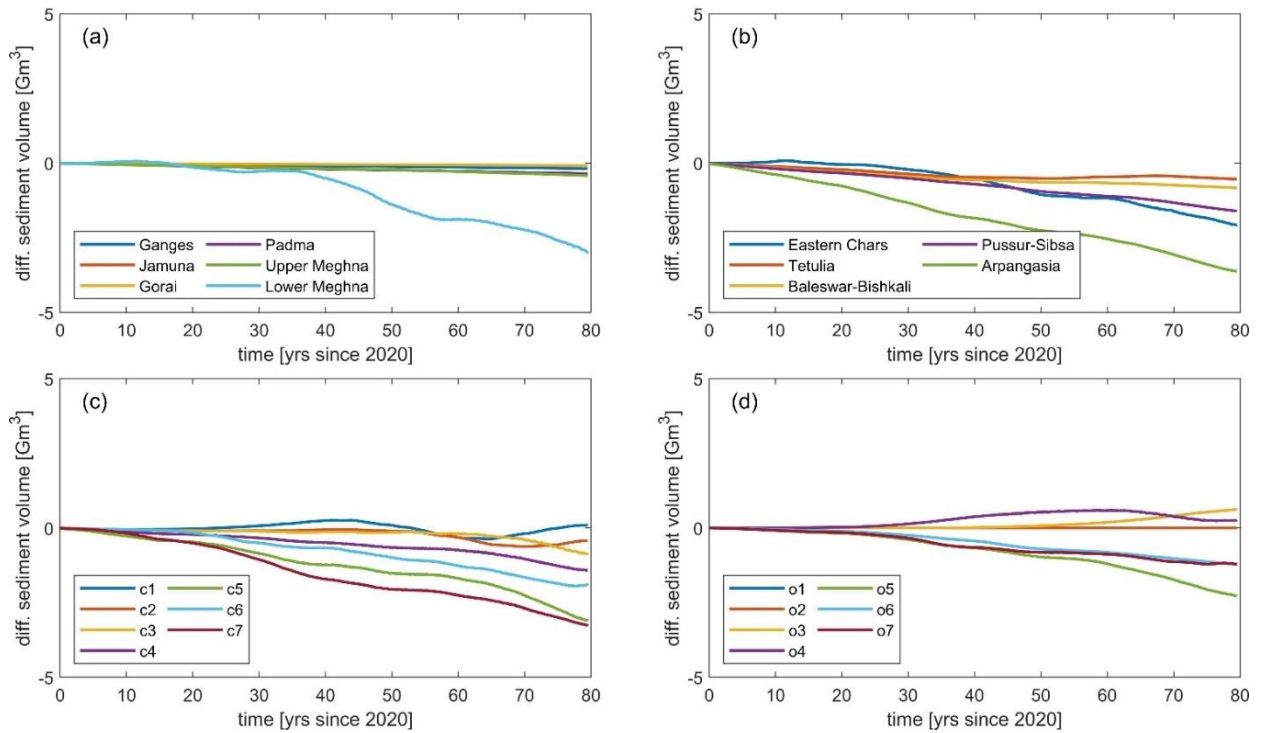


Figure 5.24 Differences in sediment volume [Gm^3] in function of time as a result of spatially varying subsidence within different parts of the GBM delta as defined in Figure 3.10.

Effect SSC reduction

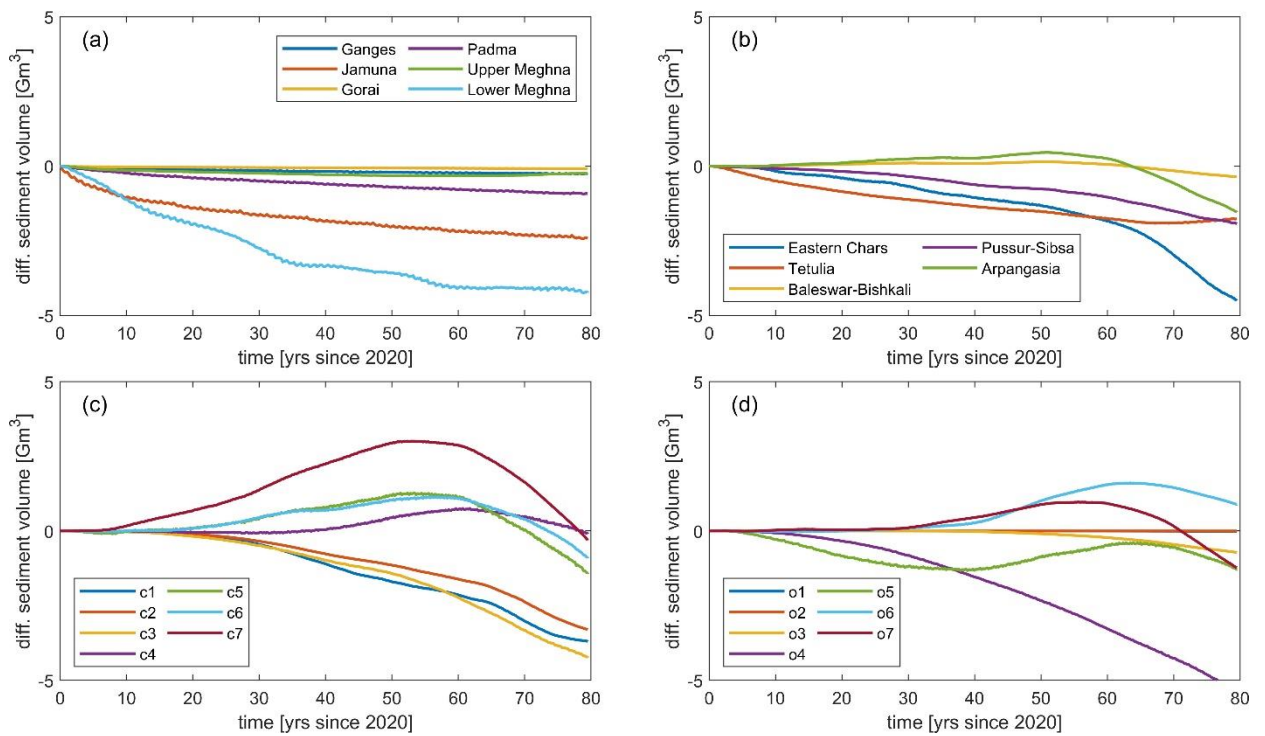


Figure 5.25 Differences in sediment volume [Gm^3] in function of time as a result of a 50% reduction of suspended sediment concentration within different parts of the GBM delta as defined in Figure 3.10.

Effect RCP8.5 vs RCP4.5 on Q

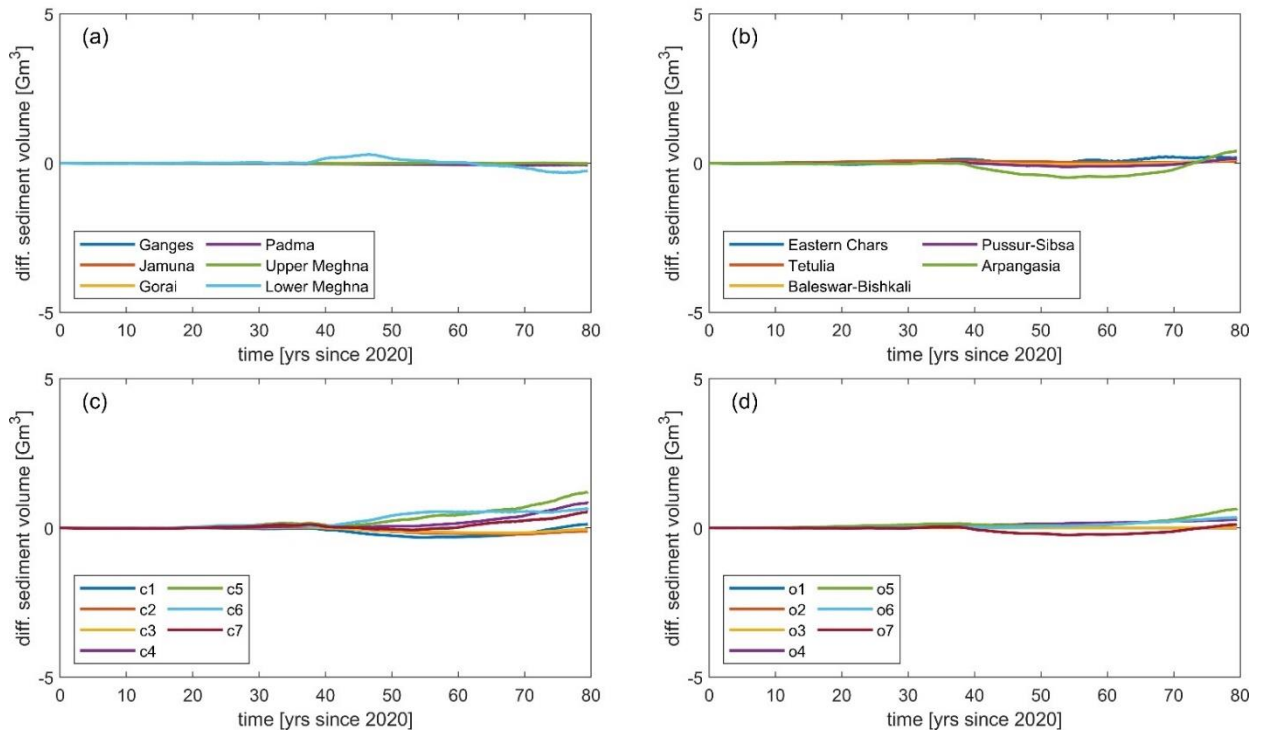


Figure 5.26 Differences in sediment volume [Gm³] in function of time as a result of using RCP8.5 instead of RCP4.5 to define upstream discharge boundaries. The different parts of the GBM delta are defined in Figure 3.10.

5.4.4 Land gain and loss

A very important parameter in assessing long-term morphology changes is the change in land and water surface area. Sarker et al. (2014) estimate that the land surface in Bangladesh increases by approx. 52 km²/yr due to sedimentation, while at the same time 32 km²/yr is lost to erosion, leading to a net change in land area of 20 km²/yr.

The Aqua Monitor (Donchyts et al., 2016), allows to inspect the land-to-water and water-to-land changes based on multiple satellite images taken over a period of 1-2 years. By adding up the pixels in each image and multiplying by the pixel size in km² total land gain, land loss and net area change can be derived from these images. This was done for the period of 1985-2016, the default in Aqua Monitor, and for 2000-2020.

Table 5.1 Observed land loss, land gain and net change in km²/yr, derived from Aqua Monitor..

	Gain (km ² /yr)	Loss (km ² /yr)	Net change (km ² /yr)
Aqua monitor 2000-2020	49	29	20
Aqua monitor 1986-2016	67	32	35
Estimate	58 +/- 10	30 +/- 5	27 +/- 10

The Aqua Monitor images are shown in Figure 5.27. There is a clear trend of sedimentation in the Padma and Lower Meghna and especially the Eastern Chars, while notably areas along Hatiya, The North side of Bhola and the areas along the Lower Meghna main channel suffer erosion.

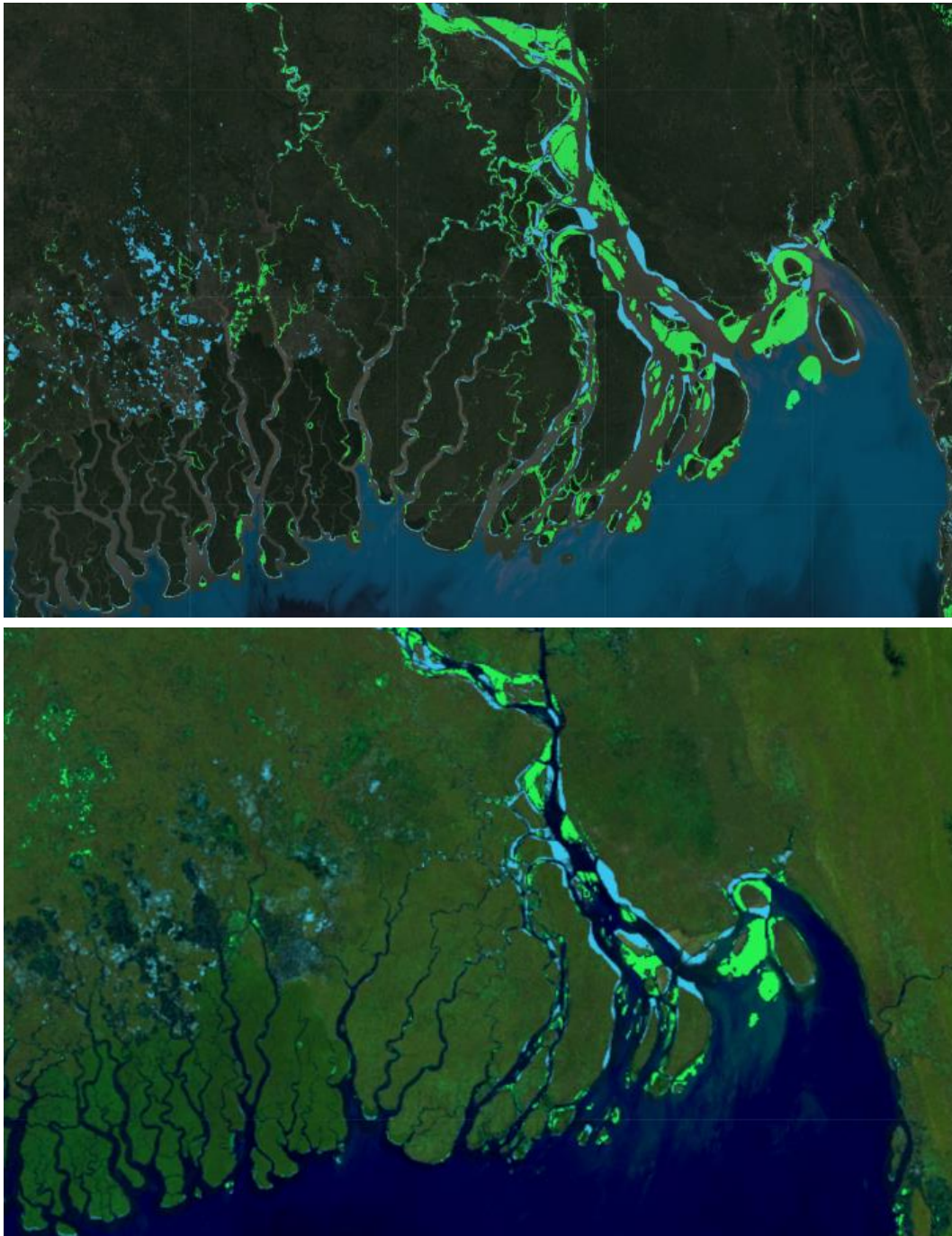


Figure 5.27 Two estimates of land gain (green) and loss (blue) from Aqua Monitor; 1985-2016 (top) and 2000-2020 (bottom).

The method to extract similar land-to-water and water-to-land changes from the model simulations has to take into account not only bed level but also water level variations; though different options could be chosen, 'land' was defined as all areas where the difference between the mean water level and the mean bed level was less than a criterion, chosen as 0.5 m, and 'water' as the areas with higher mean water depth. The averaging period was taken as 10 years, to account for the fact that the discharge forcing considered 10 different years that repeated, while undergoing slow trends of climate change.

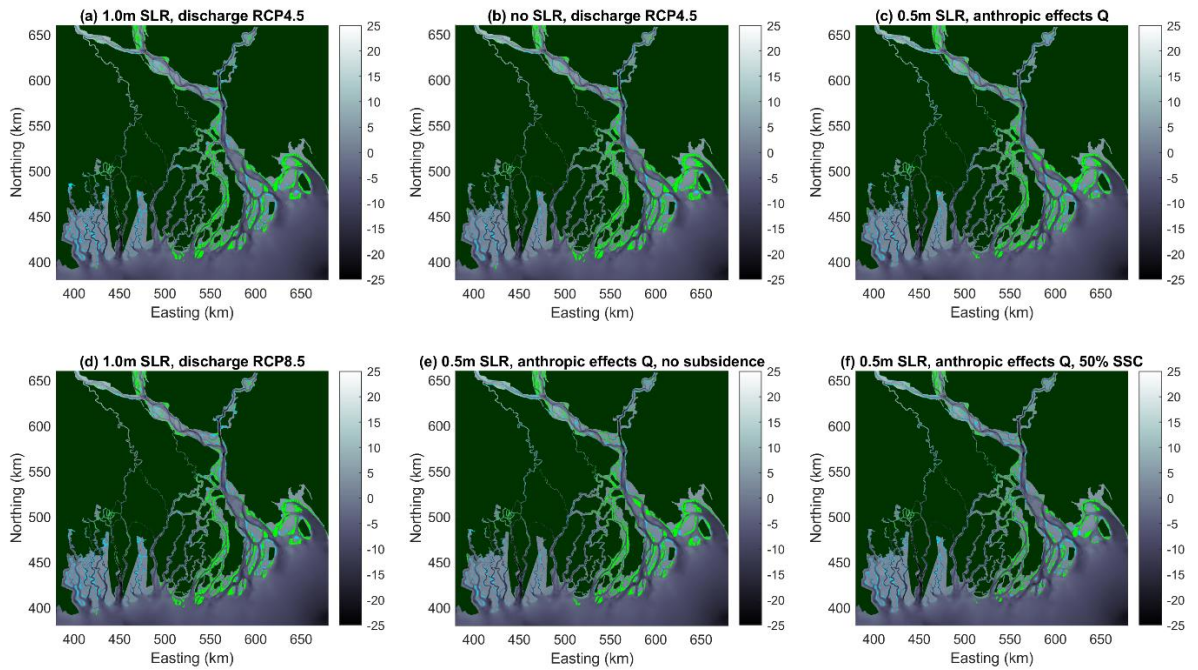


Figure 5.28 Simulated land gain due to sedimentation (green) and loss due to erosion or inundation (blue) for 2050-2060 relative to 2020-2030, for 6 different scenarios. Gray colour bar indicates bed levels.

In Figure 5.28 the land-water and water-land changes over a 30-year period, representative of changes up to 2050, are summarized for all runs. Clearly, differences between scenarios are smaller than the overall patterns, but still some conclusions can be drawn. Up to 2050, the effect of sea level rise is relatively small, as seen when comparing run (a) (+1m) with run (b) (0m). At this time horizon, only the variations in discharge have a visible effect on the land accretion areas; most conspicuously, a reduction in the upstream concentration in Ganges and Brahmaputra by 50% as in run (f) clearly leads to less sedimentation in the Eastern Chars.

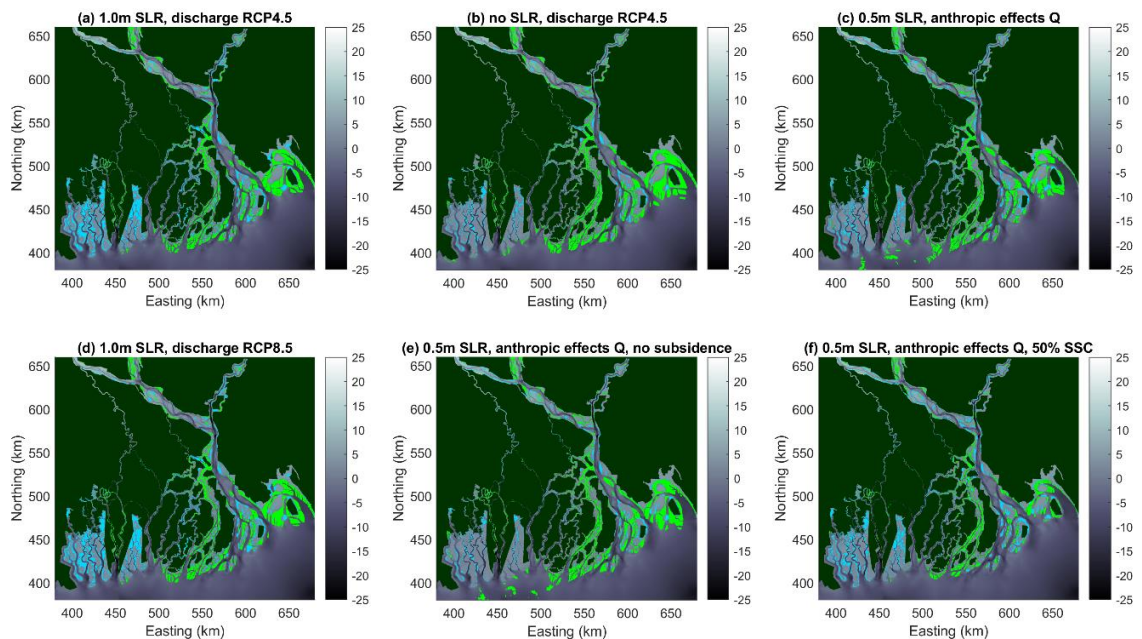


Figure 5.29 Simulated land gain due to sedimentation (green) and loss due to erosion or inundation (blue) for 2090-2100 relative to 2020-2030, for 5 different scenarios.

At the time horizon of 2100, as shown in Figure 5.29, anthropic effects on the river discharges have a limited effect of reducing sedimentation in the Eastern Chars. Sea level rise effects show up clearly in the Sundarbans, where substantial areas are lost, due to erosion and the rising water levels, as seen in runs (a) and (d).

The time series of total land gain, land loss and net change are shown in Figure 5.30. The following observations can be made:

- Land gain:
 - is not very sensitive to SLR, though it is highest in the no-SLR scenario;
 - in the long run would be higher without subsidence;
 - is very sensitive to the upstream sediment concentration
- Land loss:
 - is highest for the 1m SLR scenarios
 - is not very sensitive to the upstream discharge
 - Is lowest for no-SLR and no-subsidence scenarios
- Net change:
 - Is highest for no-SLR scenario (b) and for medium-SLR and no subsidence scenario (e)
 - Stabilizes around 2050 for scenario (c) with medium SLR and anthropic effects on discharge
 - Turns negative after 2050 for high-SLR (a), (d) or reduced upstream concentration (f) scenarios

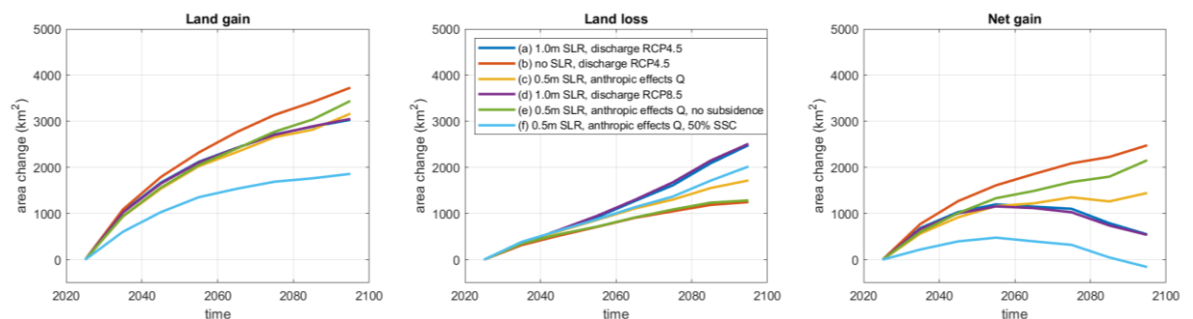


Figure 5.30 Simulated total land gain (km^2) due to sedimentation (left panel), land loss due to erosion and inundation (middle panel), and net land gain (right panel), 2020-2100.

The results in Figure 5.30 are quantified for the period 2020-2050 in Table 5.2 and for 2050-2100 in Table 5.3. Both land gain and land loss are in the same order of magnitude as the observed values in Table 5.1. The most significant deviation in this period is that due to a reduction in upstream sediment concentration. The sediment reduction actually has happened over the past decades according to Rahman et al. (2018).

After 2050 several scenarios point at a net reduction of the land area, either due to SLR or due to the expected reduction of upstream sediment concentration.

Table 5.2 Simulated land loss, land gain and net change in km²/yr , period 2020-2050.

Scenario	Land gain	Land loss	Net change
	km²/yr	km²/yr	km²/yr
(a) 1.0m SLR, discharge RCP4.5	70.7	30.8	40.0
(b) no SLR, discharge RCP4.5	77.5	23.7	53.7
(c) 0.5m SLR, anthropic effects Q	67.5	28.8	38.7
(d) 1.0m SLR, discharge RCP8.5	70.3	31.8	38.5
(e) 0.5m SLR, anthropic effects Q, no subsidence	68.4	24.0	44.4
(f) 0.5m SLR, anthropic effects Q, 50% SSC	45.2	29.2	15.9

Table 5.3 Simulated land loss, land gain and net change in km²/yr , period 2050-2100.

Scenario	Land gain	Land loss	Net change
	km²/yr	km²/yr	km²/yr
(a) 1.0m SLR, discharge RCP4.5	22.7	39.0	-16.3
(b) no SLR, discharge RCP4.5	35.1	13.4	21.7
(c) 0.5m SLR, anthropic effects Q	28.5	21.4	7.1
(d) 1.0m SLR, discharge RCP8.5	23.6	39.0	-15.4
(e) 0.5m SLR, anthropic effects Q, no subsidence	34.7	14.2	20.6
(f) 0.5m SLR, anthropic effects Q, 50% SSC	12.7	28.6	-15.9

6 Discussion

6.1 Performance of the models

This study has focused on developing a series of models that vary in complexity (from empirical to process-based), spatial scales (basin wide to individual rivers and estuaries), and temporal scales (from annual hydrographs to single tides). The distinct different approaches used for modelling ensure a substantiated outcome on the integral study results. Using this approach, the (deterministic) outcomes of the study will be placed in a context of uncertainty and can be evaluated accordingly. Moreover, the validation exercises shown in this study give for each model an indication on model performance and model uncertainty.

The **HydroTrend** hindcast model results for the reference scenario (1976-2006) capture the peak discharge in both the Ganges and Brahmaputra rivers well. Although the timing in the annual maximum (peak) discharge is modelled less accurate, the modelled hydrographs show close resemblance to the observed hydrographs. This is especially the case for the Brahmaputra river, and for a lesser extent for the Ganges river. The results show, however, that the performance of the model is largely dependent on the climate models (Deliverable D-4C) used as boundary conditions. Subsequently, the forecast results of water and sediment discharge (2006-2095) show a large range in projected output depending on the climate models used.

The **1D network model** for the GBM delta can simulate the river flow and suspended sediment transport distribution to the different river distributaries in the delta. However, due to the restrictions of the (1D) modelling approach and availability of field data, there are limitations of the present version of the model. These limitations of the model are discussed in the next paragraph and recommendations are made for further improvement of the model.

Concerning the calibration of the model an obvious remaining shortcoming of the model is the mismatch between the model results and the field observations for the water level in some upstream river channels. The simulated water level at e.g. Hardinge is lower than observed during dry season, and higher during wet season. Further reduction of the mismatch by changing e.g. the roughness in the model is not attempted during the calibration for several reasons. First, the model simulates a good flow distribution to the Gorai river, for which the water level at Hardinge is a key influencing factor. Second, a good agreement between the modelled and observed water level variations would require a physically unrealistic spatial and temporal variation of the roughness. A temporal variation of the roughness, which is not possible using Delft3D-FM, would be required because of the difference between model results and field observations. During wet season, a lower roughness in the upstream rivers than in the downstream boundaries would be required, although it is expected that it is physically the opposite. Third, as presented earlier, the mismatch is probably mainly due to the shortcomings in the used cross-sectional profiles in the model, for which the field data for the upper part (the flood plains) are too limited. Fourth, there is another possible data problem. The river discharges, prescribed at the upstream river boundaries, are not directly measured via flow velocity measurements. They are derived from water level measurements using water stage-discharge relations. The used relations are often not up to date and limited reliable. With these considerations it is recommended that further improvement of the model should be based on thorough analyses of the cross-sectional profiles and analyses of the water stage-discharge relations according to observations

The downstream (seawards) boundaries of the model are located at the mouths of the estuaries in the delta. An unavoidable data availability problem concerns the downstream boundary conditions for the suspended sediment transport concentrations. During flood, when inflow occurs at the boundaries, the sediment concentration needs to be prescribed at the open boundaries. Information for these boundary conditions at the mouths of the estuaries is not available from field observations and was based on the 2D model results. The constant conditions used in the present version of the model, however, imply that the model results on sediment transport in the most downstream part, i.e. within a distance in the order of the adaptation length for sediment concentration (flow velocity multiplied by water depth divided by settling velocity of sediment) from the boundaries, are not reliable. The model

could be improved by using time-varying information from the 2D model results for the downstream boundary conditions.

The **2D macro-scale Delft3D-FM** model has been setup and calibrated to a sufficient extent to simulate with a high confidence level morphological developments in the GBM delta over periods of up to decades (Appendix D). It is forced by relatively invariant tidal forcing far out in the Bay of Bengal, mean sea level, and by the discharges and sediment concentrations upstream in the Ganges, Jamuna and Meghna. Adding the Gorai river branch to connect the Ganges to the Pussur-Sibsa system, changing the roughness formulation and bringing down the bed roughness values, to better represent the influence of fine sediment beds, proved instrumental for improving the hydrodynamic calibration. The morphodynamic calibration, using an accelerated morphological modelling approach, was performed over the period 2000-2009. The accuracy of the outcome was sensitive to the transversal bed slope transport, dry cell erosion, and the inclusion of a sediment bed layer administration. Model results were slightly better by including wave effects. However, due to the high computational cost of running a coupled flow-wave model compared to the relatively limited improvements in results, it was decided to not include waves in the multi-decadal runs for the future scenarios.

Like any model, both the 1D model and the 2D model have limitations. As an example, concerning the sediment exchange between the Sundarbans and the coastal area both models simulate net export from the Sundarbans to the coast, whereas all information from the literature indicates the opposite. This is probably because both models ignore processes such as density flow driven by salinity gradients. The model results should therefore be interpreted and used in relative sense to identify the effects of changing environmental conditions and human interferences.

6.2 Lessons learned from the model results and future research

The active delta, the eastern part of the delta (locations 18, 21, 24 in Figure 3.10), receives the major part of the sediment supplied by the rivers (Figure 4.5 - Figure 4.8). The sediment supply is much more than needed for the area to grow with the rising sea level; the sedimentation rate here is limited by accommodation space available (see Chapter 2.5). Accordingly, the models indicate that in the future scenarios the morphological development is controlled by the upstream supply of sediment (Figure 5.3) and sea level rise has a subordinate effect (Figure 5.11, Figure 5.16, Figure 5.18, Figure 5.22 - Figure 5.26). Specifically, accretion on the Eastern Chars is significantly less under scenarios of reduced sediment supply and the Lower Meghna can even become erosive under a strong reduction (50%) of sediment load.

The river channels in the embanked (polder) area of the delta receive significantly less sediment from the upstream rivers than the active delta. The channels are considered sediment supply limited. Due to the smaller sediment supply, the estuaries have less capability to grow with sea level rise (Figure 5.18). The impact of subsidence is aggravated in the polder area because subsidence is largest here (Figure 3.8), and because the capability to fill the extra accommodation space available is limited. These observations show that the effects of relative SLR are larger in the polder area than in the active delta.

The Sundarbans area is considered accommodation space limited as the area can keep up with SLR. The sediment sources for the area are partly fluvial and partly marine. The models, however, fail to reproduce the marine import of sediment. The future scenarios indicate erosion in the Sundarbans due to relative SLR and thus a change to a supply limited system (Figure 5.21). The loss of land that is simulated under relative SLR scenarios (Figure 5.29) should be considered carefully because it is likely that sedimentation in the area is able to keep up with relative SLR due to the marine supply of sediment.

Considering the trends for the subregions described above, we can summarize for the delta as a whole that both models indicate that the changes of flow discharge and sediment transport from the upstream rivers have more effects on sediment dynamics in the delta than relative SLR. This means that the response of the morphological development of the delta lags the changing relative SLR, because the relative SLR does not cause an increase in sediment dynamics (e.g. additional import). Therefore, the rate of adjustment is influenced by the future changes in flow discharge and sediment transport. The fluvial sediment input from the river basins forms thus a very important control for delta

development. Increased sediment input in the future, due to climate change causing higher river discharge, causes more sedimentation, especially in the mouth area of the lower Meghna. Relative SLR has a less direct effect on the sediment dynamics, although a higher SLR rate does cause slightly more sedimentation throughout the delta. Land subsidence has a similar effect as SLR, even though it results into a net bed level lowering rather than a heightening in the case of SLR. The subordinate effect of relative SLR (the combined effect of SLR and land subsidence) on sediment dynamics implies that its effect on the morphological changes is most important with respect to the changing MSL. This is best illustrated by the analysis on land loss versus land gain. Relative SLR causes land loss and future accelerated SLR can turn the present net gain into net loss. According to the model results (Figure 5.30 and Table 5.3), this occurs if a value of 1.0 m SLR in 2100 is used and the upstream sediment supply remains unchanged. This effect is further aggravated when the upstream supply of water and sediment is significantly reduced, emphasizing the controlling factor of the upstream supply.

The importance of the changes in upstream river discharge and sediment transport, as shown by the model results, also mean that the distribution of the river flow and sediment transport to the distributaries will be a controlling factor in the development of the different parts of the delta. The discharge and sediment transport to the Gorai river control the development of the Sundarbans. The fluvial sediment input via the Gorai river is a direct sediment source for the Sundarbans to grow with the rising sea level, and the river flow to the Gorai also influences the sediment exchange between the Sundarbans and the coastal zone. The discharge and sediment transport to the Arial Khan river control the development of the estuaries in the middle part of the delta where the intertidal areas have been embanked into polders.

Furthermore, the 1D and 2D models indicate that mud transport is more important than sand transport for the morphological changes in the delta, although the deeper parts of the channels are dominated by coarser sandy sediments. The field data concerning the sediment load from the upstream rivers already suggested this, and the model results confirm that for the major part of the delta the morphological development is determined by mud transport.

7 Conclusions

7.1 Conclusions on model development

The modelling work within the project is carried out to improve our understanding of the long-term and large-scale dynamics of the Ganges-Brahmaputra-Meghna (GBM) delta. In this report there is focus on understanding and predicting the macro-scale (i.e. scale of the whole delta) morphodynamic processes. For this purpose, three types of models have been developed that cover the larger domain of the GBM catchment and delta (including the coastal zone):

- A basin scale hydrology model (HydroTrend). This model has been developed to simulate (future) sediment fluxes at the apex of the GBM delta. The model results of the annual mean and peak discharge (averaged over the period 1976-2000) compare well to observations. There are differences in the timing of hydrograph, which is inherent to the chosen model setup: simulations were calibrated to capture the magnitude of the peak discharge well instead of having the most accurate timing. The modelled sediment load compares well to literature values in the Ganges, but underestimates the values in the Brahmaputra. The reason for this is a large uncertainty in precipitation input for the model, and the fact that sediment discharge estimates for the Brahmaputra basin are not commonly found in the literature, and are highly variable. Future work will attempt to better constrain the sediment discharge in the Brahmaputra basin, both through detailed observations and modelling efforts.
- A 1D river branch model. This model has been developed as a computational efficient tool to estimate the distribution of discharge and suspended sediment load over the main tributaries of the GBM delta. The model compares well to observations of discharge in the Gorai and Padma and compares reasonably well to known values of sediment load in the Gorai and Arial Khan. Therefore, the model is considered appropriate to simulate the distribution of suspended sediment in the upstream part of the GBM delta. For the downstream part boundary conditions of incoming sediment fluxes need to be improved based on understanding gained in this project.
- A 2D large-scale coastal model. This model has been developed to simulate hydrodynamics, sediment transport (bed- and suspended load), morphological change and bank line changes in the GBM delta. Using flexible mesh advantages and morphological acceleration techniques with schematized boundary conditions, the model can robustly run 25-year morphodynamics within acceptable computational times (order of one week on a computational cluster). The model produces physically reasonable distributions of bed sediment composition, concentration patterns, net sedimentation areas, and agrees well to gross and net volumetric changes compared to observations. After various modifications of the 2D model, it has proven capable of simulating up to the year 2100 in continuous runs, with gradual and consistent behaviour. The addition of the 'dry-cell erosion' approach to bank line changes has been valuable in simulating land-to-water and water-to-land area changes and led to a more realistic behaviour of channels encroaching on banks. The total areas of land gain, land loss and net gain were in the correct order of magnitude compared with current trends.

7.2 Insights into the delta development and effects of climate change and human interference

Scenario simulations were carried out to study the morphodynamics of the GBM delta and investigate the effects of sea level rise, land subsidence, upstream discharge regime and the effects of a lower upstream sediment concentration. The model results improved our understanding of the development of the GBM delta and the effects of climate change and human interferences.

Under current conditions:

- Approximately 1/3th of the fluvial sediment input is exported to the deep sea, and the other 2/3th is deposited in the delta area, which agrees with literature.
- The major part of the river discharge and sediment input is transported through the Lower Meghna, being the active delta building estuary. Here, the estuary bifurcates into multiple outlets and the model results show that the most eastern outlet is increasing in importance, indicating that the eastwards building up of the delta, as reported in the geological studies, is continuing.

The effects of sea level rise are:

- A general trend of sedimentation in the tidally influenced part of the delta, however an order of magnitude less than the sea level rise itself.
- A tendency towards net land loss, especially after 2050, due to increased inundation.
- A relatively minor effect on long-term average concentrations and sediment transport patterns.

The effect of land subsidence is:

- An exacerbation of the effects of sea level rise; a SLR of 0.5 m by 2100 combined with subsidence approximately has the same effect as a 1m SLR.
- A relatively minor effect on the long-term average concentrations and sediment transport patterns.

The climate change effect on upstream discharges, according to the HydroTrend projections, is to increase discharges; this has a mildly positive effect on the sedimentation in the Lower Meghna area.

The anthropogenic effects on the upstream boundaries as simulated, are:

- An important reduction of the discharge and sediment load in Ganges and Brahmaputra;
- A strong reduction in the sedimentation in the Lower Meghna area and the shelf in front of the Sundarbans
- Relatively minor effects on land gain and loss.

A reduction of the upstream concentration, with the same discharge, leads to

- General erosion in all riverine and estuarine areas;
- A much-reduced (1/3th) land gain up to 2050 and net land loss after 2050.

In summary,

- The Macro scale development of the current GBM delta is dominated by sediment supply. Changes of the sediment dynamics in the GBM delta are mainly influenced by the changes in the river flow regime and the sediment transport regime at the upstream boundary of the models for the delta. The river flow regime and the sediment transport regime are influenced by climate change (change in precipitation, vegetation and upstream erosion) and human interferences in the river basins.
- SLR and subsidence, which combine to the relative SLR, have relatively limited influence on the current sediment dynamics of the GBM Delta, therefore limited influence on the sedimentation-erosion dynamics.
- Nevertheless, an increase in relative SLR will cause more sedimentation in the delta, however the increased sedimentation will not compensate the direct effect of relative SLR. Consequently, an increase in relative SLR has an important effect on the balance of land loss and gain. Hence an increase in relative SLR causes loss / less gain of land in the delta.
- Accelerated SLR in the future could result in to net loss of land in the delta.
- The importance of the river flow regime and sediment input from the rivers, as learned from the model results, implies that the distribution of the river discharge and sediment transport to the distributaries, like the Gorai river and Arial Khan river, will be important for the future development of the different parts of the delta. Regulation of the distributions to these distributaries are potentially important measures for the future management of the delta.

8 References

- Akter, J., Sarker, M. H., Popescu, I., & Roelvink, D. (2016a). Evolution of the Bengal Delta and Its Prevailing Processes. *Journal of Coastal Research*, 321, 1212–1226. <https://doi.org/10.2112/jcoastres-d-14-00232.1>
- Allison, M., Khan, S. R., Goodbred, S., & Kuehl, S. (2003). Stratigraphic evolution of the late Holocene Ganges–Brahmaputra lower delta plain. *Sedimentary Geology*, 155, 317–342. [https://doi.org/10.1016/S0037-0738\(02\)00185-9](https://doi.org/10.1016/S0037-0738(02)00185-9)
- Bangladesh Water Development Board (2012a). Coastal Embankment Improvement Project, Phase-I (CEIP-I). Volume I: Main Report.
- Barua, D. K., Kuehl, S. A., Miller, R. L., and Moore, W. S. (1994). Suspended sediment distribution and residual transport in the coastal ocean off the Ganges-Brahmaputra river mouth. *Marine Geology*, 120(1-2), 41-61.
- Chakrapani, G. J., Subramanian, V., Gibbs, R. J., and Jha, P. K. (1995). Size characteristics and mineralogy of suspended sediments of the Ganges River, India. *Environmental Geology*, 25(3), 192-196.
- Coleman, J. M. (1969). Brahmaputra river: Channel processes and sedimentation. *Sedimentary Geology*, 3(2), 129–239. [https://doi.org/10.1016/0037-0738\(69\)90010-4](https://doi.org/10.1016/0037-0738(69)90010-4)
- Darby, S. E.; Dunn, F.E.; Nicholls, R. J.; Rahman, M.; Ridly, L., 2015. A first look at the influence of anthropogenic climate change on the future delivery of fluvial sediment to the Ganges–Brahmaputra–Meghna delta. *Environmental Science: Processes & Impacts*, 17, 1587–1600. [10.1039/C5EM00252D](https://doi.org/10.1039/C5EM00252D).
- Datta, D. K., and Subramanian, V. (1997). Texture and mineralogy of sediments from the Ganges–Brahmaputra–Meghna river system in the Bengal Basin, Bangladesh and their environmental implications. *Environmental Geology*, 30(3-4), 181-188.
- DHI, Deltares, UNESCO-IHE, IWM, University of Colorado, & Columbia University. (2019). Coastal Embankment Improvement Project, Phase-I (CEIP-I) Long - Long Term Monitoring, Research and Analysis of Bangladesh Coastal Zone (Sustainable Polders Adapted to Coastal Dynamics). Inception report. Retrieved from <http://www.hydrology.bwdb.gov.bd/>
- Donchyts, G., Baart, F., Winsemius, H. et al. Earth's surface water change over the past 30 years. *Nature Clim Change* 6, 810–813 (2016). <https://doi.org/10.1038/nclimate3111>
- D'Alpaos, A., Lanzoni, S., Marani, M., & Rinaldo, A. (2010). *On the tidal prism – channel area relations*. *Journal of Geophysical Research*, 115(F01003), 1–13. <https://doi.org/10.1029/2008JF001243>
- Eckland, A., Overeem, I., Diermanse, F., Giardino, A., Dunn, F. E., and Kamal, F. (2022). *Modeling the recent and future water and sediment discharge regime of the Ganges-Brahmaputra delta in response to a changing climate* [Unpublished manuscript]. Department of Geological Sciences and Institute of Arctic and Alpine Research, University of Colorado Boulder.
- Egbert, G. D., & Erofeeva, S. Y. (2002). *Efficient inverse modeling of barotropic ocean tides*. *Journal of Atmospheric and Oceanic Technology*, 19(2), 183–204. [http://doi.org/10.1175/1520-0426\(2002\)019<0183:EIMOBO>2.0.CO;2](http://doi.org/10.1175/1520-0426(2002)019<0183:EIMOBO>2.0.CO;2)
- EGIS, 2001. Remote Sensing, GIS and Morphological Analyses of the Jamuna River: 2000, Part II. Dhaka, Bangladesh: EGIS for Water Resources Management, 66p.
- Fergusson, J. (1863). On Recent Changes in the Delta of the Ganges. *Quarterly Journal of the Geological Society*, 19(1–2), 321 LP – 354. <https://doi.org/10.1144/GSL.JGS.1863.019.01-02.35>
- Galappatti, R., Olesen, K. W., & Khan, A. S. (1996). Schematizing Large Active Rivers for Morphological Computations : Experience From Bangladesh.
- Garzanti, E., Andò, S., France-Lanord, C., Vezzoli, G., Censi, P., Galy, V., and Najman, Y. (2010). Mineralogical and chemical variability of fluvial sediments: 1. Bedload sand (Ganga–Brahmaputra, Bangladesh). *Earth and Planetary Science Letters*, 299(3-4), 368-381.

- Godin, G. (1972). *The Analysis of Tides*. University of Toronto Press, 264 pp.
- Goodbred, S., & Kuehl, S. (2000a). Enormous Ganges–Brahmaputra sediment discharge during strengthened early Holocene monsoon. *Geology*, 28, 1083–1086. [https://doi.org/10.1130/0091-7613\(2000\)28<1083:EGSDDS>2.0.CO;2](https://doi.org/10.1130/0091-7613(2000)28<1083:EGSDDS>2.0.CO;2)
- Goodbred, S., & Kuehl, S. (2000b). The significance of large sediment supply, active tectonism, and eustasy on margin sequence development: Late Quaternary stratigraphy and evolution of the Ganges-Brahmaputra delta. *Sedimentary Geology*, 133, 227–248. [https://doi.org/10.1016/S0037-0738\(00\)00041-5](https://doi.org/10.1016/S0037-0738(00)00041-5).
- Hagenaars, G., de Vries, S., Luijendijk, A. P., de Boer, W. P., & Reniers, A. J. H. M. (2018). On the accuracy of automated shoreline detection derived from satellite imagery: A case study of the sand motor mega-scale nourishment. *Coastal Engineering*, 133(June 2017), 113–125. <https://doi.org/10.1016/j.coastaleng.2017.12.011>.
- Hersbach, H., Bell, B., Berrisford, P., Hirahara, S., Horányi, A., Muñoz-Sabater, J., ... Thépaut, J.-N. (n.d.). The ERA5 global reanalysis. *Quarterly Journal of the Royal Meteorological Society*, n/a(n/a). <https://doi.org/10.1002/qj.3803>
- Higgins, S., Overeem, I., Rogers, K., Kalina, E., 2018. River linking in India: Downstream impacts on water discharge and suspended sediment transport to deltas. *Elementa*, 6, 1:20. DOI: 10.1525/elementa.269
- Islam, M. R., Begum, S. F., Yamaguchi, Y., & Ogawa, K. (1999). The Ganges and Brahmaputra rivers in Bangladesh: Basin denudation and sedimentation. *Hydrological Processes*, 13(17), 2907–2923. [https://doi.org/10.1002/\(SICI\)1099-1085\(19991215\)13:17<2907::AID-HYP906>3.0.CO;2-E](https://doi.org/10.1002/(SICI)1099-1085(19991215)13:17<2907::AID-HYP906>3.0.CO;2-E)
- Islam, M. R., Yamaguchi, Y., and Ogawa, K. (2001). Suspended sediment in the Ganges and Brahmaputra Rivers in Bangladesh: observation from TM and AVHRR data. *Hydrological Processes*, 15(3), 493-509. Jansen et al., 1979
- IWM; Institute for Water Modelling (2009) Use existing data on available digital elevation models to prepare useable Tsunami and storm surge inundation risk maps for the entire coastal region vol II. Institute of Water Modelling.
- IWM; Institute for Water Modelling (2010). Estuary Development Programme – EDP. Updating of Hydrodynamic & Morphological Models to Investigate Land Accretion & Erosion in the Estuary Development Program (EDP) Area.
- Kernkamp, H. W. J., Van Dam, A., Stelling, G. S., & De Goede, E. D. (2011). Efficient scheme for the shallow water equations on unstructured grids with application to the Continental Shelf. *Ocean Dynamics*, 61(8), 1175–1188. <https://doi.org/10.1007/s10236-011-0423-6>
- Kettner, A. J. & Syvitski, J. P. M. HydroTrend v.3.0: A climate-driven hydrological transport model that simulates discharge and sediment load leaving a river system. *Comput. Geosci.* 34, 1170–1183 (2008).
- Kettner, A.J.; Gomez, B.; Syvitski, J.P.M. 2007. Modeling suspended sediment discharge from the Waipaoa River system, New Zealand: The last 3000 years. *Water Resources Research*, 43, . 10.1029/2006WR005570
- Kettner, A. J.; Restrepo, J. D.; Syvitski, J. P. M.; 2010. A Spatial Simulation Experiment to Replicate Fluvial Sediment Fluxes within the Magdalena River Basin, Colombia. *The Journal of Geology*, 118, 363–379. 10.1086/652659
- Kuehl, S., Allison, M., Goodbred, S., & Kudrass, H. (2005). The Ganges–Brahmaputra Delta. In *River Deltas - Concepts, Models and Examples* (Vol. 83, pp. 413–434). <https://doi.org/10.2110/pec.05.83.0413>.
- Kuehl, S. A., Hariu, T. M., and Moore, W. S. (1989). Shelf sedimentation off the Ganges-Brahmaputra river system: Evidence for sediment bypassing to the Bengal fan. *Geology*, 17(12), 1132-1135.

- Lehner, B., Liermann, C.R., Revenga, C., Vorosmarty, C., Fekete, B., Crouzet, P., Doll, P., Endejan, M., Frenken, K., Magome, J., Nilsson, C., Robertson, J. C., Rodel, R., & Sindorf, N. (2001). Global Reservoir and Dam Database, Version 1 (GRanDv1): Dams, Revision 01 [Data set]. <https://doi.org/10.7927/H4N877QK>
- Lehner, Bernhard, Liermann, C. R., Revenga, C., Vörösmarty, C., Fekete, B., Crouzet, P., Döll, P., Endejan, M., Frenken, K., Magome, J., Nilsson, C., Robertson, J. C., Rödel, R., Sindorf, N., & Wisser, D. (2011). High-resolution mapping of the world's reservoirs and dams for sustainable river-flow management. *Frontiers in Ecology and the Environment*, 9(9), 494–502. <https://doi.org/10.1890/100125>
- MES II (Meghna Estuary Study), 2001. Hydro-Morphological Dynamics of the Meghna Estuary. Dhaka, Bangladesh: MES II, 80p.
- Morehead, Mark D.; Syvitski, James P.; Hutton, Eric W.H.; Peckham, Scott D.; 2003. Modeling the temporal variability in the flux of sediment from ungauged river basins. *Global and Planetary Change*, 39, 95–110. 10.1016/S0921-8181(03)00019-5
- Morgan, J.P. and McIntire, W.G., 1959. Quaternary geology of the Bengal Basin, East Pakistan and India. *Bulletin of the Geological Society of America*, 70, 319–342.
- O'Brien, & P., M. (1931). Estuary tidal prisms related to entrance areas. *Civil Engineering*. Retrieved from <http://ci.nii.ac.jp/naid/10016529954/en/>
- Partheniades, E., 1965. "Erosion and Deposition of Cohesive Soils." *Journal of the Hydraulics Division, ASCE* 91 (HY 1): 105–139. January.
- Payo, A., Mukhopadhyay, A., Hazra, S., Ghosh, T., Ghosh, S., Brown, S., ... Haque, A. (2016). Projected changes in area of the Sundarban mangrove forest in Bangladesh due to SLR by 2100. *Climatic Change*, 139(2), 279–291. <https://doi.org/10.1007/s10584-016-1769-z>
- Rahman, Munsur; Dustegir, Maruf; Karim, Rezaul; Haque, Anisul; Nicholls, Robert J.; Darby, Stephen E.; Nakagawa, Hajime; Hossain, Motahar; Dunn, Frances E.; Akter, Marin; 2018. Recent sediment flux to the Ganges-Brahmaputra-Meghna delta system. *Science of The Total Environment*, 643, 1054–1064. 10.1016/j.scitotenv.2018.06.147
- Roelvink, D., & Reniers, A. (2011). *A Guide to Modeling Coastal Morphology*. <https://doi.org/10.1142/7712>
- Sarker, M. H., Akter, J., & Rahman, M. M. (2013). Century-Scale Dynamics of the Bengal Delta and Future Development. 4th International Conference on Water & Flood Management (ICWFM-2013), (August), 91–104.
- Sarker, M. H., Thorne, C. R., Aktar, M. N., and Ferdous, M. R. (2014). Morpho-dynamics of the Brahmaputra–Jamuna River, Bangladesh. *Geomorphology*, 215, 45-59.
- Singh, M., Singh, I. B., and Müller, G. (2007). Sediment characteristics and transportation dynamics of the Ganga River. *Geomorphology*, 86(1-2), 144-175.
- Stummeyer, J., Marchig, V., and Knabe, W. (2002). The composition of suspended matter from Ganges–Brahmaputra sediment dispersal system during low sediment transport season. *Chemical Geology*, 185(1-2), 125-147.
- Syvitski, J.P.M. and Milliman, J.D., 2007, Geology, geography and humans battle for dominance over the delivery of sediment to the coastal ocean. *J. Geology* 115, 1–19.
- Uddin, M., Alam, J. Bin, Khan, Z. H., Jahid Hasan, G. M., & Rahman, T. (2014). Two Dimensional Hydrodynamic Modelling of Northern Bay of Bengal Coastal Waters. *Computational Water, Energy, and Environmental Engineering*, 03(04), 140–151. <https://doi.org/10.4236/cweee.2014.34015>
- Umitsu, M. (1985). Natural Levees and Landform Evolutions in the Bengal Lowland. 58(2), 149–164.
- Umitsu, M. (1993). Late quaternary sedimentary environments and landforms in the Ganges Delta. *Sedimentary Geology*, 83(3–4), 177–186. [https://doi.org/10.1016/0037-0738\(93\)90011-S](https://doi.org/10.1016/0037-0738(93)90011-S)
- VanRijn, L.C. (2007a). Unified view of sediment transport by currents and waves. I: Initiation of motion, bed roughness, and bed-load

- transport. *Journal of Hydraulic Engineering*, 133(6), 649–667. [https://doi.org/10.1061/\(ASCE\)0733-9429\(2007\)133:6\(649\)](https://doi.org/10.1061/(ASCE)0733-9429(2007)133:6(649))
- VanRijn, L. C. (2007b). Unified view of sediment transport by currents and waves. II: Suspended transport. *Journal of Hydraulic Engineering*, 133(6), 668–689. [https://doi.org/10.1061/\(ASCE\)0733-9429\(2007\)133:6\(668\)](https://doi.org/10.1061/(ASCE)0733-9429(2007)133:6(668)).
- Wang, Z. B., Winterwerp, J. C., & He, Q. (2014). Interaction between suspended sediment and tidal amplification in the Guadalquivir Estuary. *Ocean Dynamics*, 64(10), 1487–1498. <https://doi.org/10.1007/s10236-014-0758-x>.
- Wang, Z.B.; Elias, E.P.L.; Van der Spek, A.J.F.; Lodder, Q.J. (2018). Sediment budget and morphological development of the Dutch Wadden Sea-impact of accelerated sea-level rise and subsidence until 2100. *Neth. J. Geosci.* 2018, 97, 183–214.
- Williams, C. A. (1919). History of the Rivers in the Gangetic Delta, 1750-1918. Retrieved from <https://books.google.com.bd/books?id=tLfgOwAACAAJ>.
- Wilson, C. A., & Goodbred, S. L. (2015). Construction and Maintenance of the Ganges-Brahmaputra-Meghna Delta: Linking Process, Morphology, and Stratigraphy. *Annual Review of Marine Science*, 7(1), 67–88. <https://doi.org/10.1146/annurev-marine-010213-135032>
- Winterwerp, J. C., Lely, M., & He, Q. (2009). Sediment-induced buoyancy destruction and drag reduction in estuaries. *Ocean Dynamics*, 59(5), 781–791. <https://doi.org/10.1007/s10236-009-0237-y>
- Ya-feng, S., Tze-chu, H., Pen-hsing, C., & Chi-chun, L. (1980). Distribution, features and variations of glaciers in China. *World Glacier Inventory: Proceedings of the Riederalp Workshop*, 126, 111–116.

Appendices

A Data

Appendix A describes the data gathered and used for the model setup, calibration, and validation. Appendix A is attached at the end of this document.

B Development catchment hydrology model (HydroTrend)

Appendix B describes the development of a catchment hydrology model that simulates the water and sediment fluxes from the Ganges and Brahmaputra catchments at the apex of the GBM delta. Appendix B is attached at the end of this document.

C Development river network model (Delft3D-FM 1D)

Appendix C describes the development of a river network model that simulates the distribution of water and sediment over the major and most important delta tributaries in the GBM delta. Appendix C is attached at the end of this document.

D Development coastal model (Delft3D-FM 2D)

Appendix D describes the development of a large-scale depth averaged model that includes the major delta tributaries in the GBM delta as well as the coastal zone and a part of the Bay of Bengal. The model simulates the fluvial-tidal dynamics, sediment transport, and morphological developments. Appendix D is attached at the end of this document.

A Data

The macro-scale models cover a vast area of the GBM delta, and consequently, require an enormous amount of data (in-situ and remote sensed observations) of the various physical properties to force the model and to compare with model output. In this chapter all data used for the analysis, model input, and validation is described. For a more in-depth description of all data, however, reference is made to the data report of the project (Deliverable D-3; Database design).

A.1 Coordinate systems

A.1.1 Horizontal reference system

All data and models in this report are using the Bangladesh Universal Transverse Mercator (BTM) horizontal coordinate system. The BTM datum is a local projected coordinate system, which has the advantage over a global geographic system that the units are given in linear measurements (e.g. meters) rather than angular degrees. Usually, the globally available Universal Transverse Mercator (UTM) grid can be used for this purpose. The country of Bangladesh, however, is covered by two UTM tiles (UTM45N and UTM46N) which makes usage impractical. To overcome this problem a new horizontal reference system was developed in the Flood Action Plan 19 (FAP 19) in May 1992¹. Since then this reference system is used for official cartography. The projection parameters of the BTM system and transformation parameters from the global WGS84 system to BTM are shown in TableApx A.1.

TableApx A.1 Projection parameters of the BTM coordinate system and conversion parameters from WGS84.

Parameter	Value
Projection parameters	
Ellipsoid	Everest Modified Bangladesh
Projection method	Transverse Mercator
Latitude of origin	0°N
Central meridian	90°
False Northing, Easting	-2,000,000 m; 500,000 m
Scale factor	0.9996
Datum transformation parameters	
Semi-major axis	6,377,298.52400
Semi-minor axis	6,356,097.52000
Inverse Flattening 1/F	300.80170000
Rotation X, Y, Z	0, 0, 0
Translation X, Y, Z	-288.000 m, -735.000 m, -255.000 m

The BTM coordinate system is not documented in the online registry of the official EPSG Geodetic Parameter Dataset (the database for coordinate reference systems and transformation parameters), thus does not have a unique EPSG code assigned to it. The Gulshan 303 coordinate system, however,

¹ <http://socolzahid-en.blogspot.com/2012/07/bangladesh-transverse-mercator-btm.html>

has a unique EPSG code assigned to it: 3106², and the BTM system is equal to the Gulshan 303 but comprises a false northing of 2,000 km (see TableApx A.1).

A.1.2 Vertical datum

The vertical reference system used throughout the report (data and models) is the Public Works Department datum (PWD). This national vertical reference datum is maintained by the Survey of Bangladesh (SoB) through 465 benchmark stations covering the larger part of Bangladesh³. The PWD reference system is related to Mean Sea Level (MSL) which is established at Rangadia, Chittagong in 1992. The conversion from MSL to PWD is a fixed level difference, indicated as 1.5 ft (= 0.4572 m) below the MSL level⁴. However, throughout literature the following conversion is more established and is used in this study:

$$\text{PWD} = \text{MSL} + 0.46 \text{ m} \quad (1)$$

A.2 Morphology

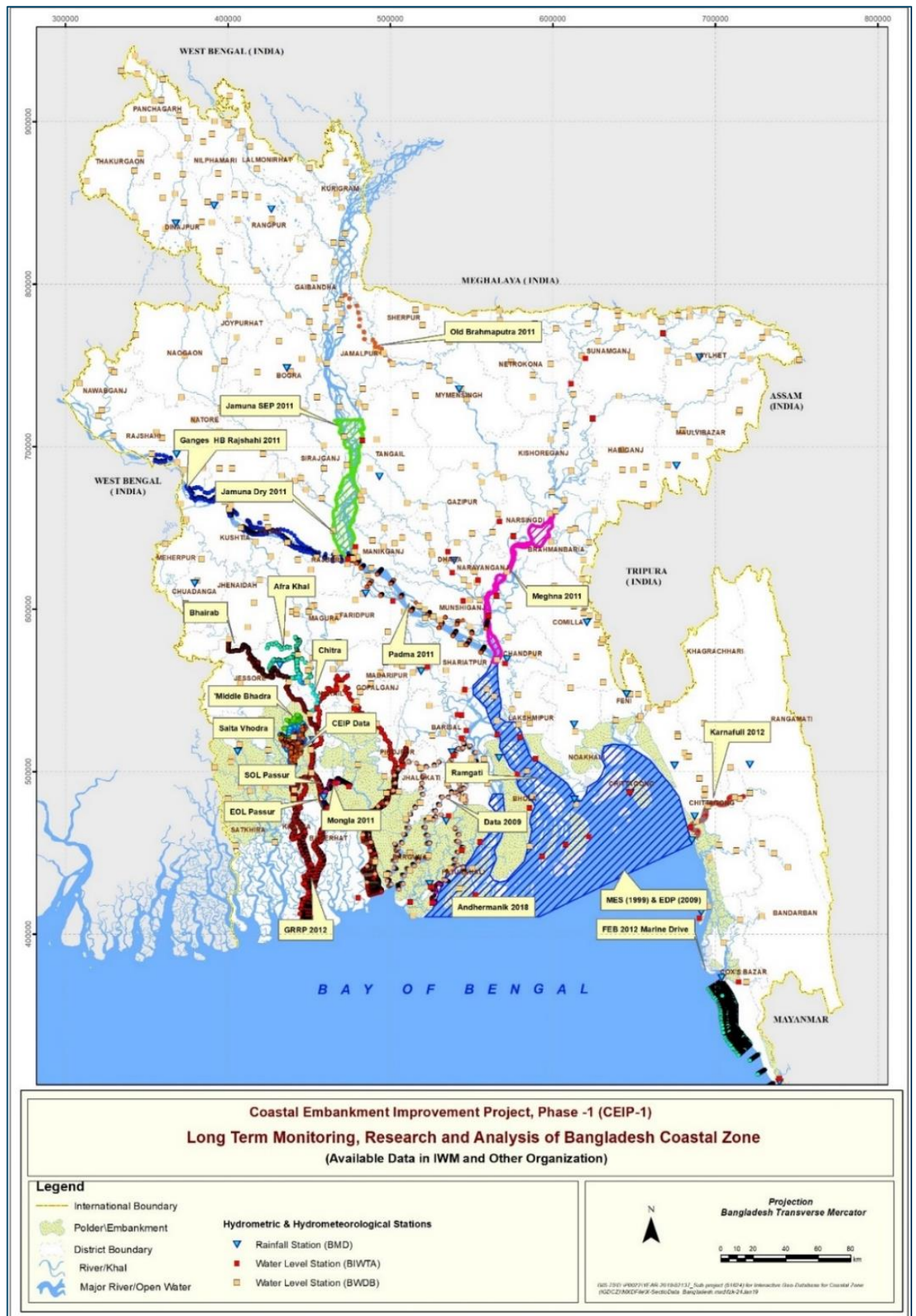
A.2.1 Bathymetry

Most of the bathymetric information on the rivers in the GBM delta and the coastal zone is available on cross-sectional transects gathered via Single Beam Echo Sounding (SBES). In-situ measurements with full spatial coverage (e.g. through Multibeam Echo Sounding, MBES) are scarce. The available observations are gathered on project basis during the past decades and were merged into a single database during the present project. Therefore, data in rivers that are monitored less frequently can be outdated while data in the most important rivers is more recent and more frequently available. Furthermore, during the project new surveys have been performed. FigureApx A1 shows the spatial coverage (enveloping polygons) of the observations available.

² <https://epsg.io/3106>

³ <http://www.sob.gov.bd/site/page/2e0fd063-09e4-4512-a470-a5fbd3668c71/Geodetic->

⁴ <http://www.ffwc.gov.bd/index.php/definitions>

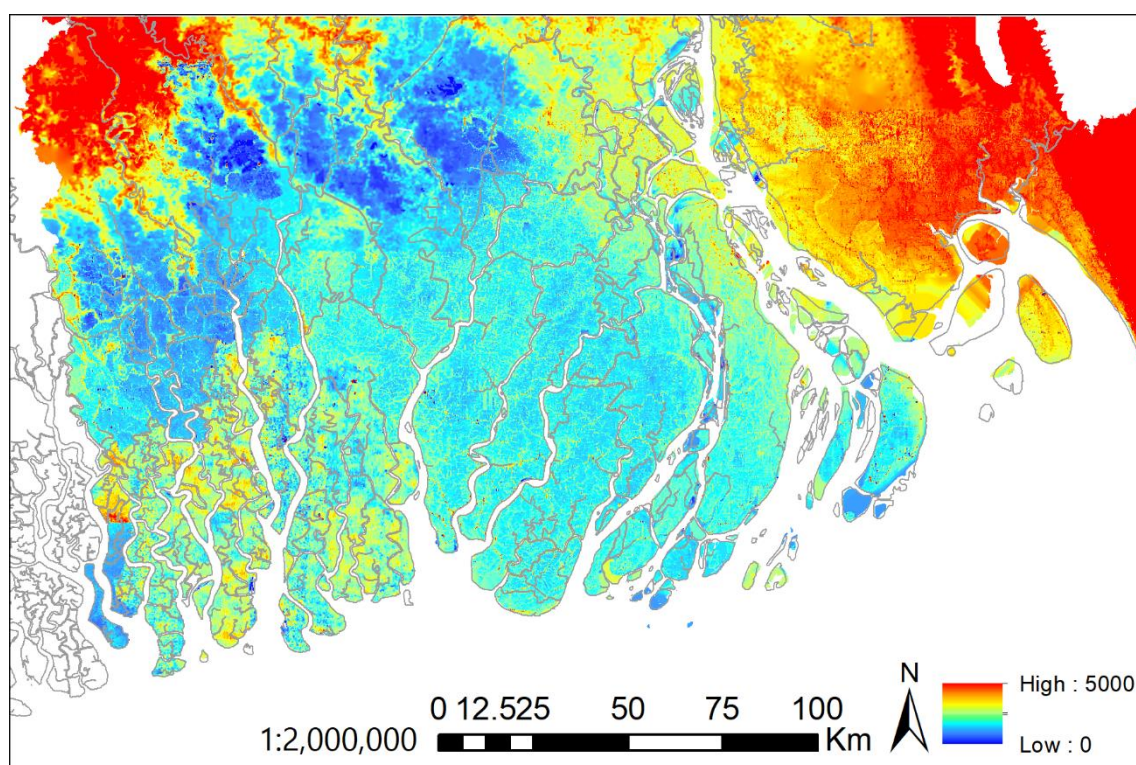


FigureApX A1 Spatial coverage of all in-situ bathymetry observations available (see colours and text boxes for name and date of bathymetry data surveys).

Besides the in-situ observations shown in FigureApx A1 a complete bathymetric dataset of the GBM delta is available from the MIKE21 Bay of Bengal (BoB) model (Uddin et al., 2014). This dataset is, besides the observations, used in the development of the coastal model (see Section Appendix D).

A.2.2 Topography

The bed level of the dry land area is available through RTK-GPS observations. However, these data are sparsely populated and therefore not suitable for input in models. A dataset that delivers full coverage of the topography of the coastal zone of Bangladesh is a satellite derived digital elevation model (DEM). This dataset was acquired by FINNMAP (a Finnish consultancy firm) in 1991 and updated by IWM in 2009 (IWM, 2009) using Google images from 2006-2007 to correct the data and to delineate the Sundarbans Forest (Payo et al, 2016). After this update the dataset has been updated regularly by IWM with land surveys executed for different projects across the delta. The dataset available for this project provides topography information on a 30 m resolution grid of the Bangladesh coastal zone (FigureApx A2). Because this dataset is acquired by remote sensing the reliability of the data must be considered carefully. It is, for example, not known if the data provides the vertical level of the land or the top of the canopy in densely vegetated areas (e.g. the Sundarbans).



FigureApx A2 Satellite derived digital elevation model (DEM) for the Bangladesh coastal zone. Elevation shown in millimetres PWD.

A.3 Hydrodynamics

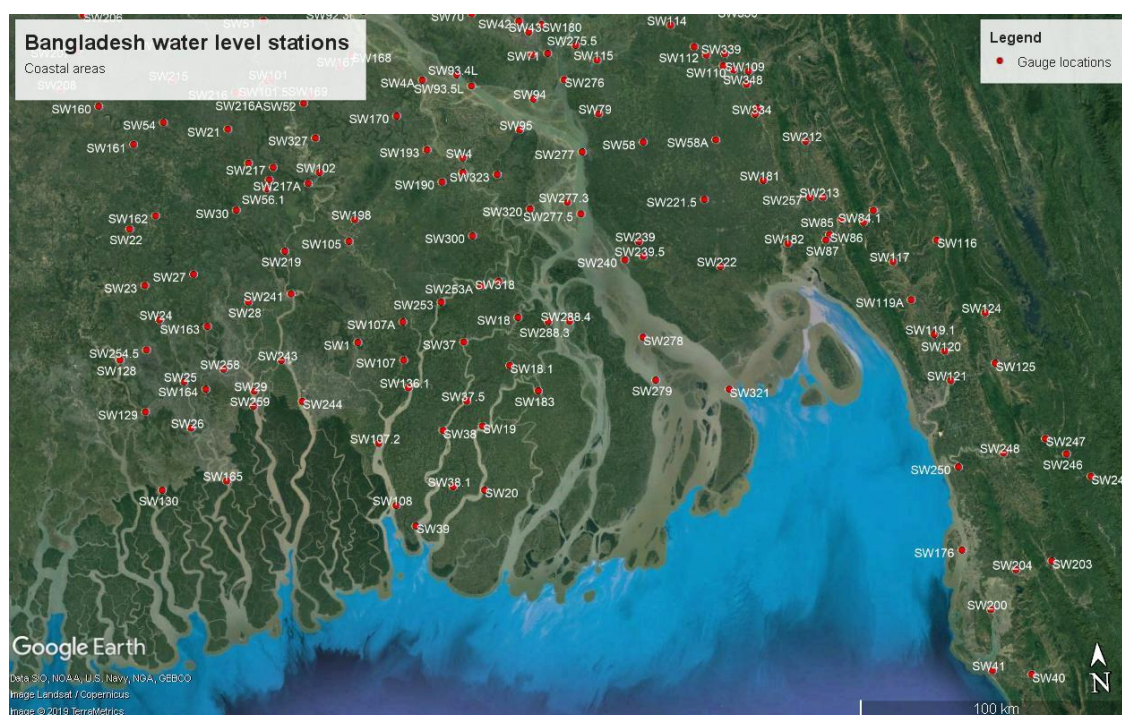
A.3.1 Water levels

A.3.1.1 Time-series

In-situ observations of the free surface elevation (water levels) are available at numerous stations in Bangladesh from two primary sources: data from the Bangladesh Water Development Board (BWBD) and Bangladesh Inland Water Transport Authority (BIWTA) monitoring stations.

The BWBD monitoring stations (FigureApX A3) are manually operated staff gauges where water levels are read and reported on 3-hour intervals, excluding the nights. A photograph showing such a staff gauge is shown in FigureApX A4 BWBD staff gauge along the Padma river.. The main purpose of these monitoring stations is to monitor monsoonal flood discharge waves and to serve as a flood early warning indicator. For this purpose, the maintained 3-hour interval is sufficient. The data is, however, less suited to derive tidal properties in the tidally influenced zone as the 3-hour time-resolution is not frequent enough for a proper representation of the tidal curve. Furthermore, because the staff gauges are often constructed from bamboo material which is positioned directly into the bed sediment, and because these constructions are relocated along the banks throughout the year to be accessible, the vertical referencing of these measurements is highly uncertain. The BWBD data was made available at the start of the project for the time period 2011-2015 on most of the monitoring stations shown in FigureApX A3. In a later stage of the project the Interactive Geo-Database for the Coastal Zone⁵ was set-up, where the BWBD data can be downloaded for long time periods.

Monitoring stations of the BIWTA (FigureApX A5) are situated in the coastal zone and data is collected automatically (using pressure sensors), and reported on varying frequencies (mostly 30-minute intervals), making it more suitable for deriving tidal properties. The availability of the BIWTA data, however, is variable and includes “no-data” gaps as well. FigureApX A6 shows the temporal availability of the BIWTA data for each monitoring gauge.

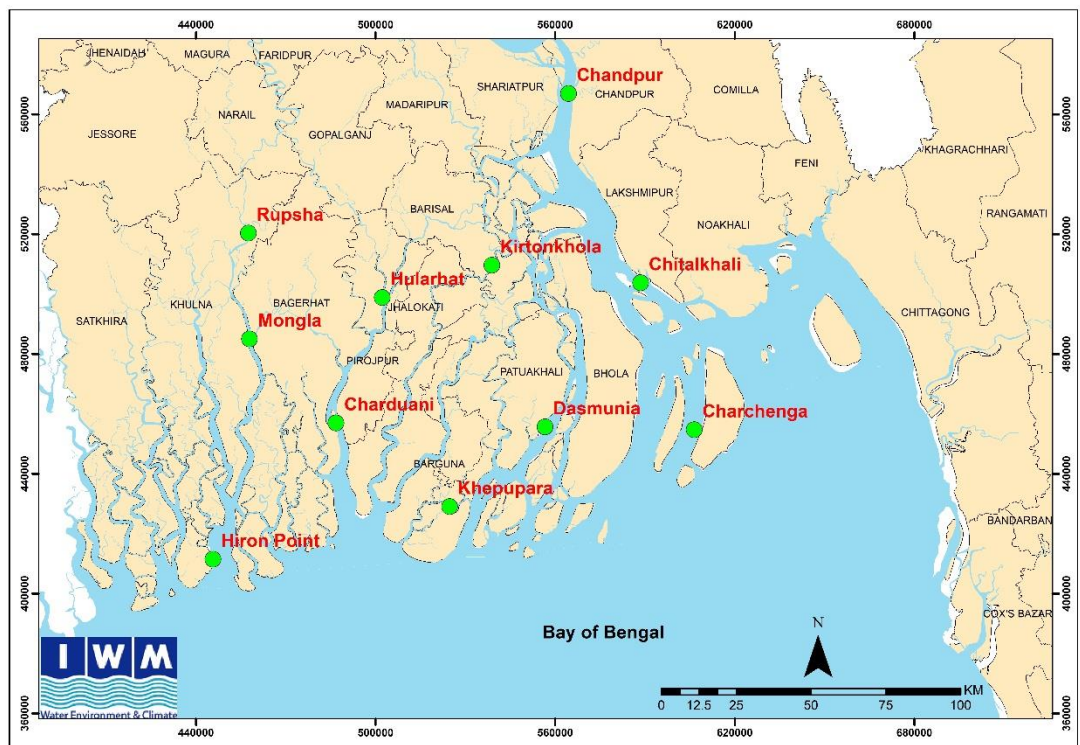


FigureApX A3 Overview of BWBD water level gauges.

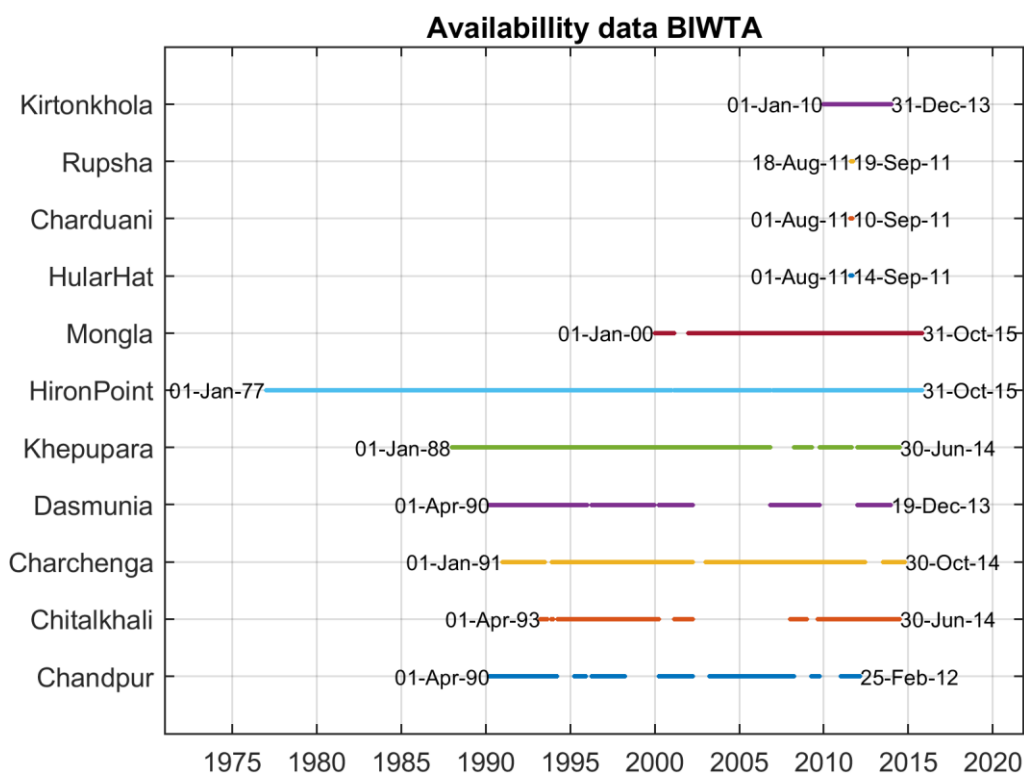
⁵ <https://gis.iwmbd.com/ceip/home>



FigureApX A4 BWBD staff gauge along the Padma river.



FigureApX A5 Overview of BIWTA water level gauges.

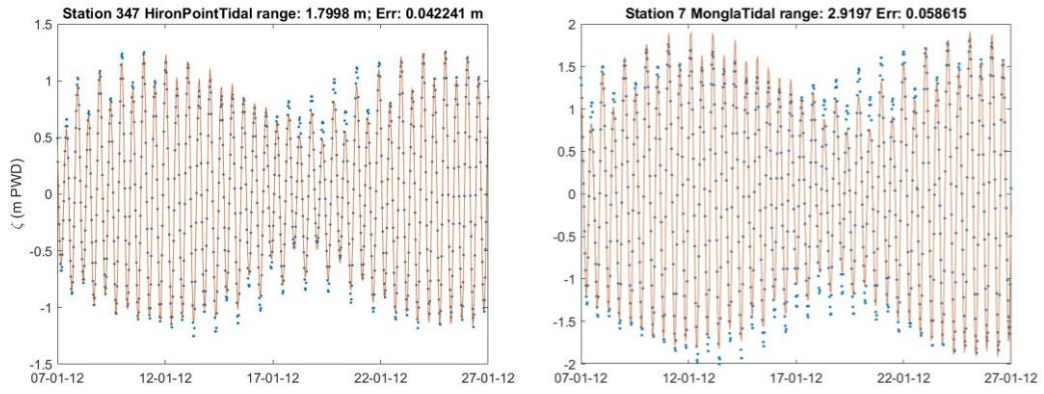


FigureApx A6 Availability of the BIWTA data.

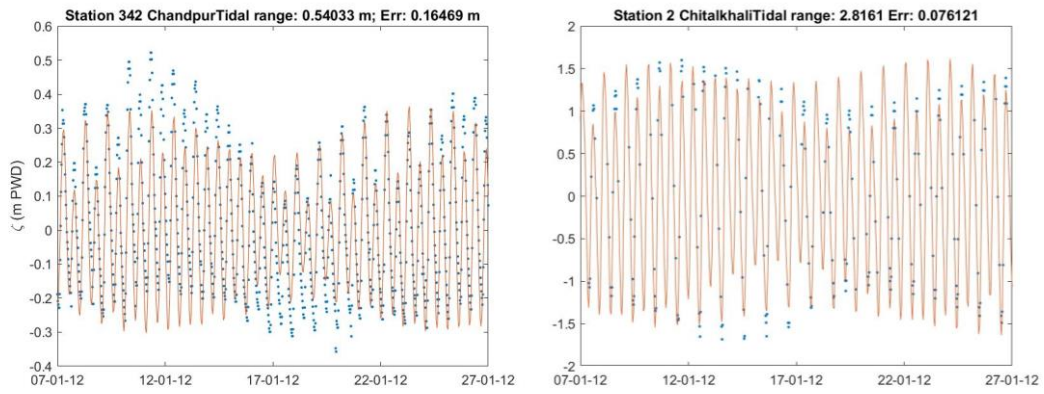
A.3.1.2 Tide in the delta

The primary use of the water level time-series data in this study is model calibration and validation, which is mainly done on the main tidal constituents, particularly M2, throughout the delta. However, performing tidal analysis on these timeseries with coarse temporal resolution, varying sampling frequency, and including data gaps, is not straightforward. Furthermore, using long timeseries (e.g. one-year duration), creates problems in areas where the tide is strongly modulated by the discharge (e.g. the Padma river), which gives rise to a highly non-stationary tidal signal. After trying various configurations, it has been chosen to perform an analysis on 28 days in January 2012 for all stations and selecting only those stations for which the root-mean-squared (rms) error between the reconstructed signal from tidal analysis and the observations was less than 16% of the mean tidal range.

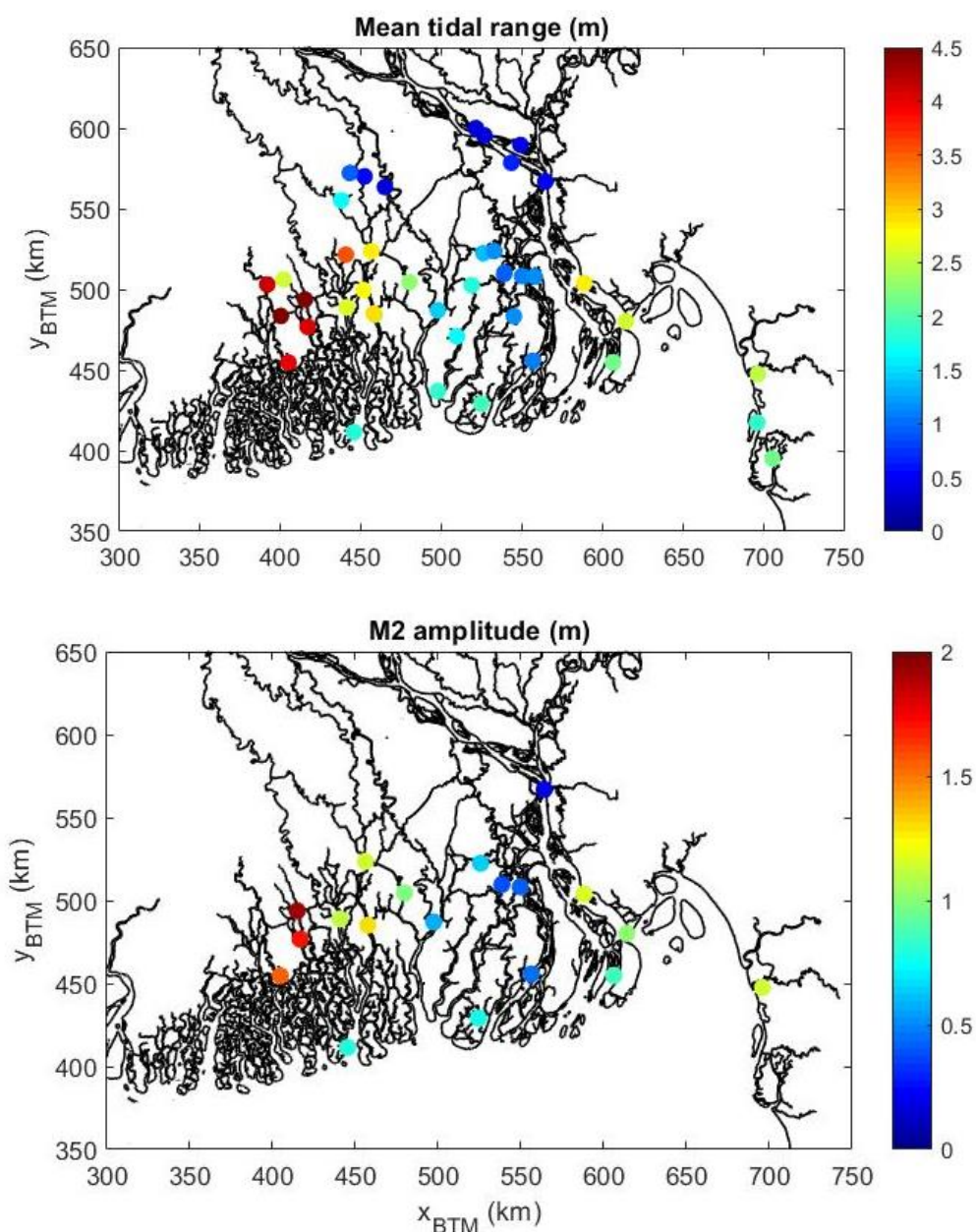
Tidal analysis was carried out using the open-source Matlab function *tidalfit* and associated *tidalval* prediction. The tidal components that could be resolved in the 28-day series were M2, M4, S2, N2, K2, O1, K1, and P1. Examples of the reconstructed signal where the input data was of good quality are shown in FigureApx A7. More problematic - but still acceptable - examples are shown in FigureApx A8 for stations Chandpur and Chitalkhali. For Chandpur, on the confluence of Upper Meghna and Padma into Lower Meghna, some discrepancy arises from mean water level variations with higher than normal values around the 11th of January and lower than normal around the 19th of January. Values of the mean tidal range and the estimated M2 tidal amplitude (used for model calibration) are shown in FigureApx A9.



FigureApX A7 Observations (blue dots) and constructed signal using tidal analysis (red lines) for Hiron Point (left) and Mongla (right).



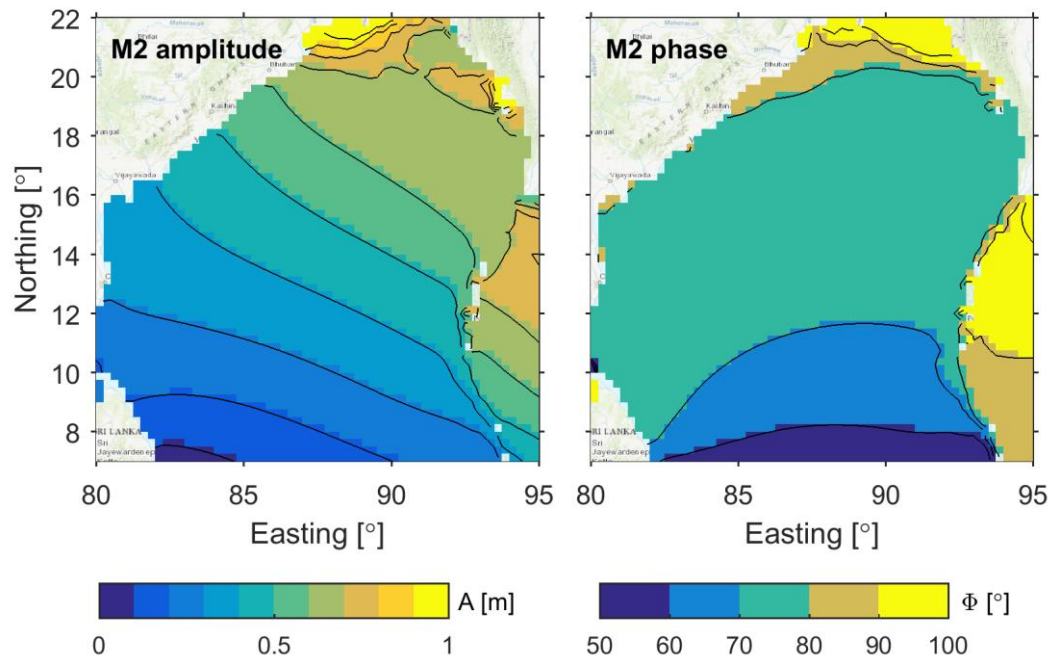
FigureApX A8 Observations (blue dots) and constructed signal using tidal analysis (red lines) for Chandpur (left) and for Chitalkhali (right).



FigureApx A9 Mean tidal range (top) and M2 tidal amplitude in the delta.

A.3.1.3 Offshore tide

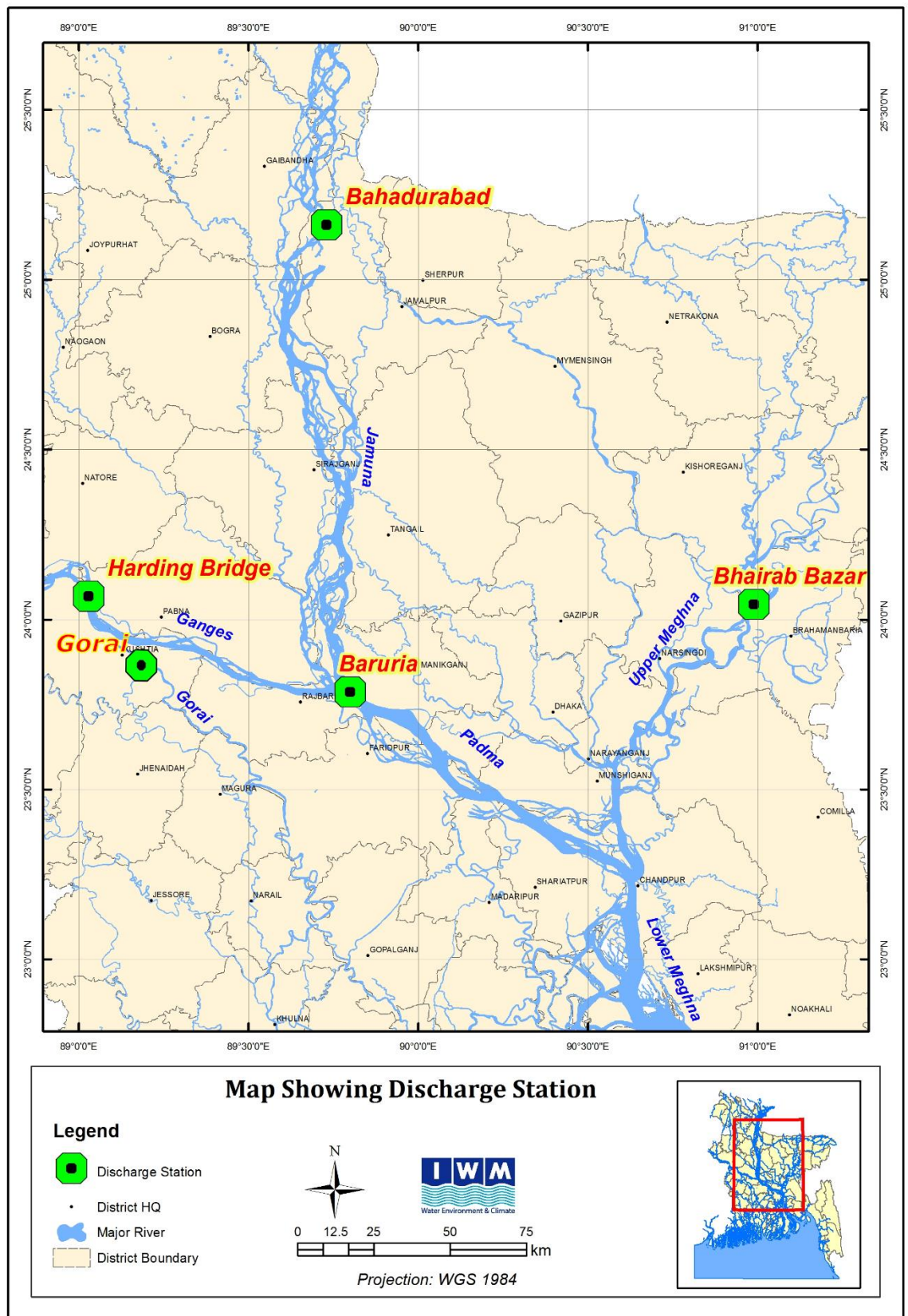
The offshore tidal environment is known from global tide models and can be used to force large scale regional models. The TPXO global tide inverse model (Egbert and Erofeeva, 2002) was used to derive offshore amplitudes and phases of the primary tidal components. The spatial distribution of the M2 tidal amplitude and phase over the Bay of Bengal is shown in FigureApx A10



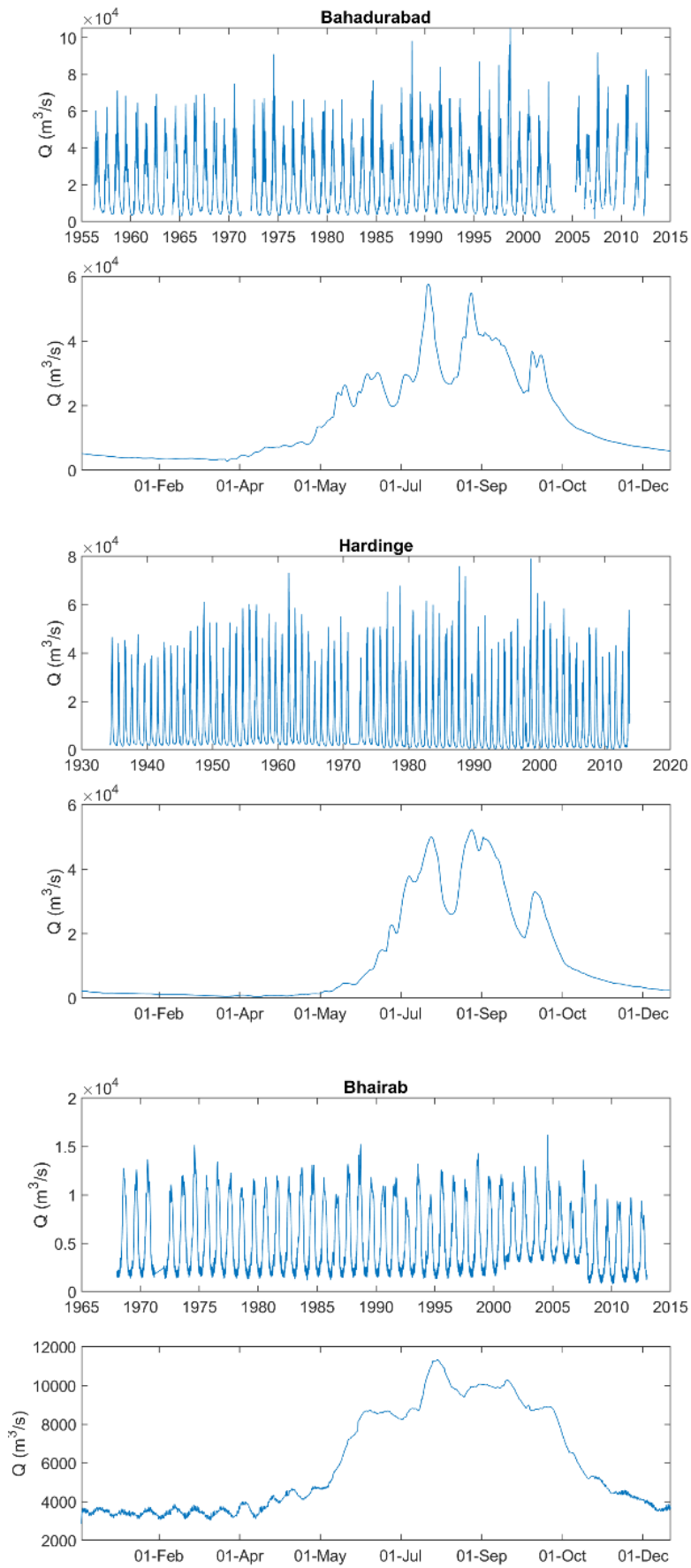
FigureApx A10 Spatial distribution of amplitude and phase of the M2 primary tidal constituent through the Bay of Bengal as computed by Egbert and Erofeeva (2002).

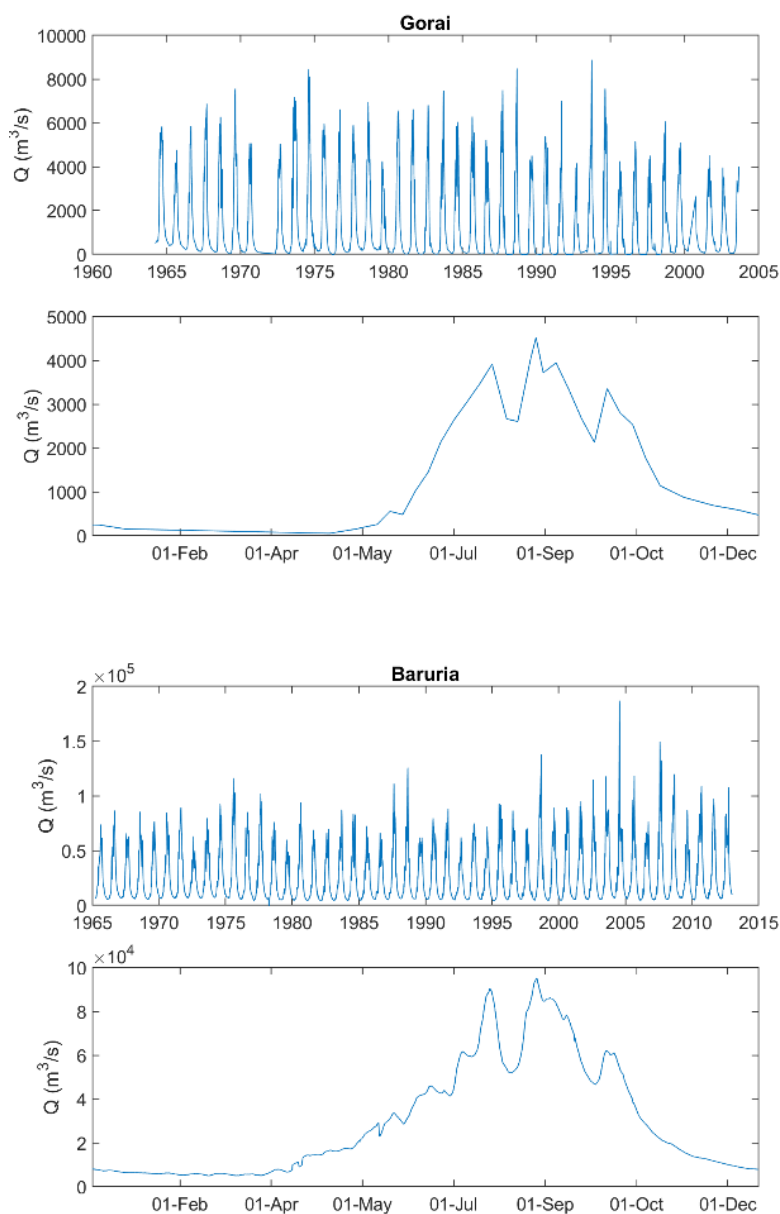
A.3.2 Discharge

The river discharge is measured at several strategic locations at the upstream reaches of the GBM delta (see the map in FigureApx A11). At these locations, the BWDB estimates the instantaneous discharge using stage-discharge relationships (or rating curves). These relationships are empirically derived functions that relate the water level at a point to the corresponding discharge. After such a relationship is established discharge can be monitored continuously by simply measuring the free surface elevation (water level stage). This method provides a simple and low-cost measure to derive continuous discharge time-series. It is, however, less accurate than deriving discharge from in-situ velocity observations. The discharge time-series available for the study are shown in FigureApx A12 for the complete time-series (top of sub-panels) and a zoom-in of the year 2001 (bottom of sub-panels). The figures show clearly that the discharge is highly variable throughout the year, with a minimum in the dry-monsoon period (Dec-Mar) and a maximum in the monsoon season (Jul-Sep).



FigureApX A11 Locations where the BWDB measures discharge through rating curves.





FigureApx A12 Time-series of discharge for all locations showing the complete time-series available (top) and a zoom-in of the year 2001 (bottom), and a map showing the locations of the stations.

A.3.3 Meteorology

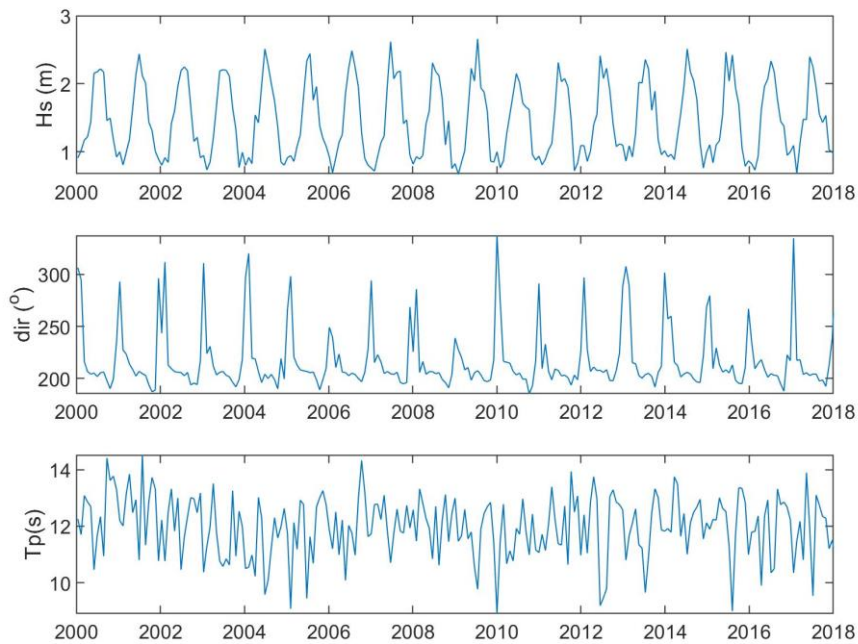
Wind and pressure field can be derived for the complete study area from global meteorological models. In this study the data from the ERA5 re-analysis (Hersbach et al., 2020) is used to acquire monthly spatially varying fields of wind velocity and direction, and pressure. The meteorological information is used in the morphological coastal model.

TableApX A.2 Parameters used to extract the ERA5 wind fields.

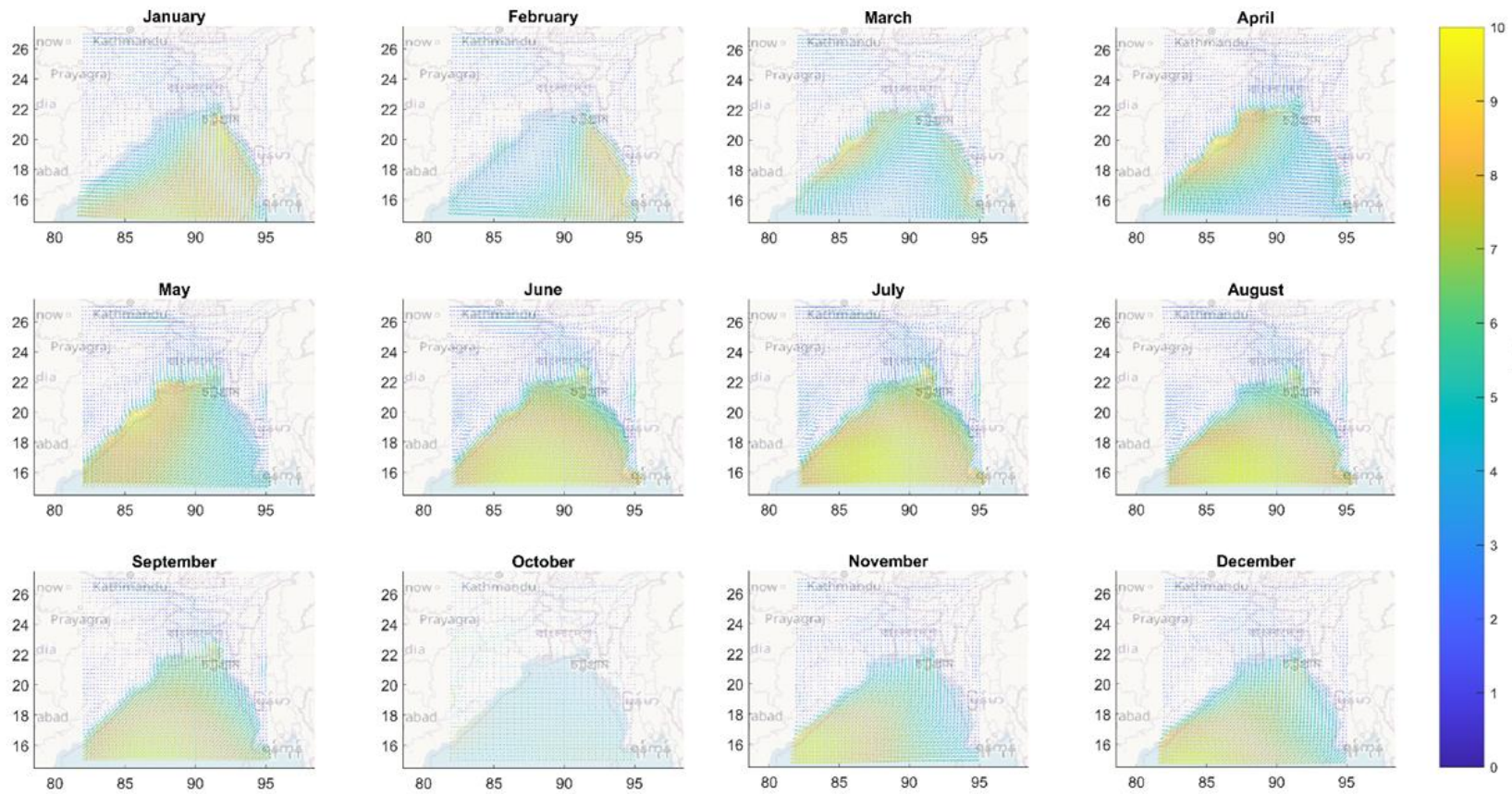
Parameter	Time frame	Easting (deg)	Northing (deg)	Timestep (h)	Resolution (deg)
10m_u_component_of_wind	1979-2019	82-95	15-27	1	0.125
10m_v_component_of_wind	1979-2020	82-96	15-28	1	0.125
mean_sea_level_pressure	1979-2021	82-97	15-29	1	0.125

A.3.4 Waves

Wave information was obtained for the offshore part of the Bay of Bengal from the ERA5 re-analysis (Hersbach et al., 2020). The data was obtained for the same period as the wind fields at the following extraction point (20.5 °N, 91.0 °E), which has a water depth of 85m and is located due south of the Meghna estuary mouth. This location has been deemed representative for the area. The monthly mean wave parameters are shown in FigureApX A13. Wave information is used in the morphological coastal model.



FigureApX A13 Monthly wave climatology at the 85m depth contour offshore of the Meghna estuary, derived from 30 years of ERA5 data



FigureApX A14 Monthly wind climatology for the Bay of Bengal, derived from 30 years of ERA5 data.

B Development basin hydrology model (Hydrotrend)

B.1 Introduction

The following sections describe the development and application of the catchment hydrology (HydroTrend) model. First, a conceptual description of the governing equations is provided (Section B.2). Second, the data sources used for model input are briefly described (Section B.3). Third, the development of the model is shown by presenting the model setup (Section B.4) and calibration procedure (Section B.5). Next, the validity of the model is discussed through a comparison to literature (Section B.6) and finally the model is applied to give projections for the future (see Section B.7).

B.2 Conceptual description

HydroTrend is an empirical model that provides estimates of discharge and suspended sediment estimates as a basin-averaged result¹. Therefore, it requires a thorough comparison of simulation results against real-world data. With careful validation the HydroTrend model has proven to be reliable in a variety of settings: smaller high sediment yield basins (Taiwan, New Zealand (Kettner et al., 2007)), complex continental-scale river basins (MacKenzie River), tropical basins with natural and intense deforestation and intensive land-use (Magdalena River; Kettner et al., 2010) and many more.

The main processes captured in HydroTrend are based on a hydrological water balance. The model incorporates a budget of basin-wide rainfall (Q_r), snow (Q_n) and glacier ice melt (Q_{ice}), evapotranspiration (Q_{Ev}) and shallow groundwater contributions (Q_g), the sum of which controls water discharge at the river mouth (Q in m^3/s):

$$Q_{tot} = Q_r + Q_n + Q_{ice} - Q_{Ev} \pm Q_g \quad (B.1)$$

An empirical relationship originates from multiple regression analysis of a global dataset of >400 rivers comprising long-term water discharge and suspended sediment load (Syvitski and Milliman, 2008). Long-term suspended sediment load, Q_s , is estimated at the river mouth (kg/s) for a basin with a mean annual temperature $T \geq 2^\circ C$ as follows:

$$Q_s = \omega B Q^{0.31} A^{0.5} R T \quad (B.2)$$

Main controls of sediment flux include the drainage basin area, A (km^2) the total water discharge at the delta apex, Q (m^3/s), the basin relief R (m), and the basin-averaged mean annual temperature, T ($^\circ C$). Additional impacts are captured in the B-factor, including the importance of lithology, L , reservoir trapping in the drainage basin, Te , and human controlled erosion and land-use practices, Eh :

$$B = L (1 - Te) Eh \quad (B.3)$$

Daily suspended sediment load at the river mouth (kg/s) (Morehead et al., 2003):

$$(Q_s[j]) / Q_s = \Psi[j] (Q[j] / Q) Ca \quad (B.4)$$

¹ <https://csdms.colorado.edu/wiki/Model:HydroTrend>

In which the Psi and C-factors accounts for individual daily measurement or modeled deviation off of the power function defined by a rating curve. This term thus introduces the day-to-day log-normal variability typically observed around a sediment rating curve. Data comparison in found that this daily variability, e.g. due to hysteresis over a flood season, is relatively modest in large basins. The factors are empirically set based on basin geometry A, and climate (more detailed equations are listed in Morehead, 2003).

Finally, daily bedload at the river mouth (kg/s) when $u \geq u_{cr}$: is computed in the following manner:

$$Qb[i] = (\rho_s / \rho_s - \rho) * (\rho g Q[i] \beta S_{eb}) / (g \tan \lambda) \quad (B.5)$$

In this modified Bagnold equation, the bedload is modelled as dependent on the grain and water densities, the river water discharge at the modelled outlet of the basin Q (m³/s) and the local channel reach slope S (-). The latter is importantly approximated from the slope of the digital elevation model at the delta apex, or specified if known from river bathymetric surveys.

B.3 Input data

Topographical information is extracted from the HydroSheds² DEM to specify each basin total area, hypsometry, slopes, river length and relief. Temperature and precipitation parameters are derived from World Meteorological Organization (WMO) Climate Stations³ and a variety of regional and global databases zoals....?.

B.4 Model set-up

HydroTrend was set up to run simulations for the Ganges and Brahmaputra basins separately in order to incorporate each basin's unique properties into the present modelling exercise. The Meghna river is the only major tributary supplying additional water and sediment to the GBM system, but it was not included in the present analysis due to its negligible contribution to the GBM's total flow volume (~1%; (Coleman, 1969; Darby, 2015). Model setup and parameterization for this project were modified after Darby et al. (2015). The locations of the respective catchment outlets were designated at the Farakka Barrage (at 24.80°N 87.93°E) in eastern India for the Ganges, and at the confluence of the Jamuna (Brahmaputra) River with the Ganges in Bangladesh (at 23.82°N 89.75°E). These locations were chosen as they are considered key boundary nodes for simulating the influx of water and sediment from the main river channels into the GBM delta.

Three input files are required to run HydroTrend. The first input file is the main input file (HYDRO.IN), which describes general drainage basin properties and physical parameters. The main input file is also used to specify the simulation time period and averaging interval (days in this case). Physical parameters include river base flow, glacier equilibrium line altitude and change per year, lapse rate to calculate freezing line, river basin length, and presence/absence of reservoirs. River length and floodplain gradient upstream of the basin outlets were derived from catchment DEMS using ArcGIS standard topographic data and catchment delineation tools (Darby et al., 2015). Lapse rate (°C/km), used to calculate daily temperatures in altitude bins, and initial equilibrium line altitude, the starting glacier equilibrium line altitude (m), were deemed identical for the two catchments. Their values were chosen with reference to the International Civil Aviation Organization standard and Ya-feng et al. (1980), respectively. Base flow for each catchment was calculated as the mean annual flow minima estimated from hydrological records for the gauging stations located at Hardinge Bridge (period of record 1973-1995) on the Ganges river and Bahadurabad Bridge (1973-1995) on the Brahmaputra river (Darby et al., 2015). The Farakka Barrage on the Ganges was the only significant large reservoir specified under "reservoir storage capacity" in the input file setup (Lehner et al., 2001, Lehner et al., 2011).

² <https://www.hydrosheds.org/>

³ http://www.wmo.int/pages/prog/wcp/wcdmp/CON_3.php

Hypsometric curves represent the topography of each of the respective drainage basins upstream of their catchment outlets and define the drainage areas. The second input file to the model describes this basin hypsometry (HYDRO0.HYPS). In this file, the total number of hypsometric bins are specified, followed by two columns containing values for altitude (m) and associated cumulative drainage area (km²). This data represents the topography of the drainage basins upstream of their catchment outlets and define the drainage area encompassed within a series of elevation bins (spaced at 25 m intervals). The Advanced Spaceborne Thermal Emission and Reflection Radiometer (ASTER) Global Digital Elevation Model (GDEM) product was used to calculate and model the Ganges and Brahmaputra's hypsometric curves, while drainage basin area in each elevation bin was derived using the ArcGIS toolbox (following Darby et al., 2015).

The third input file contains climate data (HYDRO.CLIMATE). This file specifies the number of rows of input values, followed by two columns containing total precipitation (mm) and average temperature (°C) data. Climate projections used for the present project were developed from five climate models: GFDL-ESM2M, HadGEM2, IPSL-CM5A, MIROC_ESM_CHEM, and NORESM-M. From each model, the climate data was gathered for the following three periods: reference scenario (time period 1951-2005), RCP4.5 global warming emission scenario (time period 2006-2099), and RCP8.5 global warming emission scenario (time period 2006-2099). The following time periods are considered: 1976-2006 (reference scenario), 2006-2035 (representative for the climate of the year 2020), 2026-2055 (representative for the climate of the year 2040), 2046-2075 (representative for the climate of the year 2060), and 2066-2095 (representative for the climate of the year 2080). Temporal resolution was set to one day (daily data).

The HydroTrend model is originally coded in C, but this version was made accessible through the Python Modelling Tool (pymt), an Open Source Python package developed by the Community Surface Dynamics Modelling System (CSDMS). The Jupyter Notebook application was used to run HydroTrend through the pymt package. Separate Jupyter notebooks were run for each 30-year simulation for each basin, emission scenario, climate model, and time period, for a total of 90 HydroTrend simulations. 30-year simulations were conducted over the period 1976-2099 rather than a single century-long simulation to prevent a timing offset associated with leap year, which cannot be resolved by HydroTrend itself. Output ASCII files were generated with daily data for each model run. A summary statistics csv file was also written for each model run, which computed statistics averaged over each simulation time period (30 years), allowing for easy data analysis and comparison between model runs.

B.5 Model calibration

B.5.1 Calibration approach

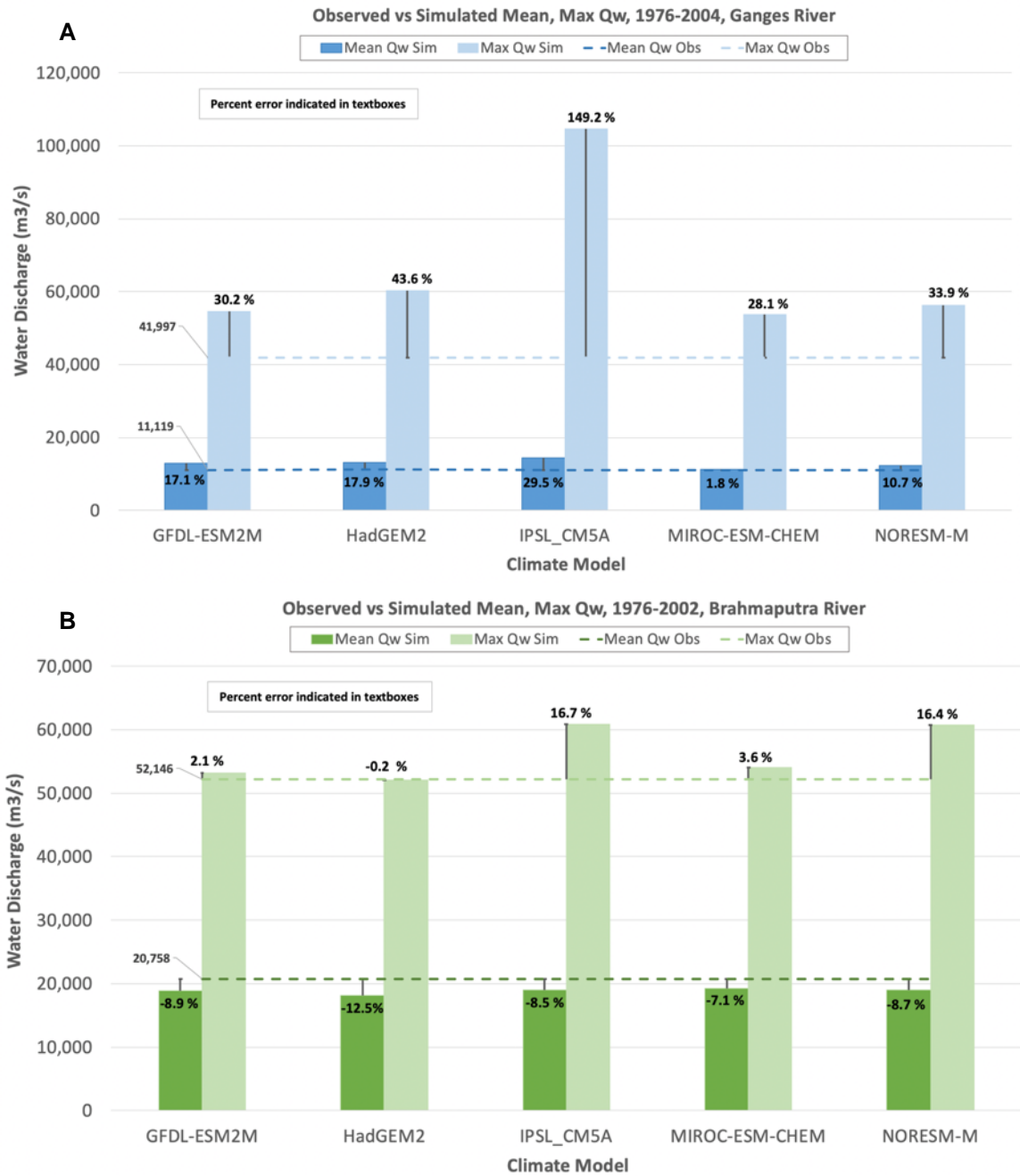
HydroTrend model outputs from the reference scenario (1976-2006) simulations were compared with observed records in order to calibrate and validate the HydroTrend model setup. Climate hindcast data from five climate models (GFDL-ESM2M, HadGEM2, IPSL-CM5A, MIROC_ESM_CHEM, and NORESM-M) were used to drive the reference scenario simulations. Observed data were provided by the Institute of Water Modelling (IWM). Observed records consist of water discharge values for the Ganges river at Hardinge Bridge and the Brahmaputra river at Bahadurabad. Rated discharge values were utilized for comparison with simulated values. Observed (rated) daily discharge values at Hardinge Bridge range from January 1934 to October 2004 and at Bahadurabad from January 1956 to July 2002.

The observed (rated) sediment load for the Ganges and Brahmaputra rivers were calculated using sediment-rating curves, since direct sediment measurements from the rivers are lacking. Sediment-rating curves from Higgins et al. (2018) were utilized. Curves were established using Ganges river water discharge data from Hardinge Bridge over the period 1980-1995 (Islam et al., 1999) and Brahmaputra river discharge data from Bahadurabad Gauging Station over the period 1989-1994 (Islam et al., 1999). The sediment-rating curve equation for the Ganges river is $Q_s = 0.007 \times Q^{1.51}$ ($R^2 = 0.68$) and for the Brahmaputra river is $Q_s = 0.005 \times Q^{1.56}$ ($R^2 = 0.78$), with units of kg/s for Q_s and m³/s for Q . The observed sediment record was not used extensively for calibration and validation

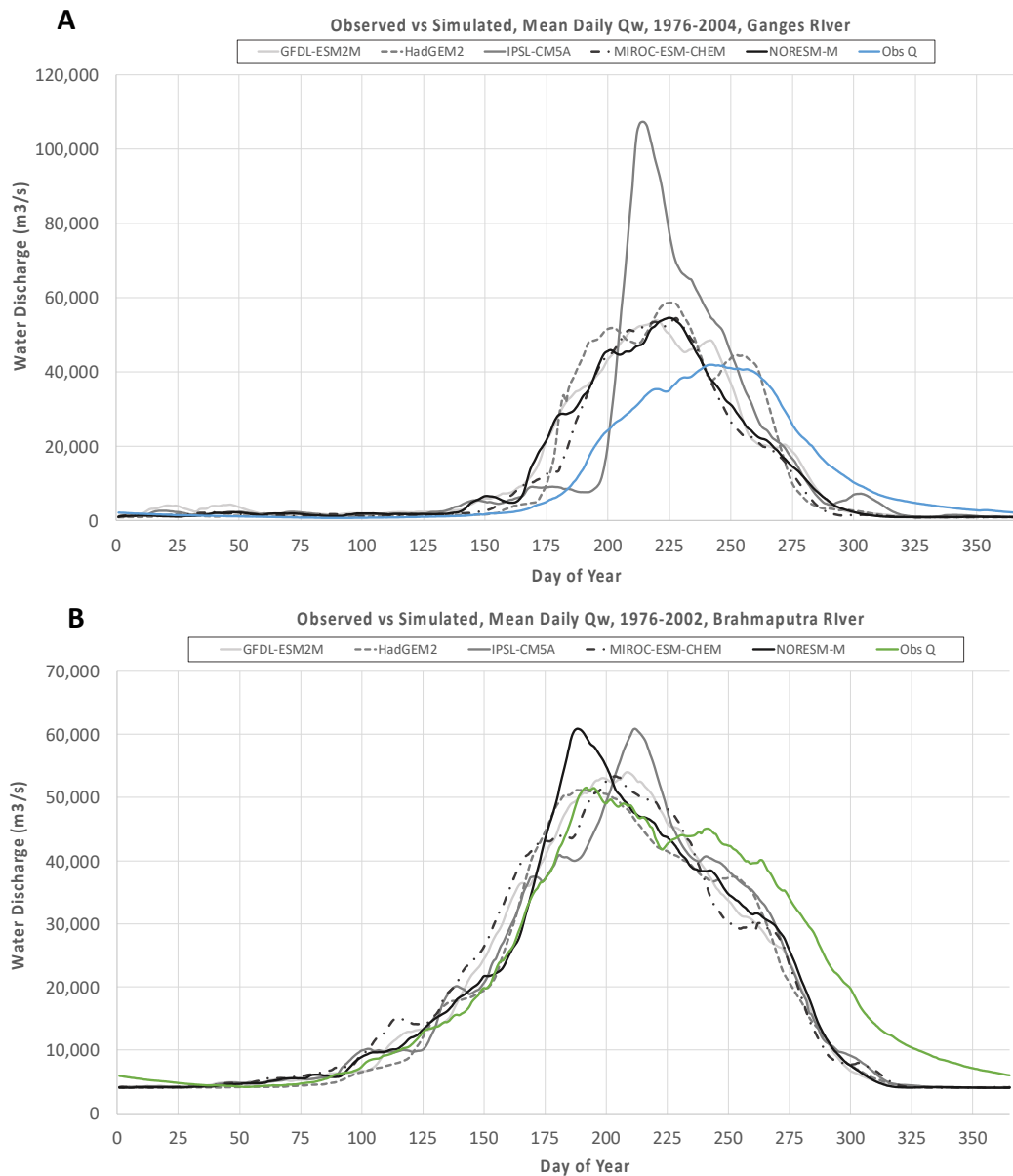
purposes since this dataset does not encapsulate direct sediment measurements; however, the observed sediment discharge record will be used for evaluating the timing of annual peak sediment discharge, which will be discussed in more detail in the following sections.

B.5.2 Results of reference scenario: Data-model comparison

The reference scenario (1976-2006) model outputs forced by five climate models (GFDL-ESM2M, HadGEM2, IPSL-CM5A, MIROC_ESM_CHEM, and NORESM-M) were compared with observed water discharge records from the Ganges and Brahmaputra rivers. Overall, HydroTrend simulated mean water discharge well for both rivers. Percent error between observed and simulated values for mean water discharge for the Ganges river ranged from +1.8% (MIROC-ESM-CHEM) to +29.5% (IPSL_CM5A). The largest water discharge that was simulated during each 30-year long model run is hereby referred to as the maximum water discharge. Percent error for maximum water discharge ranged between 28.1% (MIROC-ESM-CHEM) and 149.2% (IPSL_CM5A). For the Brahmaputra river, mean water discharge ranged from -7.1% (MIROC-ESM-CHEM) to -12.5% (HadGEM2). Percent error for maximum water discharge ranged between -0.2% (HadGEM2) and 16.7% (IPSL_CM5A). FigureApx A.1 portrays HydroTrend model performance by comparing mean and maximum simulated water discharge values with observed records.



FigureApX A.1 Observed vs. simulated mean and maximum water discharge for the A) Ganges river and B) Brahmaputra river. Percent error values are written as percentages next to error bars. Average and maximum observed water discharge are written to the left of the dotted lines and are reported in units of m³/s.



FigureApx A.2 Observed vs. simulated mean annual daily water discharge for the A) Ganges river and B) Brahmaputra river. Discharge data were trimmed from the initial reference time period of 1976-2006 to 1976-2004 for the Ganges and 2002 for the Brahmaputra, since the observed discharge records were missing a considerable number of values at the tail end of their respective records.

Observed and simulated mean annual daily discharge were also assessed to see how well HydroTrend simulated the rivers' hydrographs over the reference scenario. HydroTrend performed well in this regard considering the reduced complexity of this model, particularly in simulating the Brahmaputra rivers' annual flow regime (FigureApx A.2). In FigureApx A.3 it is illustrated how the mean annual daily discharge from the five climate-model-hindcasts compares with observed discharge records over the reference scenario time period (1976-2004/2002). The averaging interval was trimmed by 2 and 4 years for the Ganges and Brahmaputra rivers, respectively, depending on the comprehensiveness of the observed discharge record. TableApx A.1 reports how the timing of peak flow compares to observed and simulated values over the reference scenario. Differences in timing are to be expected for a basin-averaged precipitation in a 1D model. First, timing may be inaccurate because precipitation is not uniformly distributed throughout the basin and the timing of monsoonal arrival may already be off in the primary climate simulations. This is illustrated by the fact

that the different models have different delays (TableApX A.1) Then, the basin-wide 1D model takes into account a lag between input precipitation and arrival of high discharge for long rivers (approximated by a simplified shockwave dampening approach). In reality there could be distinct spatial variations in delay of the river runoff routing due to for example irrigation management or reservoir storage at the small farm pond scale, thus timing at the daily timescale can be complex to resolve. Simulations are calibrated to optimize to capture the peak discharge instead of the most accurate timing. This strategy was deliberately chosen to most accurately represent peak input flow dynamics and peak potential sediment transport characteristics for the macroscale model, but it compromises some of the precision in timing of daily predictions.

TableApX A.1 A comparison of the observed and simulated timing of peak flow and sediment transport averaged over the reference scenario (1976-2006) for the Ganges and Brahmaputra rivers. Values are reported as days of the calendar year (Julien day). The “difference” column represents the difference, in days, between observed and simulated peak flow. A positive difference indicates that simulated timing of peak flow occurred later in time than was observed, and a negative difference indicates that peak flow occurred earlier in time than was observed.

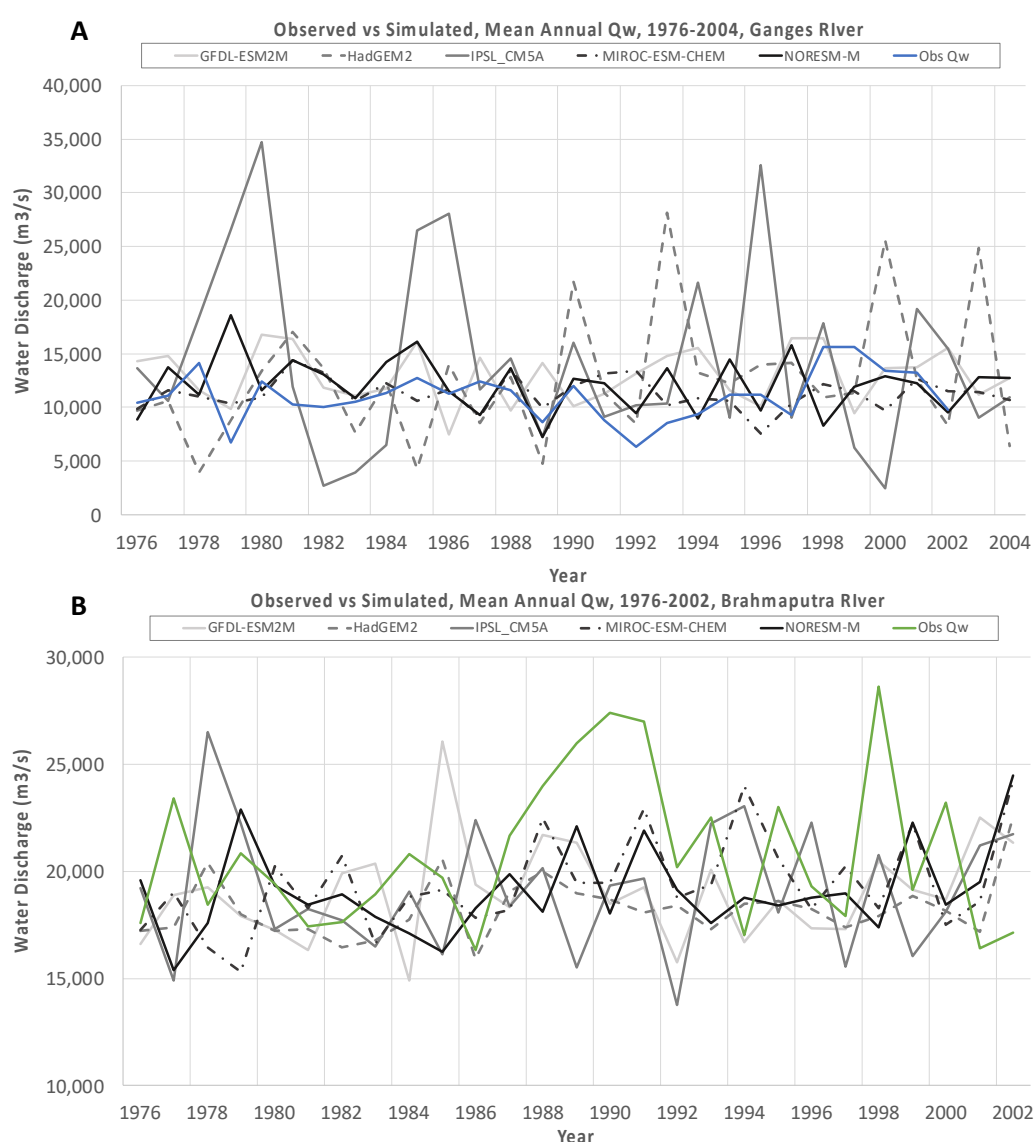
Day of Year of Peak Qw						
	Brahmaputra			Ganges		
Climate Model	Observed	Simulated	Difference	Observed	Simulated	Difference
GFDL-ESM2M	200	200	0	244	220	+24
HadGEM2	200	192	+8	244	227	+17
IPSL_CM5A	200	214	-14	244	216	+28
MIROC-ESM-CHEM	200	206	-6	244	227	+17
NORESM-M	200	190	+10	244	228	+16
Day of Year of Peak Qs						
GFDL-ESM2M	200	202	-2	259	217	+42
HadGEM2	200	184	+16	259	228	+31
IPSL_CM5A	200	213	-13	259	217	+42
MIROC-ESM-CHEM	200	203	-3	259	228	+31
NORESM-M	200	201	-1	259	217	+42

Finally, observed and simulated mean annual water discharge data were assessed to complete the model-data comparison. The purpose of this task was to investigate how mean water discharge varied in reality, compared to simulated discharge. FigureApX A.3 portrays mean annual water discharge from the five climate-model-hindcasts compared with observed discharge records over the reference scenario.

The Ganges and Brahmaputra basins show different trends in inter-annual variability of water discharge for both modelled and observed data (FigureApX A.3). For the Ganges basin, the model results illustrate large inter-annual variabilities compared to observed discharge. The IPSL-CM5A model generated about twice as much variability than the other four models. In addition, between the other four models, variability is larger than the observed differences in annual mean water discharge. Hence, the IPSL-CM5A model is an outlier with respect to water discharge, which is largely controlled

by its predictions of annual and monsoonal rainfall. The IPSL-CM5A model shows outliers on both the high and low ends of water discharge (FigureApx A.3A).

The large differences in inter-annual variability between climate models are not consistent over the entire GBM basin. For example, in FigureApx A.3B, the modelled discharge in the Brahmaputra basin shows similar intra-annual variability to the observed water discharge record. Also, the variation from the mean in the Brahmaputra basin is less than the variation from the mean in the Ganges basin – especially for the IPSL-CM5A model. This can be explained by the fact that mean annual precipitation is lower in the western part of the GBM basin, where the Ganges basin is located. In turn, the variation in the Ganges basin is substantially larger than the variation in the Brahmaputra basin, which is located in the eastern part of the GBM basin. This discussion is supported by takeaways from Section 4.3 of the Climate Change Scenarios report (Deliverable D-4D).



FigureApx A.3 Observed vs. simulated mean annual water discharge for the A) Ganges river and B) Brahmaputra river, averaged over the reference scenario time period of 1976-2004 for the Ganges River and 1976-2002 for the Brahmaputra River.

B.6 Comparison with existing GBM sediment load observations and estimates

The simulated results shown above in TableApx A.2 and TableApx A.3, and presented visually in FigureApx A.4 and FigureApx A.5, allow for the calculation of annual sediment discharge for the Ganges and Brahmaputra basins. In this section, only sediment discharge calculated over the reference scenario (1976-2006) is reported, since simulated data over this time period can be directly compared with observations. The HydroTrend simulations, averaged over the five climate models, simulated an annual sediment discharge of 496 MT/year for the Ganges basin and 251 MT/year for the Brahmaputra basin. Together, these values sum up to 747 MT/year for the entire GBM basin.

The simulated sediment discharge for the Ganges basin is close to values predicted from previous work. The current report (Chapter 2) presents an annual sediment discharge for the Ganges basin of 550 MT/year, which is close to the 496 MT/year that the HydroTrend model runs estimated. However, the simulated annual sediment discharge for the Brahmaputra basin is much lower than has been previously estimated in past work. In this report, annual sediment discharge for the Brahmaputra basin is documented at 590 MT/year, which is more than twice as much as HydroTrend simulated in the present modeling exercise, which estimates an annual sediment discharge of 251 MT/year.

The underestimation of sediment discharge at the Brahmaputra basin outlet can be explained by a few possible reasons. First, large uncertainties in the hindcasted precipitation data exist, which in turn produces a large uncertainty in the sediment load estimates. Another potential explanation is that previous work overestimated the annual sediment discharge in the Brahmaputra river. This is possible since sediment discharge estimates for the Brahmaputra basin are not commonly found in the literature, and among previously published work, estimates for annual sediment discharge are highly variable. Future work will attempt to better constrain the sediment discharge in the Brahmaputra basin, both through detailed observations and modeling efforts. The figure below (FigureApx A.6) places the presently estimated annual sediment discharge values for the Ganges and Brahmaputra basins in the context of previous estimations.

B.7 Results on future projections

The HydroTrend model has been run for the Ganges and Brahmaputra rivers for the time period from 1976-2099 for the two global climate change scenarios, RCP4.5 and RCP8.5. Hence, this section evaluates potential changes in water and sediment discharge in the Ganges and Brahmaputra basins due to predicted future climate change scenarios. The results are presented per basin in the following chapters.

B.7.1 Ganges basin

HydroTrend model results for the Ganges basin show both water discharge and sediment discharge increasing in the Ganges river from 1976-2099. Mean water discharge (averaged across all climate models) for the RCP4.5 emission scenario increased by 37% over the simulation, while mean sediment discharge increased by 29%. For the RCP8.5 emission scenario, mean water discharge increased by 46% and sediment discharge increased by 45%. Bedload discharge also increased over the simulation time period by 37% (RCP4.5) and 46% (RCP8.5) (Details are listed in TableApx A.2). Suspended sediment concentration increases less dramatically, with a percent increase of 17% (RCP4.5) and 3% (RCP8.5). FigureApx A.4 portrays average simulated water discharge, sediment discharge, bedload discharge, and suspended sediment concentration as average values over the time periods representative of the years 2020, 2040, 2060, and 2080. Climate hindcasts from the reference scenario are also included in the line plots to amplify trends and to extend the analysis timeframe. Simulated values averaged over each time period are also reported numerically in

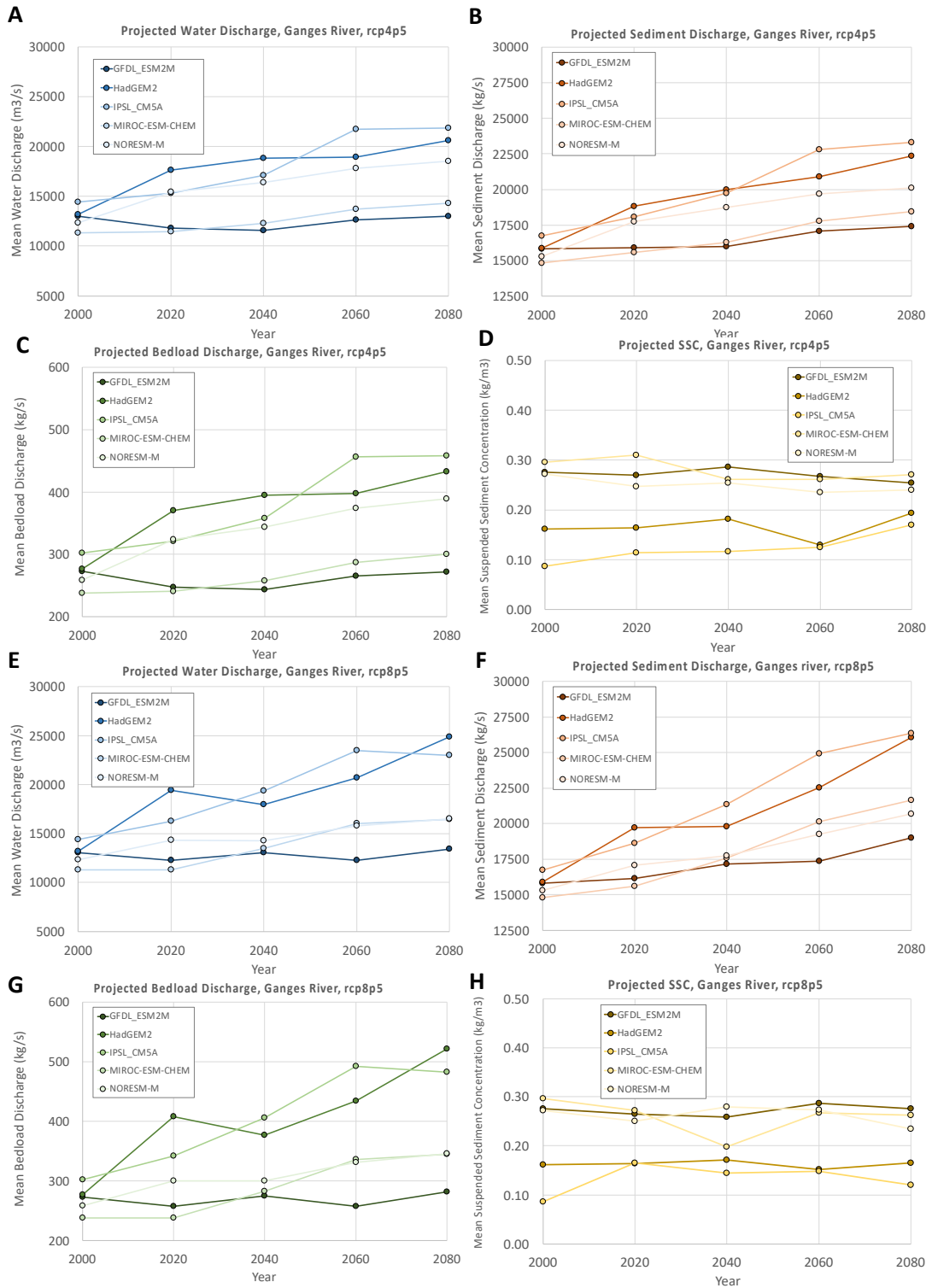
TableApX A.2. Percent change calculations reported were calculated by subtracting the statistic/value from the year 2000 statistic/value by the year 2080 statistic/value, dividing by the year 2000 statistic/value, and multiplying by 100; this simple calculation illustrates how discharge and other parameters changed from the reference time period (1976-2006) to the end of 20th century time period (2066-2099) of the simulation timeframe.

Maximum annual water discharge (peak flow) shifted earlier in time in the Ganges river as the simulations progressed through time. For example, the MIROC-ESM-CHEM climate model under the RCP4.5 emission scenario generated a peak flow on the 227th day of the year in 2020, whereas peak flow occurred on the 202nd day of the year in 2080, equivalent to a 25-day shift earlier in time (nearly a month). Averaged across the climate models, peak flow occurred earlier in time in the Ganges basin by 3% and 5% for RCP4.5 and RCP8.5, which is equivalent to 12 and 17 days, respectively.

B.7.2 Brahmaputra basin

Similar to the Ganges basin, model results for the Brahmaputra basin show both water discharge and sediment discharge in the Brahmaputra river increasing from 1976-2099. Mean water discharge (averaged across all climate models) for the RCP4.5 emission scenario increased by 21% over the simulation time period, while mean sediment discharge increased by 52%. For the RCP8.5 emission scenario, mean water discharge increased by 29% and mean sediment discharge increased drastically by 88%. Bedload discharge also increased over the simulation time period by 21% (RCP4.5) and 29% (RCP8.5). Finally, suspended sediment concentration increased by 15% (RCP4.5) and 16% (RCP8.5). FigureApX A.5 shows average simulated water discharge, sediment discharge, bedload discharge, suspended sediment concentration as averaged values representative of the years 2020, 2040, 2060, and 2080. Climate hindcasts from the reference scenario were included in the line plots to amplify trends and to extend the analysis timeframe. Simulated values averaged over each time period are also numerically reported in TableApX A.3.

Maximum annual water discharge (peak flow) shifted earlier in time in the Brahmaputra river under the RCP8.5 emission scenario but did not shift significantly for the RCP4.5 scenario. The day of peak flow for the RCP4.5 scenario (averaged across climate models) shifted slightly later in time with a percent change of 0.2%, equivalent to $\frac{3}{4}$ of a day. Contrastingly, for the RCP8.5 emission scenario, peak flow shifted earlier in time by 4%, equivalent to 14 days.

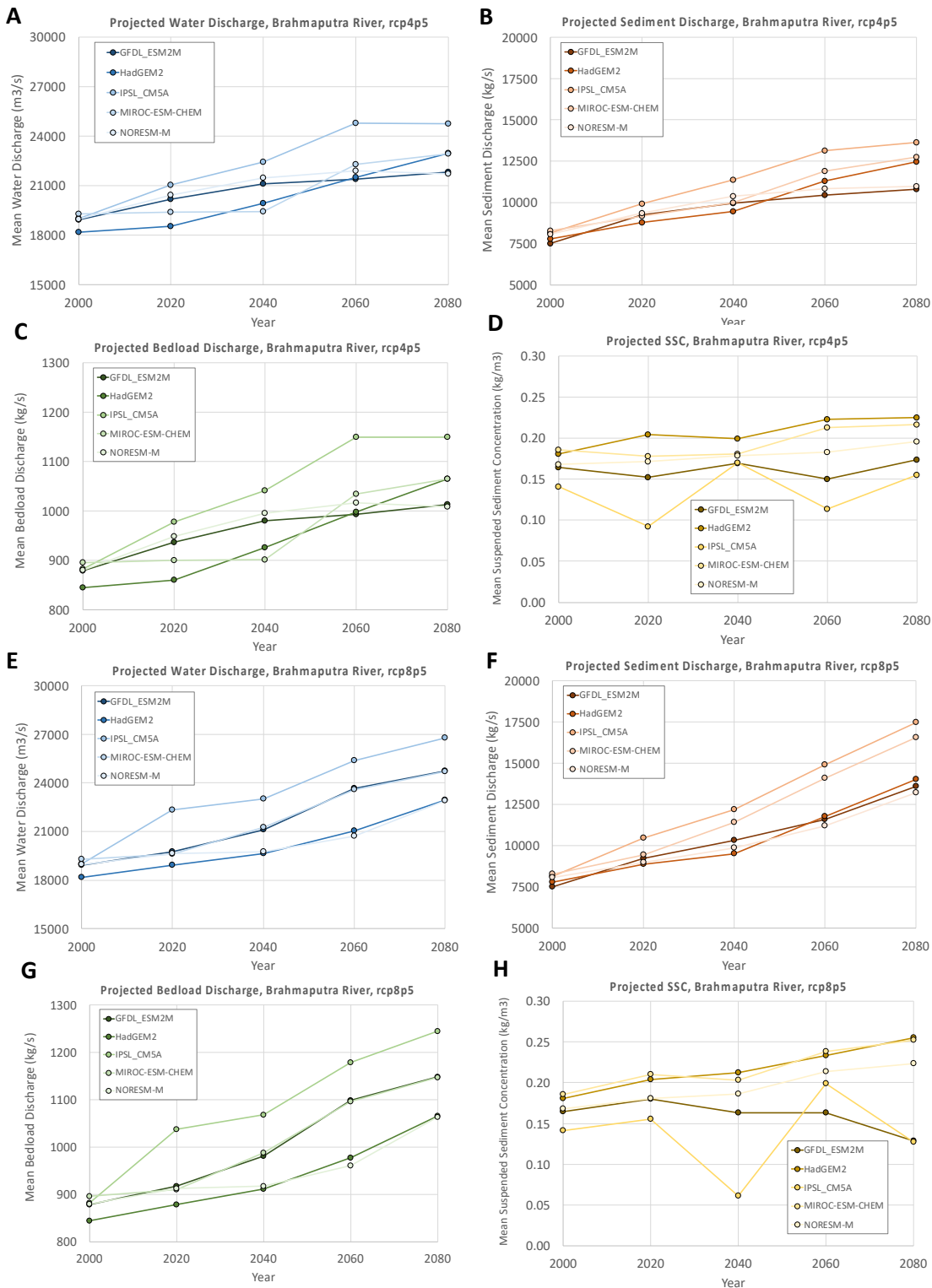


FigureApX A.4 Projected water discharge, sediment discharge, bedload discharge, and suspended sediment concentration for the Ganges river driven by climate representative of the years 2020, 2040, 2060, and 2080 under the RCP4.5 emission scenario (A-D) and RCP8.5 emission scenario (E-H). Data for the reference scenario representative of the year 2000 are included in the line plots to amplify trends and to extend the analysis timeframe.

TableApX A.2 Summary statistics from HydroTrend simulations of the Ganges basin for the reference, RCP4.5, and RCP8.5 scenarios. Reference scenario statistics are averaged over the time period 1976-2006. RCP4.5 and RCP8.5 emission scenario values are averaged over the time periods representative of the years 2020, 2040, 2060, and 2080 (see model setup section for more details). Statistics from the reference scenario (2000) are included within each climate model section in the RCP4.5 and RCP8.5 portions of the table for ease of analysis.

Ganges Basin Summary Statistics					
Reference Scenario (1976 – 2006)					
Unit/description:		Mean Qw	Mean Qs	Mean SSC	Mean Qb
		m ³ /s	kg/s	kg/m ³	kg/s
Climate model:	GFDL-ESM2M	13018	15823	0.276	273
	HadGEM2	13184	15894	0.162	277
	IPSL_CM5A	14399	16752	0.087	302
	MIROC-ESM-CHEM	11315	14827	0.296	237
	NORESM-M	12311	15310	0.272	258
RCP4.5 (2006 – 2099)					
Unit/description:		Mean Qw	Mean Qs	Mean SSC	Mean Qb
		m ³ /s	kg/s	kg/m ³	kg/s
Climate Model	Representative Climate of Year and Averaging Interval				
GFDL-ESM2M	2000 (1976-2006)	13018	15823	0.276	273
	2020 (2006-2035)	11783	15916	0.270	247
	2040 (2026-2055)	11587	15990	0.286	243
	2060 (2046-2075)	12649	17069	0.267	265
	2080 (2066-2095)	12979	17423	0.254	272
HadGEM2	2000 (1976-2006)	13184	15894	0.162	277
	2020 (2006-2035)	17622	18810	0.164	370
	2040 (2026-2055)	18804	19984	0.182	395
	2060 (2046-2075)	18938	20907	0.129	397
	2080 (2066-2095)	20620	22374	0.194	433
IPSL_CM5A	2000 (1976-2006)	14399	16752	0.087	302
	2020 (2006-2035)	15319	18078	0.114	322
	2040 (2026-2055)	17060	19725	0.117	358
	2060 (2046-2075)	21737	22828	0.124	456
	2080 (2066-2095)	21826	23308	0.170	458
MIROC-ESM-CHEM	2000 (1976-2006)	11315	14827	0.296	237
	2020 (2006-2035)	11450	15571	0.310	240
	2040 (2026-2055)	12270	16281	0.262	258
	2060 (2046-2075)	13686	17793	0.261	287
	2080 (2066-2095)	14304	18454	0.270	300
NORESM-M	2000 (1976-2006)	12311	15310	0.272	258

	2020 (2006-2035)	15427	17733	0.247	324
	2040 (2026-2055)	16369	18729	0.254	344
	2060 (2046-2075)	17807	19679	0.235	374
	2080 (2066-2095)	18538	20114	0.240	389
RCP8.5 (2006 – 2099)					
Unit/description:		Mean Qw	Mean Qs	Mean SSC	Mean Qb
		m ³ /s	kg/s	kg/m ³	kg/s
Climate Model	Representative Climate of Year and Averaging Interval				
GFDL-ESM2M	2000 (1976-2006)	13018	15823	0.276	273
	2020 (2006-2035)	12280	16160	0.264	258
	2040 (2026-2055)	13070	17149	0.259	274
	2060 (2046-2075)	12245	17388	0.286	257
	2080 (2066-2095)	13393	19016	0.276	281
HadGEM2	2000 (1976-2006)	13184	15894	0.162	277
	2020 (2006-2035)	19412	19703	0.164	407
	2040 (2026-2055)	17972	19823	0.171	377
	2060 (2046-2075)	20669	22528	0.152	434
	2080 (2066-2095)	24853	26049	0.165	522
IPSL_CM5A	2000 (1976-2006)	14399	16752	0.087	302
	2020 (2006-2035)	16281	18634	0.166	342
	2040 (2026-2055)	19343	21345	0.144	406
	2060 (2046-2075)	23447	24920	0.148	492
	2080 (2066-2095)	22993	26353	0.120	483
MIROC-ESM-CHEM	2000 (1976-2006)	11315	14827	0.296	237
	2020 (2006-2035)	11312	15588	0.272	237
	2040 (2026-2055)	13450	17565	0.198	282
	2060 (2046-2075)	16012	20128	0.267	336
	2080 (2066-2095)	16429	21662	0.263	345
NORESM-M	2000 (1976-2006)	12311	15310	0.272	258
	2020 (2006-2035)	14312	17059	0.250	300
	2040 (2026-2055)	14274	17753	0.279	300
	2060 (2046-2075)	15755	19275	0.273	331
	2080 (2066-2095)	16488	20706	0.235	346

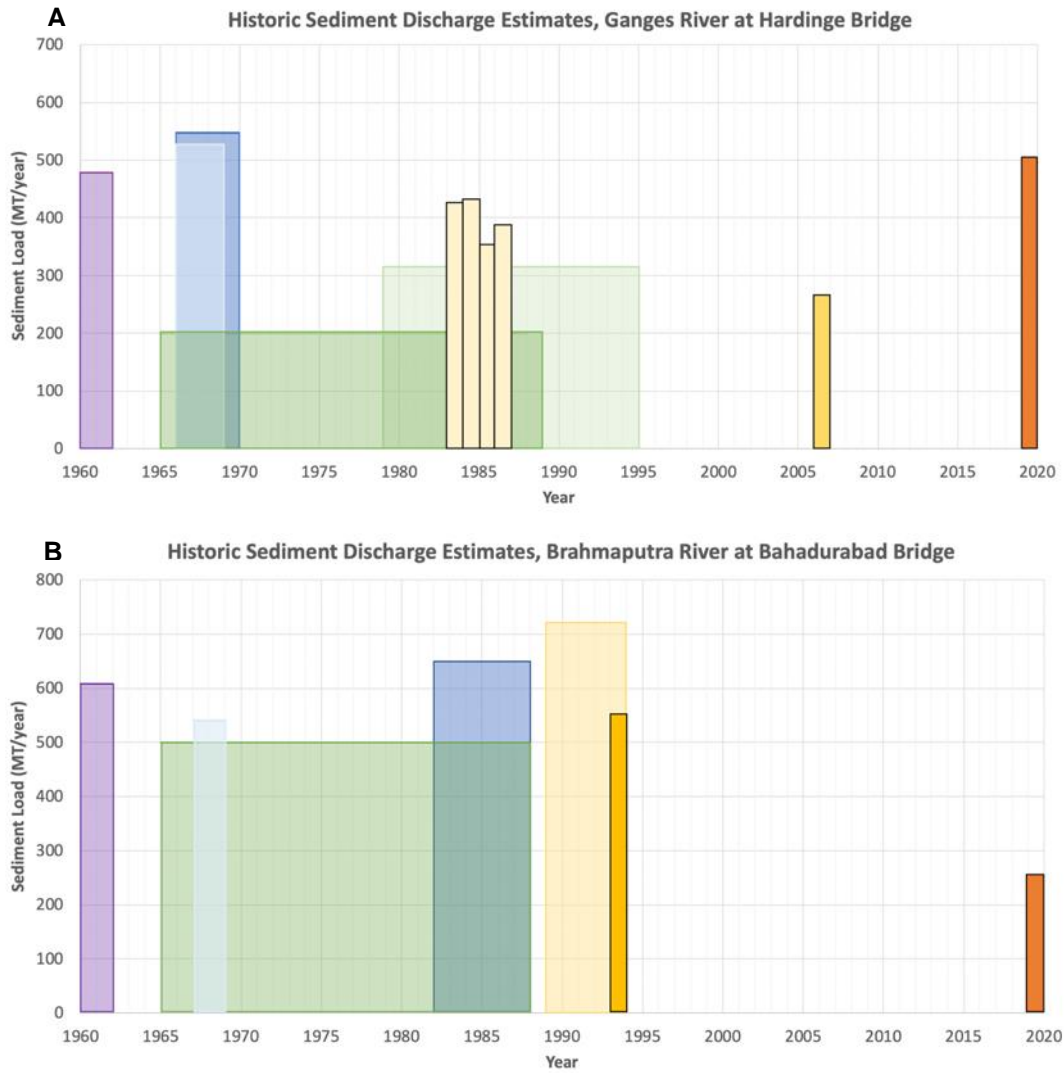


FigureApX A.5 Projected water discharge, sediment discharge, bedload discharge, and suspended sediment concentration for the Brahmaputra River driven by climate representative of the years 2020, 2040, 2060, and 2080 under the RCP4.5 emission scenario (A-D) and RCP8.5 emission scenario (E-H). Climate hindcasts for the reference scenario representative of the year 2000 are included in the line plots to amplify trends and to extend the analysis timeframe.

TableApx A.3 Summary statistics from HydroTrend simulations of the Brahmaputra basin for the reference, RCP4.5, and RCP8.5 scenarios. Reference scenario statistics are averaged over the time period 1976-200a6. RCP4.5 and RCP8.5 emission scenario values are averaged over the time periods representative of the years 2020, 2040, 2060, and 2080 (see model setup for more details). Statistics from the reference scenario (2000) are included within each climate model section in the RCP4.5 and RCP8.5 portions of the table for ease of analysis.

Brahmaputra Basin Summary Statistics					
Reference Scenario (1976 – 2006)					
Unit/description:		Mean Qw	Mean Qs	Mean SSC	Mean Qb
		m ³ /s	kg/s	kg/m ³	kg/s
Climate model:	GFDL-ESM2M	18916	7501	0.164	879
	HadGEM2	18172	7795	0.181	844
	IPSL_CM5A	18990	8159	0.141	882
	MIROC-ESM-CHEM	19284	8291	0.186	896
	NORESM-M	18947	8061	0.168	880
RCP4.5 Emission Scenario (2006 – 2099)					
Unit/description:		Mean Qw	Mean Qs	Mean SSC	Mean Qb
		m ³ /s	kg/s	kg/m ³	kg/s
Climate Model	Representative Climate of Year and Averaging Interval				
GFDL-ESM2M	2000 (1976-2006)	18916	7501	0.164	879
	2020 (2006-2035)	20164	9243	0.152	936
	2040 (2026-2055)	21088	9943	0.169	979
	2060 (2046-2075)	21374	10438	0.150	993
	2080 (2066-2095)	21807	10803	0.174	1013
HadGEM2	2000 (1976-2006)	18172	7795	0.181	844
	2020 (2006-2035)	18521	8779	0.204	860
	2040 (2026-2055)	19928	9455	0.199	926
	2060 (2046-2075)	21477	11303	0.223	997
	2080 (2066-2095)	22938	12455	0.225	1065
IPSL_CM5A	2000 (1976-2006)	18990	8159	0.141	882
	2020 (2006-2035)	21038	9925	0.093	977
	2040 (2026-2055)	22416	11379	0.170	1041
	2060 (2046-2075)	24762	13144	0.114	1150
	2080 (2066-2095)	24749	13638	0.155	1149
MIROC-ESM-CHEM	2000 (1976-2006)	19284	8291	0.186	896
	2020 (2006-2035)	19378	9167	0.178	900
	2040 (2026-2055)	19407	9975	0.181	901
	2060 (2046-2075)	22269	11885	0.213	1034
	2080 (2066-2095)	22926	12748	0.216	1065
NORESM-M	2000 (1976-2006)	18947	8061	0.168	880

	2020 (2006-2035)	20406	9356	0.172	948
	2040 (2026-2055)	21436	10388	0.179	996
	2060 (2046-2075)	21882	10834	0.183	1016
	2080 (2066-2095)	21696	10966	0.196	1008
RCP8.5 Emission Scenario (2006 – 2099)					
Unit/description:		Mean Qw	Mean Qs	Mean SSC	Mean Qb
		m ³ /s	kg/s	kg/m ³	kg/s
Climate Model	Representative Climate of Year and Averaging Interval				
GFDL-ESM2M	2000 (1976-2006)	18916	7501	0.164	879
	2020 (2006-2035)	19751	9230	0.180	917
	2040 (2026-2055)	21107	10337	0.163	980
	2060 (2046-2075)	23647	11594	0.163	1098
	2080 (2066-2095)	24724	13589	0.128	1148
HadGEM2	2000 (1976-2006)	18172	7795	0.181	844
	2020 (2006-2035)	18919	8881	0.204	879
	2040 (2026-2055)	19622	9509	0.213	911
	2060 (2046-2075)	21047	11762	0.233	977
	2080 (2066-2095)	22947	14025	0.255	1066
IPSL_CM5A	2000 (1976-2006)	18990	8159	0.141	882
	2020 (2006-2035)	22339	10480	0.155	1037
	2040 (2026-2055)	23002	12188	0.061	1068
	2060 (2046-2075)	25384	14907	0.199	1179
	2080 (2066-2095)	26780	17452	0.127	1244
MIROC-ESM-CHEM	2000 (1976-2006)	19284	8291	0.186	896
	2020 (2006-2035)	19595	9435	0.210	910
	2040 (2026-2055)	21262	11403	0.203	987
	2060 (2046-2075)	23598	14090	0.238	1096
	2080 (2066-2095)	24683	16555	0.252	1146
NORESM-M	2000 (1976-2006)	18947	8061	0.168	880
	2020 (2006-2035)	19639	8975	0.180	912
	2040 (2026-2055)	19756	9871	0.186	918
	2060 (2046-2075)	20697	11222	0.213	961
	2080 (2066-2095)	22887	13203	0.224	1063



FigureApX A.6 Historic annual sediment discharge estimates from published work. A) Ganges river evaluated at Hardinge Bridge, and B) Brahmaputra river evaluated at Bahadurabad Bridge. References from left to right (A): Coleman, 1969 (purple); FAP24, 1996 (dark blue); BWDB, 1972, in Islam et al., 1999 (light blue); Islam et al., 1999 (dark green); CBJET, 1991 (light green); Hossain, 1992 (yellow); Rice, 2010 (dark yellow), present study (orangey red). References from left to right (B): Coleman, 1969 (purple); CBJET, 1991 (green); BWDB, 1972, in Islam et al., 1999 (light blue); Hossain, 1992 (dark blue); Islam et al., 1999 (light yellow); Kabir and Ahmed, 1996 (dark yellow); present study (orangey red).

C Development river network model (Delft3D-FM 1D)

C.1 Introduction and outline

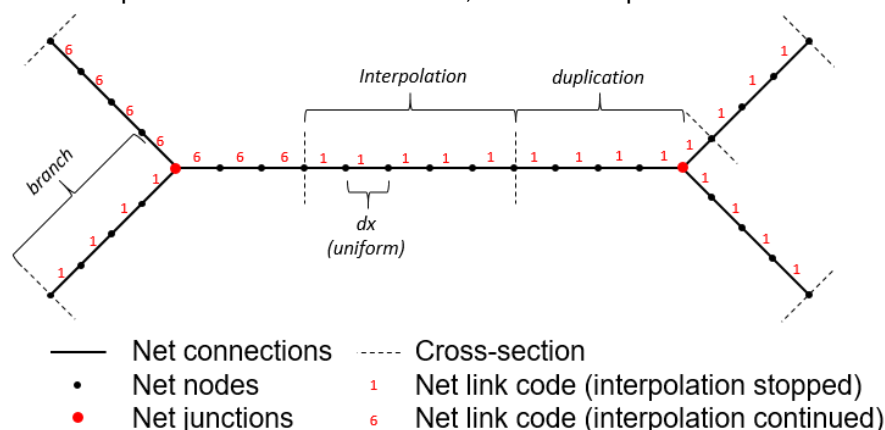
The following sections of this appendix discuss all aspects of the development of the Delft3D-FM 1D river branch model. The model set-up is discussed in Section C.2 through Section C.8. The procedure can be summarized as:

- Setting up a numerical network that covers the most important river branches of the GBM delta
- Constructing cross-sectional profiles to give a proper representation of the dimensions of the channels
- Imposing boundary conditions of hydrodynamics and sediment input

Subsequently, hydrodynamic calibration of the model is shown in Section C.9 and a sediment balance is derived in Section 0. These results are discussed in the last section (Section C.11) as part of model performance and the application of the model to simulate future projections on changes in climatic conditions is elaborated on.

C.2 Numerical network

The numerical domain of Delft3D-FM consists of a fully unstructured network (Kernkamp et al., 2011). In the 1D mode the network can be expressed as a set of converging and diverging lines, representing for example river branches including confluences and bifurcations. In FigureApx C.1 a schematic diagram of a simplified 1D numerical network is shown. The physical properties (e.g. bed level, water depth) are specified and calculated at the net nodes of the network, which are linked through 1D net links (connections) with a (uniform) spatial discretization. The net links that are located between net nodes joining more than two net links (a junction) make up a (river) branch. The cross-sectional area and base level at the net nodes is specified by user-defined profiles. To reduce the required input, these profiles do not have to be specified for each net node in a network. The cross-sectional area and base level are interpolated (between profiles) or duplicated (between a profile and junction) from neighbouring profiles within a single branch. In the default case, interpolation is not continued along connecting branches at a junction (net link code = 1). However, the user can continue the interpolation (net link code = 6) along a junction so that the cross-sectional profile and base level change smoothly over the course of the main branch (e.g. in case of a confluence of a large and a smaller river). In the model set-up of the 1D GBM delta model, both these options will be used.



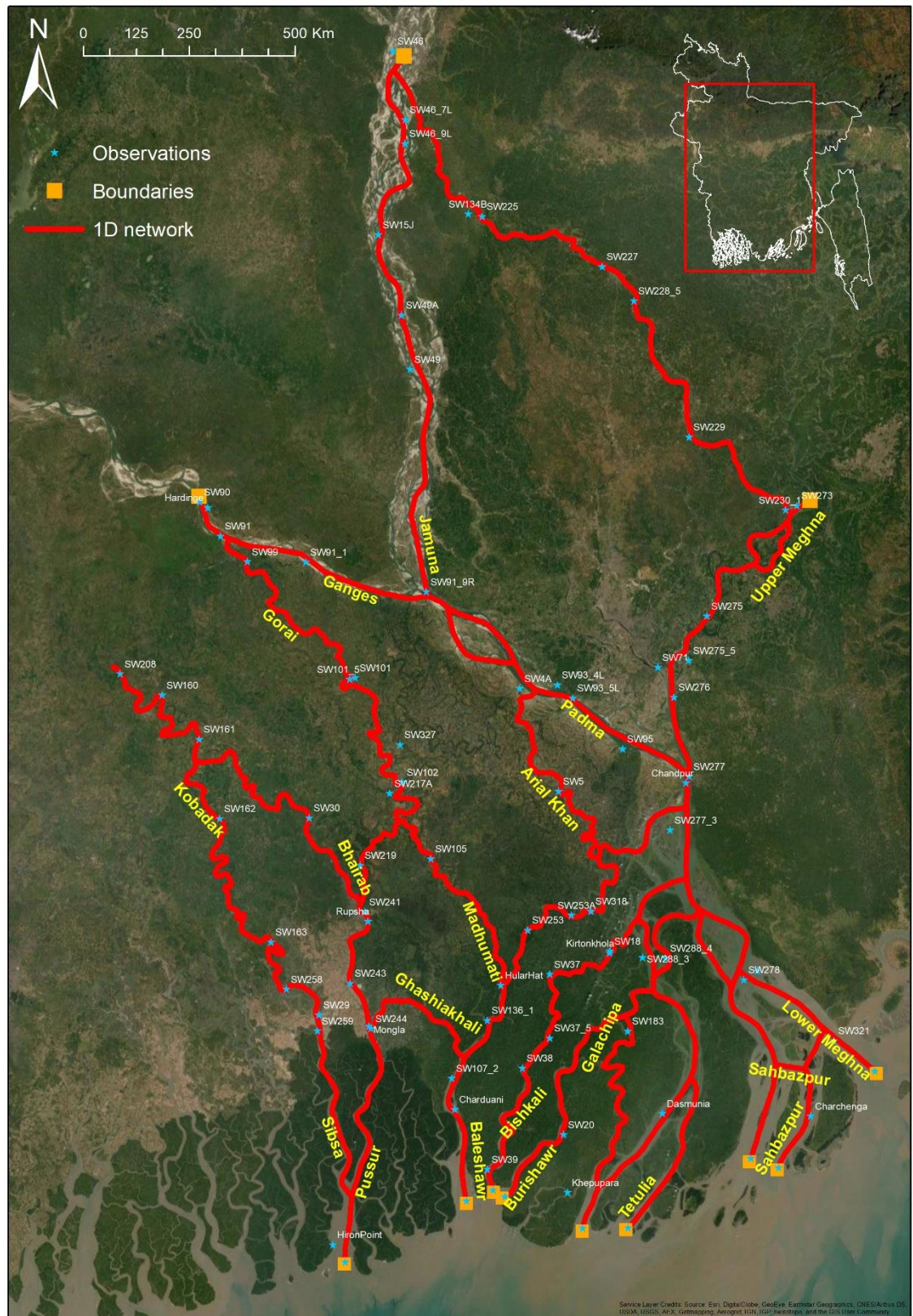
FigureApx C.1 Interpolation scheme of the Delft3D-FM 1D model.

The GBM delta is schematized in a 1D network from the upstream part of the three major rivers (Ganges, Brahmaputra, and Meghna) up to the seaward limit of the major estuaries (from west to east: Pussur-Shibsha, Baleshawr, Bishkali, Burishawr, Galachipa, Tetulia, Sahrpazpur, and the main branch of the Lower Meghna). The network is schematized using GIS software and the choice for the extent of the model (i.e. which branches to include) is based on experience and local knowledge (pers. comm. IWM). The schematization is converted to a numerical network suitable for the modelling suite using the embedded RGFRID tools. In this procedure a spatial discretization of 1500 m is used for the spatially uniform distance between net nodes. The spatial interval is chosen as a compromise between accuracy of the river branch geometries and computational efficiency. The network is shown with the names of the rivers in FigureApx C.2.

Properties of the numerical network are shown in TableApx C.1 Parameters of the 1D GBM model network. Although Delft3D-FM calculates a maximum allowed computational time step during the simulation based on the Courant-Friedrichs-Lewy (CFL) number, a couple of other time steps need to be set and are network (grid) dependent. The initial time step (dt_{ini}) specifies the time step for the very first computational step which is needed because no model results are available yet to calculate the CFL conditions (this value should be small). The user time step (dt_{user}) specifies the time step used for updating the boundary conditions, and the maximum time step (dt_{max}) specifies a maximum limit during the simulation (irrespective of CFL conditions).

TableApx C.1 Parameters of the 1D GBM model network.

Property	Values
Coordinate system	Bangladesh Transverse Mercator (BTM)
Vertical datum	Public Works Datum (PWD)
Extent of domain	$x_1 = 276017, y_1 = 448780$ $x_2 = 807850, y_2 = 696230$
Number of net nodes	1950
dx	1500 m
dt_{ini}	1 s
dt_{user}	300 s
dt_{max}	60 s



FigureApX C.2 Schematization of the major river branches in a network for the 1D GBM model, including locations where boundary conditions are forced and observation points used for model-data comparison.

C.3 Cross-sectional profiles

C.3.1 Bathymetric dataset

The 1D GBM model covers a vast area of the Bangladeshi part of the delta, and as such, an extensive dataset of bathymetric measurements is used to define the cross-sectional profiles. The data is described in Appendix A.

C.3.2 Profile types

In Delft3D-FM 1D (river branch) models the cross-sectional area and base level in the model environment are provided by the geometry of profiles specified at branches in the network. The cross-sectional profiles can be schematised and prescribed to the model in different ways. In all cases it is essential to know that a 1D model uses the model input to calculate storage and conveyance. The storage width is represented by the total width at the water surface, and the conveyance is represented by two parameters, viz. the flow-carrying cross-sectional area and the hydraulic radius:

$$R = A/P \tag{1}$$

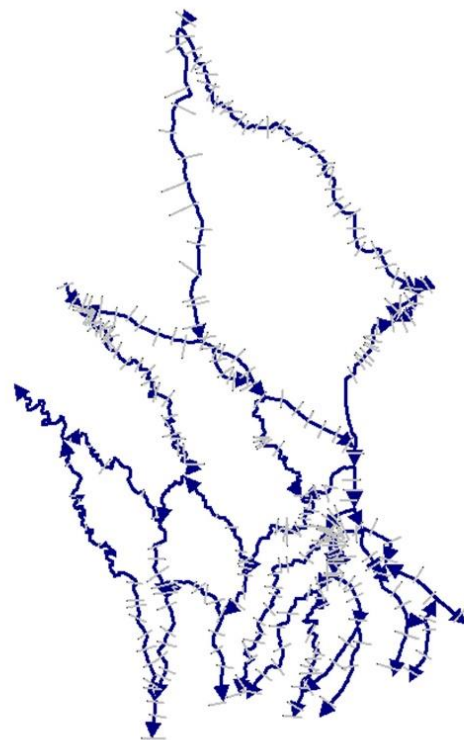
Here, A is the flow-carrying cross-sectional area and P is the wetted perimeter. This means that any way of schematisation of the cross-sectional profiles can be used as long as these parameters are correctly represented. It should further be noted that these parameters vary spatially (along a branch) and temporarily (with the varying water level due to tidal motion or river discharge variation). Thus, the specified cross-sectional profiles for a branch in the river network need to represent the variations in these parameters along the branch at any possible water level.

In this study two alternative types of profiles are used:

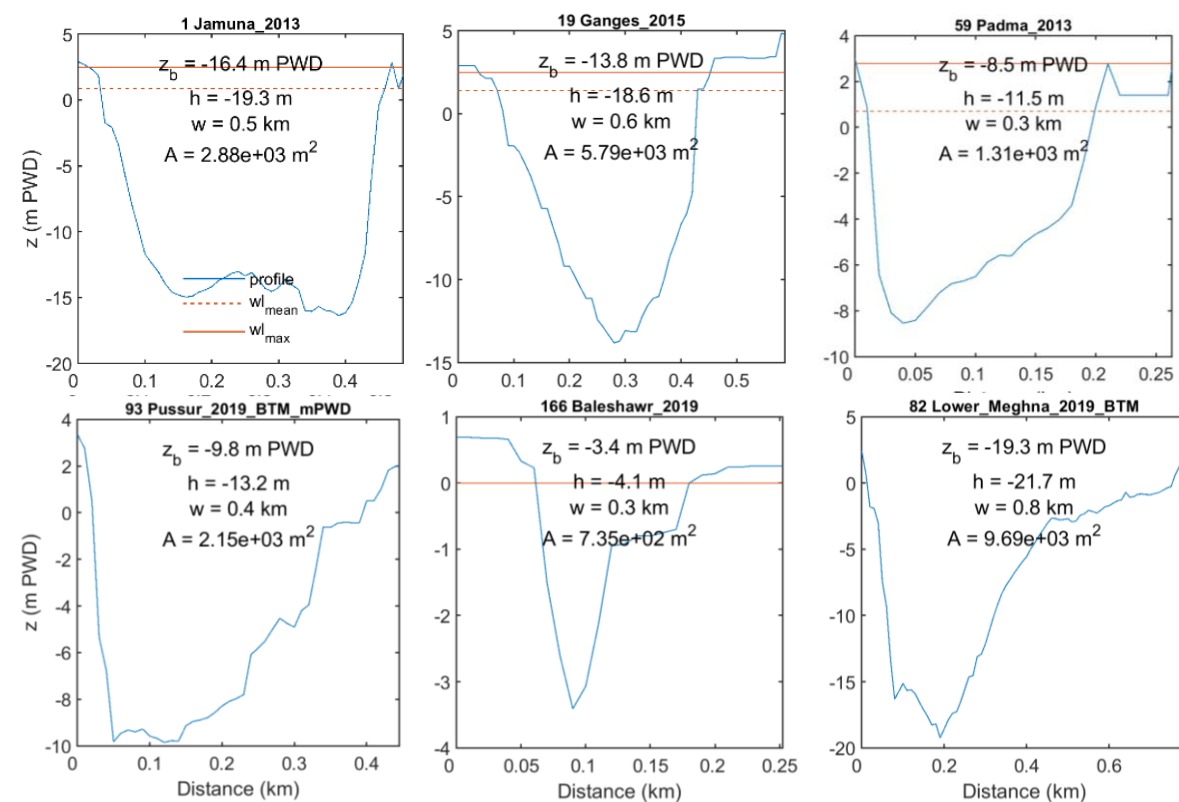
- Measured
- Hybrid (schematized from bathymetric observations)

C.3.3 Measured profiles

The model set-up with measured profiles uses the most recent dataset of each river if the spatial coverage of this dataset is sufficient, otherwise an older dataset is used. The selection of the profiles is done using GIS software and the shapefiles of the datasets, shown in FigureApx C.3. The original profiles filtered out of the datasets consist of very high-resolution data (i.e. several measurements in one-meter length). Forcing the model with such an enormous amount of data is unnecessary. The spatial resolution of the profiles is therefore reduced to a 10 m resolution for profile with widths less than 500 m and 50 m resolution for profiles with widths more than 500 m. Showing figures of all profiles would be excessive, therefore a few examples are shown in FigureApx C.4.



FigureApX C.3 Map showing the selection of measured profiles.



FigureApX C.4 Examples of a few selected profiles (source dataset shown in figure titles), including the base level (z_b), the height to the banks (h), the maximum width (w), and the cross-sectional area (A).

C.3.4 Hybrid profiles

The model set-up with hybrid profiles has the advantage over the measured profiles that the measurements of several profiles (in time as well in space) can be used to derive a characteristic cross-sectional profile for a section of a river branch. The hybrid profiles are constructed from subsets of the bathymetric dataset. The selection of the subsets is done by (manually defined) polygons that cover a part of a river branch (FigureApx C.5). The size of the polygons depends on the change in geometric properties of the river and data availability. The size should not be too small as the geometry of the constructed 'characteristic' profile will resemble the geometry of an actual observed profile (reducing the advantage of the schematization) and not too large as longitudinal variations will be discarded.

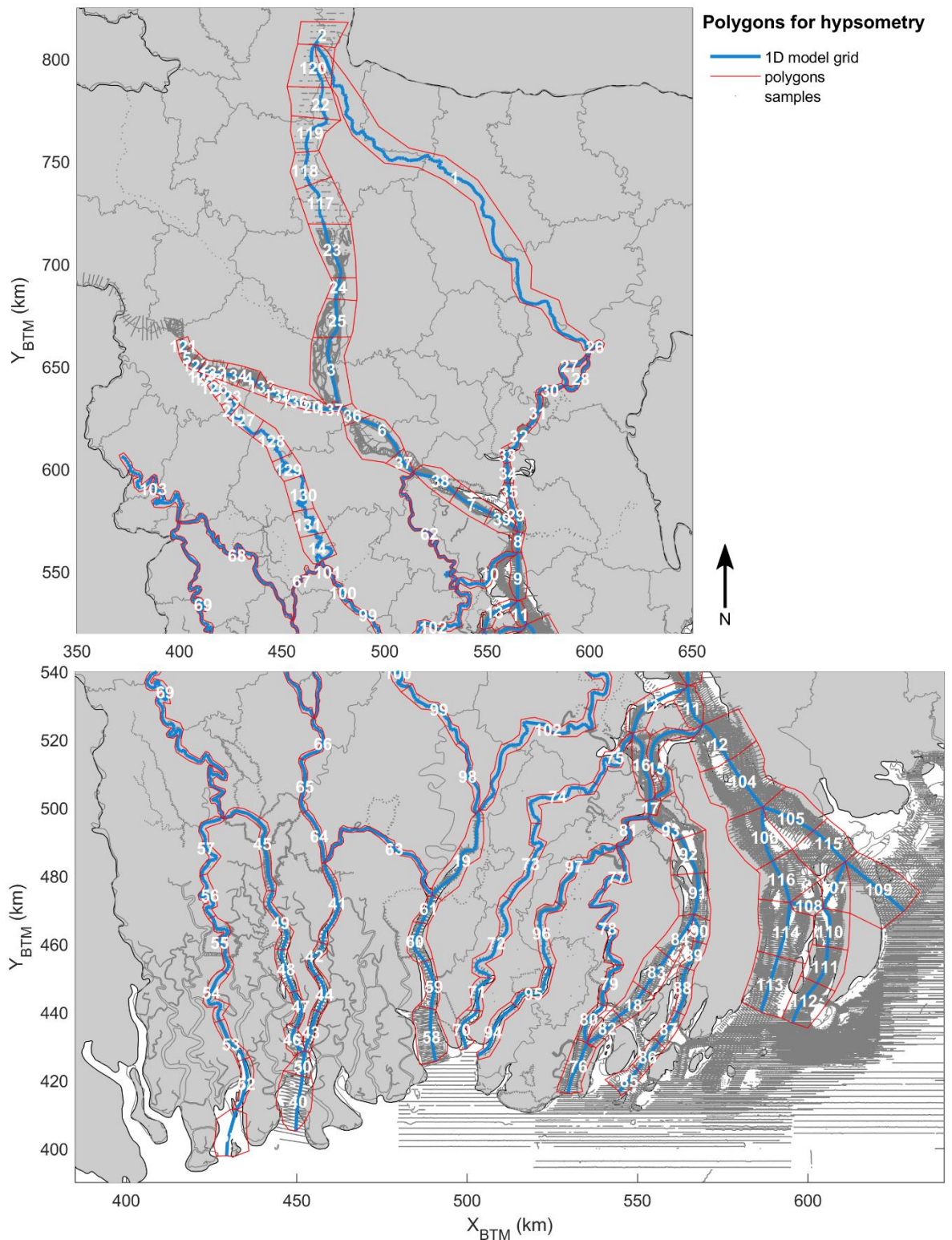
The subsets of the bathymetric dataset are used to create a tightly fitting polygon on the data (inner polygon in FigureApx C.6). This polygon is used to set-up a local mesh grid where the values of the grid cells are determined by the median of all samples that fall within a grid cell. From the gridded dataset the following properties are calculated:

- The total area of grid cells that contain data,
- The distribution in elevation (histogram) of the subset of the data.

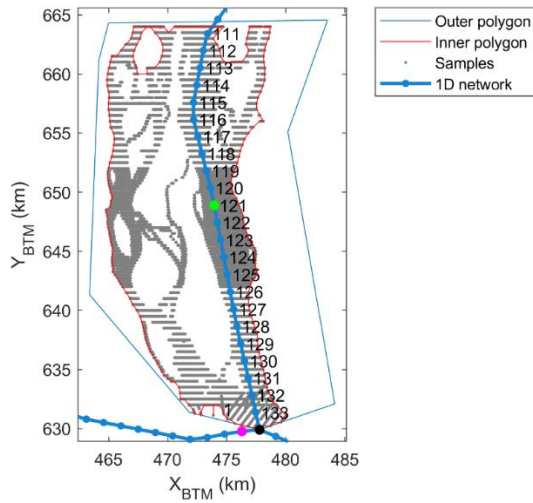
Grid cells with no data coverage are not taken into account. The distribution in elevation is schematized by establishing a probability density histogram (FigureApx C.7a) on the height level of the gridded topo-bathymetric observations (the width of the bins is determined via an automated algorithm). Subsequently, a hypsometric curve is established based on the total area of the grid cells and the values of the binned dataset of elevation (FigureApx C.7b).

To set-up a schematized profile, the width of the river should be known as well. In other (e.g. SOBEK) type of 1D river branch models this is an easy procedure as the length of a river branch is known from the model architecture. Because the Delft3D-FM 1D model network is fully unstructured, this quantity is hard to derive, and the river width is therefore inserted as manual input for each manually defined polygon. With the information on the width of the river section and the hypsometric curve, a characteristic and symmetric profile can be established (FigureApx C.7c). Finally this profile is defined in x,y,z coordinates and positioned at the net node closest to the centre of the boundary fitted polygon (FigureApx C.7d).

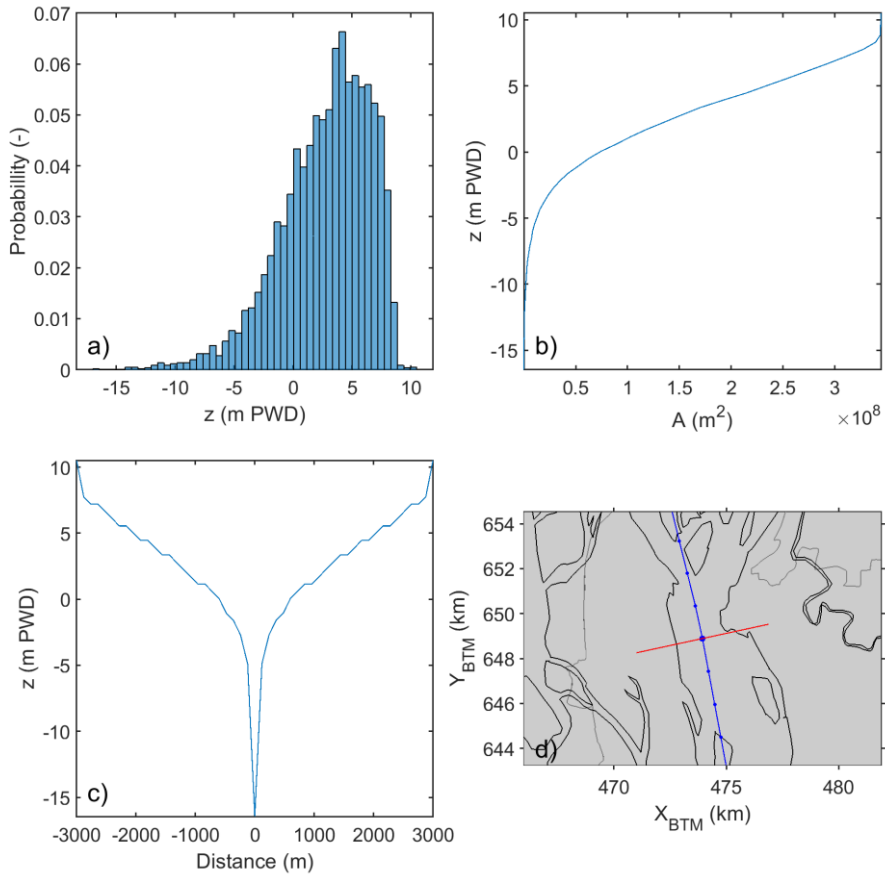
The validity (correctness) of the schematization procedure is studied by comparing the morphological characteristics of the river from the hybrid profiles with respect to these properties derived directly from the observed profiles (FigureApx C.8). The figure shows that mean and maximum bed level of the hybrid profiles compare well to the observed profiles (FigureApx C.8c), both for a tidal and non-tidal river. The width is manually inserted and, therefore logically, compares well to the data as well, leading to a proper presentation of the cross-sectional area in the schematized profiles.



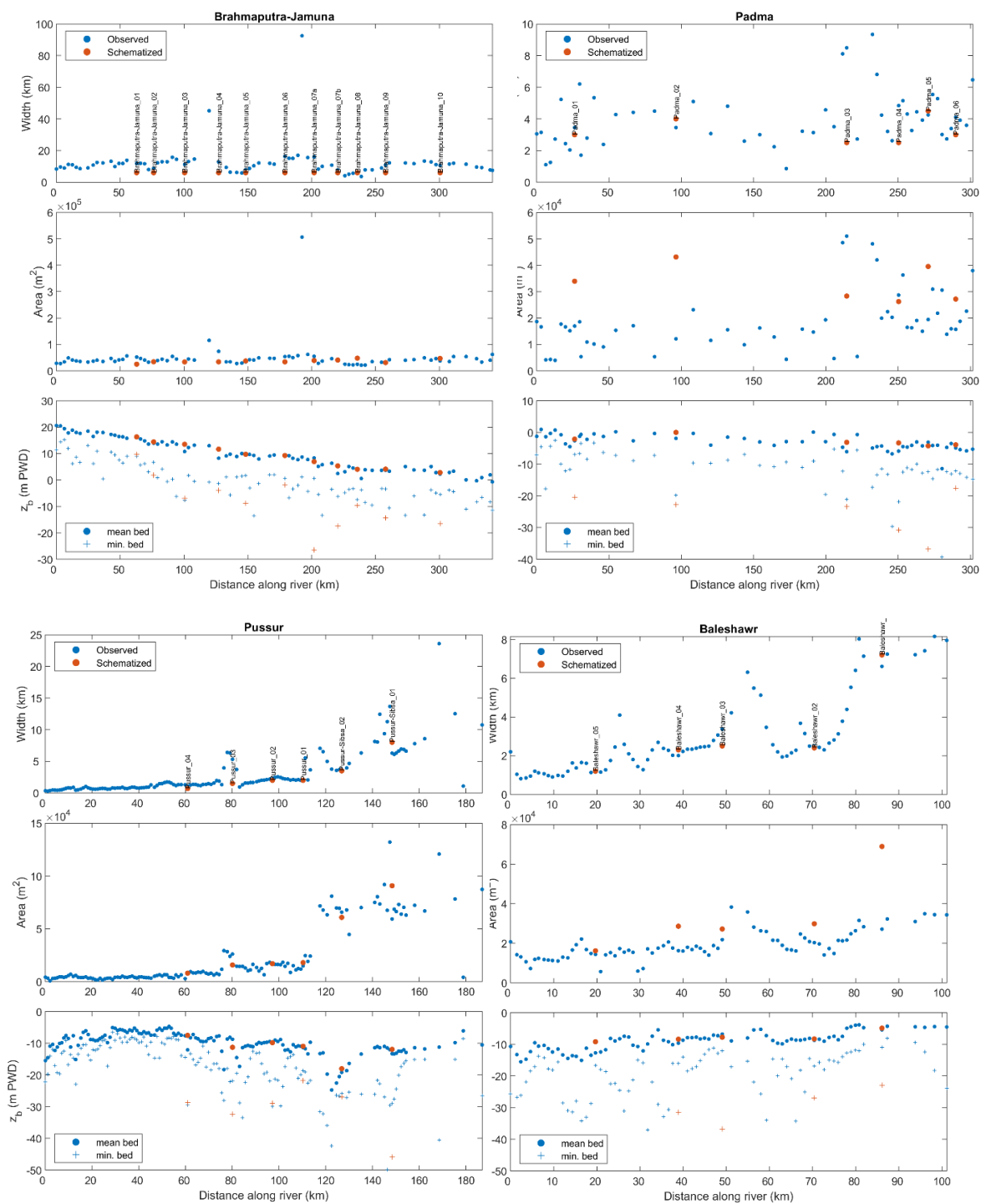
FigureApX C.5 Map of the GBM delta with the model network (blue), the topo-bathymetric observations (gray dots), and the polygons (red) defining sub areas of the river branches for schematization of the hybrid profiles.



FigureApX C.6 Example of methodology to derive an area and river length based on a tightly data-fitting polygon (red), which is found by the definition of manually defined outer polygons (blue).



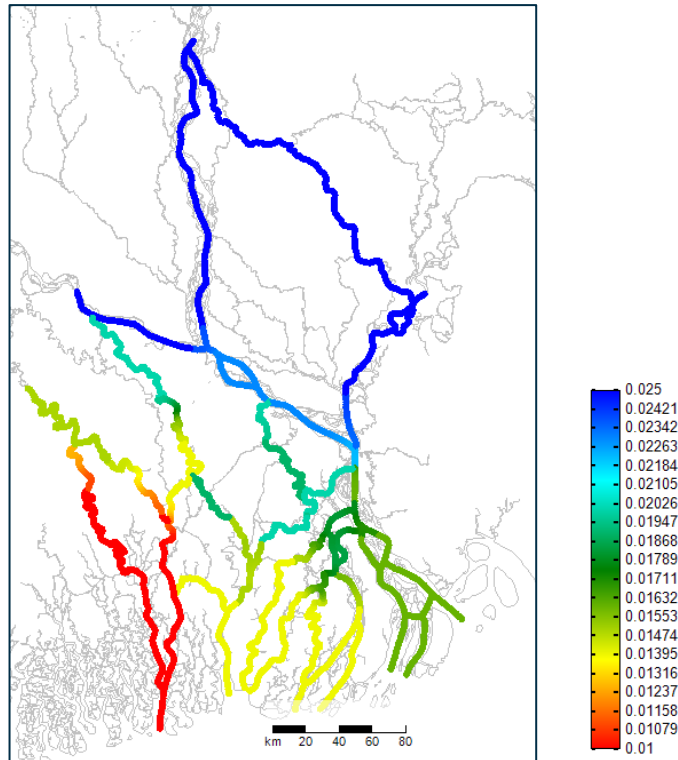
FigureApX C.7 Methodology of schematizing cross-sectional profiles, illustrated for the downstream part of the Brahmaputra: a) histogram of the gridded topo-bathymetric observations within the sub area defined by the polygon; b) hypsometric curve derived from the histogram; c) schematized cross-sectional profile constructed from the hypsometric curve and the river width; d) positioning of the cross-sectional profile on to the model network.



FigureApX C.8 Morphological characteristics of the Jamuna (non-tidal) and Pussur (tidal) rivers derived from observed profiles (blue) and schematized hybrid profiles (red). Figures shows river width (a), cross-sectional area (b), and mean and minimum bed level of the profiles (c).

C.4 Friction

A spatially varying Manning's coefficient (Manning's n) is imposed on the model as roughness coefficient. The values shown on the map in FigureApX C.9 are the final result of a best comparison with waterlevel and discharge data.



FigureApX C.9 Spatially varying roughness field (Manning's n) imposed on the 1D model.

C.5 Sediment model

Sediment transport is modelled via built-in sediment transport formulations that are coupled online (updated every computational time-step) to the hydrodynamics. A cohesive (mud) and non-cohesive (sand) sediment fraction is modelled. The transport formulations and the associated parameter values are identical to the sediment model used for the (2D) coastal model (see Appendix D).

C.6 Boundary conditions

C.6.1 Upstream

The upstream open model boundaries are situated at the three major rivers (from west to east) Ganges, Brahmaputra, and Meghna (FigureApX C.2). Due to the availability of long-term discharge observations at Hardinge Bridge (Ganges), Bahadurabad (Brahmaputra), and Bhairab Bazar (Meghna) (see Appendix A) the open boundaries are situated exactly at these locations (and not at Bangladesh' national border). At these upstream boundaries the model is forced hydrodynamically with measured discharge time series (FigureApX C.10) for calibration and validation purposes. For model application (see Section C.8) the model is forced by a hydrograph that resembles the mean annual discharge variation. The construction of this hydrograph is described in the set-up of the coastal model (see Appendix D).

Suspended sediment concentrations are derived from literature (see Chapter 2) and are prescribed as mean annual values. For non-cohesive sediment an equilibrium concentration is prescribed and for cohesive sediment constant values of 900 mg/l (Jamuna and Ganges) and 100 mg/l (Upper Meghna) are included in the model (similar to the coastal model).

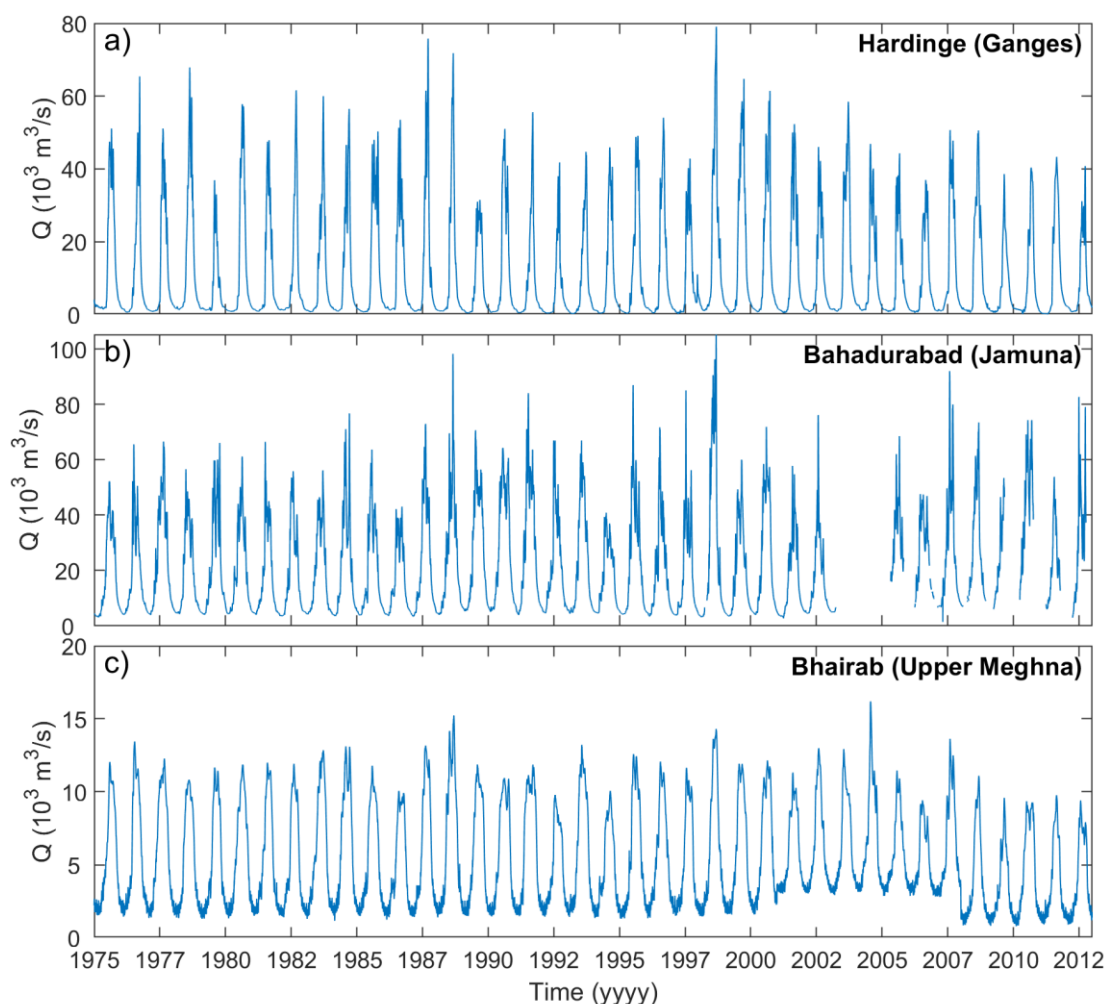


Figure C.10 Timeseries of discharge from 1975 up till 2012 at the three measurement locations (Hardinge, Bahadurabad & Bhairab) used to force the model at the upstream boundaries.

C.6.2 Downstream

The downstream boundary conditions are imposed at the seaward boundaries of the estuaries (Figure C.2). The hydrodynamic boundary conditions consist of astronomical tidal constituents, prescribing the amplitude and phase of the tidally induced water level fluctuations. The 1D and 2D models are set-up in such a way that they are independent of each other, therefore the constituents are derived from the MIKE21 Bay of Bengal model (Uddin et al., 2014). The boundary information includes all tidal constituents that could be solved from two-year (2014 – 2015) model results.

C.7 Initial conditions

To reduce the spin-up time of the model – and to avoid numerical instabilities in the initial stage of the model simulation – a best estimate for the initial conditions are imposed on the model. The initial water level is derived from the observations and interpolated to the model net nodes. Second, a new initial conditions file is created from the output of a previous model simulation to deliver the best spatially

varying conditions. The initial bed composition is spatially uniform and equal to the coastal model (see Appendix D).

C.8 Model simulations

The boundary conditions imposed on the model for the hindcasts allow to simulate any time period within the availability of the discharge data (see FigureApx C.10). Two time periods were chosen to serve the following purposes: a short time period that overlaps with the availability of data for water level comparison, and a long time period that allows for a proper comparison of the model with daily discharge measurements. Subsequently, the model is applied to derive the mean annual flow and sediment budget in the GBM delta for the purpose of (a qualitative) validation. In TableApx C.2 the settings and the purpose of the model simulations are summarized.

TableApx C.2 Simulation types with the period modelled and the purpose of the simulation.

Simulation type	Time period	Purpose	Section
Calibration	1 Apr 2012 – 7 Oct 2012	Comparison to observations (several months) on water levels	C.9.1
	1 Jan 1975 - 1 Jan 2000	Comparison to long-term (25 years) observations on daily discharge	C.9.2
Validation	Hydrograph (25 reps.)	Mean annual flow and sediment budget	0

C.9 Calibration of hydrodynamics

This section describes the results of the calibrated models with measured and hybrid profiles. The model input parameters that are used to calibrate the models are the cross-sectional profiles and the spatial variation in the roughness coefficient. In a 1D model a large portion of a branch is represented by a single cross-sectional profile and therefore the model is most sensitive to (small errors in) the cross-sectional profiles. Consequently, most of the calibration effort has been devoted to the representation of the bed level; i.e. an appropriate choice of representative measured profiles and the method of constructing hypsometric curves from the measurements. Variations in spatially varying roughness values were tested to optimize model outcomes. The full calibration procedure is not reported but rather the final calibrated model outcomes are shown for both the measured and schematized profiles.

C.9.1 Water levels

The model variants with measured and hybrid profiles are both run for a short period (several months) to directly compare to observations of water levels. First, a time-series analysis is made and secondly performance of the model is evaluated in the tide-dominated part of the GBM delta using harmonic analysis.

C.9.1.1 Time-series

FigureApx C.11 shows for both models target-diagrams of the error statistics BIAS and Root Mean Squared Error (RMSE);

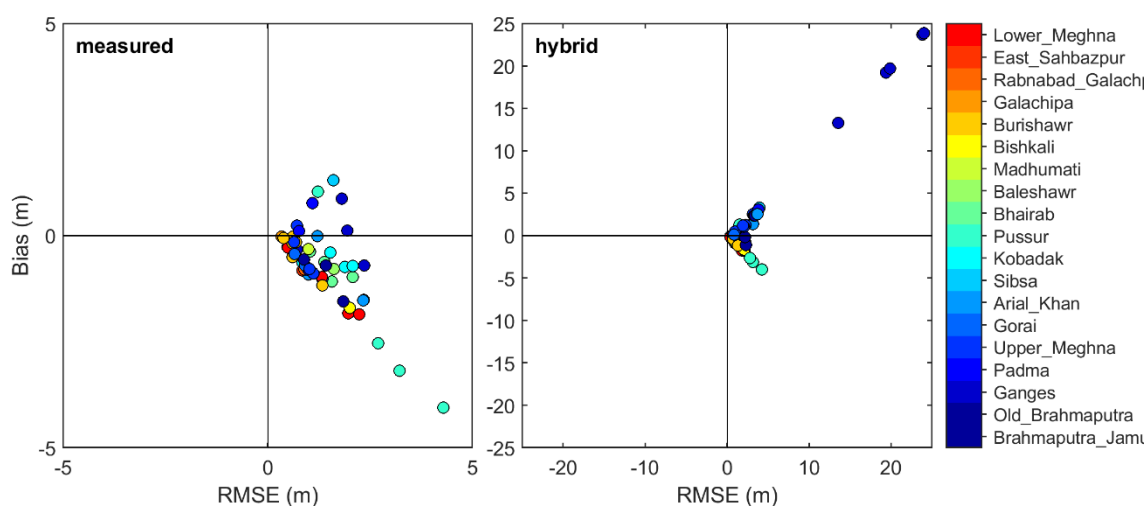
$$(2) \quad BIAS = \frac{1}{n} \sum (X_{sim} - X_{obs})$$

$$(3) \quad RMSE = \sqrt{\frac{1}{n} \sum (X_{sim} - X_{obs})^2}$$

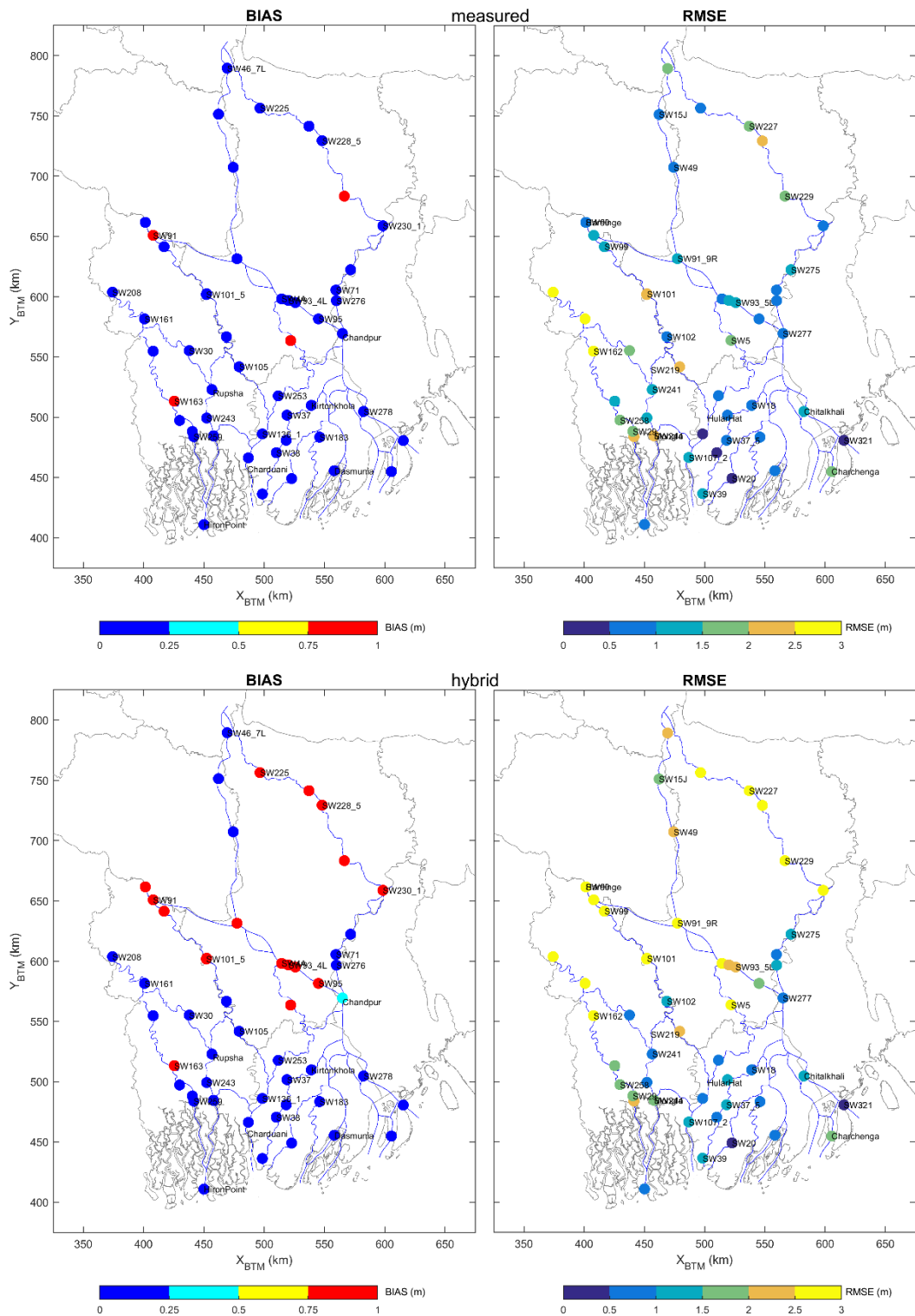
subdivided per river system as indicated by the colouring. The figure shows that model results for both measured and hybrid profiles cluster near similar error values for both statistics but clearly perform less for specific river systems. FigureApX C.12 shows the spatial distribution of the error statistics. The figure shows that the Kobadak river performs poor in both models, which is mainly due to a lack of bathymetry measurements to construct realistic cross-sectional profiles. Therefore, the Kobadak river will not be considered in this study. The hybrid model shows, contrary to the measured model variant, that it is not performing well for the upstream (non-tidal) rivers (red colours). Timeseries plots of the (mainly) non-tidal rivers Ganges (FigureApX C.13) and Padma (FigureApX C.14) show that both model variants perform well in dry-season (April-May) and perform less in monsoon-season (after July). This model mismatch in the monsoon season is the worst for the hybrid model variant.

The reason for the model mismatch is the availability of bathymetry measurement on the floodplains (chars) in the upstream rivers. In the monsoon season, the floodplains become an important part of the flow-carrying (conveying) cross-section of the river and hence, a detailed description of the hypsometry of the floodplains is required. Bathymetry measurements are scarce at the floodplains which means they are not represented well in the hybrid model variant. In the measured model variant, this effect is present as well but reduced because the hypsometry of the floodplains (gaps in the cross-sections) is estimated using linear interpolation (FigureApX C.15). Improvement of model performance can be achieved by a more detailed bathymetry of the floodplains.

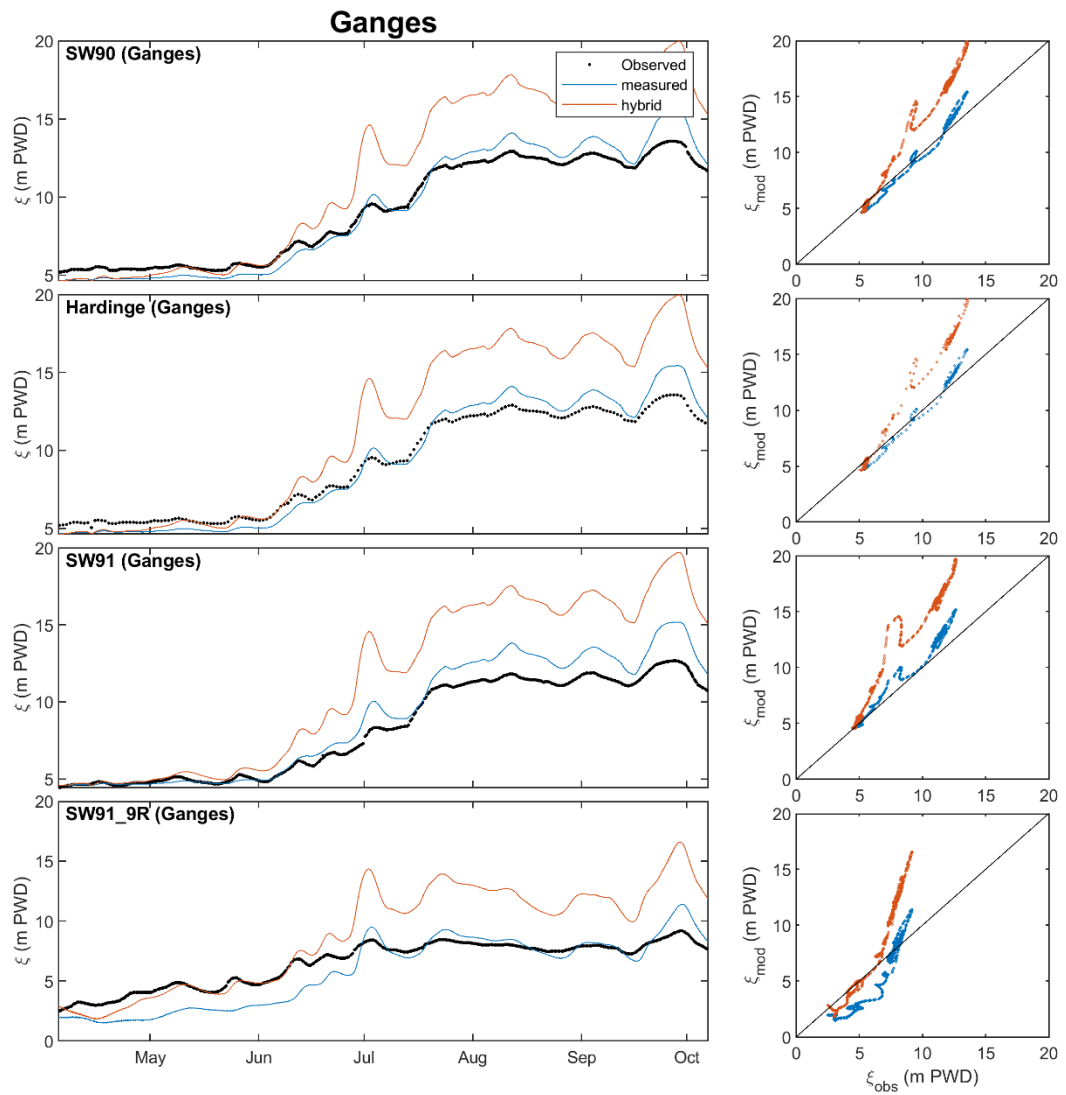
Timeseries of the modelled and observed water levels in the tidally dominated part are pre-processed by removing low-frequency variation by means of a Godin filter (Godin, 1972) to show the performance of the tidal reproduction. An example is visualized for the Pussur estuary (FigureApX C.16). The timeseries show a similar performance of both models but also reveal that this analysis does not give a proper indication the tide-dominated part; a small phase shift results in a large mismatch and there is no overlap on data availability in each station. Therefore, the tidal reproduction of tidal properties is evaluated in the next section through harmonic analysis.



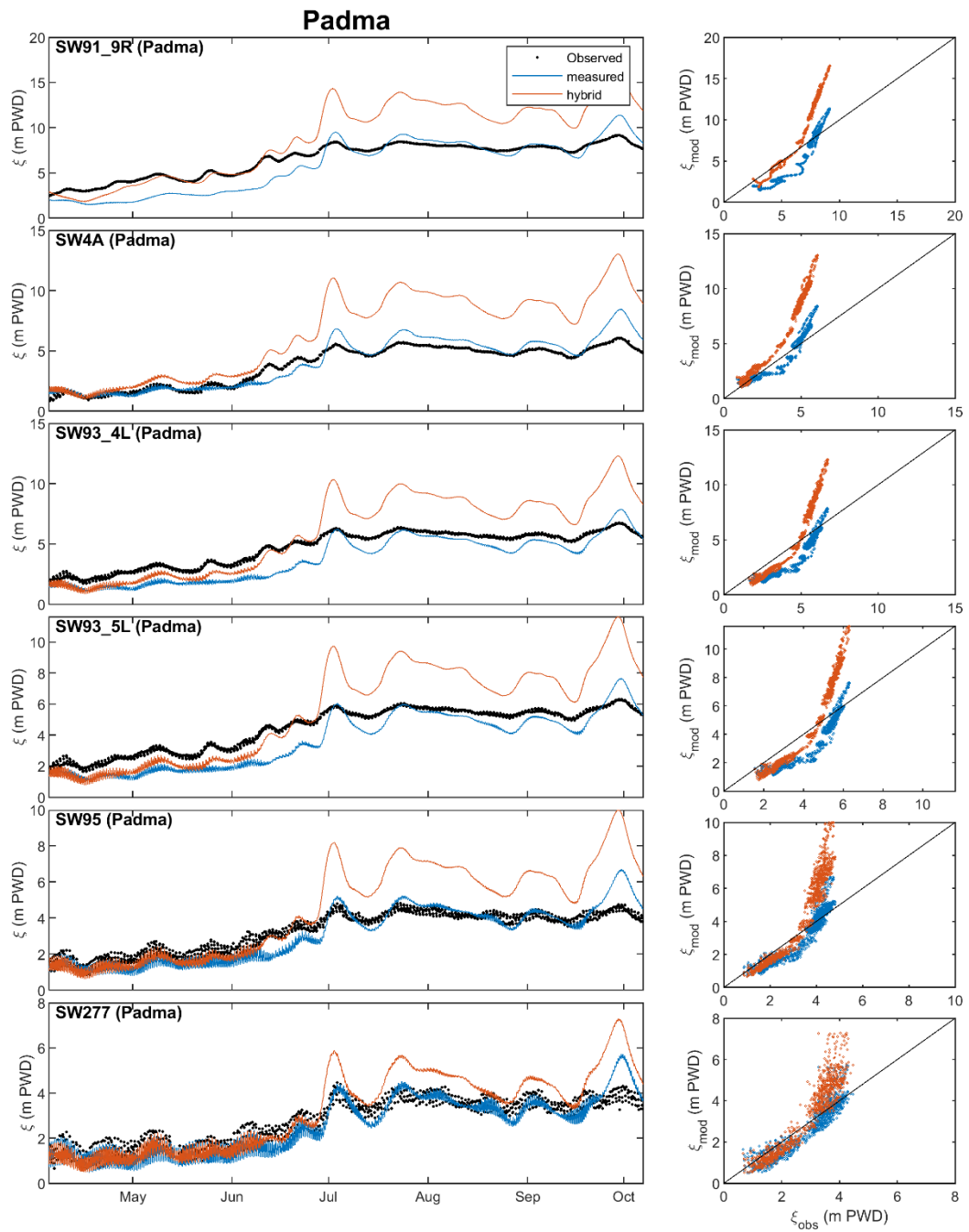
FigureApX C.11 Target diagram of the BIAS and RMSE between model results and observations on water levels, for the model with measured (left) and hybrid (right) profiles. River systems are indicated by the colours. Scales are different on both figures.



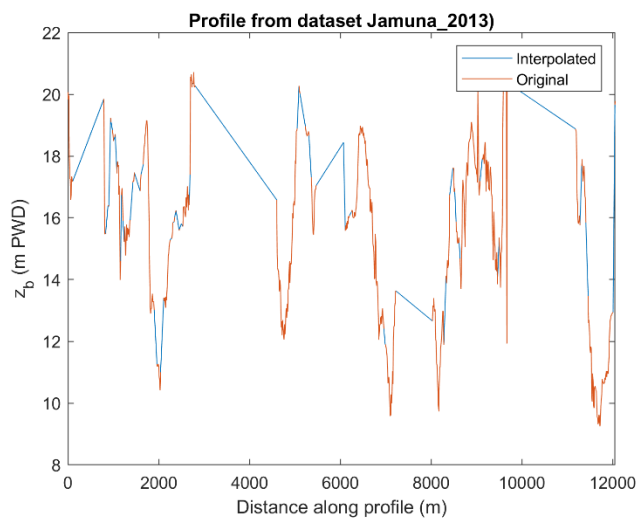
FigureApX C.12 Map overview of the BIAS (left) and RMSE (right) between the model with measured (top) and hybrid (bottom) cross-sections and observations.



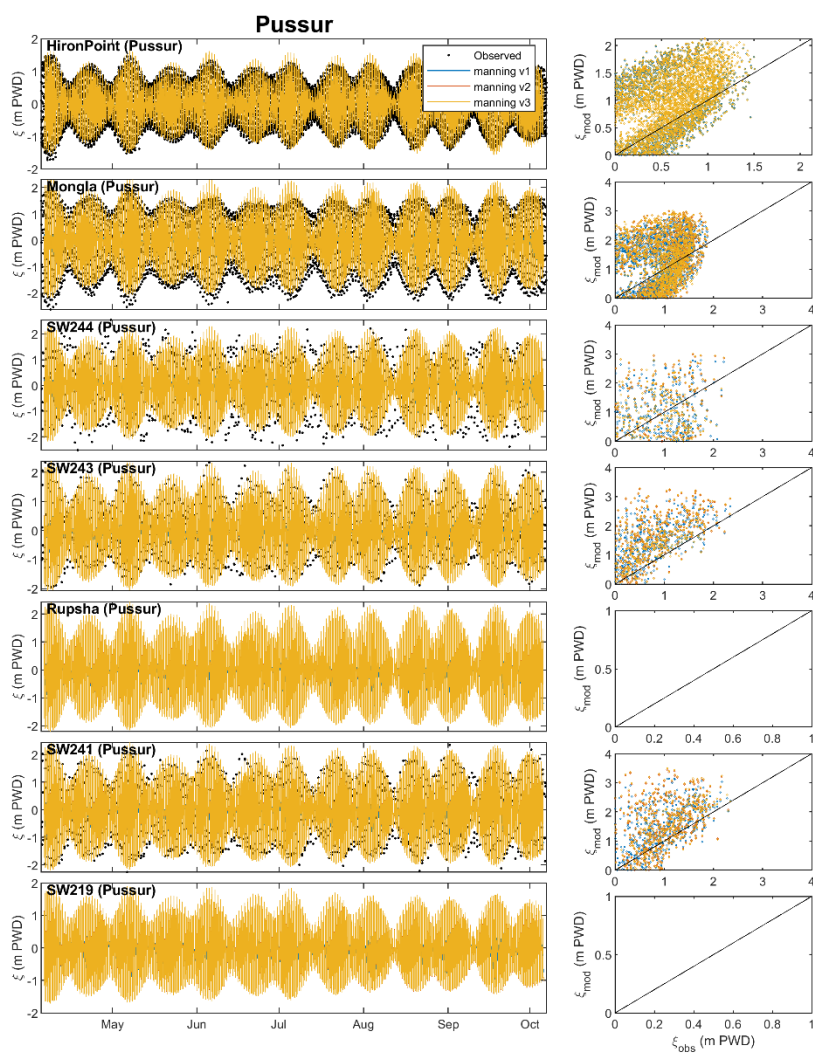
FigureApX C.13 Timeseries of the modelled and observed water levels in the Ganges from upstream (Hardinge Bridge) to the downstream confluence of the Ganges and Jamuna in to Padma.



FigureApX C.14 Timeseries of the modelled and observed water levels in the Gorai-Madhumati river from upstream (bifurcation of Ganges) to the downstream bifurcation towards the Baleshavr (upstream of Khulna).



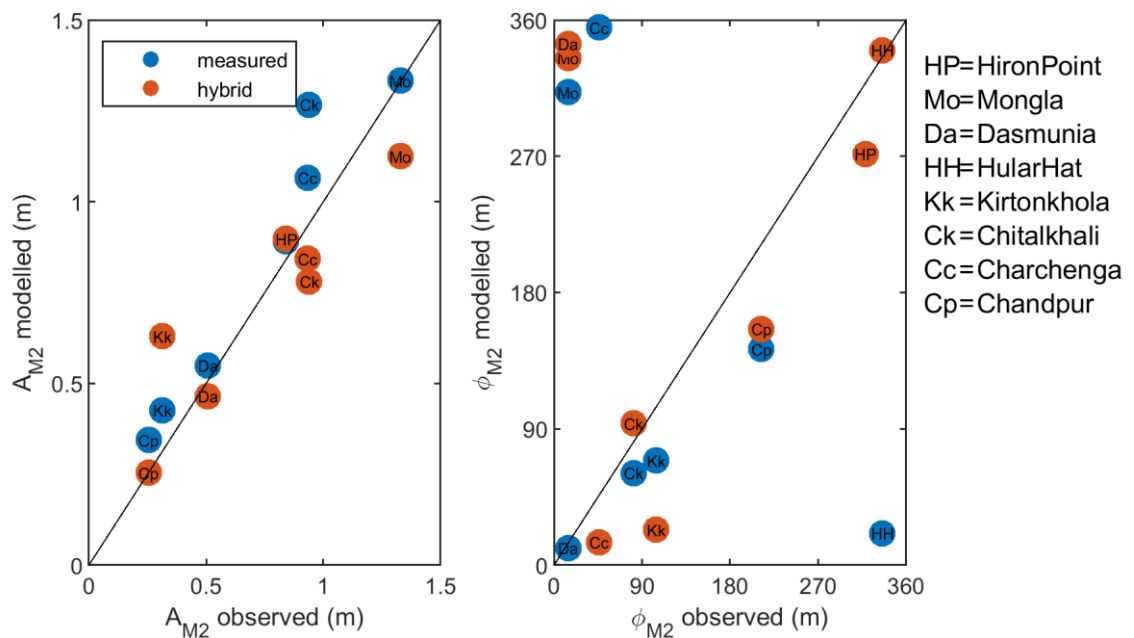
FigureApX C.15 Cross-sectional profile in the Jamuna, showing observed values (red) and char sections which are filled in by interpolation (blue).



FigureApX C.16 Comparison of modelled and observed water levels in the tidally dominated Pussur estuary, for the model with measured (left) and hybrid (right) profiles.

C.9.1.2 Tide

Harmonic analysis is a powerful way to analyse tidal propagation in the GBM delta and provides a good measure for model comparison. However, as explained in Appendix A, harmonic analysis on the available data is not straightforward as tidal signals are highly non-stationary and the coarse temporal resolution hampers the analysis. The consequence is that this analysis can only be done for the 30-min interval data from the BIWTA, at locations where sufficient data is available, the 3-hr interval data from the BWDB are omitted. FigureApx C.17 shows a comparison of modelled and observed amplitudes and phases for the main semi-diurnal tidal constituent (M_2). The figure shows that both models perform similar in the tide-dominated part of the delta; the model variant with measured profiles shows a slight overprediction of amplitudes, and the model variant with hybrid profiles a slight underprediction. The reproduction of tidal phases is shown on the right side of FigureApx C.17, the figure gives the impression that there are a few outliers, but this is caused by a difference close to 360° . In general, it can be concluded that both model variants perform reasonably well for the tide-dominated part of the GBM delta.



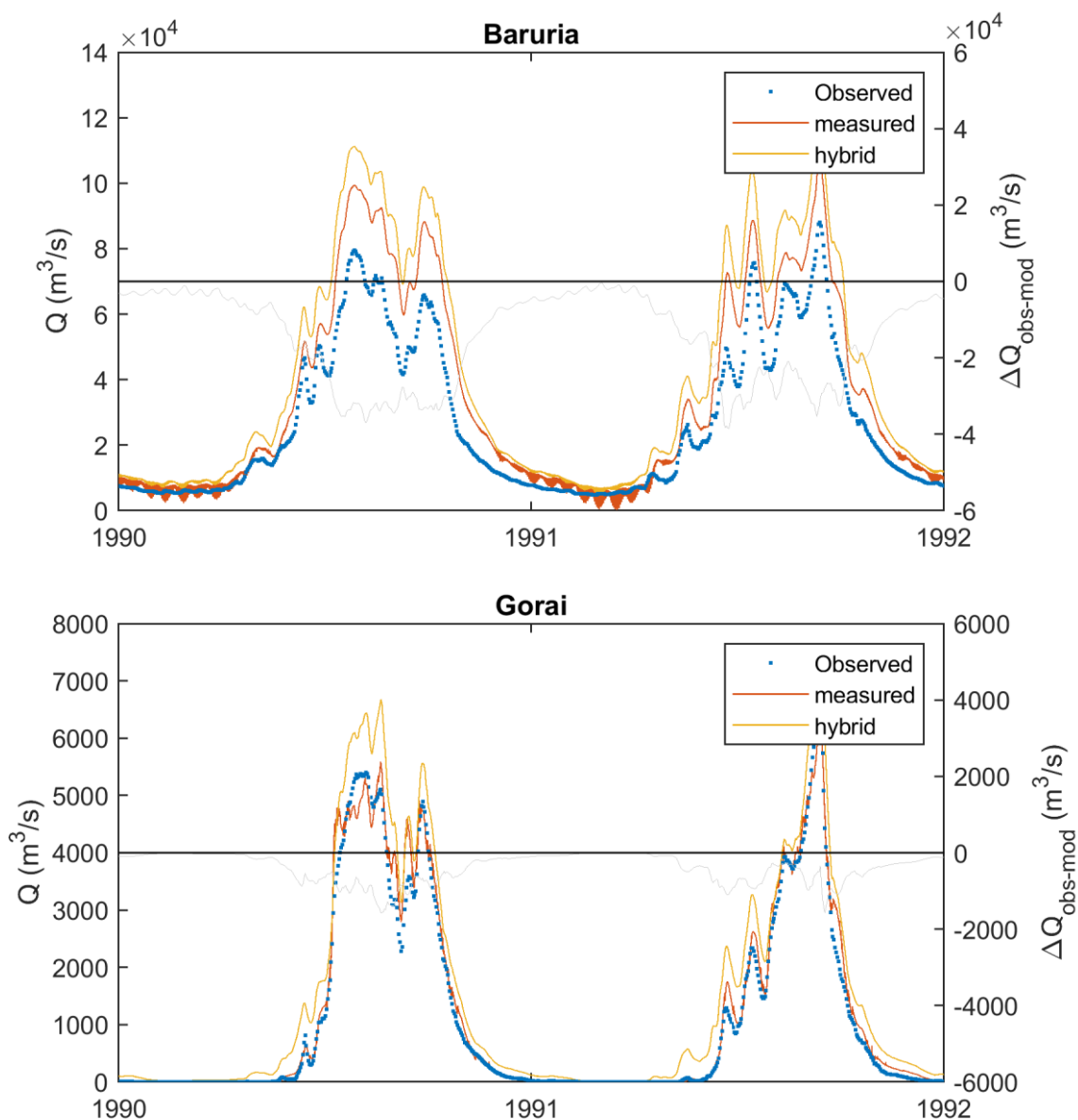
FigureApx C.17 Observed and modelled M_2 tidal amplitude (left) and phase (right) for the model with measured and hybrid cross-sectional profiles.

C.9.2 Discharge

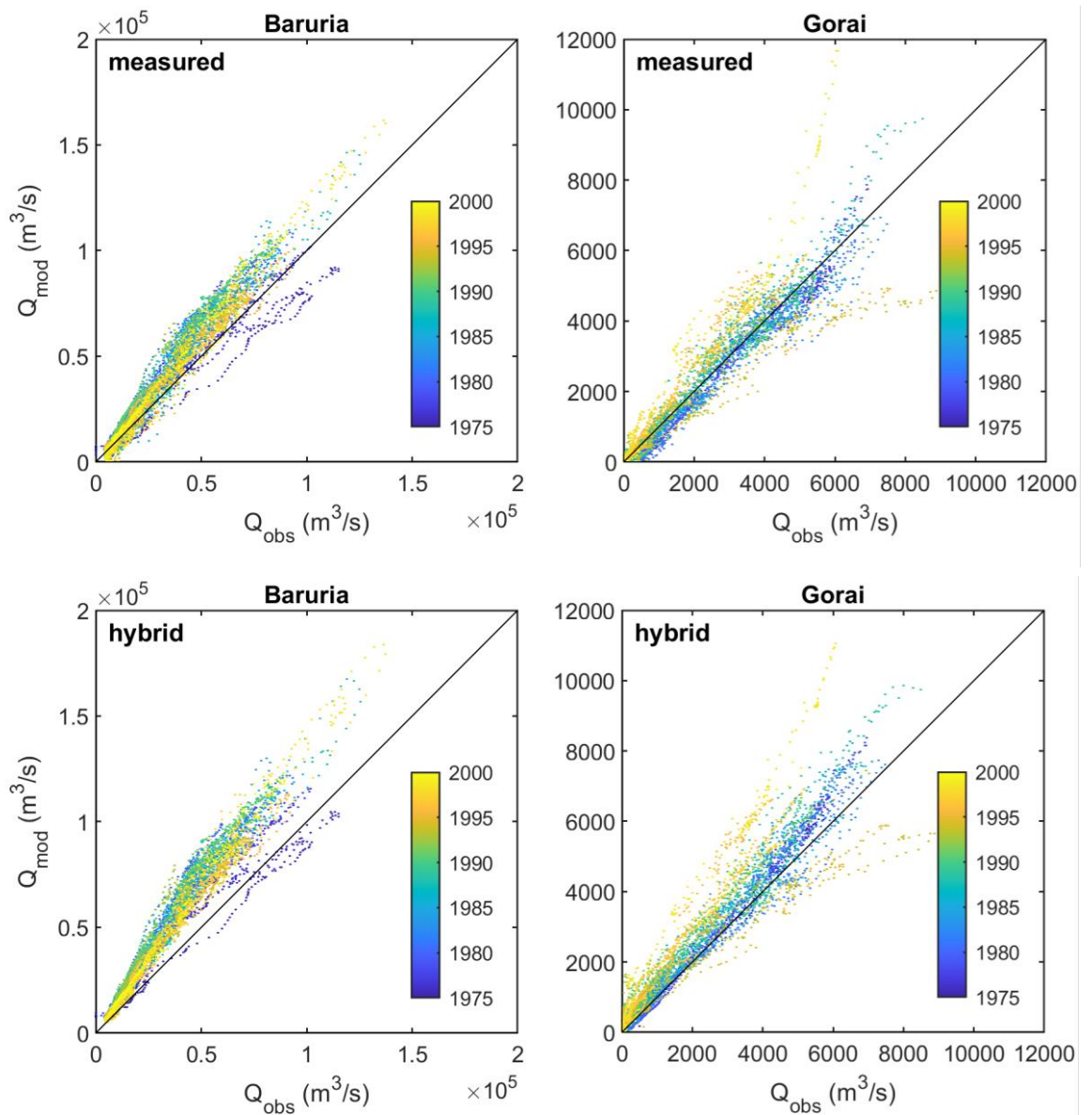
Both model variants are run for a time period of 25 years to allow for a good comparison with long-term daily discharge data available at the confluence of the Ganges and the Jamuna (Baruria) and the bifurcation of the Gorai (Gorai Railway Bridge). The performance of the models is visualized in timeseries (FigureApx C.18), scatter plots (FigureApx C.19), and a table with error statistics (TableApx C.3). These figures and tables show that both models perform quite well in distributing the discharge and that the distribution is modelled well at the Gorai bifurcation during the monsoonal fluctuation. The model-data comparison is also nearly perfect in the Gorai (for the measured variant), but at Baruria both model variants show an over-estimation of the discharge for most of the modelled period. The over-estimation is smaller for the model with the measured profiles.

To get a better understanding on the over-estimation of the models at Baruria, the observed discharge at Baruria is plotted with a discharge that is calculated by adding the contributions from Jamuna and Ganges and subtracting the contribution from the Gorai. The time-series and scatterplot (FigureApx C.20) explain the model-data mismatch observed: part of the discharge from the Jamuna and Ganges

is flowing towards locations elsewhere and does not flow to Baruria. These locations can be smaller distributaries, but also overland flooding, water-intake, and evaporation. These processes are not included in the present set-up of the 1D model (the model results present a closed flow budget, but the data does not). Another source of data-model mismatch can be attributed to the accuracy of the stage-discharge derived measurements (see Appendix A).



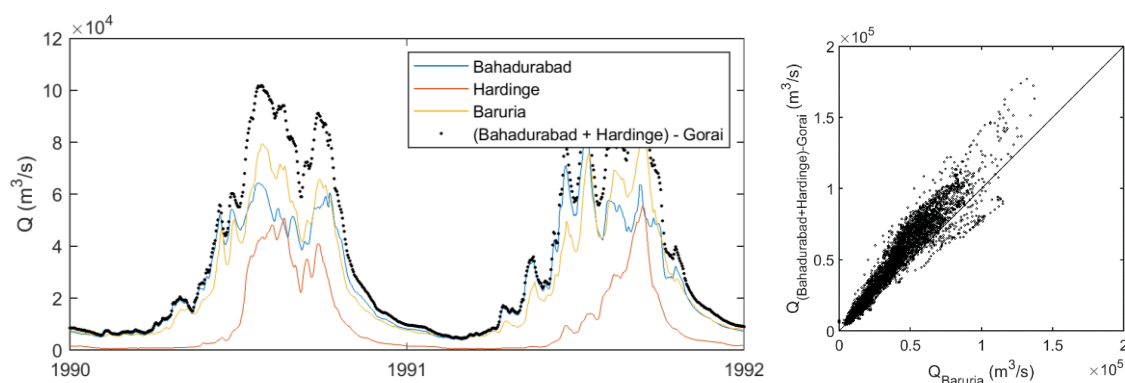
FigureApX C.18 Timeseries of the modelled and observed discharge at Baruria (upstream of Padma) and the Gorai (Gorai Railway Bridge). Figures are zoomed-in on a two-year period to highlight the monsoon-drive discharge fluctuations.



FigureApx C.19 Scatter plots of the modelled and observed discharge for the confluence of Ganges and Jamuna (Baruria, left) and the bifurcation of the Gorai (right), for both model variants.

TableApx C.3 Error statistics of the measured and modelled daily discharge.

Model	Station	Bias (m ³ /s)	RMSE (m ³ /s)	Corr. Coeff. (R)
Measured profiles	Baruria	4325	8392	0.98
	Gorai	-26	485	0.97
Hybrid profiles	Baruria	10367	14565	0.98
	Gorai	243	599	0.97



FigureApx C.20 Time-series and scatter plot of the observed discharge at Baruria and the combined discharge from the observations of Bahadurabad, Hardinge with the Gorai subtracted.

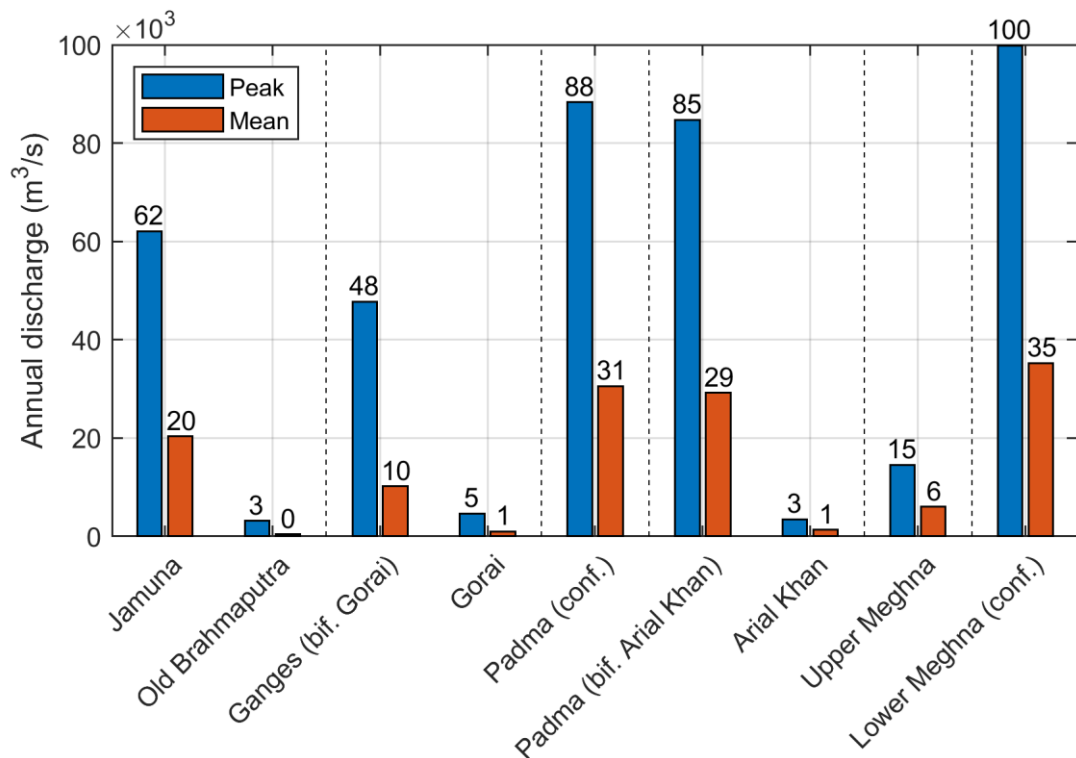
C.10 Model validation

The analysis of water levels shows that the model variants with measured and hybrid profiles perform similar in the tide-dominated part of the GBM delta, and that the model with measured profiles performs better in the upstream fluvial dominated part. The key property to simulate with the 1D model is the distribution of discharge and suspended sediment load over the river tributaries. The discharge analysis shows that the model with measured profiles performs best. Therefore, the model variant with measured profiles is used for the scenario-analysis. The following sections show the results of the ‘measured’ model variant which is run for a period of 25 years and forced with a representative hydrograph (see Appendix D. The annual flow and sediment dynamics are analysed and, if possible, compared to literature as an aggregated form of validation.

C.10.1 Flow budget

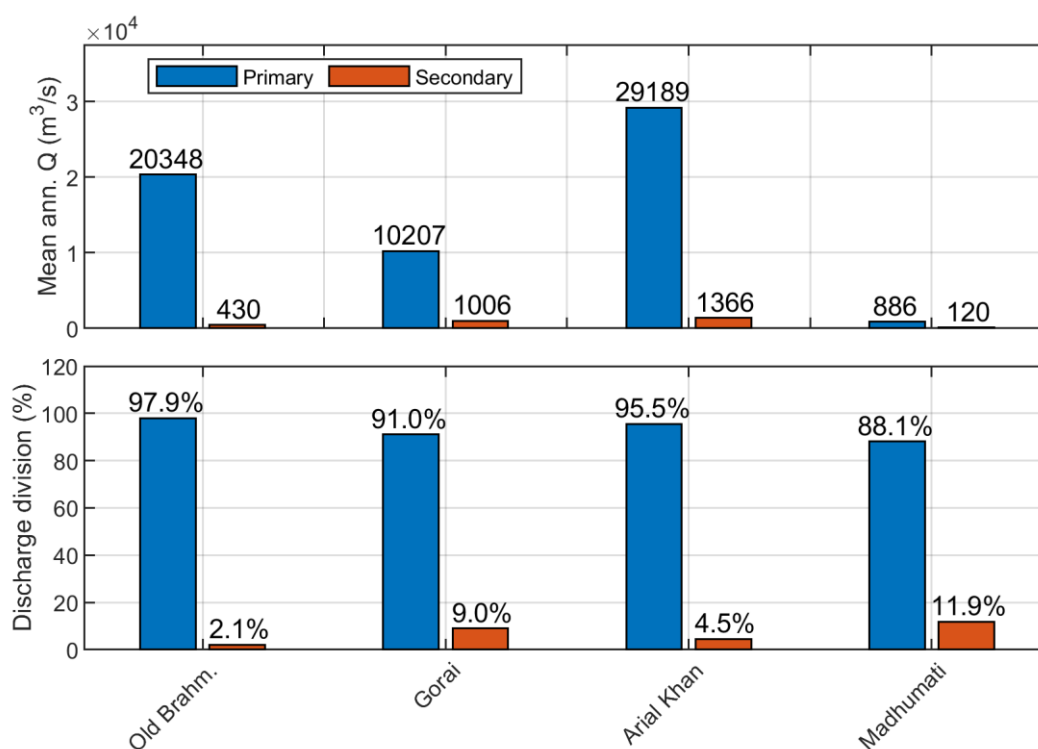
Upstream

The mean and peak annual discharge is shown for the upstream (non-tidal) rivers in FigureApx C.21. The figure shows for both the Gorai tributary and Arial Khan tributary a mean annual discharge of $\sim 1,000 \text{ m}^3/\text{s}$. At the confluence of the Jamuna and Ganges, flowing into the Padma, the figure indicates that a mean annual discharge of $\sim 30,000 \text{ m}^3/\text{s}$ and peak annual discharge $\sim 88,000 \text{ m}^3/\text{s}$ flows into this confluence. These values compare well to the values known from literature (see Table 2.1). At the other branches of the GBM delta - that are included in the 1D model - there is no information available for a quantitative comparison. However, it is apparent from the figure that the ratio between mean and peak annual discharge is approximately 1:3 – 1:4 in the upstream (non-tidal) branches of the GBM delta.



FigureApx C.21 Mean and peak annual discharge budget for the upstream (non-tidal) rivers in the GBM delta. Vertical dotted lines indicate connecting tributaries. Values on top of the bars show the value of the bar multiplied by $1 \times 10^3 \text{ (m}^3/\text{s)}$.

In FigureApX C.22 the distribution of the mean annual discharge is shown for the most important bifurcations in the upstream part of the delta. The figure shows the discharge flowing towards the primary branch (blue) and to the secondary (bifurcating) branch (red), in absolute values (top panel) and percentages (bottom panel). The figure shows the largest part of the mean annual discharge is flowing towards the Padma (and subsequently the Lower Meghna) and that the Gorai and Arial Khan roughly receive the same amount of discharge annually. The amount of the annual discharge flowing from the Gorai river in to the Madhumati is ~12%. This is smaller than the known distribution of ~20% (pers. comm. IWM) but the order of magnitude is correct. Given the model uncertainties these results can be qualified as reasonable.

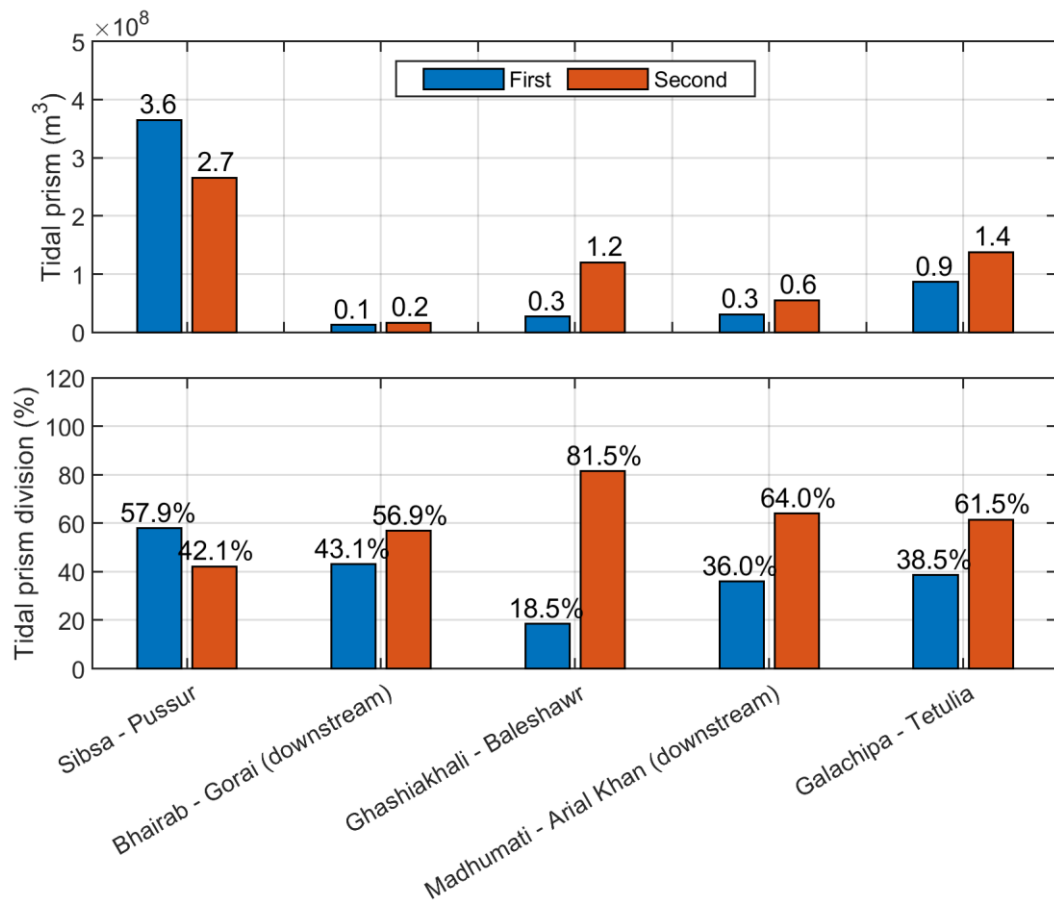


FigureApX C.22 Discharge division for the three most important bifurcations in the upstream part of the GBM delta. Absolute values (top panel) and percentages (bottom panel).

Downstream

The bifurcations at the coastal part of the GBM delta is tidally influenced, and the tidal prism is a more representative metric for the distribution of the discharge. The tidal prism is defined as the volume of water entering a river branch during the flood period of the tide (averaged over the simulation period). The tidal prism is shown in FigureApX C.23 for the most important bifurcations in the coastal part of the GBM delta, in absolute values (top) and percentages (bottom).

The figure shows that at the bifurcation of Sibsa-Pussur the largest part of the tidal prism (~60%) is conveyed by the Sibsa estuary, which complies with other studies (e.g. Deliverable D-4A-2; meso scale Pussur-Sibsa). The Ghashiakhali conveys a small part of the tidal prism, which matches to the fact that this connecting channel of the Pussur and Balesawr systems has been siltating over the past decades (perc. comm. IWM).

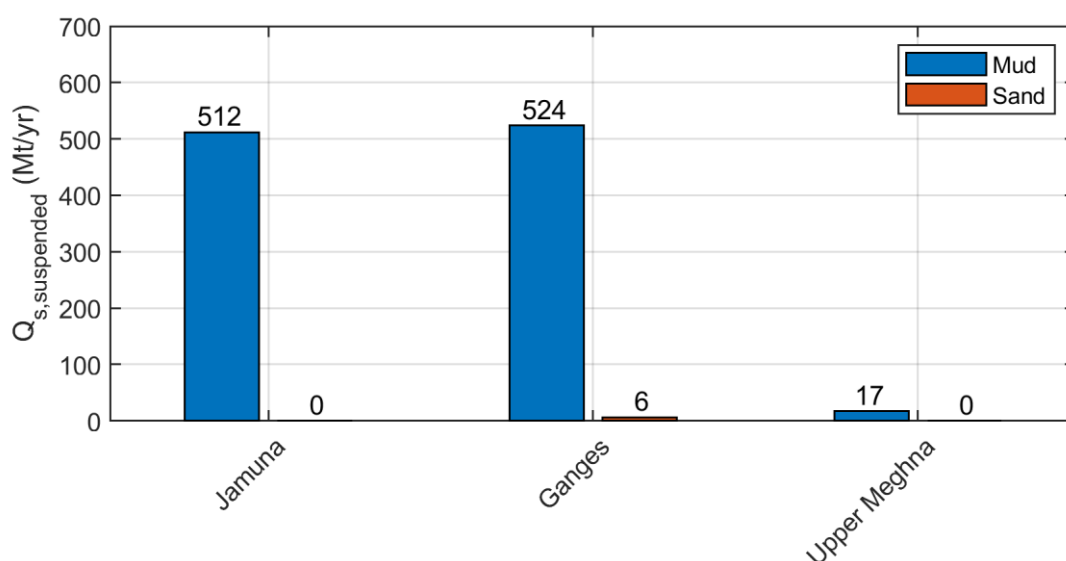


FigureApX C.23 Division of the tidal prism for downstream bifurcations in absolute values (top panel) and percentages (bottom panel). Colours indicate the first (blue) and second (red) river system indicated in the labels on the horizontal axis (see FigureApX C.2 for names of the river systems).

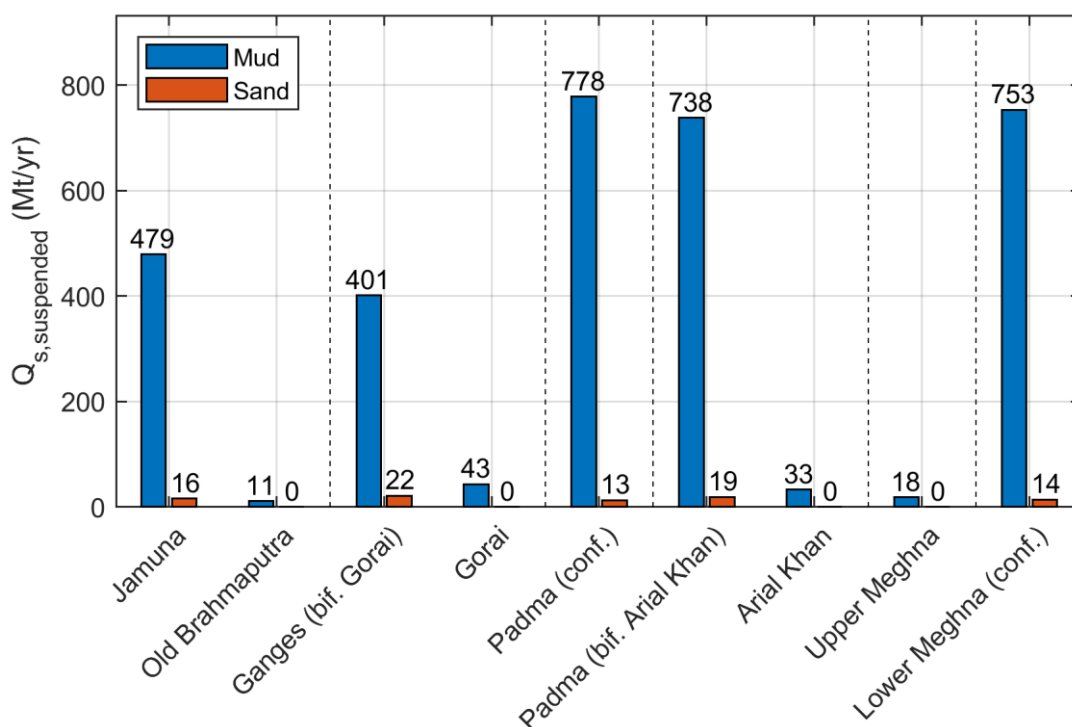
C.10.2 Suspended sediment budget

The suspended sediment load that is distributed over the tributaries in the upstream part of the GBM delta is calculated and presented as a mean annual value over the 25 years that are simulated. FigureApX C.24 shows the mean annual suspended sediment load at the upstream boundaries of the model domain. The figure shows that ~500 Mt/yr of fine sediment is flowing in to the model domain at the Ganges and Jamuna rivers, which compares well to the general understanding of sediment received at the delta. The influx of suspended sediment at the Upper Meghna is more than an order of magnitudesmaller. The figure shows that the influx of sand is negligible at all rivers. The suspended sediment concentration (SSC) of non-cohesive sediment (sand) is, contrary to cohesive sediment (mud), forced to the model as a Neumann type (no gradient) conditions, which can be seen as an equilibrium concentration. The modelled cross-sectionally averaged flow conditions apparently do not entrain any non-cohesive sediment at the boundaries. The implications of this are discussed in the following section.

In FigureApX C.25 the distribution of the suspended sediment load is shown for the most important distributaries in the upstream part of the delta. The figure shows a load of 43 Mt/yr and 33 Mt/yr for the Gorai and Arial Khan tributaries, respectively. This is ~25% larger than the values shown in Table 2.1. In the Lower Meghna the total suspend load constitutes up to ~750 Mt/yr, which is ~25% smaller than the ~1000 Mt/yr given in literature. Given the uncertainties in sediment loads known from literature, the 1D model produces plausible results in terms of the large scale sediment budget of the GBM delta.



FigureApX C.24 Mean annual suspended influx at the upstream boundaries of the model.



FigureApX C.25 Mean annual suspended sediment budget for upstream part of the GBM delta. Bars between vertical dotted lines indicate connecting tributaries. Values on top of the bars show the value of the bar multiplied by $1 \cdot 10^3$ (m^3/s).

C.11 Model performance and applicability

The Delft3D-FM 1D river branch model that is set-up for the GBM delta with measured cross-sectional profiles shows a good reproduction of water levels, tidal amplitudes, and the distribution of discharge at several locations in the delta. The model is applied to assess the annual flow and sediment budget and a qualitative validation shows a general agreement with values known from literature. Therefore, the performance of the model is reasonable, and the model can be considered appropriate to study

the effects of a change in future boundary conditions on the hydrodynamics and sediment dynamics in the delta. This applies in particular to the relative effects, where any linear mistake cancels out. However, there are two points of discussion:

- There are no high discharge conditions considered in the upstream forcing. The current upstream boundary conditions used for model application consist of a representative hydrograph that represent the mean annual conditions. Neglecting large peak discharges most likely leads to an underestimation of the sediment flux. In the future scenarios a more realistic type of forcing should be considered that includes year-to-year variations in the peak discharge.
- There is lack of non-cohesive sediment input at the upstream boundaries of the model. The influx is determined by the model, based on the modelled cross-sectionally averaged flow conditions. Apparently - despite the comparison to observed water levels - the model does not correctly reproduce flow velocities at the boundaries. The implications for model application are, however, limited. The adaptation length (the distance to reach equilibrium suspended sediment concentrations) is a function of the flow velocities, water depth, and sediment fall velocity and is for the present model set-up in the order of kilometres. This means that the suspended sediment flux of non-cohesive sediment at a certain location is determined by the local interaction with the bed, instead of the distant supply to the delta. For cohesive sediment this is not the case as the sediment fall velocity is several orders smaller.

D Development coastal model (Delft3D-FM 2D)

D.1 Introduction

The development of the 2D coastal model is described in the following sections. An overview of the procedure is as follows:

- Construct an unstructured-grid model of the entire GBM delta and a large part of the Bay of Bengal, covering the main rivers and estuaries with widths greater than 500 m, in a mesh of which the cell sizes range from 8 km to 500 m, with rectangular grid cells except where areas of different resolution are connected by triangles. Rectangular grids are the most efficient and effective grid shapes.
- Run and calibrate the model hydrodynamically with realistic boundary conditions for river flow of the three main rivers and full astronomical boundaries at the sea boundary. The calibration focuses on reproducing the M2 amplitude variations throughout the delta, in comparison with data from a large number of tidal stations, for each of which a limited tidal analysis is carried out.
- Verify the discharges through a number of cross-sections, mainly in the Meghna and the Pussur-Sibsa system and where necessary adjust the model parameters.
- The main variables in the calibration are the bathymetry, ensuring the continuity of channels in the relatively coarse grid, and the roughness, which is varied only on a very large scale (e.g. different values for sea –estuaries – rivers).
- The model has been developed in three stages:
 - In the first stage, up to the confluence of Jamuna and Ganges at Baruria;
 - In the second stage, the Ganges and Jamuna up to Hardinge Bridge and Bahadurabad, respectively, were included. In the Meghna the model runs up to Bhairab Bazar.
 - The final stage includes the Gorai River as it was seen as an important source of sediment to the Pussur-Sibsa system. It is included as a curvilinear grid section connected to the overall grid using triangles and quadrilaterals to smoothen the transition from higher to lower resolution.
- Two types of morphodynamic simulations are carried out:
 - Short-term (~1 year) runs with realistic time series boundaries and full astronomical sea boundary components;
 - Long-term (5-100 year) runs with schematized *representative* boundary conditions for the river discharges and simplified *representative* tidal components, combined with a *morphological factor* approach to accelerate the morphodynamic simulations.
- Calibration of the sediment model on the shorter time scale is carried out using available sediment concentration measurements, for selected periods where bathymetric, hydrodynamic and sediment concentration measurements are available. Calibration was carried out by adjusting sediment properties like fall velocity, critical erosion shear stress and the erosion factor for mu and sand diameter for sand
- Calibration of the decadal-scale morphological development is carried out using the accelerated approach.

It must be noted that having a good calibration for sediment concentrations on the short term is no guarantee that the same settings will lead to good morphological behaviour. This is in part because the longer-term evolution is influenced by parameters that have little influence on short time-scales,

but also because there are different paths towards a reasonable concentration distribution that may have quite different resulting sedimentation/erosion patterns.

Therefore, our approach in calibrating the sediment and morphology behaviour consists of trying to **reconcile** the settings for both types of simulations, rather than taking the settings resulting from the sediment calibration and assuming them to be equally valid for the morphological runs.

The calibrated model mesh and setup was improved for the 80-year scenario runs including sea level rise and anthropic interventions. These adaptations are described in the last section of this appendix.

D.2 Grid and bathymetry

D.2.1 Automated grid generation

Given the objectives of the model as outlined in Section D.1, the generated grid must fulfil the following requirements:

1. Boundary conditions far from the region of interest and allowing both effects of sea level rise and changes in upstream flow and sediment discharges to be accounted for;
2. Grid resolution fine enough to represent the major river system but coarse enough to allow long-term simulations in acceptable runtimes of several days;
3. Grid covering recent channel areas, potentially flooded areas and areas prone to erosion;

Given these requirements a model domain was created covering the Bay of Bengal up to the seaward limit of the MIKE21 storm surge model and up to the confluence of Ganges and Jamuna (for initial model calibration) and up to Hardinge Bridge on the Ganges and Bahadurabad on the Jamuna; in all cases up to Bhairab Bazar on the Meghna .

Rather than constructing a complicated mesh consisting of curvilinear and triangular elements, a 'quadtree' type approach was opted for with rectangular grid cells that can locally be refined by a factor of two in both directions. The connections between such areas are made of triangles. This approach can be automated to a large extent and guarantees that no small grid cells are generated that may reduce the time step, and does not lead to preferential orientation of channels. Besides, the resulting grids are perfectly orthogonal.

The basis for generating the grid is a rectangular grid with cells of 16x16km², aligned at the seaward boundary with the Bay of Bengal Mike21-FM grid. The parameters for this overall grid are given in TableApx D.1.

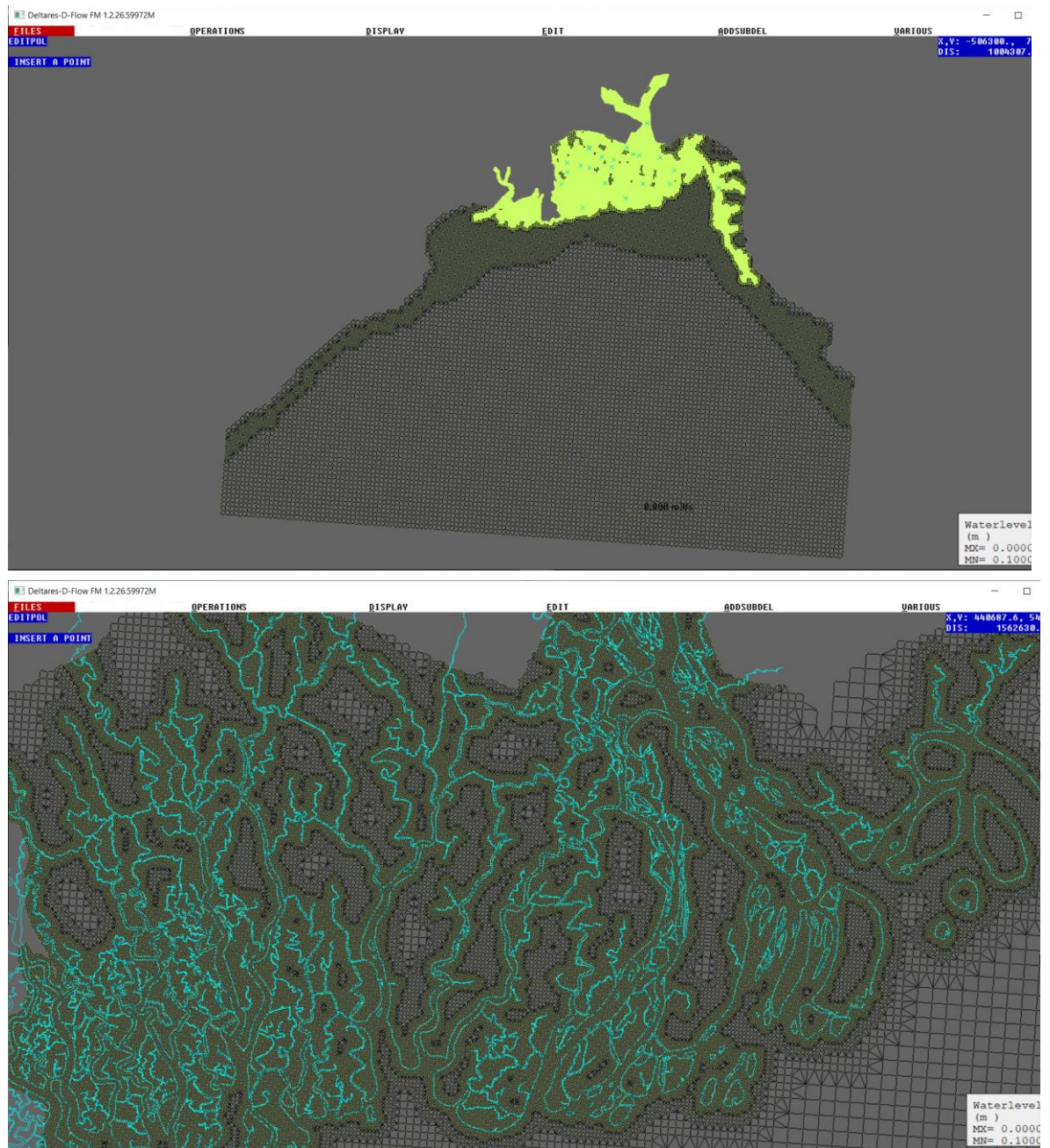
TableApx D.1 Parameters of the base grid from which the quad grid is developed

X origin	-320 km	Grid size x	16 km
Y origin	-150 km	Grid size y	16 km
Orientation	-4°	Number of cells x	81
		Number of cells y	72

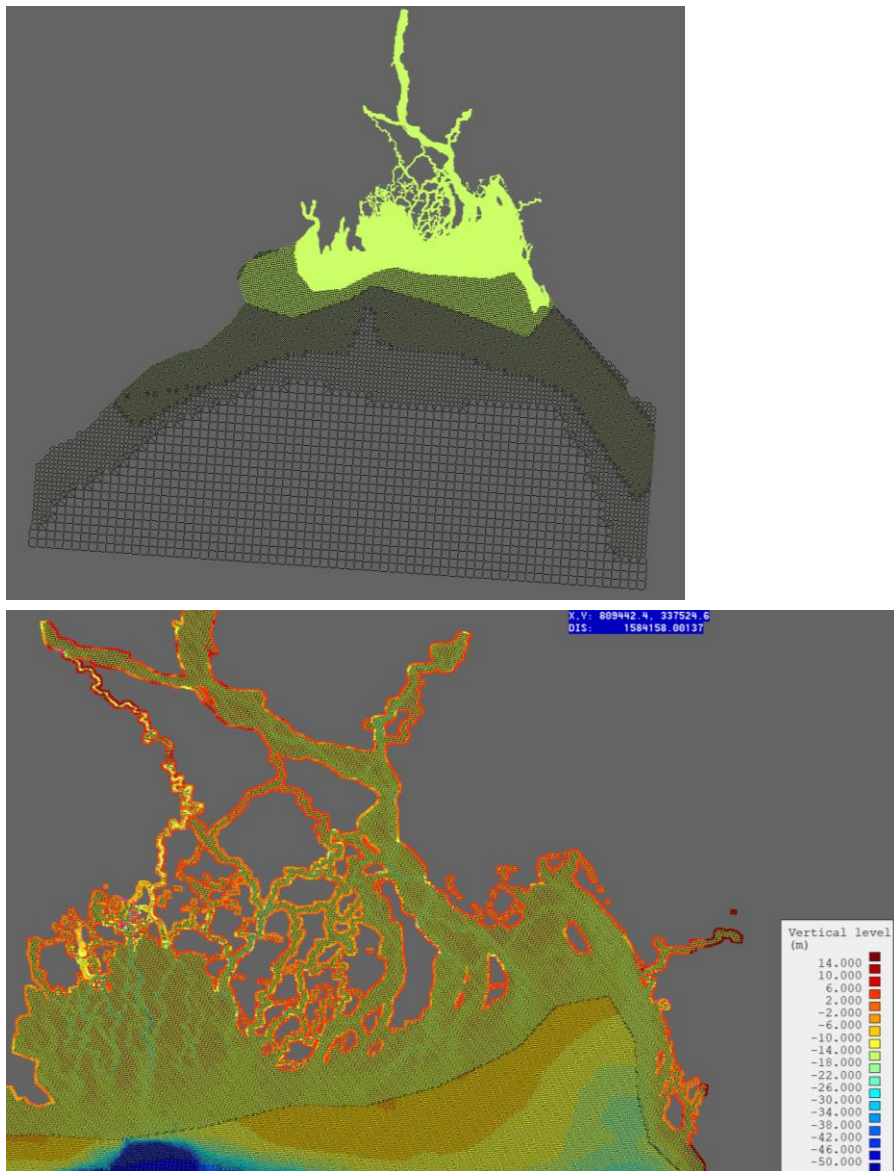
Next, the grid was automatically refined based on a combination of distance to the nearest bank line and water depth. Areas that are not expected to ever flood are excluded by taking out entire grid cells, based on polygons. The resulting grid is shown in FigureApx D.1.

Since the automated procedure based on a combination of distance to banklines and depth was rather complicated and could still lead to some areas with rather deviating shapes, the procedure for the final stage of the model was simplified to one where successive two by two refinement was carried

out using user-defined polygons, which gave more and easier control over the resolution and the removing from areas that are certain not to flood. The resulting mesh is shown in FigureApX D.2.



FigureApX D.1 Overall mesh (top panel) and detail of delta (lower panel) for stage 1 model.

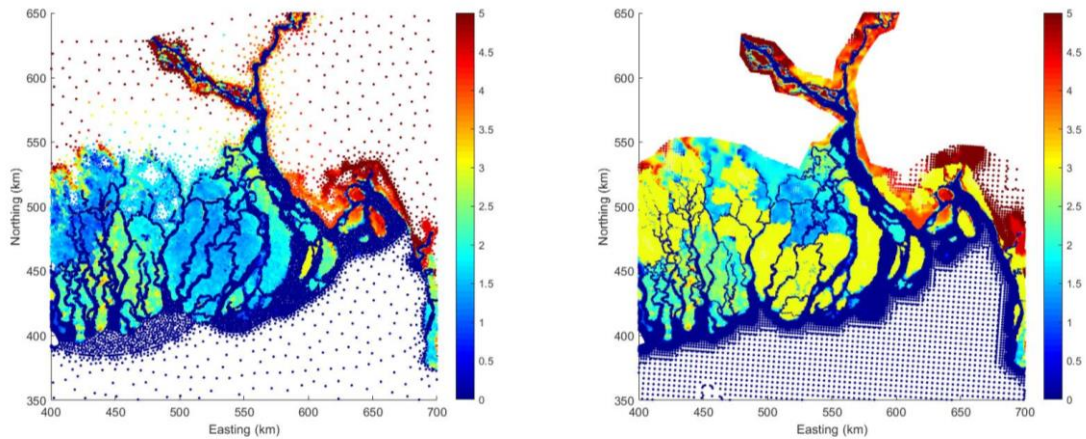


FigureApX D.2 Overall mesh (top panel) and detail of delta (bottom panel), stage 3 model.

D.2.2 Bathymetry

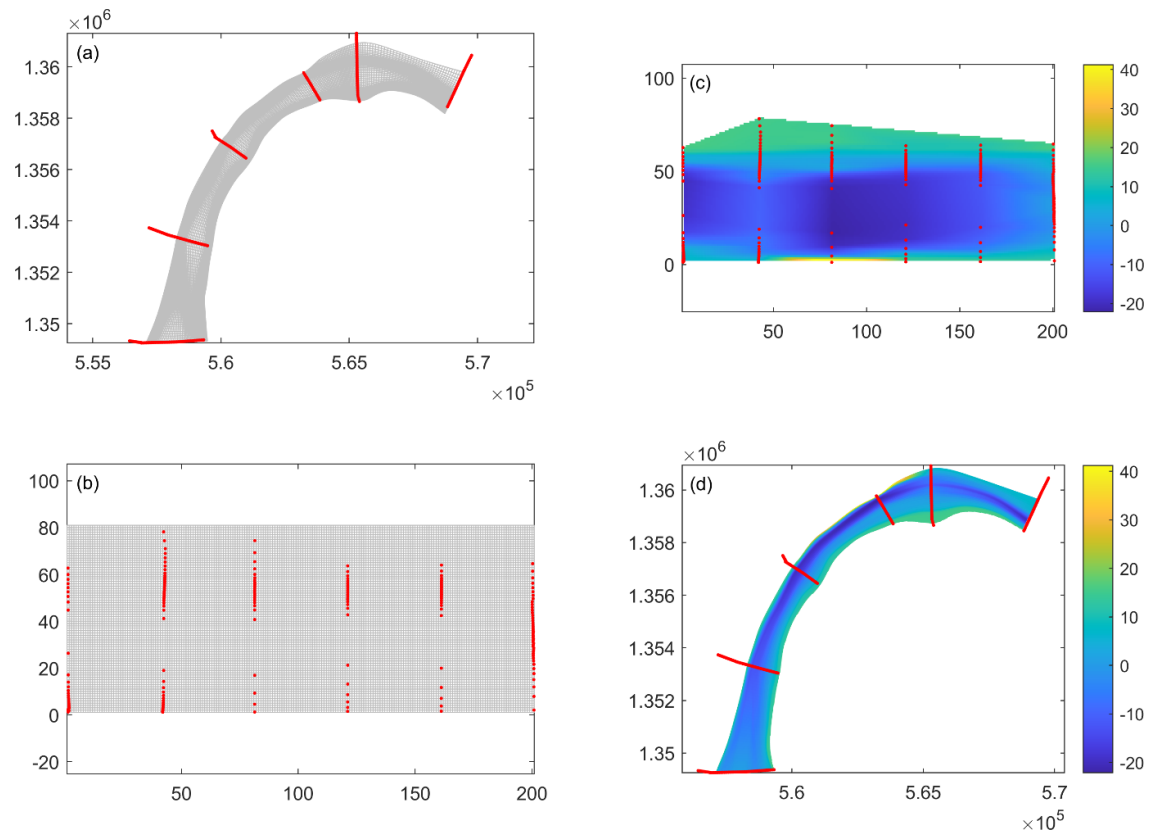
The bathymetry for the macro 2D hydrodynamic model was initially based on that of the validated MIKE21-FM Bay of Bengal model (IWM, 2010), which generally has a finer grid size than the current model. It is based on bathymetric datasets close to the reference year 2010 (FigureApX D.4).

Additionally, several datasets exist for different parts of the system and during different periods. These were used to generate up-to-date initial bathymetric sample sets for morphological calibration/validation runs, in the following manner: if bathymetric surveys for a given area exist for times T1 and T2, then the overall model bathymetry will be initialised as much as possible with data from time T1. For river branches where the available datasets only contain cross-sections that are sparsely distributed in space, the methodology of Vo et al. (2020) has been applied to generate comprehensive sample sets with bathymetric information: construct a curvilinear grid of the river reach under consideration and apply a coordinate transformation of the cross-sectional data to the curvilinear grid administration. The actual interpolation happens in the curvilinear coordinate space, after which the data is transformed back to real world geographical space. This process is illustrated in FigureApX D.4. A full overview of all available bathymetries is available in the data inventory and is not repeated here.

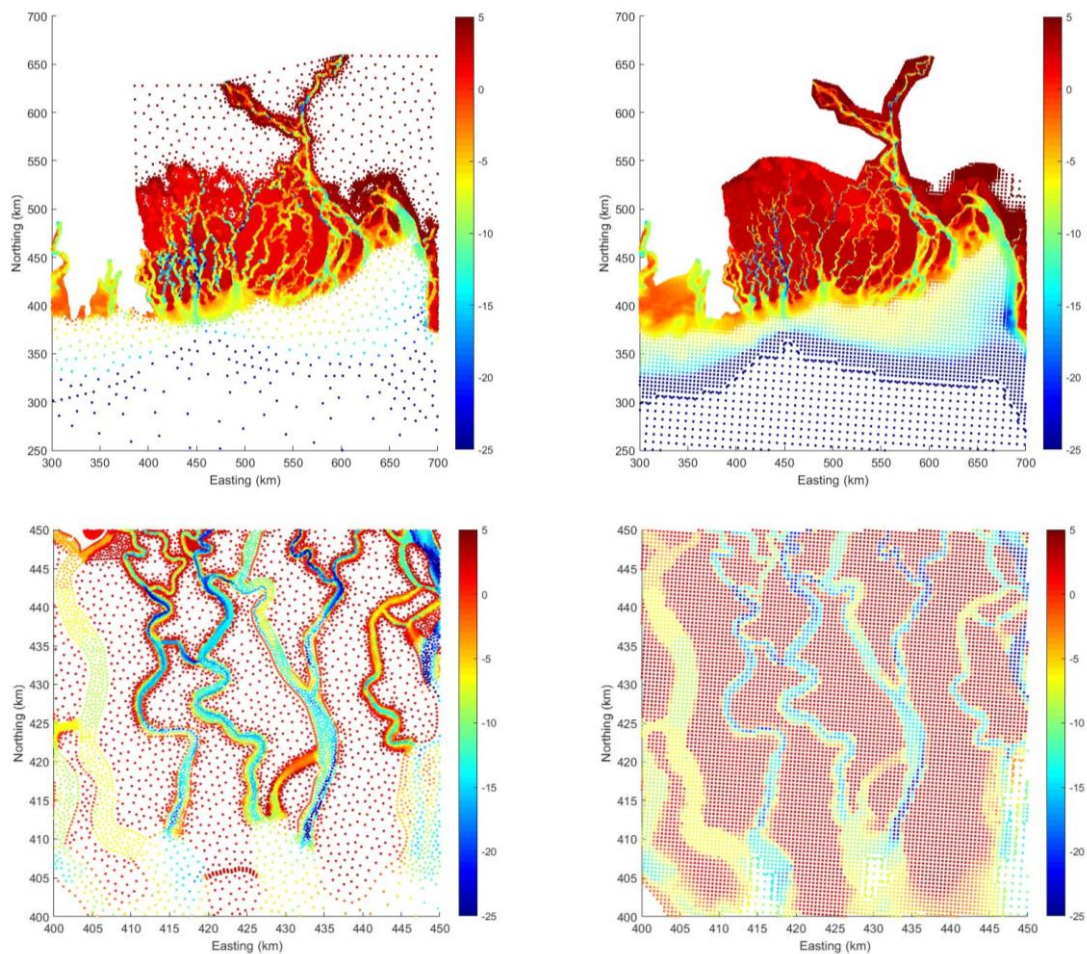


FigureApX D.3 Comparison between MIKE21-FM Bay of Bengal storm surge model elevation (left panels) and the representation in Delft3D-FM large-scale morphological model (right panels).

The DEM of the non-poldered areas, mostly in the Sundarbans, was taken over from the MIKE21-FM Bay of Bengal storm surge model as these areas may be inundated during regularly occurring events. The poldered areas were put at a level of +3m, preventing inundation under normal circumstances. A comparison between the MIKE21-FM model representation of the DEM and that in the Delft3D-FM morphological model is given in FigureApX D.3.



FigureApX D.4 Bathymetry interpolation procedure for river reaches. (a) curvilinear grid and sample set in geographic space; (b) Sample set in curvilinear space; (c) Interpolated bathymetry in curvilinear space; (d) Back transformed bathymetry in geographic space. The channel now smoothly follows the correct thalweg even though only sparse cross-sections are given.



FigureApX D.5 Comparison between MIKE21-FM Bay of Bengal storm surge bathymetry (left panels) and the representation in Delft3D-FM large-scale morphological model (right panels). Top panels: overview of coastal areas; Bottom panels: zoom area in Sundarbans.

D.3 Hydrodynamic calibration: tidal propagation

The hydrodynamic calibration concentrated on the distribution of the tidal amplitudes throughout the lower Meghna delta and Sundarbans. It was carried out both for the stage 1 and stage 3 model setups and focused on a period of one month, January 2012, which was close to the date most of the bathymetric data was obtained and had a large number of functioning tide gauges.

D.3.1.1 Boundary conditions

The upstream boundary conditions varied little during the month of January 2012 and were hence taken as constant, with values of 8,340 m³/s for the Padma and 1,440 m³/s for the Meghna.

At the sea boundary, astronomical components of the water level were imposed, extracted from the global tidal model of (Egbert and Erofeeva, 2002) derived from the TOPEX-Poseidon laser altimetry data. These components vary along the southern sea boundary; a typical set at the middle of this boundary is shown in TableApX D.2. The component A0 represents the mean sea level and its value is consistent with the use of the BTM vertical datum.

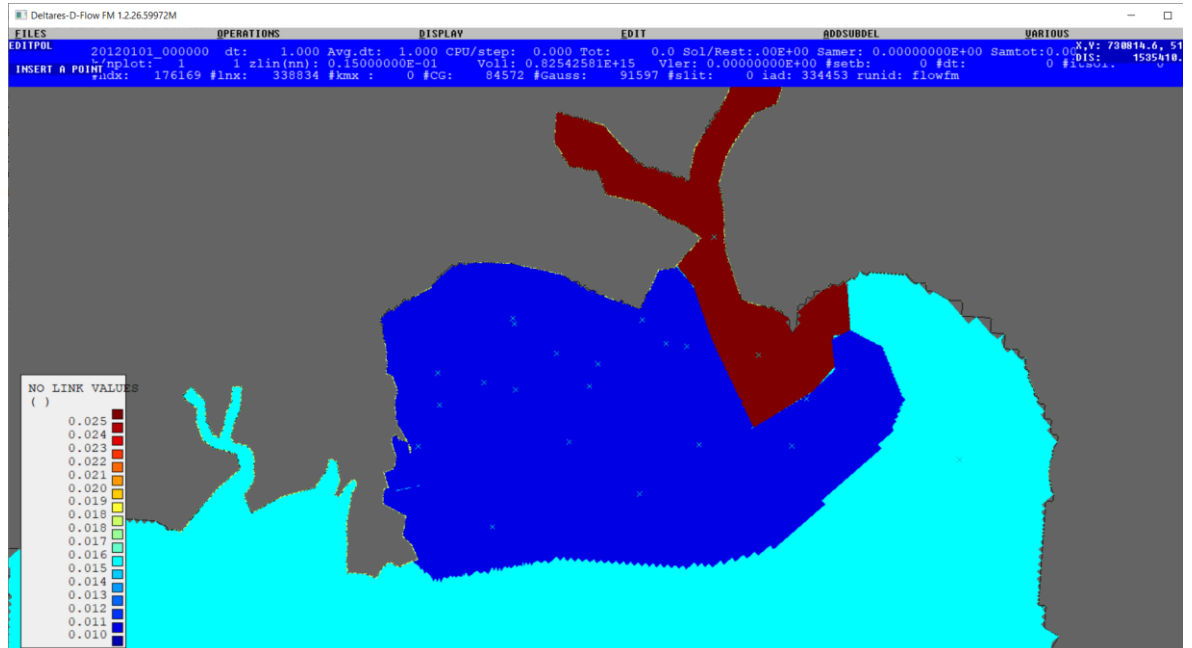
TableApX D.2 Astronomical components at centre of sea boundary

Component	Amplitude (m)	Phase (deg.)
A0	0.460	0
M2	0.523	76
S2	0.232	106
N2	0.112	70
K2	0.064	103
K1	0.114	245
O1	0.042	233
P1	0.035	239
Q1	0.002	307
MF	0.012	12
MM	0.006	5
M4	0.002	46
MS4	0.001	209
MN4	0.000	173

D.3.1.2 Tuning bathymetry and roughness

The two main variables determining the tidal propagation are the bathymetry and the roughness. In the bathymetry, especially for the narrower rivers it is important that the channel depth is well represented and narrow channels are connected even in a grid this is too coarse to resolve it. This has been achieved by taking the maximum sample depth in each cell instead of the average depth. This leads to good connectivity, although the average depth will be a bit overestimated.

As for the roughness, only very large-scale variations in roughness were allowed, which are specified per polygon, as shown below as an example (FigureApX D.6).

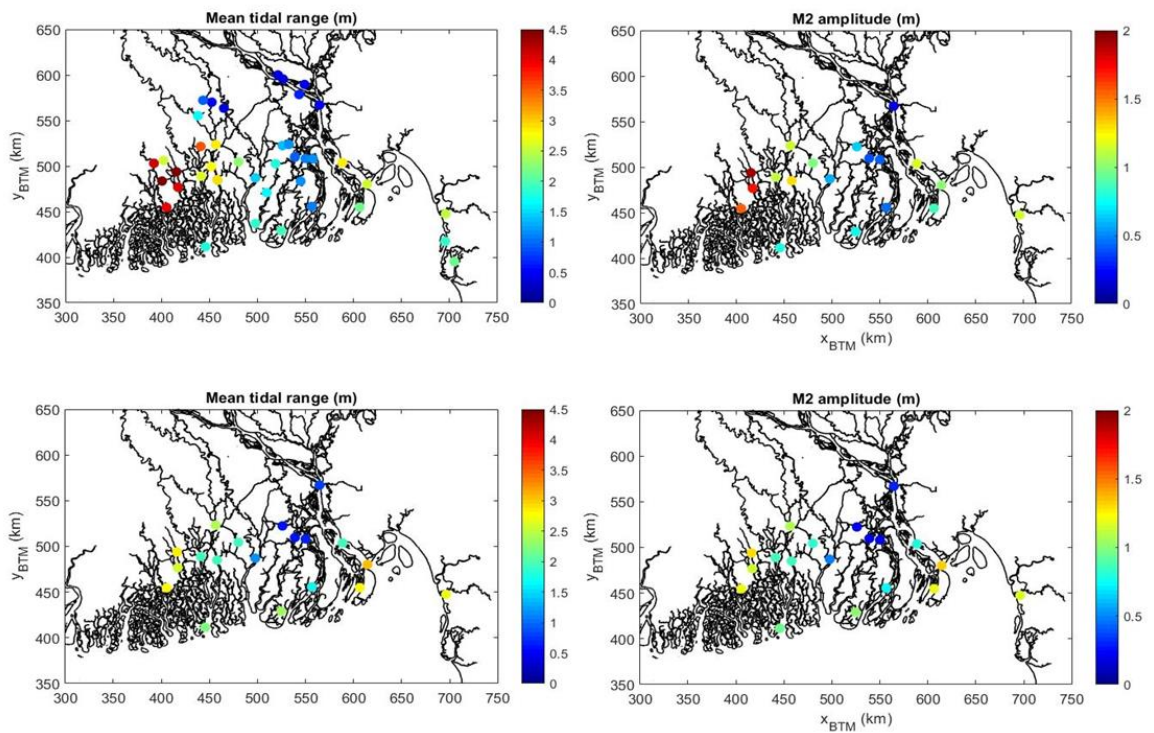


FigureApX D.6 Example manning roughness ($s/m^{1/3}$) map distinguishing sea (cyan), estuaries (blue) and Meghna/Padma (brown)

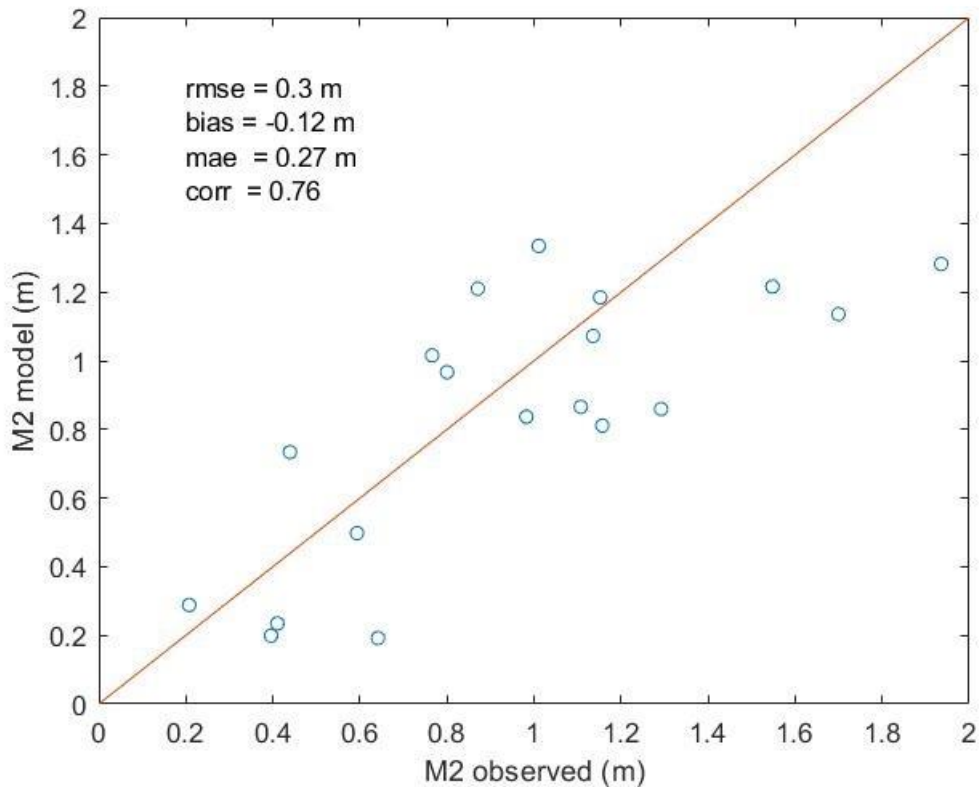
D.3.1.3 Results stage 1 model

The main variable that has been calibrated for in this coarse large-scale model is the distribution of the tidal amplitudes, and especially the M2 amplitude. The same tidal analysis procedure is applied to the simulation data as for the observations.

After a number of calibration runs, the following results were obtained, as shown in FigureApx D.7 and FigureApx D.8. In general, a reasonable distribution of the mean tidal range and the M2 amplitude is obtained, though there is some underestimation for the westernmost observation points, which are far up relatively narrow channels. Although further optimization may be possible, this situation was deemed acceptable to proceed to the sediment and morphology simulations.



FigureApx D.7 Observed (top panels) and simulated (bottom panels) mean tidal range (left panels) and M2 amplitude (right panels).



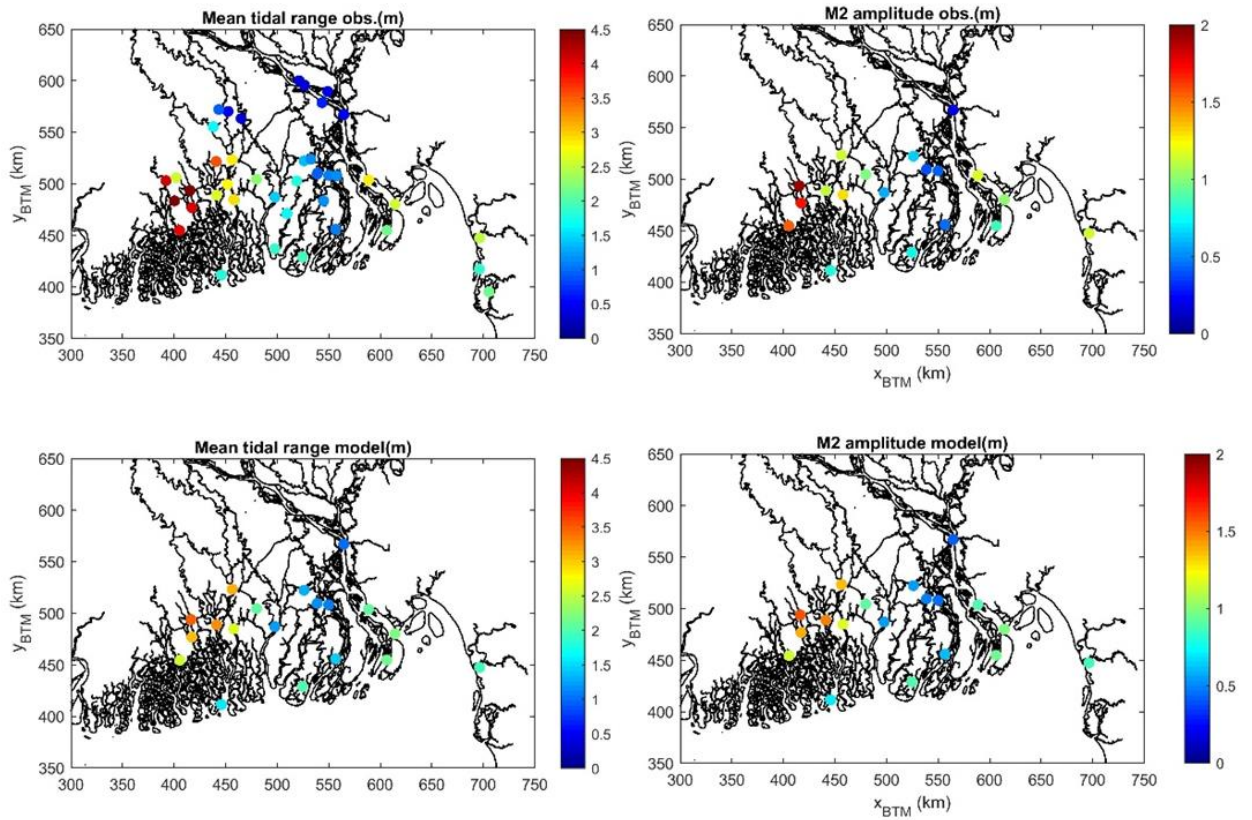
FigureApX D.8 Simulated vs. observed M2 amplitude in points shown in FigureApX D.9. (rmse = root mean square error, mae = mean average error, corr = correlation coefficient)

D.3.1.4 Results stage 3 model

After extending the model with the Ganges, Jamuna and Gorai rivers, it was recalibrated against the same dataset for the tidal propagation. The settings of run 13 showed a marked improvement going from the stage 1 model to the stage 3 model, particularly in the Pussur/Sibsa area. In the meantime, it was noticed that morphodynamic results were smoother and met with fewer problems when Chézy roughness was chosen rather than the Manning formulation. An explanation for this fact is that with a constant Chézy, the roughness increases with depth, and therefore tidal flats are automatically smoother than channels which typically have large bedforms. In view of this several combinations of different Manning's and Chézy values were tried, as listed in TableApX D.3. Although the differences are not enormous, a good fit was obtained with Chézy values of $120 \text{ m}^{0.5}/\text{s}$ in most of the area, with a bias of just 4 cm, an RMS error of 0.22 m and a correlation coefficient of 0.89 (see run 19). These Chézy values are very high and imply very low roughness values. However, similar validation values were found in the Yangtze River with a similar model approach. Both systems consist mainly of high concentration, fine sediments. A possible explanation is that the presence of ample fine sediments leads to limited bed forms and form friction, while high sediment concentrations suppress turbulence limiting bed friction impact on the water flow.

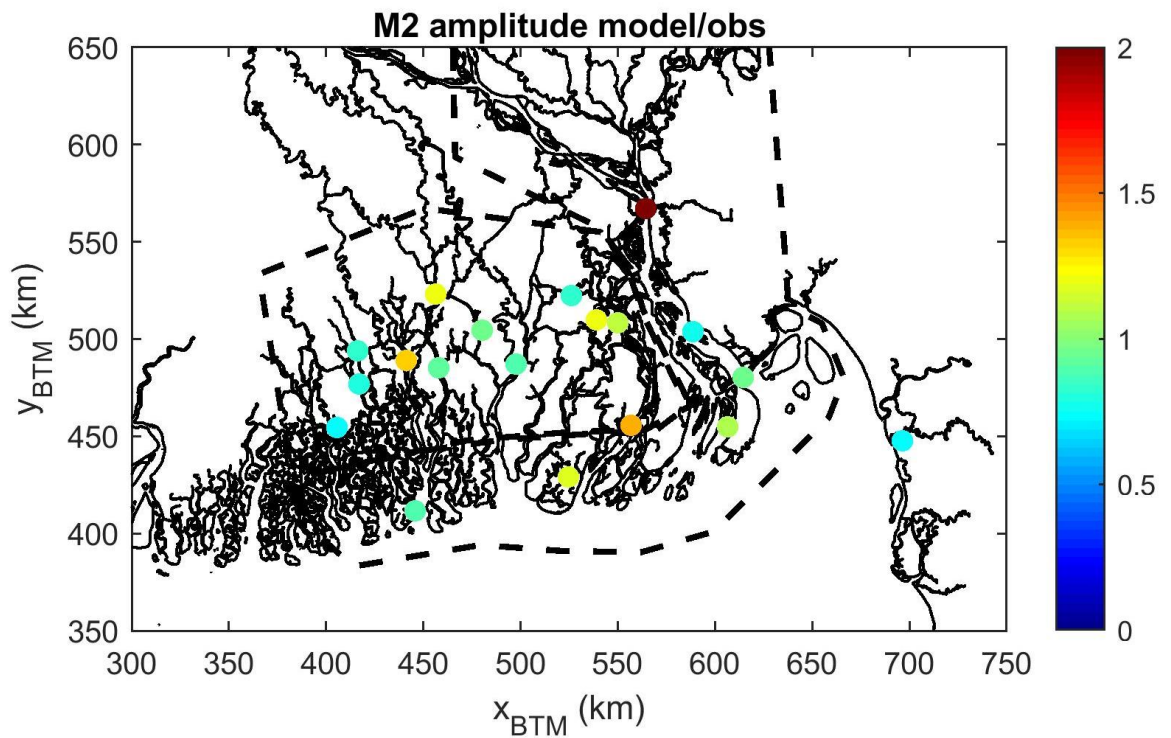
TableApX D.3 Overview of calibration tests and results

Run	Manning/ Chezy	Uniform	Estuaries	West	Meghna/ Padma	Model stage	Bias	RMSE	corr
13	M	0,015	0,01	0,01	0,025	1	-0,12	0,30	0,76
13	M	0,015	0,01	0,01	0,025	3	0,11	0,23	0,88
14	C	65	100	100	65	3	-0,14	0,23	0,88
15	C	65	80	80	65	3	-0,21	0,24	0,88
16	C	65	100	150	65	3	-0,10	0,23	0,87
17	M	0,015	0,015	0,01	0,025	3	-0,04	0,23	0,87
18	M	0,015	0,015	0,015	0,015	3	-0,06	0,23	0,88
19	C	65	120	120	120	3	-0,04	0,22	0,89
20	C	120	120	120	120	3	0,04	0,24	0,86



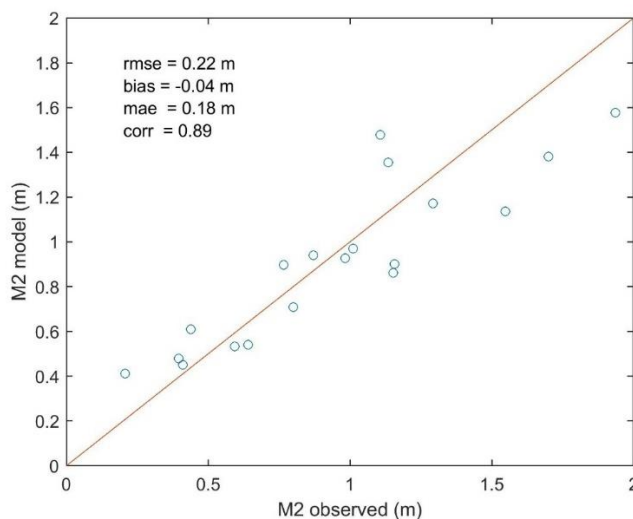
FigureApX D.10 Observed and modelled mean tidal range (left panels) and M2 amplitude (right panels) for calibration run 19.

The distribution of observed and modelled mean tidal range and M2 tidal amplitude is quite similar as shown in FigureApX D.10. The ratio between modelled and observed M2 tidal amplitude does not show a particular trend as shown in FigureApX D.11.



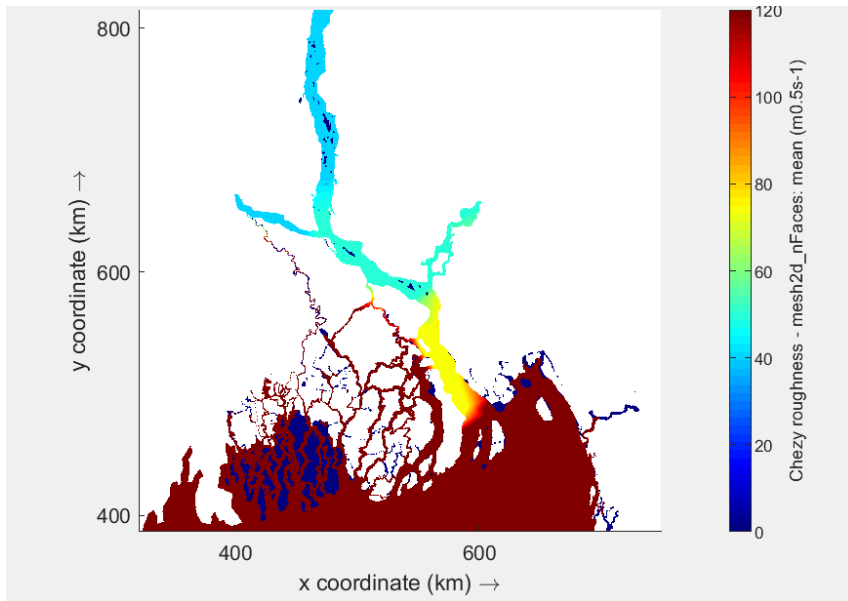
FigureApX D.11 Ratio of modelled vs. observed M2 tidal amplitude, run 19.

Finally, the scatter plot in FigureApX D.12 shows an acceptable correspondence between the observed and modelled M2 amplitudes.



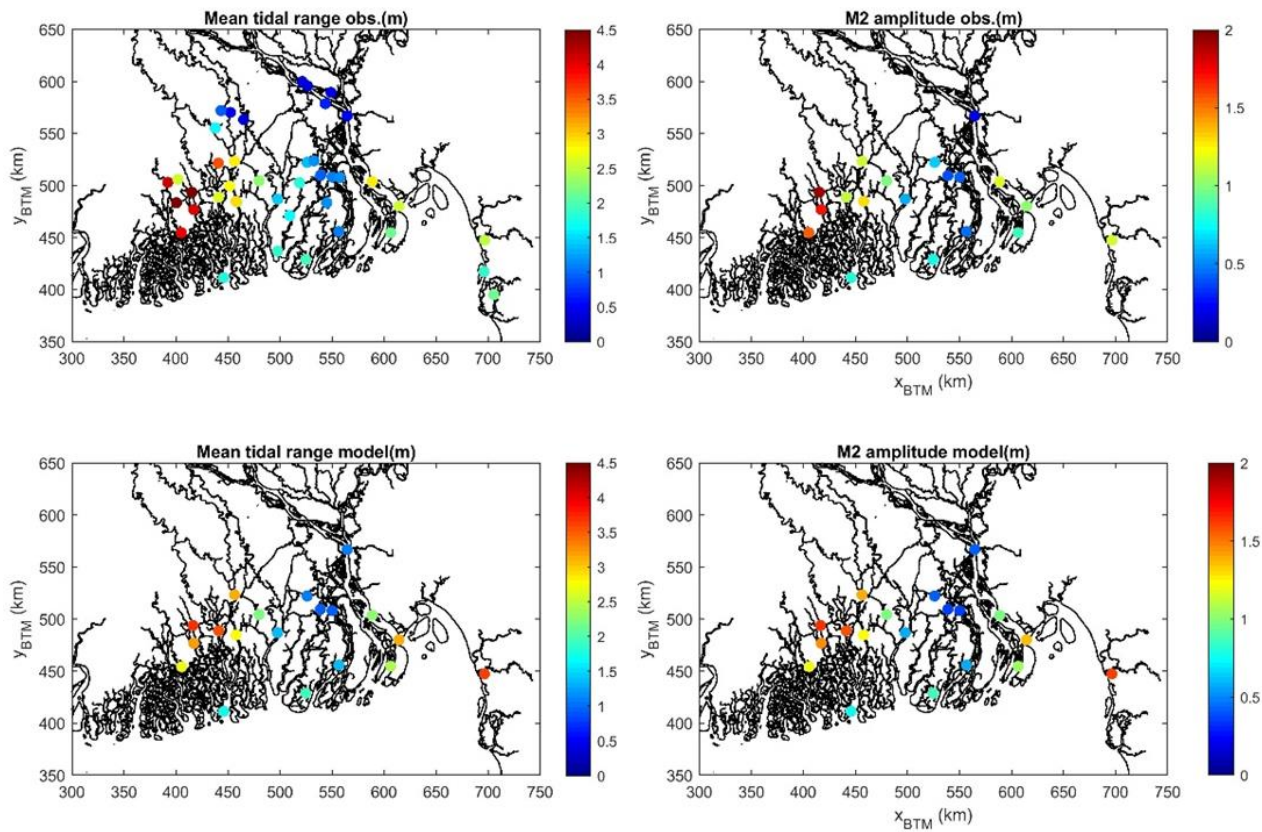
FigureApX D.12 Modelled vs. observed M2 tidal amplitude, run 19.

A final modification to the roughness map was made based on a) morphological results that showed distinct patterns where the roughness changed abruptly, b) severe underestimation of discharges through section Hatiya North (see next Section) and c) an underestimation of water levels at Hardinge Bridge, in turn leading to too low discharges through the Gorai. The final roughness map for this report can be seen in FigureApX D.13 as a spatial distribution.

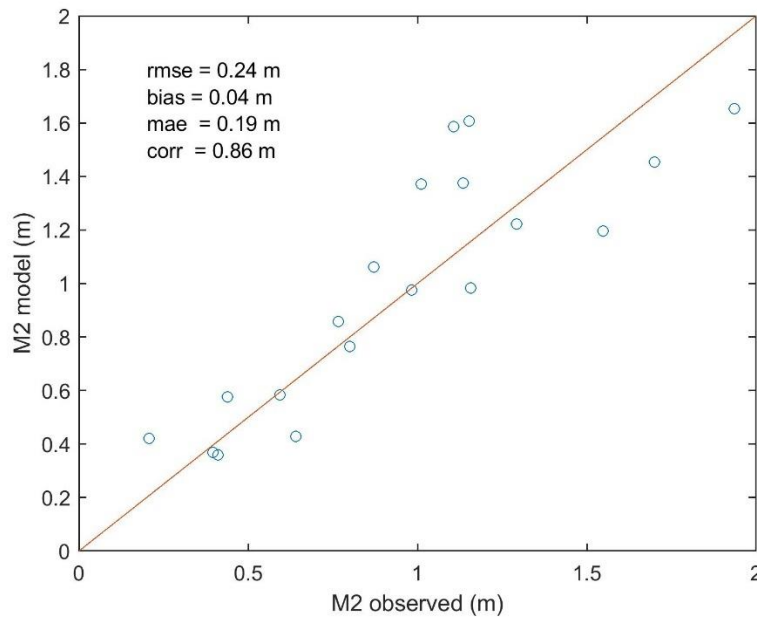


FigureApX D.13 Spatial Chézy roughness distribution

The comparison between the water level amplitudes and tidal range from observations and model in this final setup is shown in FigureApX D.14 and FigureApX D.15. The differences are small although there is a slight deterioration in the correlation coefficient, from 0.89 (run13) to 0.86 (runc20). However, this leads to a more realistic distribution of flows as addressed in Section D.4.



FigureApX D.14 Observed and modelled mean tidal range (left panels) and M2 amplitude (right panels) for calibration run 20.

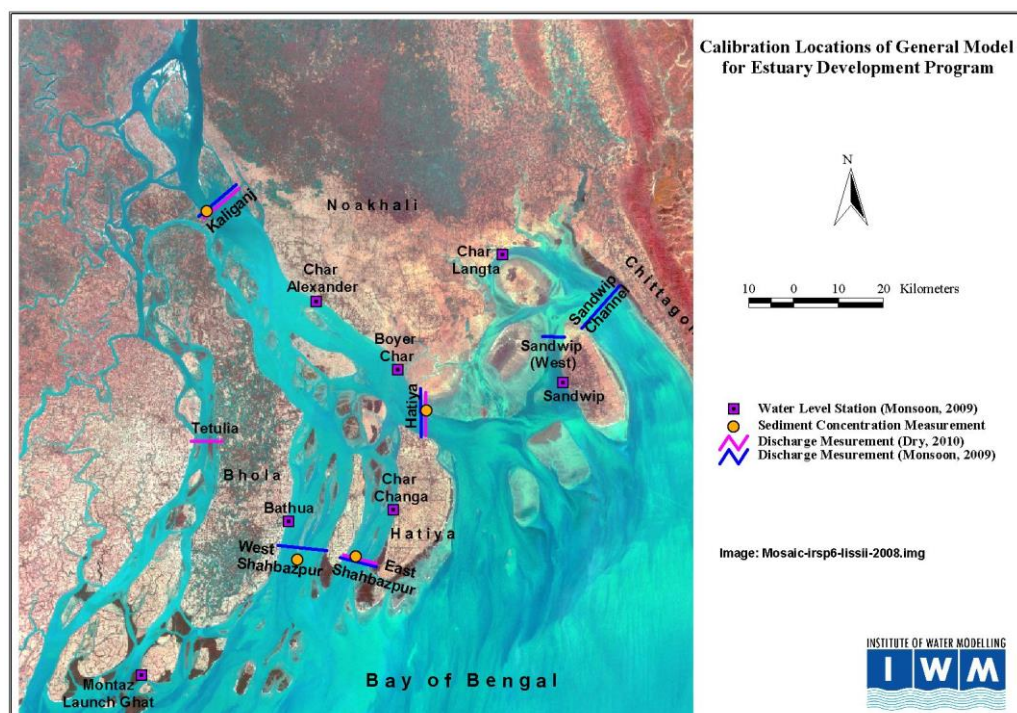


FigureApX D.15 Modelled vs. observed M2 tidal amplitude, run 20

D.4 Hydrodynamic calibration: modelled vs. observed discharges

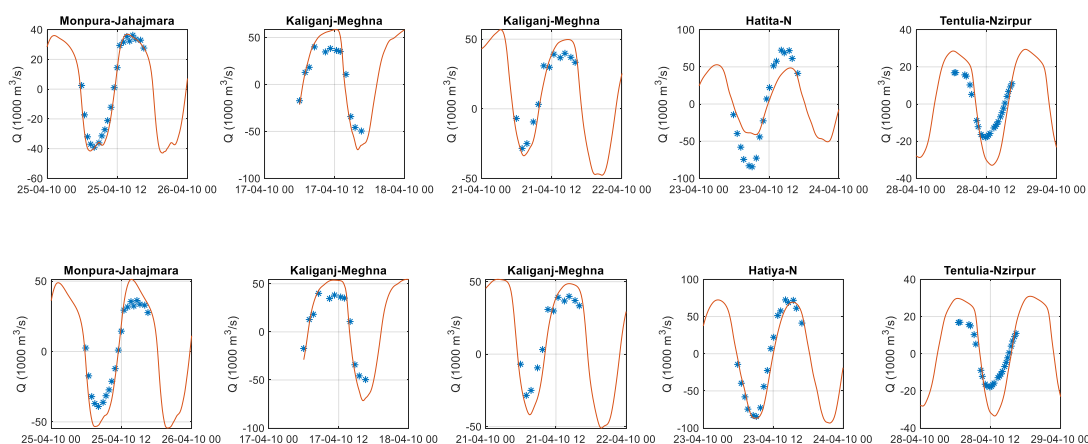
D.4.1.1 EDP 2009/2010

During the Estuary Development Programme in 2009/2010 several 13-hrs measurements were carried out in the Meghna estuary. These data were also used in the calibration of the meso-scale model of the lower Meghna and Tetulia. The location map is given below in FigureApX D.16.



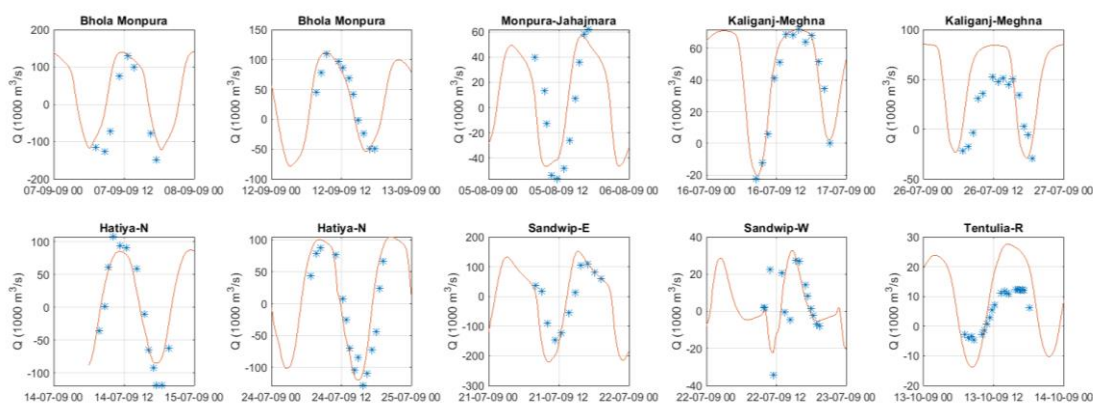
FigureApX D.16 Location map of 13-hrs measurements during EDP programme

For the dry period the results are presented in FigureApX D.17. The top panels show the comparison for the settings as in run 19; especially at Hatiya North the discharges are strongly underestimated; the main cause of this is the uneven roughness distribution in the area, forcing the flow more to the west. In run 20 this gradient in roughness has been removed, leading to much better agreement at Hatiya North. It is possible that a slight reduction of Chézy values in the whole area would improve the overall performance even further, but for now these results are acceptable, and further tuning has not been carried out at this stage. The Tentulia -Nazpur cross-section and the Monpura-Jahipura section show a modest overestimation of the discharge amplitudes.



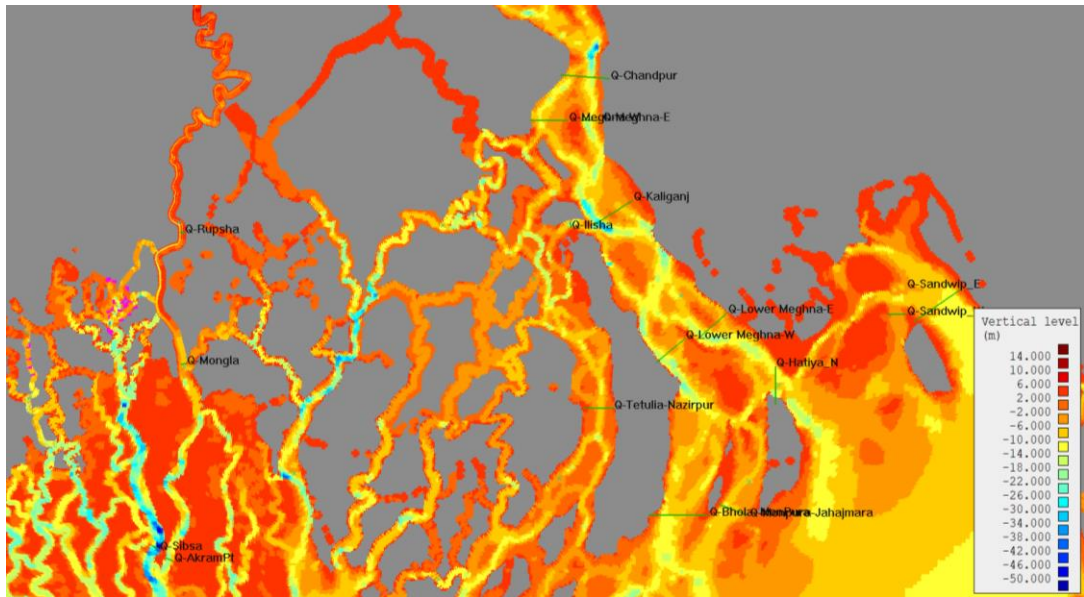
FigureApX D.17 Calibration of discharges in Lower Meghna area. Top: with settings as in run 19; bottom: with roughness distribution as in FigureApX D.18 (run 20). Dry period.

During the monsoon period most cross-sections show good agreement in amplitudes and phases (FigureApX D.19), with the exception of Kaliganj and Tentulia cross-sections; in the first, the mean discharge seems to be overestimated whereas in the second, both amplitude and mean discharge are overestimated. This is likely due to the fact that the schematized annual hydrographs were used for the upstream boundary conditions.



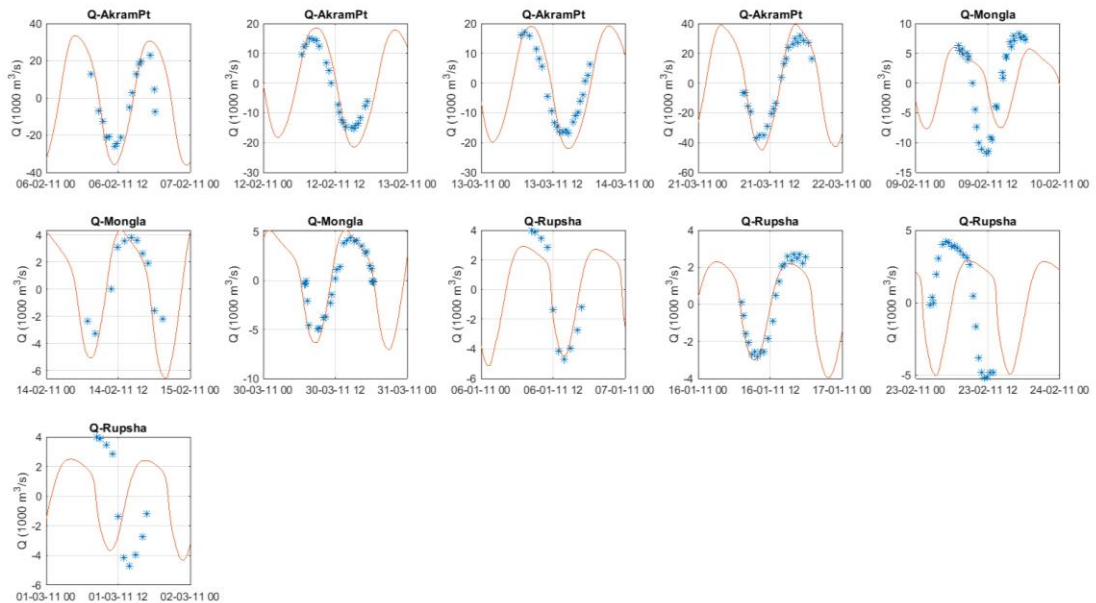
FigureApX D.19 Calibration of discharges in Lower Meghna area. Top: with settings as in run 19; bottom: with roughness distribution as in FigureApX D.20 (run 20). Monsoon season.

D.4.1.2 Pussur-Sibsas 2011



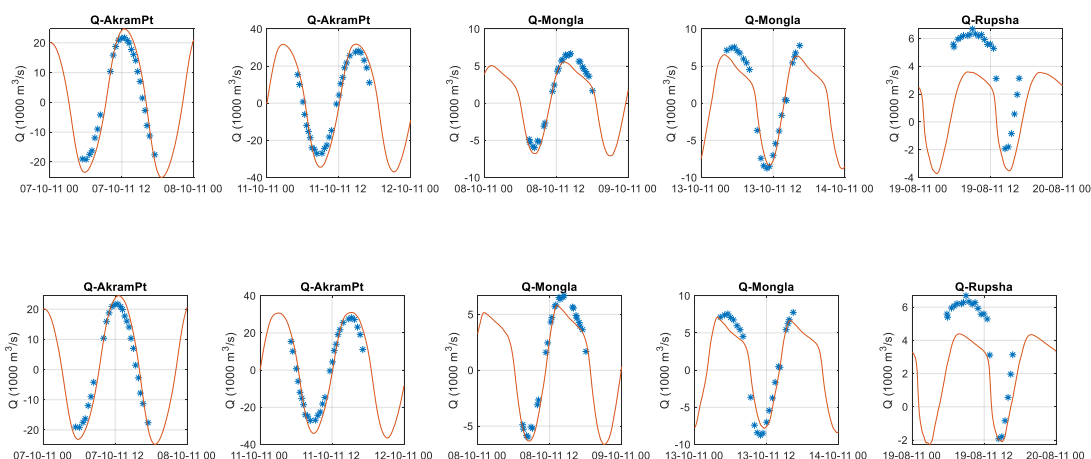
FigureApX D.21 Cross-section definition in Pussur-Sibsas and lower Meghna system.

In the stage 1 model the upper reaches of the Pussur-Sibsas system were incompletely represented and the Gorai was not included. With the modifications in the stage 3 model the tidal amplitudes and discharges have much improved. The cross-sections considered are Akram Point, Mongla and Rupsha, see FigureApX D.21. For the dry period (FigureApX D.22), Akram Pt measurements are generally simulated well, as is Mongla on March 30, 2011; both underestimation and overestimation occur for the other two dates for Mongla. Rupsha data are followed closely on January 6 and 16, while there are unknown time shifts in the data around February 23 and March 1. Overall the agreement is acceptable given the scale of the model.

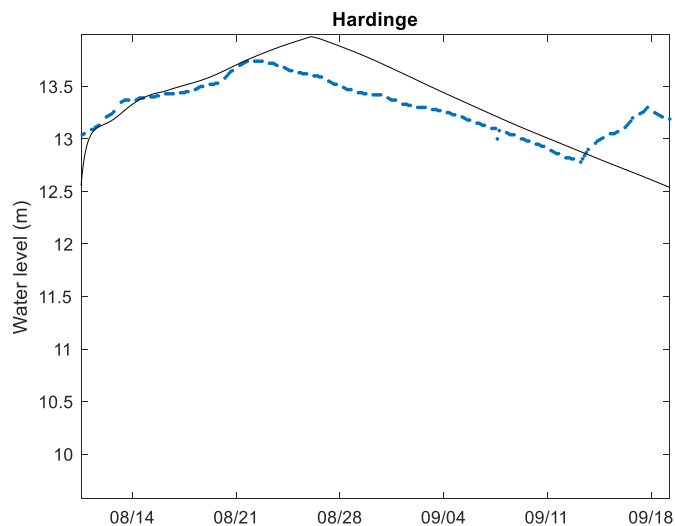


FigureApX D.22 Comparison model – observations for Pussur-Sibsas area, dry period.

For the monsoon period, as shown in FigureApX D.23, the agreement is generally quite good. Extra attention was given to the Rupsha cross-section and as the bottom panel shows, some improvement is created by using the alternative roughness map given in FigureApX D.13 and applying measured discharges at the upstream boundaries. A key factor in this is whether the water levels at Hardinge, which to a large extent drive the flow through the Gorai, are accurately represented. As FigureApX D.24 shows, this is the case for the combination of roughness map and imposed discharges used in run 20. Earlier runs showed underestimation of the Hardinge Bridge water levels by up to metres.



FigureApX D.23 Comparison model – observations for Pussur-Sibsra area, monsoon period. Top panels: with schematized hydrograph; bottom panels: with measured discharges at upstream boundaries.



FigureApX D.24 Comparison modelled (black) and observed (blue) water levels at Hardinge Bridge, monsoon period. Settings as in run 20.

D.5 Sediment model

D.5.1.1 Sediment Data

The literature review suggests that grain sizes of sediment of the GBM delta range from fine sands to clays ($D = xx - xx$ mm), with seasonal variability in transport due to monsoons. Ganges bed sediment samples are 76% fine to very fine sands (idesm), with silt-sized grains making up the remaining bed layer (Datta and Subramanian, 1997). Downstream of the junction of the Ganges and Jamuna rivers, bed sediments are even finer with very coarse silts (Singh et al., 2007). In the coastal region, samples showed the dominant size class were also fine to very fine sands (Stummeyer et al., 2002). Sundarbans sediments are muddy, especially in the more inland located areas, while deeper portions of the Sundarbans estuaries may be sandier.

Suspended sediment in the main rivers of the GBM delta consists of fine silts and clays. Datta and Subramanian (1997) show fine silts and clays in the Ganges, Meghna, Jamuna and Padma Rivers, while the grain size of more than 95% of the suspended material is fine silt and clays (≤ 16 microns). Median grain sizes sampled in the Meghna estuary range from 13.8 to 25 microns, or fine to medium silts (Kuehl et al. 1989, Barua et al., 1994).

D.5.1.2 Model sediment settings

Following the data described in literature, the model includes both finer (mud) and coarser (sand) sediment fractions, each forced by its own sediment transport formula.

Mud transport will dominate suspended sediment concentrations, so that mud sediment settings play a major role in the calibration of concentrations and transports. The Krone-Partheniades transport formula describes the erosion and deposition of mud, while an advection-diffusion equation transports the mud (Krone 1962, 1993; Ariathurai 1974).

$$\begin{aligned} E &= MS_e(\tau_{cw}, \tau_{cr,e}) \\ D &= w_s c_b S_d(\tau_{cw}, \tau_{cr,d}) \end{aligned} \quad (0.1)$$

With

- E erosion flux, $\text{kg/m}^2/\text{s}$,
- M erosion parameter, $0.001 \text{ kg/m}^2/\text{s}$
- D deposition flux, $\text{kg/m}^2/\text{s}$
- w_s sediment fall velocity, 0.001 m/s
- c_b near bed sediment concentration, kg/m^3
- T_{cw} maximum shear stress due to waves and current, N/m^2
- $T_{cr,e}$ critical shear stress for erosion, 0.3 N/m^2
- $T_{cr,d}$ critical shear stress for deposition, 1000 N/m^2
- S_e erosion factor
- S_d deposition factor

and

$$\begin{aligned} S_e(\tau_{cw}, \tau_{cr,e}) &= \left(\frac{\tau_{cw}}{\tau_{cr,e}} - 1 \right) \text{ for } \tau_{cw} > \tau_{cr,e} \\ &= 0 \text{ for } \tau_{cw} \leq \tau_{cr,e} \end{aligned} \quad (0.2)$$

$$S_d(\tau_{cw}, \tau_{cr,d}) = \begin{cases} \left(1 - \frac{\tau_{cw}}{\tau_{cr,d}}\right) & \text{for } \tau_{cw} < \tau_{cr,d} \\ 0 & \text{for } \tau_{cw} \geq \tau_{cr,d} \end{cases} \quad (0.3)$$

Values for the different parameters applied in the standard settings of current study are given next to the parameter definitions. It was considered that mud deposition is not a function of shear stress ($\tau_{cr,d} \gg 1$) and that, in our 2D model, mud is uniformly distributed over the water column. The near bed mud concentration is then given by a concentration constant over depth.

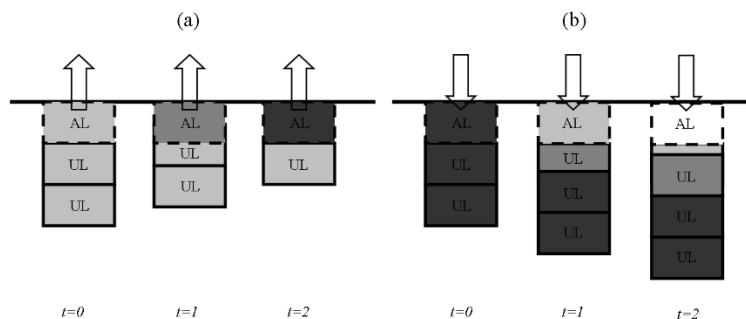
For the bed and suspended transport of non-cohesive sediment, Van Rijn et al. (2000) is followed as described in the D-morphology user manual (Deltares, 2020). Standard settings apply a sediment diameter of 150 μm , a bed slope factor (α_{bn}) of 200 and a maximum bed slope of 1:50. The latter parameters are explained in the next section.

D.5.1.3 Bed composition

In case of multiple sediment fractions, the model applies bed layering with an active layer concept to account for different bed sediment composition across the domain, over time and in the bed. FigureApX D.25 shows the concept of the bed layer model. Initially, in the model setup, the bed consists of two underlayers (UL) of 0.25 m, and a 0.25m active layer that may vary in height depending on the initial sediment availability and erosion and deposition processes during a run. The active layer (AL) is present on top of the fixed layers. The active layer will rise during deposition and lower during erosion, respectively transferring and retrieving sediments and bed composition to/from underlying layers.

The initial bed composition consists of 15 m of sand and 15 m of mud that is equally distributed over a 30 m bed column. Then, during the first phase of a model run (e.g. a year), the model redistributes different sediment fractions throughout the domain, changing the bed composition based on prevailing shear stress and transport variations while bed level changes are not allowed. It is called the BCG (Bed Composition Generation) phase. Van der Wegen et al. (2011) further describe and validate the methodology. The BCG phase typically leads to sandier cells in higher energy environments. After this phase also bed level changes are allowed and the full morphodynamic runs starts.

Transport rates of different sediment fractions (sand, mud) will be proportional to their presence in the active layer. A larger percentage of sand in a cell will thus decrease mud erosion rates. The sand-mud interactions, where e.g. the presence of mud would influence the critical erosion shear stress of sand, has been classified as a second order effect and is not taken into account.



FigureApX D.25 Conceptual multi-fraction bed layer model under conditions of (a) erosion of finer fractions (b) deposition of finer fractions. Darker colours indicate the presence of more, coarser fractions.

D.5.1.4 Morphology

Generally, in the model, sandy sediments will shape the morphology of the bed such as the meander length scale and cross-sectional profile of channels. Important parameters are the transverse bed slope parameter (α_{bn}) driving down-slope sediment transport, and the maximum bed slope parameter limiting the slope of the bed to a maximum value (wetslope). If this bed slope is exceeded, numerical avalanching will redefine the bed until bed slopes are lower than the maximum bed slope. These model parameters are used to calibrate model results against observed channel-shoal patterns. Mud will generally settle in areas of limited shear stress, typically being shoals and wave sheltered areas. Mud transport is not affected by the transverse bed slope effect (α_{bn}) and the maximum bed slope factor. Entirely muddy environments will thus show relatively narrow, deep channels with steep banks.

D.6 Sediment transport boundary conditions

Based on the data analysis presented in Section 3.2 and given the wide variation in estimates of the sediment loads, the following simple conditions were taken, where the seasonal variation of the suspended load and wash load concentration was neglected. For both Ganges and Jamuna rivers a constant concentration of 0.9 kg/m^3 was assumed, well within the reported range of $0.75\text{-}1.25 \text{ kg/m}^3$; for the Meghna at Bhairab Bazar a much lower value of 0.1 kg/m^3 . For the bedload transport equilibrium conditions were assumed depending on local and time varying flow velocities. The total suspended load transport imposed on the upstream boundaries amounts to $(20,200 \cdot 0.9 + 11,300 \cdot 0.9 + 4,600 \cdot 0.1) \text{ kg/s} = 28,810 \text{ kg/s} = 913 \text{ Mt/yr}$, which is well within the range of estimates.

In order to produce the actual sediment fluxes mentioned in Akter (2014) it would be better to increase the mean concentration in the Ganges to 1.5 kg/m^3 , as follows from the table below (TableApx D.4). However, for the runs reported in this report the earlier estimate of 0.9 kg/m^3 has been maintained.

TableApx D.4 Characteristic values for the Ganges, Brahmaputra, and Meghan.

Rivers	Ganges	Brahmaputra	Meghna
Annual average discharge (m^3/s)	11,300	20,200	4,600
Sediment (million tonnes/y)	550	590	13
Annual average concentration (kg/m^3)	1.5	0.9	0.1
Average flood discharges (m^3/s)	52,000	70,000	13,700
D_{50} of the bed material (mm)	0.15	0.2	0.14

D.7 Sediment transport calibration

Since only infrequent and sparse concentration measurements are available, it was not considered useful to try and calibrate this large-scale model against individual measurements; rather, it was tried to reproduce the range and variability of sediment concentrations, based on the following approximate data, collected from various meso-scale reports:

Rupsha: $0.2\text{-}0.8 \text{ kg/m}^3$ for discharges between 0 and $6000 \text{ m}^3/\text{s}$;

Akram Pt: $0.2\text{-}1.5 \text{ kg/m}^3$ for discharges between 0 and $30,000 \text{ m}^3/\text{s}$;

Mongla: $0.4\text{-}1.0 \text{ kg/m}^3$ for discharges between 0 and $5,000 \text{ m}^3/\text{s}$;

Lower Meghna: in the range of $0.5\text{-}1.0 \text{ kg/m}^3$.

D.8 Morphodynamic model setup

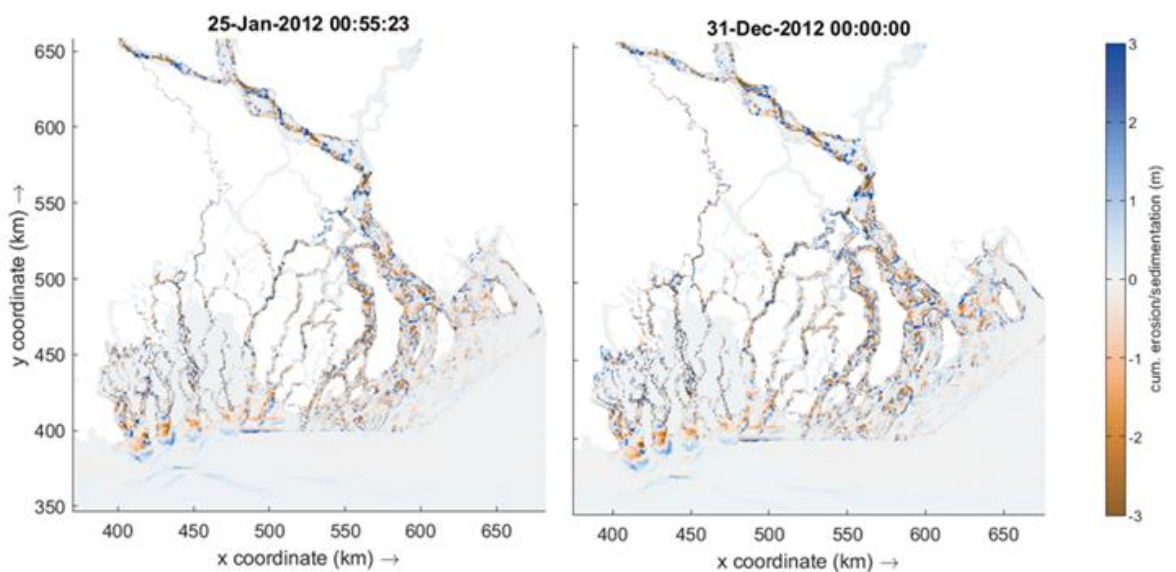
D.8.1.1 Method

D.8.1.2 Real-time simulations vs. MorFac approach

The computational time for simulating a single year of hydrodynamics, sediment transport (?) and morphology with a model such as this is in the order of 12-24 hours on a heavy computational cluster; therefore, 'brute-force' simulations of the morphological evolution over decades would be extremely cumbersome. Therefore, the well-established approach of 'morphological acceleration' or MorFac method (Roelvink 2006, Ranasinghe et al, 2011) has been applied. This works as follows: in Delft3D the model solves hydrodynamics, sediment transport and bottom updating at every timestep; however, the morphological changes are multiplied by the MorFac (the Morphological Acceleration Factor), effectively accelerating the morphological evolution. Thus, after one tidal cycle, the effect on the morphology is as if a number of cycles equal to MorFac had been run. This approach is acceptable as long as the bed level changes within one tidal cycle, even accelerated, are small relative to the water depth.

The tidal cycle can be left unchanged or can be schematized to a single representative tide. However, the yearly discharge curve has a much longer timescale and has to be treated in a different way. As long as the discharge curve changes slowly, the flow distribution can be considered quasi-stationary. The hydrograph can then be accelerated, or 'squeezed' into a shorter time period, by the same MorFac. Squeezing the yearly hydrograph into two weeks does not fundamentally alter the flow distribution; after these two weeks all flow and transport events of a year have passed by. If now a MorFac of 26 (52 weeks divided by 2) is applied, then after one two-week cycle the morphological evolution of one year will have been simulated at the correct (morphological) speed; one hydrodynamic year with 26 such cycles thus represents 26 years of morphological change.

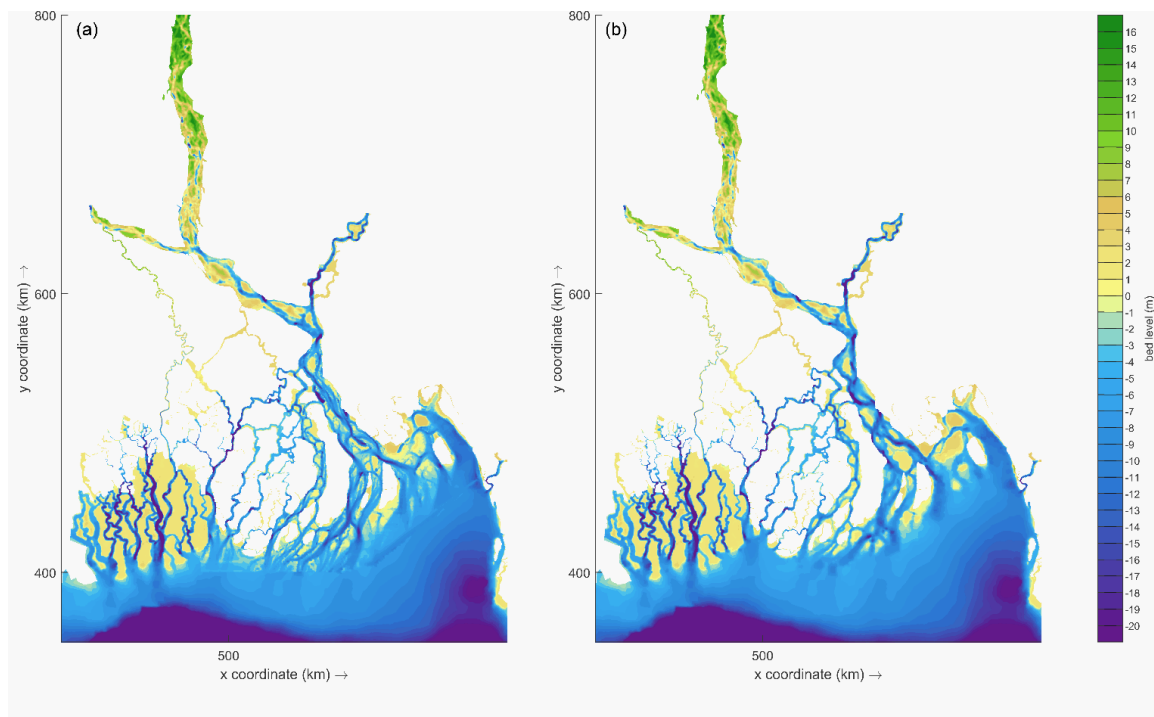
This methodology was tested by comparing a run forced by a 1-year hydrograph with a MorFac of 1 (run Sq1) to a run forced by a 14-days hydrograph (equal in shape, but different in duration) with a MorFac of 26 (run Sq26). Both runs applied a spin-up time of 14 days that allowed for suspension and transport of sediments but not for bed level updating and bed composition updating. Waves were included in these runs. FigureApx D.26 shows that the differences are indeed minimal.



FigureApx D.26 Erosion and sedimentation patterns for Run Sq1 after 1 year (upper panel) and Run Sq26 after 14 days (lower panel).

D.8.1.3 Domain and initial bathymetry

The domain of the morphodynamic model is the stage 3 model described in Section D.3.1.4 and depicted in FigureApx D.27. The model bathymetry sample sets were derived for two points in time, 2000 and 2012, using the datasets described in Appendix A. Where multiple datasets were available, the one closest to the target date was used, in all other cases the available set was used. The initial bathymetry in the model runs is determined at runtime, by Delaunay triangulation of samples onto the mesh nodes. The depth is assigned to the grid cell centre using a tile approach.

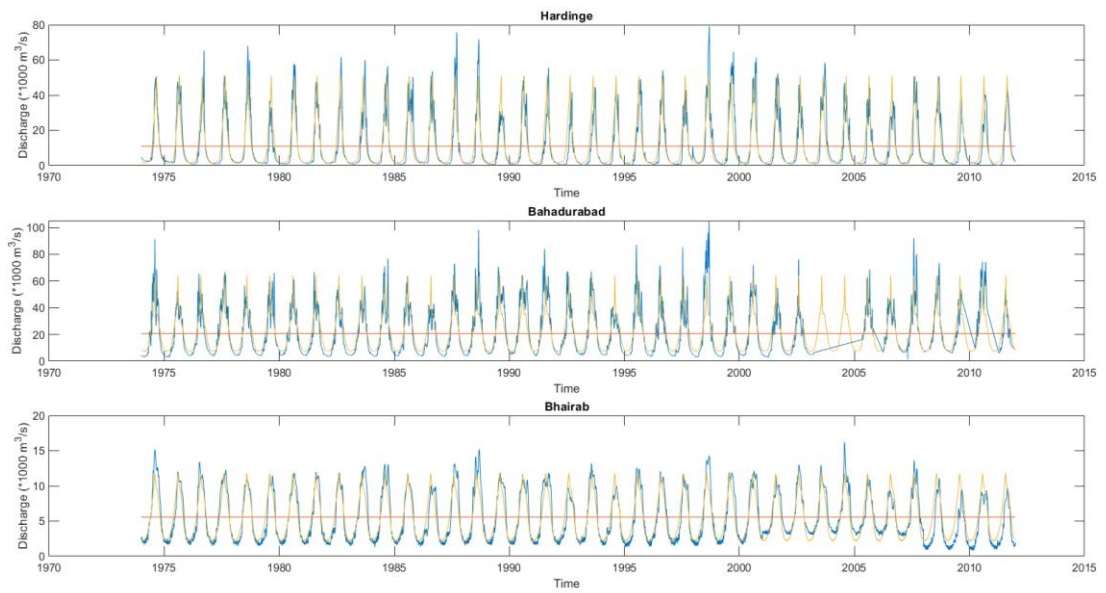


FigureApx D.27 Morphodynamic model domain and bathymetry. (a) Bathymetry for runs starting in 2000; (b) Bathymetry for runs starting in 2012.

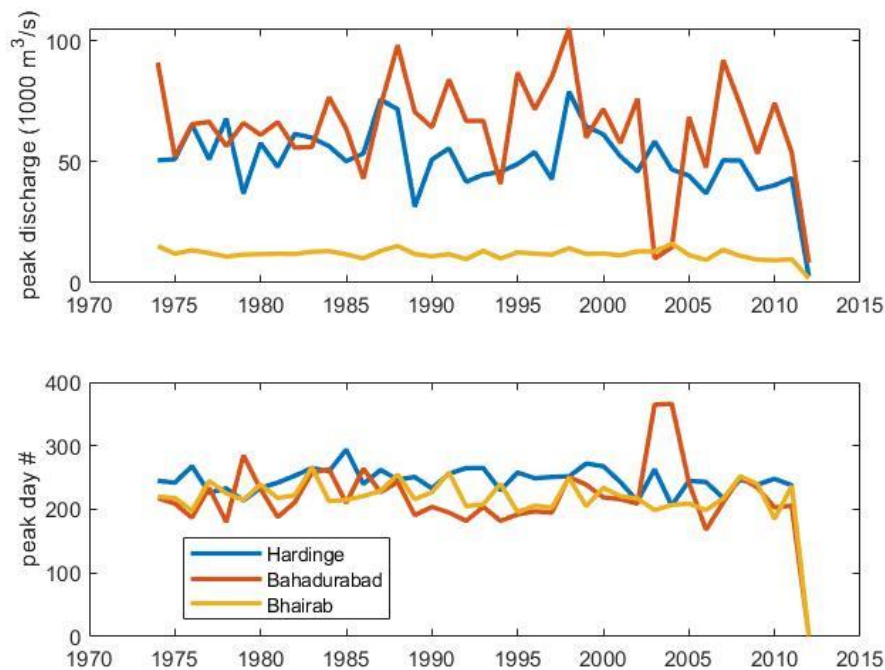
D.8.1.4 Boundary conditions

River boundary conditions

River discharge boundary conditions are prescribed at Hardinge Bridge (Ganges), Bahadurabad (Jamuna) and Bhairab Bazar (Meghna). They are based on multi-year measurements by BWDB covering the period 1974-2012 as shown in FigureApx D.28 (blue lines). A representative discharge curve was determined by determining the year day of the peak discharge for each year and then taking the average of all discharges that are the same number of days before or after the peak. In this way smoothing out the discharge curve was avoided because of the variation in the peak discharge time. The result is shown in the yellow lines in the same figure. The variation in peak discharge and year day of the peak discharge is shown in FigureApx D.29. For the long-term simulations it is the intention to use one representative hydrograph as described above, but the variation shown here could later be used in more stochastic runs where the peak discharge is allowed to vary from year to year.



FigureApX D.28 Observed river discharges of the main three rivers, 1974-2012. Blue lines: observed actual discharges. Yellow lines: multi-year average discharge curve based on days before/after peak.



FigureApX D.29 Observed peak discharges and year day on which peak discharge took place, for Hardinge, Bahadurabad and Bhairab Bazar.

Wind fields

Wind fields are needed in the morphodynamic simulations to drive monsoon-related wind-driven circulation, and to generate local wind waves close to the coast, that add to the swell waves imposed on the boundaries. Spatial- and time-varying wind fields were sourced from the ECMWF ERA5 hindcast database (Hersbach et al., 2020), and were shown in Appendix A.

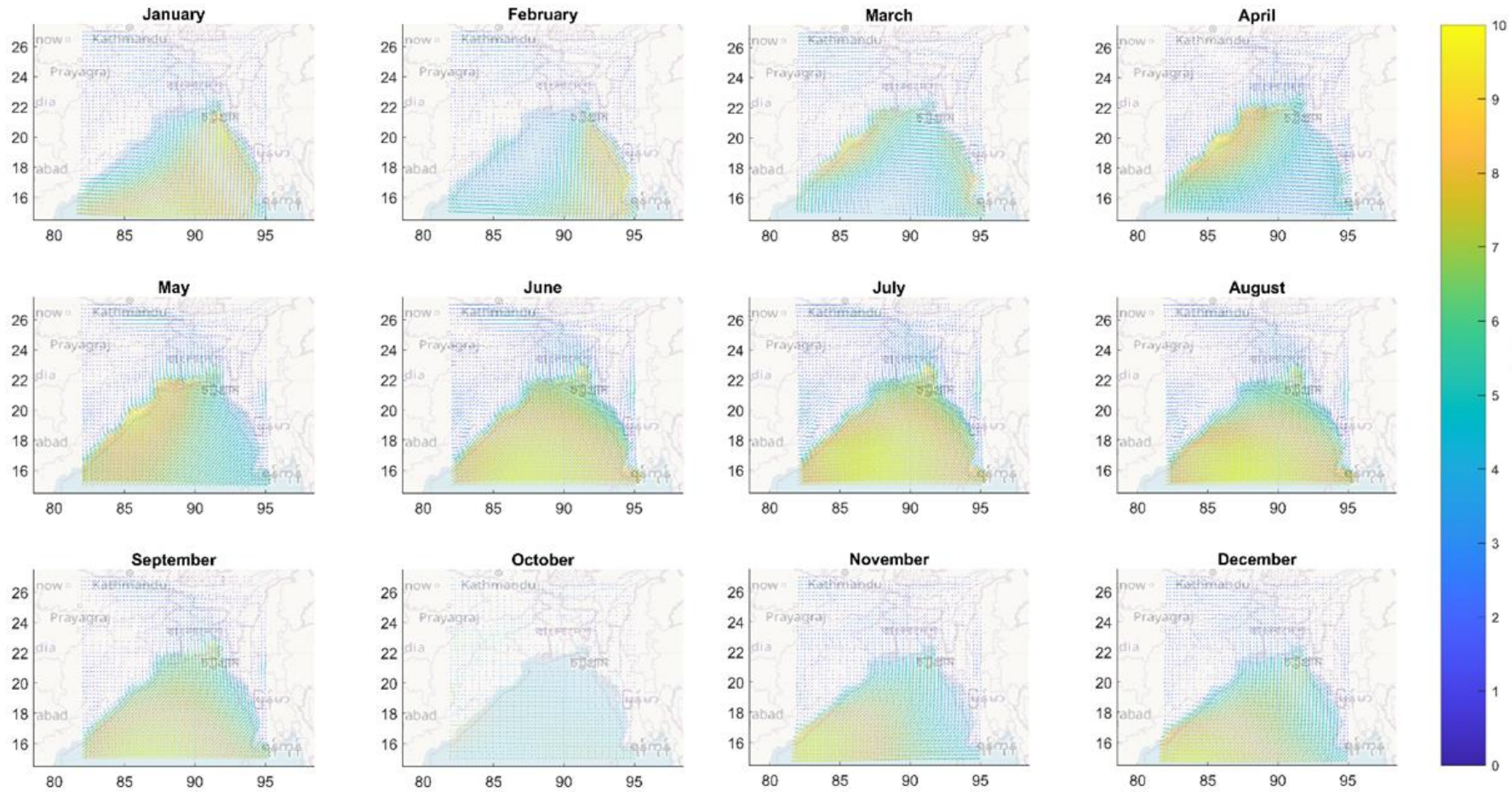
The hourly meteo fields were averaged over the period 1979-2019 for each month, in order to get a clean yearly wind climatology over the year (FigureApx D.30). The resulting data was converted to Delft3D compatible files for spatially- and time-varying meteorological forcing.

Wave boundary conditions

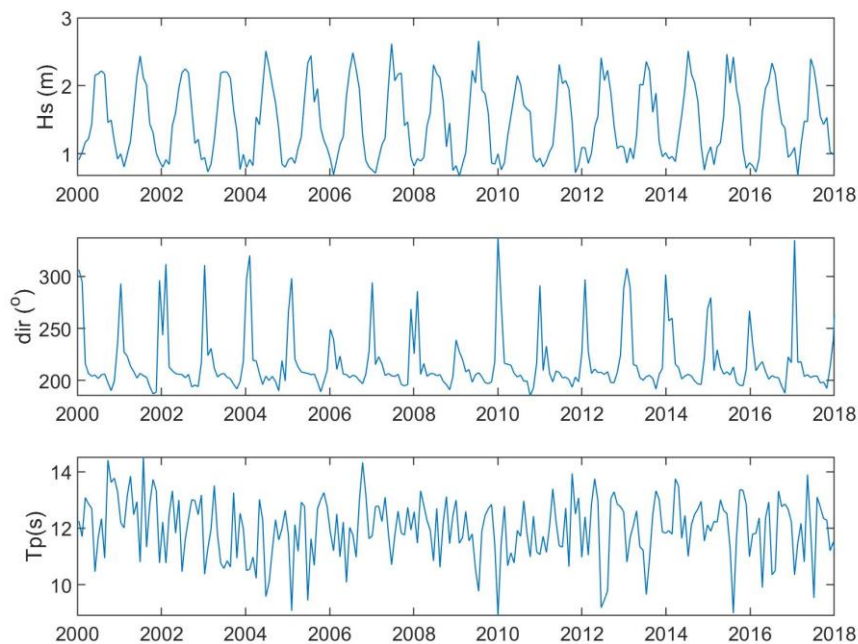
Wave data was obtained for the same period as the wind fields at the following extraction point (20.5 °N, 91.0 °E), which has a water depth of 85m and is located due south of the Meghna estuary mouth. This location is considered to be representative for the area. From the same location, for the purpose of long-term simulations, monthly weighted average values of wave height period and direction were taken. These monthly weighted average values of wave height period and direction were applied as boundary conditions after 'squeezing' the time series by a MorFac of 26, resulting in time steps of variation of the wave conditions of a little over one day. The original time series is shown in FigureApx D.31 for the period after 2000.

Assessing the effect of wind and waves

Because the effect of wind and waves on the large-scale sediment transport fluxes and erosion-sedimentation patterns was not known beforehand, as so far no existing models of the GBM delta had considered it, two base simulations were carried out, one without wind and waves and one with both. In the following sections, the results of both simulations will be compared with each other and with data, where possible.



FigureApX D.30 Monthly wind climatology for the Bay of Bengal, derived from 30 years of ERA5 data



FigureApX D.31 Monthly wave climatology at the 85m depth contour offshore of the Meghna estuary, derived from 30 years of ERA5 data. Direction in degrees North

D.8.1.5 Sediment settings

Given the enormous scale of the model domain, sediment settings have to be a compromise between local knowledge and overall consistency. The modelling process starts from the simplest possible setup, whereby one sand fraction and one mud fraction are combined. Different initial distributions of the sand and mud have been tried and it was tested how these fractions interact in the bottom, where a layered bed composition model is applied. To avoid large morphological changes due to a wrong distribution of the sediments, so-called 'bed composition generation' (BCG) runs can be run, where the bed composition changes but the bathymetry is not updated. This provides a better starting point for morphological simulations. Alternatively – or additionally – an initial distribution of sediment thicknesses can be prescribed.

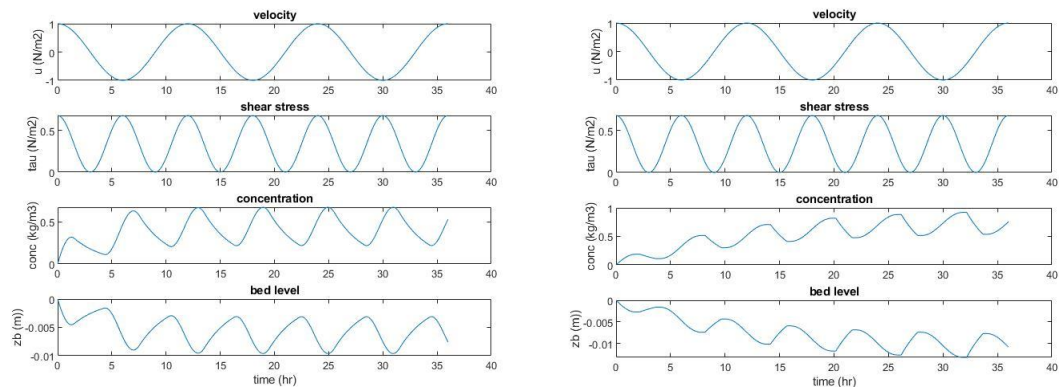
It is tried to adapt similar settings to those used in meso-scale models and in the 1D macro model, but this is not always possible, for instance because a meso model may be in a totally muddy area and hence have no sand fraction, which leads to different behaviour.

The following simple tool can help us to assess the effect of sediment parameters on sediment concentration variations for a given area, under the assumption of spatially uniform conditions. It is focused on mud concentrations and uses the same input parameters as the Mike and Delft3D systems. Because different modelling practices exist at Deltares and DHI, it is useful to compare the effects of different settings, especially with respect to sedimentation and erosion thresholds. As shown in TableApX D.5, this does not have to lead to very different outcomes.

TableApX D.6 Typical parameter settings for sediment, comparison Deltares and DHI approaches.

Variable	Description	Typical Deltares setting (left panel)	Typical DHI setting (right panel)
u_{mean}	mean velocity (m/s)	0	0
u_{amp}	tidal velocity amplitude (m/s)	1.0	1.0
h	water depth (m)	10	10
frac	availability of mud fraction	1	1
M	Erosion parameter (kg/s/m ²)	0.001	0.0002
w_s	fall velocity (m/s)	0.001	0.001
$\tau_{u_{\text{ce}}}$	critical shear stress for erosion (N/m ²)	0.3	0.2
$\tau_{u_{\text{cd}}}$	critical shear stress for deposition (N/m ²)	1000	0.1
C	Chézy value (m ^{1/2} /s)	120	120
c _{ref}	bed concentration (kg/m ³)	700	700

The result for the case defined in TableApX D.6 is a time series of velocity, shear stress, concentration and bottom variation over the tidal cycles (TableApX D.6, FigureApX D.32). It can be seen that, for a fully muddy bottom (availability=1), and for these velocities of 1 m/s amplitude, a variation of the concentration between 0.5 and 1 g/l will be achieved, a typical value for the Pussur-Sibsa area. However, there are many combinations of parameters that can produce a similar time series of concentration. While Deltares practice is to apply continuous deposition (by setting a very high critical shear stress for deposition), DHI typically applies a low threshold for deposition; both approaches are well established in practice. In FigureApX D.32 the values and results on the left are applying Deltares settings; on the right the DHI settings; both can clearly lead to similar results, though the DHI approach takes a little more time to reach an equilibrium response. The fall velocity is the dominant parameter in determining how far the concentration falls back during slack tide.



FigureApx D.32 Behaviour of sediment concentration and bottom change as a function of sediment parameters as computed by ...; left panel: typical Deltares settings with no critical shear stress for deposition; right panel: typical DHI setting with critical shear stress for deposition

For the morphological simulations, settings of bed composition and sediment properties were varied until a satisfactory longer-term behaviour was achieved for both the morphological changes and the sediment concentration. TableApx D.7 shows the sediment settings applied in the final setup.

TableApx D.7 Overview of sediment parameters current model

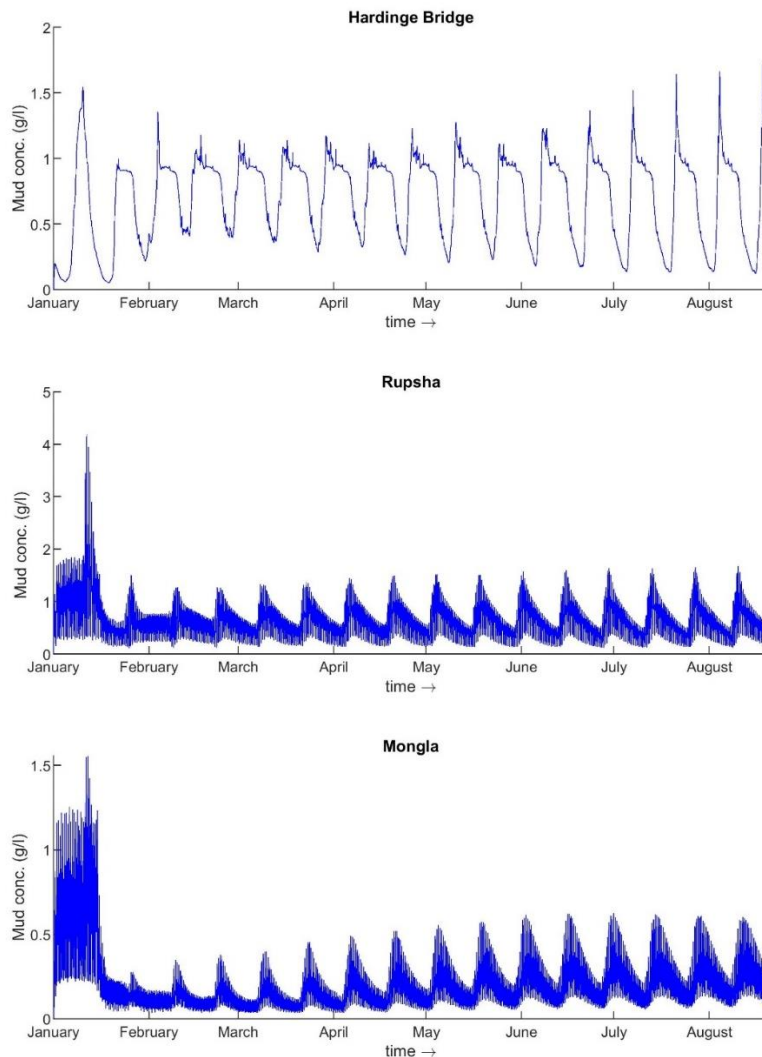
Variable	Description	Current setting
D50	Sand median diameter (mm)	0.15
IniSedThick sand	Initial thickness of sand layer (m)	15
Cref, sand	Bed concentration sand (kg/m ³)	2650
IniSedThick mud	Initial thickness of mud layer (m)	15
frac	Availability of mud fraction	Depending on bed composition sand/mud, variable.
M	Erosion parameter (kg/s/m ²)	0.001
w _s	Fall velocity (m/s)	0.001
tau _{ce}	Critical shear stress for erosion (N/m ²)	0.3
tau _{cd}	Critical shear stress for deposition (N/m ²)	1000
C	Chézy value (m ^{1/2} /s)	120
Cref, mud	Bed density (kg/m ³)	700

With these settings, the sediment concentrations in the model range between 0.2 and 1.5 g/l. This is in line with observations both in the Pussur-Sibsa area and in the Meghna estuary mouth. These concentrations vary with the tide and throughout the monsoon.

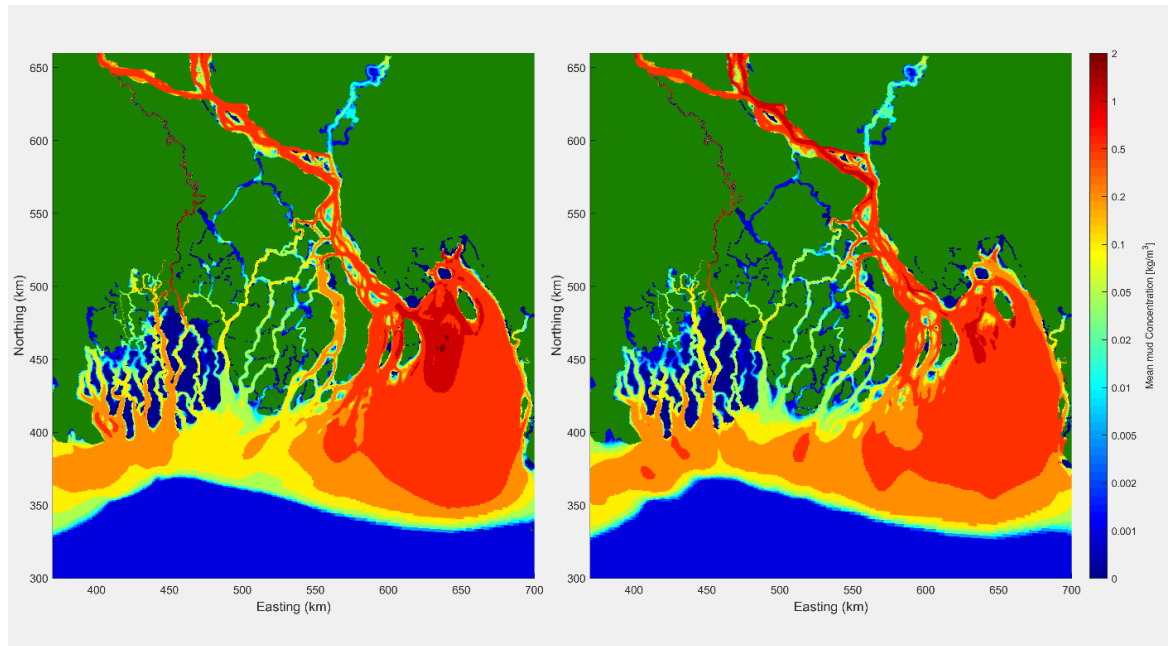
In FigureApx D.33 some time series of sediment concentration are shown from upstream at Hardinge to the Pussur-Sibsa estuary at Mongla. During the first (hydrodynamic) weeks the concentrations can be relatively high because of an initial availability of mud in the top layer of 50%. When the bed composition and morphology updating kicks in, the mud availability rapidly adapts to the local shear stresses and also the bottom profile, which can have local irregularities, tends to be smoothed by the morphodynamic updating. The evolution of the concentration with each (accelerated) hydrograph tends to a recurring pattern, and the concentrations level out at a range similar to the observations.

The spatial patterns of the time-averaged concentration are depicted in FigureApx D.34, for both the simulation without and the one with wind and wave forcing. The overall pattern appears reasonable and the effect of the waves is to raise the level of sediment concentrations in the nearshore shelf areas.

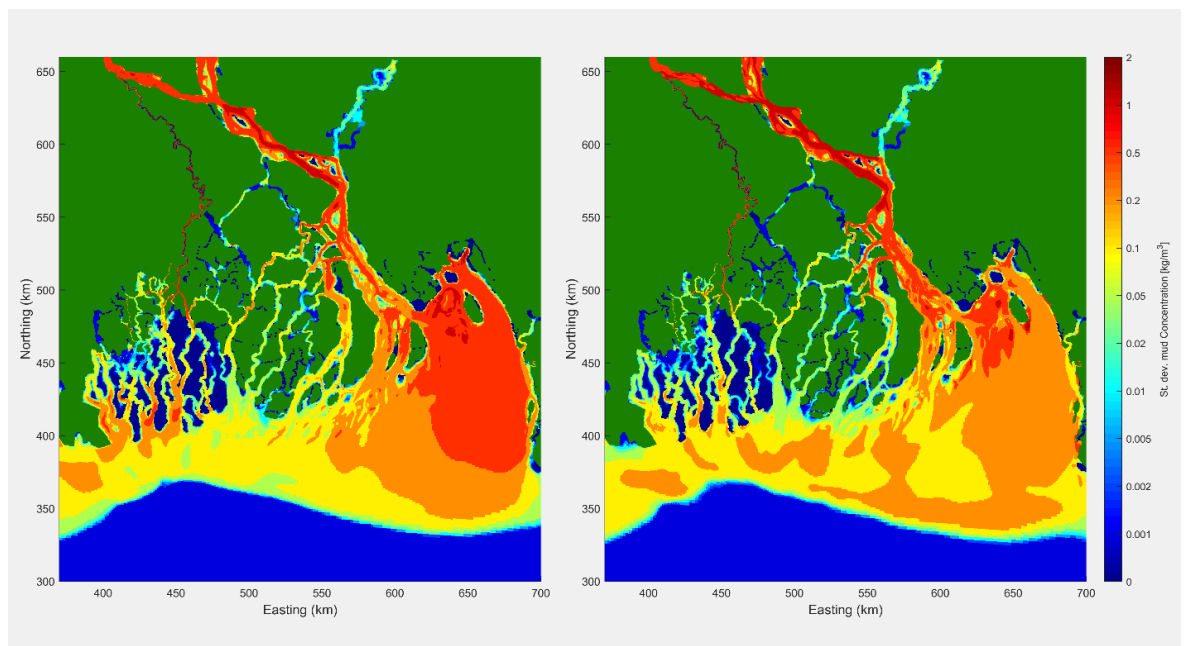
A measure of the variability of the sediment concentration is the standard deviation in time of this concentration. As FigureApx D.35 shows, the variability is substantial, almost of the same order of magnitude as the mean concentration, which is understandable due to the strong seasonal modulation and the intra-tidal and spring-neap variation. The wind and wave forcing does not add much to this variability, and in places it actually reduces it, e.g. around Sandwip Island.



FigureApx D.33 Time series of sediment concentration computed with the xxx model at Hardinge, Rupsha and Mongla.



FigureApX D.34 Time-averaged sediment concentration pattern in delta; left: without wind and wave forcing, right: with wind and wave forcing.



FigureApX D.35 Standard deviation of sediment concentration pattern in delta; left: wind and wave forcing, right: with wind and wave forcing.

D.8.1.6 Morphological settings

In TableApX D.8 the morphology model settings are summarized. Most parameters are set to default or have already been discussed, such as the MorFac and spin up interval MorStt; noteworthy are AlfaBn, a transverse bed slope gradient term that works only on the bedload part of the transport of the sand fraction. Since this is only a small part of the total sediment transport it needs to be set to relatively high values to have any effect and results in smoothing the bed evolution to a reasonable extent. Using the Wetslope keyword avalanching is activated when slopes get too high. As the grid is generally very coarse (500 m square cells in most cases) it is noted that a 1:50 wetslope still allows bed level differences of 10 m between neighbouring cells.

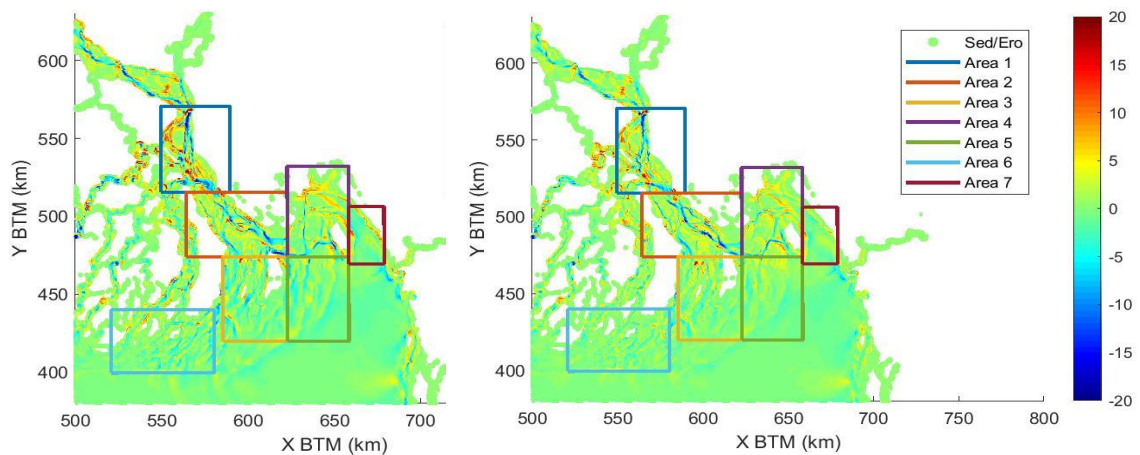
As was discussed before, the underlayer model is essential to create a realistic spatial distribution of the sediment fractions in the top layer, which in turn greatly influences the sediment concentrations.

TableApX D.8 Overview of morphological parameters current model

[Morphology]			
MorFac	26	[-]	Morphological scale factor
MorStt	1209600	[s]	Spin-up interval from TStart till start of morphological changes (14 d)
Thresh	0.05	[m]	Threshold sediment thickness for transport and erosion reduction
MorUpd	true	[-]	Update bathymetry during FLOW simulation
NeuBCMud	false	[-]	Neumann condition for upstream mud boundary
NeuBCSand	true	[-]	Neumann condition for upstream sand boundary
AksFac	1	[-]	van Rijn's reference height = AksFac * ks
RWave	2	[-]	Wave related roughness = RWAVE * estimated ripple height.
AlfaBs	1	[-]	Streamwise bed gradient factor for bed load transport
AlfaBn	200	[-]	Transverse bed gradient factor for bed load transport
Sus	1	[-]	Multiplication factor for suspended sediment reference concentration
Bed	1	[-]	Multiplication factor for bed-load transport vector magnitude
SusW	0	[-]	Wave-related suspended sed. transport factor
BedW	0	[-]	Wave-related bed load sed. transport factor
SedThr	0.2	[m]	Minimum water depth for sediment computations
ThetSD	0	[-]	Factor for erosion of adjacent dry cells
Wetslope	0.02	[-]	Threshold bed slope for avalanching
[Underlayer]			
IUnderLyr	2	[-]	Flag for underlayer concept 1 = one well mixed layer 2 = multiple layers
ExchLyr	false	[-]	True/false separate exchange layer
TTLForm	1	[-]	Transport layer thickness formulation
ThTrLyr	0.25	[m]	Thickness of the transport layer
MxNULyr	2	[-]	Number of underlayers (excluding final well mixed layer)
ThUnLyr	0.25	[m]	Thickness of each underlayer

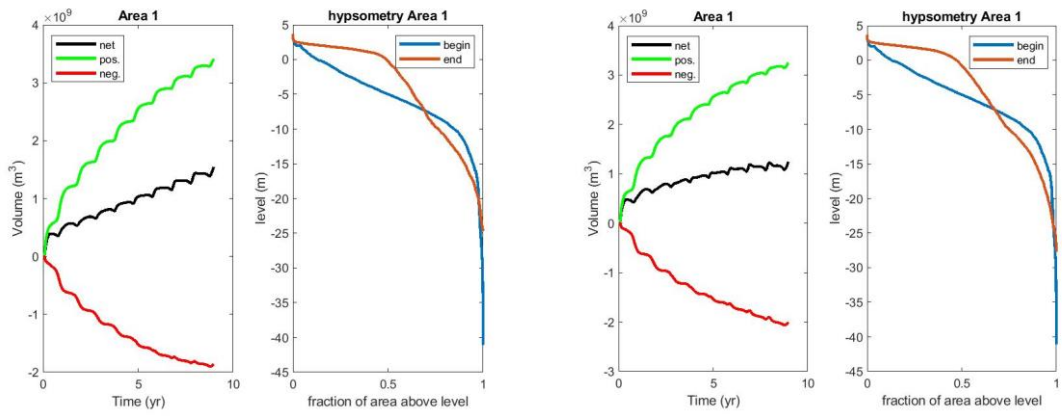
D.8.2 Calibration

The most complete morphological calibration data available is the comparison of bathymetric surveys from 2000 and 2009, as described in the EDP report on updating of the morphological model of the EDP area (IWM, 2010). The areas used in the volume balance were converted to the BTM coordinate system and the same analysis was applied namely the rate of change of the erosion, deposition and net volumes per area. The areas are shown in FigureApx D.36 along with the simulated erosion-sedimentation patterns over the same period of 2000 to 2009. In the left panel, as with the subsequent figures, the results without wind and wave effects are presented; in the right panel the erosion/sedimentation is shown for the simulation with the monthly averaged wind and wave time series.

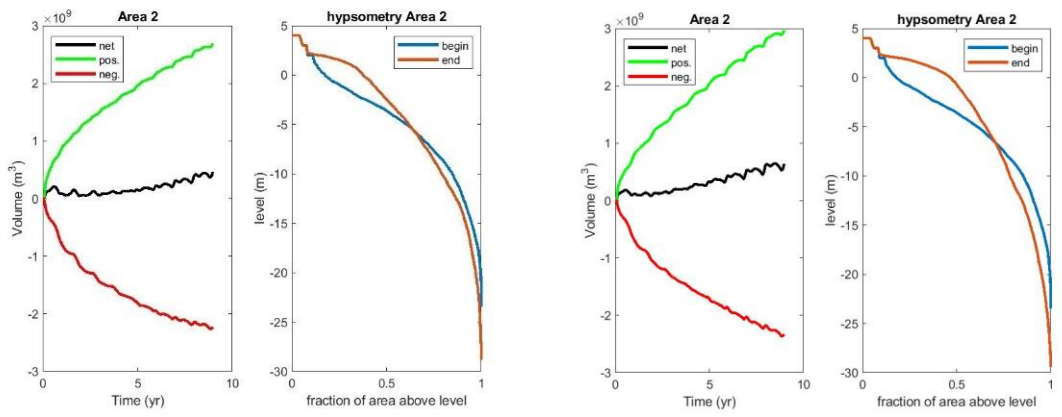


FigureApx D.36 Sedimentation/erosion pattern (in warm/cold colours) over period 2000-2009 in lower Meghna area, and volume balance areas applied in EDP study (2009). Left panel: simulation without wind and waves; right panel: simulation with realistic time series of wind and waves.

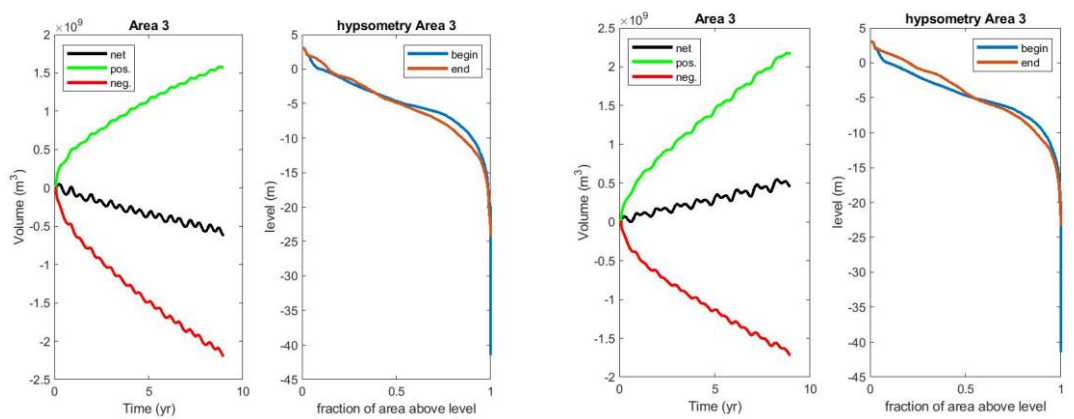
In FigureApx D.37 up to and including FigureApx D.43 the evolution of the erosion, sedimentation and net volumes is shown in time, clearly showing the effect of the seasonal variation on top of the trends. Also, the hypsometry change (the change in how the surface area is distributed as a function of bed level) is shown in the panel next to it. For each area, the trends are shown without (left) and with (right) wind and waves included. The effect is negligible in Area 1 and 2, as they are mostly sheltered from the waves, but for Area 3 the wind and waves are able to reverse the net erosion to net accretion especially leading to more sedimentation in shallow areas. In Area 4, which in the measurements showed the strongest accretion, an already positive net trend is enhanced; in Area 5 the negative net trend is reduced and then reversed to accretion. Area 6, southwest of Bhola, shows subtle differences with slightly more accretion with waves, and a hypsometry that is almost stable. Finally, Area 7 shows strong accretion in the shallow areas but a deepening of the channels, and a net positive trend.



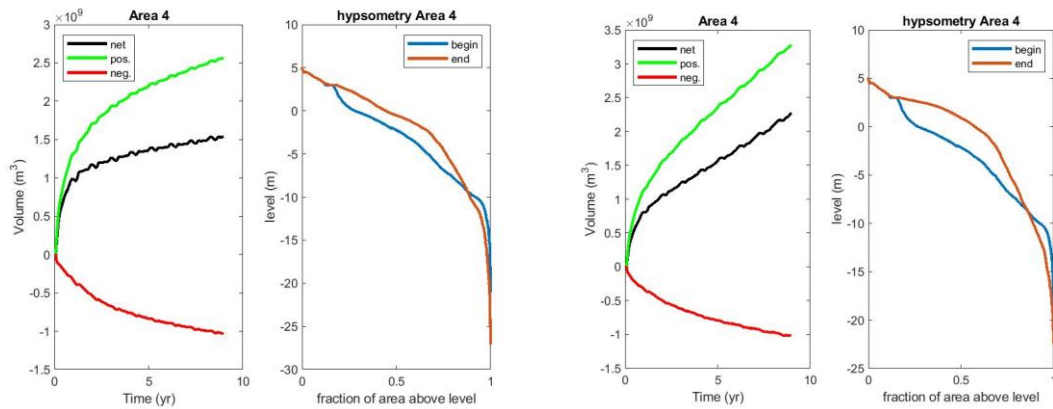
FigureApX D.37 Volume and hypsometry change 2000- 2009 area 1; without (left) and (right) wind and waves.



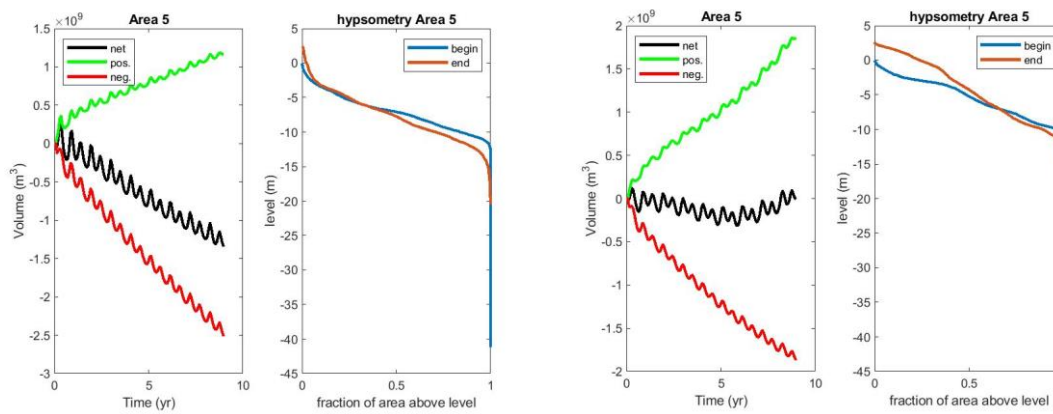
FigureApX D.38 Volume and hypsometry change 2000- 2009 area 2; without (left) and (right) wind and waves.



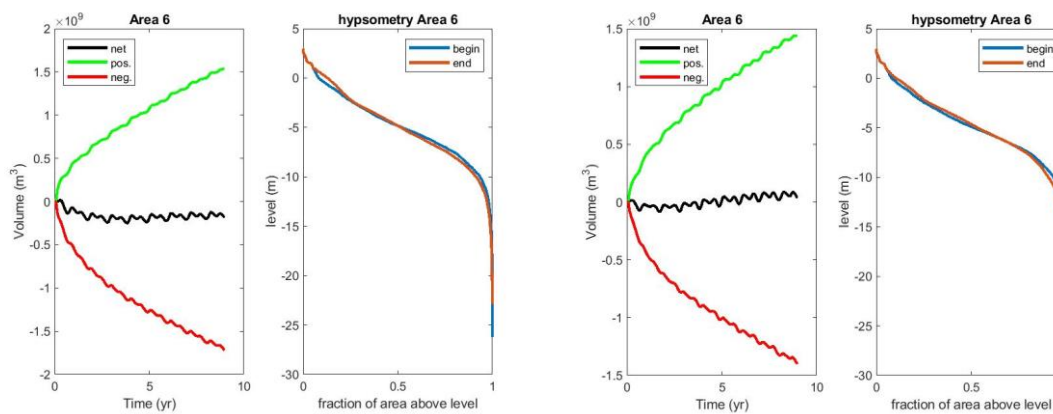
FigureApX D.39 Volume and hypsometry change 2000- 2009 area 3; without (left) and (right) wind and waves.



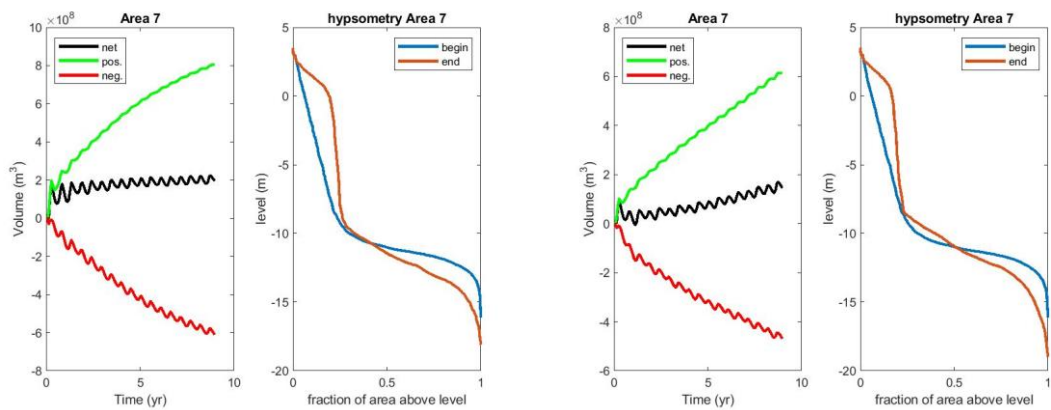
FigureApX D.40 Volume and hypsometry change 2000- 2009 area 4; without (left) and (right) wind and waves.



FigureApX D.41 Volume and hypsometry change 2000- 2009 area 5; without (left) and (right) wind and waves.

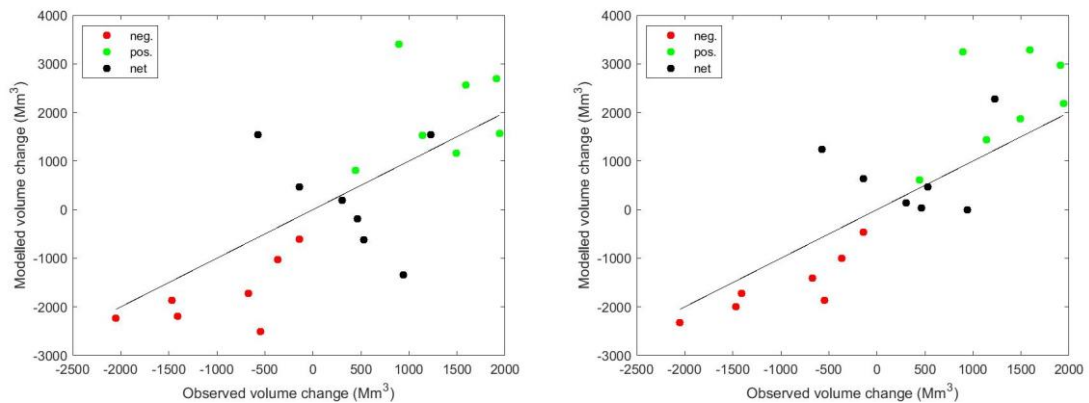


FigureApX D.42 Volume and hypsometry change 2000- 2009 area 6; without (left) and (right) wind and waves.



FigureApX D.43 Volume and hypsometry change 2000- 2009 area 7; without (left) and (right) wind and waves.

The erosion, accretion and net volume change over the period from 2000 to 2009 as simulated is compared with the observed volumes in FigureApX D.44. The results of the simulation without wind and wave effects show some agreement, albeit with a large scatter, to the measured gross volume changes but the net changes are uncorrelated or even negatively correlated. When the wind and waves are included the scatter in the gross changes reduces significantly and 5 out of the 7 areas show the correct sign of the net trend.



FigureApX D.44 Computed vs. observed erosion (red), sedimentation (green) and net volume change (black) in the period 2000-2009 for the 7 areas as defined in Figure xxx, for a simulation without (left) and with (right) wind and waves.

The observed and modelled volume changes are also listed in the table below (TableApX D.9). It is important to note that the overall trends are comparable, and erosion and sedimentation volume changes are highly to moderately correlated (0.85 resp. 0.53). Although the net volume change is the difference of two uncertain numbers, there is still a correlation of 0.13 and the total changes (negative, positive and net) are all overestimated by the same factor of approx. 1.6. Overall this result is as good as could be expected given the large uncertainties in the observed data, the boundary conditions and the model settings.

TableApx D.9 Observed and modelled volumetric changes.

	Observed volume change (Mm ³)			Modelled volume change (Mm ³)		
	Neg.	Pos.	Net	Neg.	Pos.	Net
1	-1467	892	-574	-2003	3247	1245
2	-2050	1908	-142	-2325	2968	643
3	-1408	1941	533	-1721	2182	462
4	-366	1594	1228	-1005	3283	2278
5	-547	1492	944	-1871	1863	-7
6	-672	1138	465	-1403	1438	35
7	-139	444	305	-469	614	145
<i>Total</i>	<i>-6649</i>	<i>9409</i>	<i>2759</i>	<i>-10796</i>	<i>15596</i>	<i>4801</i>

Parameter	Neg.	Pos.	Net
RMSE	367	854	962
BIAS	-592	884	292
MAE	592	884	752
SLOPE	1.62	1.66	1.74
CORR	0.85	0.53	0.13

D.8.2.1 Sensitivity analysis

Due to long computation times only a limited sensitivity analysis was carried out. The findings are summarized below:

- Excluding Coriolis' force has a very limited effect;
- Increasing the sand diameter from 150 μm (standard settings) to 250 μm has a very limited effect on morphodynamics. This is probably due to the fact that, for morphodynamic development, spatial sediment transport gradients are more important than actual transport magnitudes;
- Increasing the transverse bed transport parameter (α_{bn}) from 200 to 500 has a limited effect, whereas lower values (50,100) lead to much narrower and deeper channels;
- Applying a bed slope parameter of 1:200 instead of 1:50 (standard settings), leads to shallower and wider channels. For the Jamuna and Meghna estuary this looks reasonable. However, narrower estuaries like Pussur and Sibsa lose too much channel depth so that tidal intrusion is limited too much. Applying a muddier bed composition to the Pussur-Sibsa system (which is quite muddy) would lead to steeper slopes and deeper channels since the bed slope effect only applies to sand transports.

D.9 Conclusions calibrated model

Based on the calibration results for hydrodynamics and morphology change over periods in the order of 10-20 years the following conclusions may be drawn:

- The macro scale morphodynamic model runs robustly on a 25-year timescale, with acceptable run times (in the order of days on a cluster).
- Some important parameters have been identified and a clear parameter setting has been arrived at.
- This setting leads to a physically reasonable distribution of bed sediment, concentration patterns, net sedimentation areas including delta top set, and erosion hotspots.

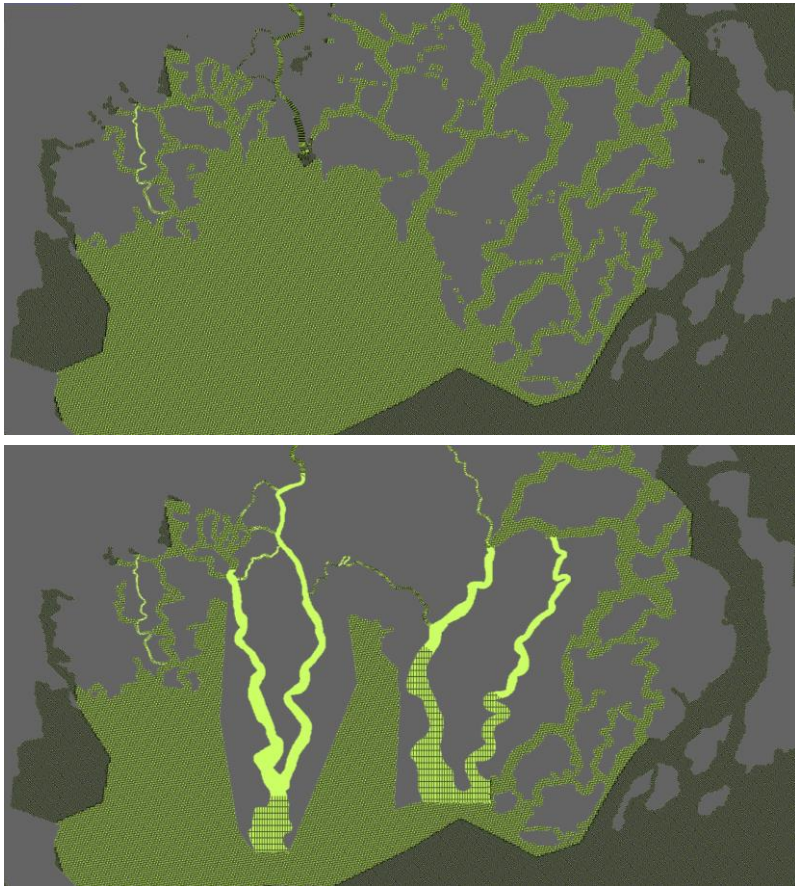
- The model shows a predictable behaviour as a function of processes and boundary conditions;
- A detailed validation over a ~9 year period shows reasonable agreement for gross and net volume changes and general patterns; there is an overestimation of overall sedimentation, erosion and net volume changes by factor 1.6, which is well within an acceptable range for morphodynamic models.
- Inclusion of wind and waves significantly improves the performance of the model in terms of reproduction of sedimentation, erosion and net volume changes.
- Straightforward boundary conditions can be applied that are easy to adjust to future scenarios.

In short, the macro-scale model has been developed to an acceptable level and can serve as a basis for future scenario runs.

D.10 Adaptations for scenario runs

Based on improved systems insight and continuous model optimization, some adaptations of the calibrated model mesh and model setup were made for the 80-year scenario runs. These are summarized in this section. It is stressed that the adaptations have been minor and aimed at improving local dynamics and will not have significantly affected the macro scale model performance described in previous sections.

- The possibility of local refinement of the mesh is one of the assets of D3D FM. The mesoscale meshes of the Pussur-Sibsa system and the Baleswar-Bishkali system were integrated in the macro scale mesh (see FigureApx D.46). This was done to generate optimal boundary conditions for meso scale modelling that, in this way, would not be affected by coarser mesh schematization of the calibrated mesh. In addition, this inclusion allowed for an integral assessment of the dynamics at meso- and macro-scale level. Mesh resolution improved from about 200 to 100 m in the meso scale regions.
- The bathymetry was updated with new area parts as long as they were available and more recent than the 2010 bathymetry of the calibrated model. We refer to this version as the 2020 bathymetry, although the majority of the updated parts were from around 2015.
- Preliminary morphodynamic model runs showed that the Gorai would dramatically erode over 80 years taking about 50% of the discharge from the Ganges in the end. This was considered an unrealistic scenario. We therefore increased the friction by decreasing Chezy values from 120 to 45 in the Gorai.
- Preliminary morphodynamic model runs showed a large impact of the initial sediment availability in the bed. Basically, the 15m to 15m initial mud and sand availability lead to unrealistically deep and shallow channels after decades because mud was washed out. A division of 1m to 15m for mud and sand lead to more realistic results.
- The dry cell erosion factor, which in earlier phases gave problems, was switched on for the scenario runs. This allows to simulate large-scale bank erosion following encroachment of channels and avoids the problem of encroaching channels becoming unrealistically deep. An important factor in this modelling is the depth of the adjacent channel that has to be reached before the dry cell erosion kicks in. This depth, H_{MaxTH} , was set to 10m.
- Based on additional sensitivity analysis we adapted the mud fall velocity from 1 mm/s to 0.25mm/s, the sand diameter from 150 μ m to 250 μ m, the bed slope parameter α_{bn} from 200 to 500 and disregarded the bed steepness calibration factor, wetslope. Finally, we increased the critical shear stress for erosion in the Sundarbans region from 0.3 Pa to 1 Pa for areas above 1m BTM vertical datum to stimulate deposition at the higher, mangrove covered intertidal flats.



FigureApx D.45 Mesh of calibrated model (upper panel) and mesh of scenario model (lower panel).